Design, Synthesis and Mechanistic Studies of Boron and Phosphorus Heterocycles and Their Applications in Asymmetric Catalysis

by

Shuang Qiao

B.A. Chemistry, Harvard University (1994)

Submitted to the Department of
Chemistry in Partial Fulfillment of the
Requirements for the Degree of

DOCTOR OF PHILOSOPHY
IN ORGANIC CHEMISTRY

at the

Massachusetts Institute of Technology

June 1999

Signature of Author _____
Department of Chemistry
May 24, 1999

Certified by _____
Gregory C. Fu
Thesis Supervisor

Accepted by _____
Dietmar Seyferth
Chairman, Departmental Committee on Graduate Students

This doctoral thesis has been examined by a committee of the Department of Chemistry as follows:

Professor Satoru Masamune _____
Chairman

Professor Gregory C. Fu _____
Thesis Supervisor

Professor Peter H. Seeberger _____

Design, Synthesis and Mechanistic Studies of Boron and Phosphorus Heterocycles and Their Applications in Asymmetric Catalysis

by

Shuang Qiao

Submitted to the Department of Chemistry
on May 24, 1999 in partial fulfillment of the
requirements for the Degree of Doctor of Philosophy at the
Massachusetts Institute of Technology

ABSTRACT

In Part I of this thesis, detailed synthetic and mechanistic studies of borabenzene and boratabenzene complexes are discussed. A comprehensive mechanistic study of nucleophilic aromatic substitution reactions of borabenzene-PMe_3 complexes strongly favors an associative pathway, an addition-elimination mechanism, over all the other potential alternatives. Boratabenzenes are found to be capable of undergoing nucleophilic aromatic substitutions as well. Structurally interesting complexes have been synthesized and characterized.

In Part II, a new approach to chiral phosphines in asymmetric catalysis is discussed. A series of enantiopure phosphaferrocenes have been synthesized. One of them has been demonstrated to be an effective ligand in the enantioselective hydrogenation of dehydroamino acids. This marks the first application of an sp^2 hybridized phosphorus based compound as a chiral ligand in asymmetric catalysis. The versatility of this phosphaferrocene has also been demonstrated in a second reaction, asymmetric hydrogenation of aryl enamides to generate secondary aryl-alkyl amines. The key finding is the additive KBr which increases the enantioselectivity to above 90%. The remarkable success of the phosphaferrocene in enantioselective hydrogenation of enamides demonstrates its superiority over many existing phosphine ligands (e.g. BINAP) in certain reactions. Efforts to utilize chiral phosphaferrocenes in other transition-metal catalyzed processes are discussed. Preliminary studies of Rh catalyzed asymmetric isomerization of allylic alcohols have shown up to 86% ee.

Thesis Supervisor: Gregory C. Fu
Title: Professor of Chemistry

ACKNOWLEDGMENTS

As my life up to now has been that of a student, I have numerous people to thank at the conclusion of my Ph.D. study.

Blessed from childhood on with the best teachers I could ask for, it is literally impossible for me to fully express my gratitude in words. All my middle-school and high school teachers (where my mother teaches still) encouraged me to always strive for the best while maintaining a sense of modesty. During my college years at Beijing University (1990-1992) and Harvard University (1992-1994), I had the opportunity to be educated among some of the brightest students (my husband was one of them) by some of the best professors.

Professor Peter Chen, my academic advisor at Harvard, will always remain a role model for me. His integrity, kindness and enthusiasm for science will continue to inspire me. Professor George M. Whitesides in whose laboratory I had the fortune to conduct supervised research, is a great scientist with formidable intelligence and vision. His confidence in my potential helped me through graduate school as much as the knowledge and skills I gained under his guidance. I would also like to thank my Ph.D. advisor Professor Gregory C. Fu for allowing me to work independently on challenging projects. I have learned much from working for him.

I owe a million thanks to those I have learned from in research. Drs. Eric E. Simanek, Mathai Mammen, Watson J. Lees, John P. Folkers and Jinming Gao taught me much while I was in Whitesides lab. I have no reluctance staying up all night to do experiments after working with these dedicated researchers. At MIT, I have been lucky to work next to many talented and devoted chemists. Dr. David S. Hays was my baymate for three years, whose scientific ability can only be matched by his honesty and hard work. Beata Tao is the best labmate and friend that anyone could ask for. I have no doubt that she will continue to be successful. The contagious enthusiasm of Michael M-C. Lo for chemistry prompted me to think harder and more creatively on my projects. Thanks also to Dr. Christine E. Garrett, Dr. Hallie A. Latham, Dr. Rosa Lopez and Jennifer Tweddell, whose courage, dedication and talent have inspired me. I only hope that I am worthy of being one of them. I have been fortunate to learn from these hard-working and gifted colleagues: Jack Liang, Adam Littke, Dr. Michinori Suginome, Shih-yuan Liu, Mike Smith, Dr. Jordi Tormo, Dr. Ken Stockman, Yutaka Ie, Dr. Chaoyang Dai, Dr. Stephane Bellemin-Laponnaz and Dr. Shigeru Arai. Thank you all for helping to make my past few years a success.

Many of my friends deserve a special thanks for reminding me constantly what is most important in life. Edith Wun, Qing He, Melissa Klein and Yingnan Zhang were the four beautiful bridesmaids at my wedding. They passed their own lessons in life on to me with intelligence and humanity. I hope that I can do as much for them as they have for me. Zhuqing Dong, Tony Wong, Albert Lee, Uljana Mayer and Betty Bhudhikanok all have a great sense of humor which cheered me up when I was down.

Thanks to every member of my extended family, especially my grandmother in heaven, who used to tell me so much about her own school days abroad in France. I hope that I have inherited some of her style, culture, and joie de vivre. Finding and

reading my great-grandfather's biography in the Harvard library helped to inspire as well as humble me. I will try my best to live up to his expectations. I would also like to thank my kind and generous parents-in-law, Mr. and Mrs. Kang-yi Lin for being most understanding and loving.

This thesis is dedicated to the most extraordinary woman I know — my dearest mother, whose love knows no bounds and whose character is above reproach. She has taught me with her own example to embrace honesty and integrity above everything. Were it not for her, I would not have been where I am or what I am today. I only wish that I could make her half as proud of me as I am of her.

Lastly and most importantly, I do not know how in earthly words I can express my gratitude to my husband Michael Lin for his unwavering support and unconditional love. I have never met anyone else who combines the kindest heart with the smartest mind. Thank you, Michael, for being there for me all the time and for possessing everything it takes to achieve whatever you desire. You have never ceased to amaze me. You are the better half of my soul.

DEDICATION

To my dearest mother
the most remarkable woman on earth

PREFACE

Parts of this thesis have been adapted from the following articles co-written by the author.

Highly Enantioselective Hydrogenation of Aryl Enamides Catalyzed by a Rh(I)-Phosphaferrocene Complex. Qiao, S.; Lo, M. M-C.; Fu, G. C. Manuscript in preparation.

The First Application of a Planar-Chiral Phosphorus Heterocycle in Asymmetric Catalysis: Enantioselective Hydrogenation of Dehydroamino Acids. Qiao, S.; Fu, G. C. *J. Org. Chem.* **1998**, *63*, 4168-4169.

Synthesis, Resolution, and Crystallographic Characterization of a C_2-Symmetric Diphosphaferrocene. Qiao, S.; Hoic, D. A.; Fu, G. C. *Organometallics* **1998**, *17*, 773-774.

Synthesis and Structure of Borabenzene-(4-Phenylpyridine), a Heterocyclic Analogue of *p*- Terphenyl. Qiao, S.; Hoic, D. A.; Fu, G. C. *Organometallics* **1997**, *16*, 1501-1502.

Nucleophilic Aromatic Substitution Reactions of Borabenzene-Trimethylphosphine: A Versatile Route to 1-Substituted Boratabenzenes. Qiao, S.; Hoic, D. A.; Fu, G. C. *J. Am. Chem. Soc.* **1996**, *118*, 6329-6330.

TABLE OF CONTENTS

ABBREVIATIONS

cod	1,5-cyclooctadiene
Cp	cyclopentadienide
Cp^*	pentamethylcyclopentadienide
Cy	cyclohexyl
d	doublet
eq	equation
equiv	equivalent(s)
GC	gas chromatography
hr	hour(s)
HRMS	high resolution mass spectroscopy
IR	infrared
L	ligand
LDA	lithium diisopropylamide
min	minute(s)
NMR	nuclear magnetic resonance
ppm	parts per million
q	quartet
quint	quintet
r.t.	room temperature
s	singlet
t	triplet
Tf	trifluoromethanesulfonyl
THF	tetrahydrofuran
TLC	thin-layer chromatography
TMS	trimethylsilyl

Part I

Synthetic and Mechanistic Studies of Borabenzene and Boratabenzene Complexes

Chapter 1
Introduction

Lewis acids are known to catalyze a broad range of reactions, including some important carbon-carbon bond-forming reactions such as Diels-Alder, Mukaiyama aldol, Sakurai, and ene reactions.[1,2] The growing need for optically active compounds has stimulated an active interest in developing new asymmetric methodologies in the chemical community. Despite significant advances, the discovery of a versatile chiral Lewis acid catalyst remains elusive.[3-7]

Until recently, the efforts to discover chiral Lewis acid catalysts were essentially based on a "trial and error" strategy. Within the past few years, more rational approaches have resulted in some successes albeit limited. One of the examples is illustrated in Figure 1.1.[8,9] The key design element of the catalyst is a π-donor-acceptor interaction between the naphthalene system of the catalyst and the dienophile.

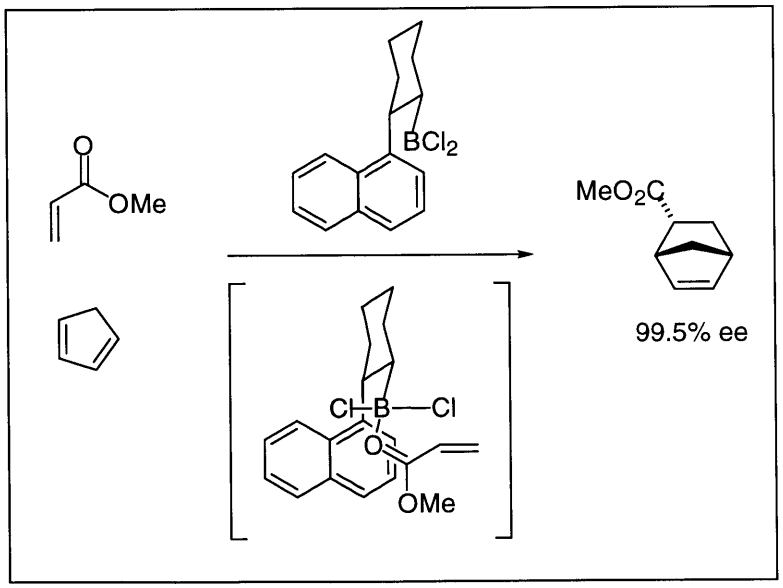

Figure 1.1. Hawkins' chiral Lewis acid catalyst.

However, this catalyst is incapable of effecting Lewis-acid catalyzed processes other than a number of Diels-Alder reactions. This may be due to the fact that the

stacking interaction which assists in organizing the substrate-(Lewis acid) complex does not explicitly activate this complex relative to other conformers.

Our goal is to develop a versatile chiral Lewis acid catalyst for reactions with aldehydes utilizing both π-activation and σ-activation (Figure 1.2). By σ-activation, we are referring to the interaction between the oxygen lone pair and the empty sp^2 orbital of the metal. This interaction which polarizes the carbonyl system has been the conventional approach to activate aldehydes by Lewis acids. However, this σ-symmetry interaction does not activate the π-carbonyl system towards nucleophilic attack. In addition, the strength of this interaction is essentially independent of the rotation around the M-O bond. By π-activation, we are referring to the interaction between the filled π-orbital of the carbonyl group and the empty p orbital of the π-symmetry metal center. This interaction not only explicitly activates the carbonyl towards nucleophilic attack but also couples organization and activation as the strength of this interaction is greatest when the p-type orbitals are parallel to each other.

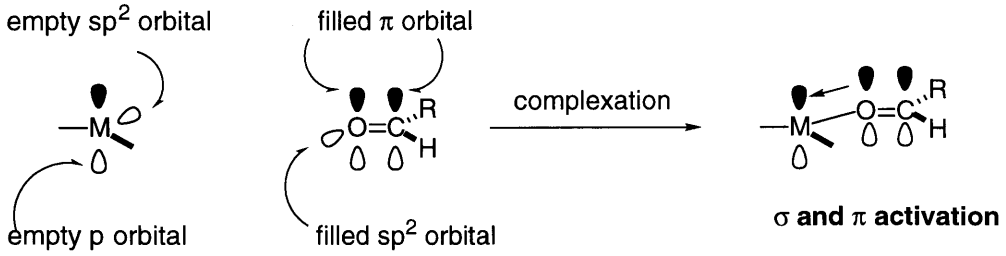

σ activation: complexation of the oxygen lone pair to the empty sp^2 orbital of the metal leads to polarization of the carbonyl system.

π activation: interaction between the π system of the carbonyl and the empty sp^2 orbital of the metal activates the carbonyl towards nucleophilic attack.

Activation and organization are coupled.

Figure 1.2. Proposed simultaneous π-activation and σ-activation of a prochiral aldehyde.

Borabenzene appears to be an ideal candidate for this design as it has a Lewis-acidic σ-symmetry orbital as well as a low-lying π*-orbital (Figure 1.3). The ortho-substituent R and the π-complexation of borabenzene to $Cr(CO)_3$ effectively destroy the symmetry of the molecule, resulting in a planar-chiral system. L should be a labile Lewis base which stabilizes the borabenzene as well as dissociates from it in the presence of an aldehyde substrate. The binding mode of the aldehyde to borabenzene illustrated in Figure 1.3 is probably the most favorable in terms of sterics. With a bulky $Cr(CO)_3$ blocking the bottom face, the nucleophile most likely will attack from the top face, leading to a stereoselective reaction.

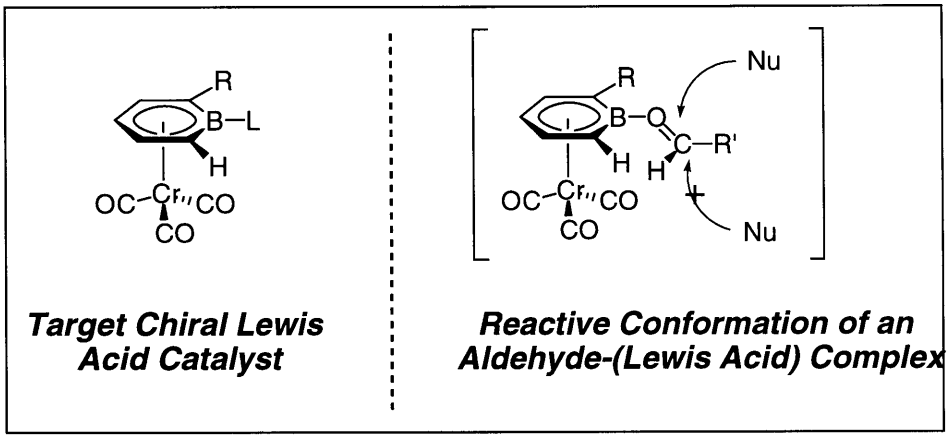

Figure 1.3. Target chiral Lewis acid and the proposed reactive conformation of the aldehyde-(Lewis acid) complex.

In order to accomplish the goal of developing the chiral Lewis acid based on borabenzene, it is important to be familiar with the chemistry of this class of heterocycles. While borabenzene chemistry is generally considered esoteric, there has been significant progress in this area in the past few years.[10-13] There are two classes of complexes in borabenzene chemistry - neutral borabenzene complexes and anionic boratabenzene complexes (Figure 1.4). Prior to our group's effort, only two neutral borabenzene complexes[14,15] had been reported while the field of anionic

boratabenzene complexes had been relatively more active.[13] Free borabenzene itself has never been detected and is estimated to be a highly energetic species.[16-22]

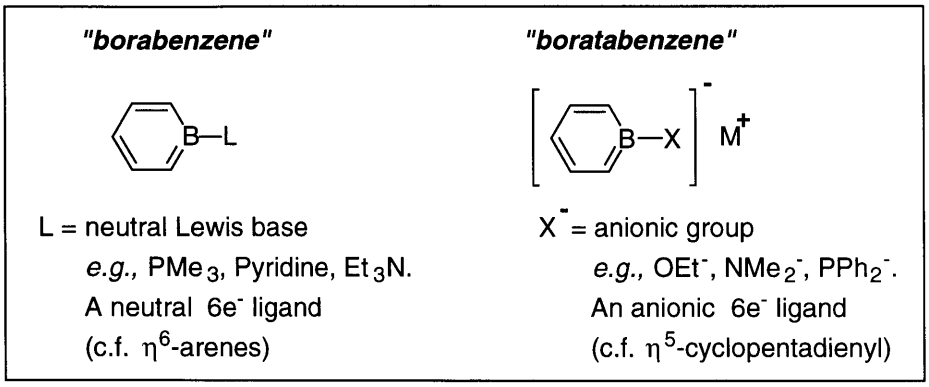

Figure 1.4. The two classes of complexes in borabenzene chemistry.

Efforts from our laboratory have greatly enriched borabenzene chemistry. Following the discovery of a facile synthesis of neutral borabenzene complexes,[23] nucleophilic aromatic substitution, a new mode of reactivity for borabenzene complexes was successfully used to accomplish ligand exchange at boron.[24] As ligand exchange at boron is essential for our proposal, a detailed mechanistic study of nucleophilic aromatic substitution reaction was deemed necessary. Chapter 2 discusses extensively the approach to understand the mechanism of this reaction. Our findings strongly suggest that the nucleophilic substitution reaction of borabenzene-PMe_3 complexes undergoes an associative pathway (Figure 1.5).

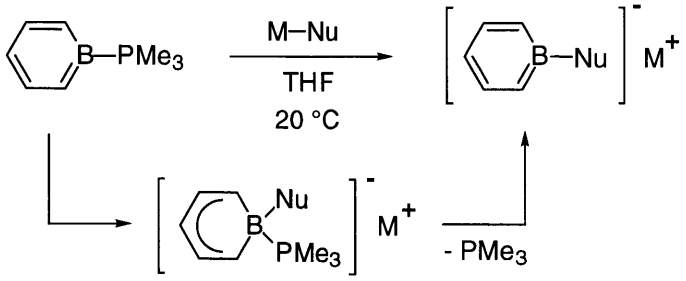

Figure 1.5. The addition-elimination mechanism favored by our mechanistic study.

While many attempts to functionalize the borabenzene ring have failed due to the fragility of the system,[25] some fascinating chemistry has been discovered in the meantime. In Chapter 3, results from our study of the fundamental reactivity of borabenzene and boratabenzene complexes are discussed. Molecules which might possess interesting material properties have been synthesized. The scope of nucleophilic aromatic substitution reaction in borabenzene chemistry has been explored. The successes as well as the failures have since taught us how to work with this class of molecules which undoubtedly will be beneficial to the ongoing pursuit of a chiral borabenzene-based catalyst.

Despite considerable efforts, synthesis of the proposed chiral Lewis acid catalyst (see Figure 1.3) has not yet been achieved. However, with the knowledge and expertise gained in the effort to date, the author is optimistic that some application of borabenzenes in asymmetric synthesis, if not the exact proposed model, will be accomplished in the future.

References

1 *Selectivities in Lewis Acid Promoted Reactions*; Schinzer, D., Ed.; Kluwer: Boston, 1989.
2 Yamaguchi, M. In *Comprehensive Organic Synthesis*; Trost, B. M., Ed.; Pergamon: New York, 1991; Vol. 1; Chapter 1.11.
3 Narasaka, K. *Synthesis* **1991**, 1-11.
4 Kagan, H. B.; Riant, O. *Chem. Rev.* **1992**, *92*, 1007-1019.
5 Mikami, K.; Shimizu, M. *Chem. Rev.* **1992**, *92*, 1021-1050.
6 Deloux, L.; Srebnik, M. *Chem. Rev.* **1993**, *93*, 763-784.
7 Bach, T. *Angew. Chem., Int. Ed. Engl.* **1994**, *33*, 417-419.
8 Hawkins, J. M.; Loren, S. *J. Am. Chem. Soc.* **1991**, *113*, 7794-7795.
9 Hawkins, J. M.; Loren, S.; Nambu, M. *J. Am. Chem. Soc.* **1994**, *116*, 1657-1660.
10 Amendola, M. C. M.S. Thesis, MIT, 1995 and references therein.
11 Hoic, D. A. Ph.D. Thesis, MIT, 1998 and references therein.
12 Tweddell, J. M. S. Thesis, MIT, 1997 and references therein.
13 Herberich, G. E.; Ohst, H. *Adv. Organomet. Chem.* **1986**, *25*, 199-236.
14 Boese, R.; Finke, N.; Keil, T.; Paetzold, P.; Schmid, G. *Z. Naturforsch., B* **1985**, *10*, 1327-32.

15 Boese, R.; Finke, N.; Henkelmann, J.; Maier, G.; Paetzold, P.; Reisenauer, H. P.; Schmid, G. *Chem. Ber.* **1985**, *118*, 1644-54.
16 Maier, G. *Pure Appl. Chem.* **1986**, *58*, 95-104.
17 Cioslowski, J.; Hay, P. J. *J. Am. Chem. Soc.* **1990**, *112*, 1707-10.
18 Schulman, J. M.; Disch, R. L. *Organometallics* **1989**, *8*, 733-7.
19 Raabe, G.; Schleker, W.; Heyne, E.; Fleischhauer, J. *Z. Naturforsch., A* **1987**, *42*, 352-60.
20 Schulman, J. M.; Disch, R. L.; Sabio, M. L. *J. Am. Chem. Soc.* **1982**, *104*, 3785-3788.
21 Maier, G.; Wolf, H. J.; Boese, R. *Chem. Ber.* **1990**, *123*, 505-11.
22 Maier, G.; Reisenauer, H. P.; Henkelmann, J.; Kliche, C. *Angew. Chem., Int. Ed. Engl.* **1988**, *27*, 295-296.
23 Hoic, D. A.; Wolf, J. R.; Davis, W. M.; Fu, G. C. *Organometallics* **1996**, *15*, 1315-18.
24 Qiao, S.; Hoic, D. A.; Fu, G. C. *J. Am. Chem. Soc.* **1996**, *118*, 6329-6330.
25 We have failed to functionalize the borabenzene ring before or after the formation of the aromatic system.

Chapter 2
Nucleophilic Aromatic Substitution Reactions of Borabenzene-PMe_3

Background

Although borabenzene complexes **1** are one of the simplest families of heterocycles, very little is known about their chemistry.[1-3] As part of a program directed towards the development of applications of borabenzenes in organic synthesis (see Chapter 1), we have initiated studies of their fundamental reactivity.

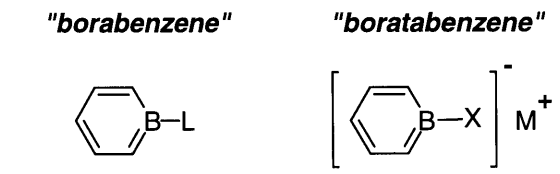

1 **2**

The only neutral borabenzene complex known prior to our group's efforts was borabenzene-pyridine and its $Cr(CO)_3$ complex.[1,2] The synthetic route illustrated in Figure 2.1 tends to be laborious and lacks generality. Another disadvantage is that the diyne is not commercially available.

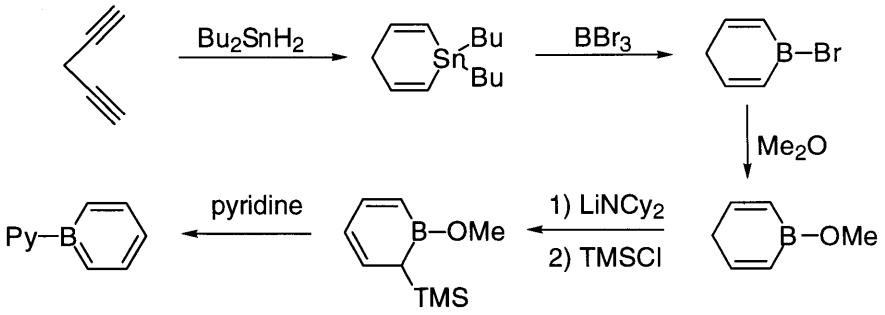

Figure 2.1. The first reported synthesis of a neutral borabenzene complex.

A modified procedure reported from our group has been demonstrated to be a more facile and more general route to neutral borabenzene complexes (Figure 2.2)[3]. The changes in the synthesis have allowed the preparation of a family of neutral

complexes exhibiting varied substitutions at boron. In addition, it is a less expensive and more efficient route due to the commercial availability of the starting material diyne.

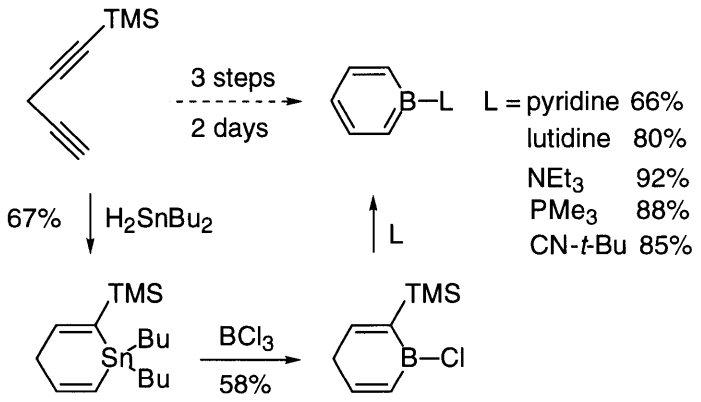

Figure 2.2. An improved and versatile synthesis of neutral borabenzene complexes.

Unlike neutral borabenzene complexes, for which only one synthetic route was available prior to our group's effort, several syntheses of boratabenzenes **2** have been reported.[4-8] However, they all have serious drawbacks, the most common of which is the limited scope as the procedures tend to be rather specific for synthesis of certain boratabenzenes only.

Since boratabenzenes **2** can serve as surrogates in organometallic chemistry for the ubiquitous cyclopentadienyl groups,[9] the synthesis of boratabenzenes **2** with various steric and electronic properties is worthy of exploration. Taking advantage of the readily available borabenzene-PMe_3 synthesized according to Figure 2.2, a facile synthesis of boratabenzenes **2** through aromatic substitution has been developed (Figure 2.3) by Dr. Diego A. Hoic.[10] Aromatic substitution, which has been investigated thoroughly in the case of benzenes[11] but was not known for borabenzenes, caught our attention as a possible means of generating a series of desired boratabenzenes.

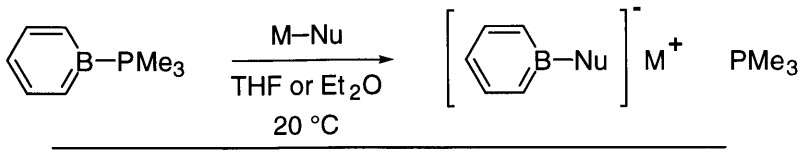

Nucleophile	Product	Yield (%)
$LiAlH_4$	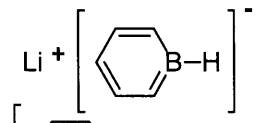	71
Li—≡—$SiMe_3$	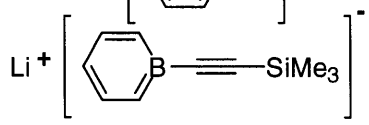	68
Li—NMe_2	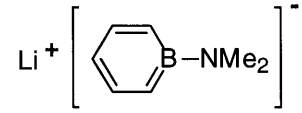	78
Na—OEt	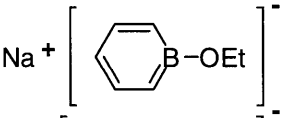	78
K—PPh_2	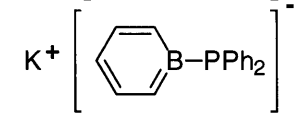	91

Figure 2.3. A versatile synthesis of boratabenzene complexes through aromatic substitution.

A detailed study of the mechanism of this newly discovered reaction would serve two purposes. One, it would enable us to better understand the fundamental chemistry of this family of heterocycles. Two, as ligand exchange at boron is supposed to occur in our proposed model of the chiral borabenzene catalyst, understanding the mechanism of this substitution reaction could give us further insight into the validity of our proposal and may potentially help modify the proposal to facilitate the process of developing this catalyst.

Results and Discussion

To understand the mechanism of this nucleophilic aromatic substitution reaction, we initially chose to study the reaction between borabenzene-PMe_3 (**B**) and $LiNMe_2$. However, the reaction was too fast at room temperature for us to follow. Speculating that bulkier groups on the amide nitrogen would slow down the reaction, we changed the nucleophiles to $LiNEt_2$. To our surprise, during the course of the reaction, we observed a new species by both ^1H and ^{11}B NMR which eventually disappeared to yield the desired product. When the groups on the amide nitrogen were changed to bulkier isopropyl groups, we observed only the new species with no trace of the desired substitution product **Q**. The phenomena could be best explained by Figure 2.4.

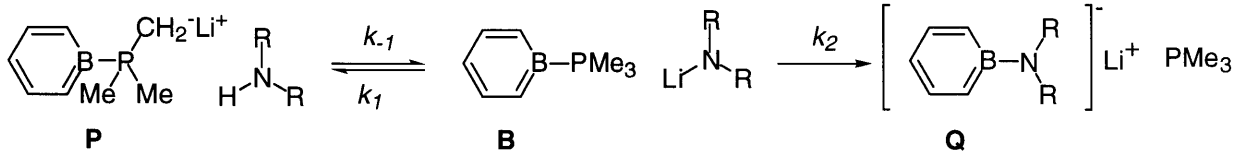

R = Me	***k_2 very large.***	***"P" not observed at r.t. Reaction complete instantaneously at r.t.***
R = Et	***$k_1 > k_2$***	***"P" observed in the beginning.***
R = *i*-Pr	***k_2 minimal.***	***Only "P" observed. "Q" never observed.***

Figure 2.4. Basicity versus nucleophilicity.

All three amides have roughly the same pKa's (around 36), which implies that all of them are capable of deprotonating the methyl groups of the PMe_3 moiety. While they are of comparable basicity, their levels of nucleophilicity are drastically different. As $LiNMe_2$ is the most nucleophilic of the three, we observed

instantaneous conversion to **Q** at room temperature. We indeed observed the transient formation of **P** at -78°C with $LiNMe_2$. $LiNEt_2$ is less nucleophilic than $LiNMe_2$ which results in a slower substitution reaction. The deprotonation became competitive. In the case of LDA, the isopropyl groups render it too bulky to act as a nucleophile. It essentially serves as a base and generates only **P**. As our primary interest is the substitution reaction, we decided to look into less basic nucleophiles to avoid complicated mechanistic situations such as the one described above.

The model system we have finally chosen to study the mechanism of aromatic substitution is the reaction between borabenzene-PMe_3 (**B**) and lithium trimethylsilylacetylide (**T**) (Figure 2.5). First, the reaction at room temperature generally takes a few hours to complete, which is convenient for the purpose of monitoring the conversion. Second, by ^1H NMR, the PMe_3 in both the product and the reactant is a sharp doublet corresponding to nine protons. Similarly, the TMS group in both the reactant and the product is a sharp singlet corresponding to nine protons by ^1H NMR. This enables us to follow the conversion by ^1H NMR with more accuracy. Third, there is no side reaction as lithium trimethylsilylacetylide is much less basic (pKa ~ 25) than amides.

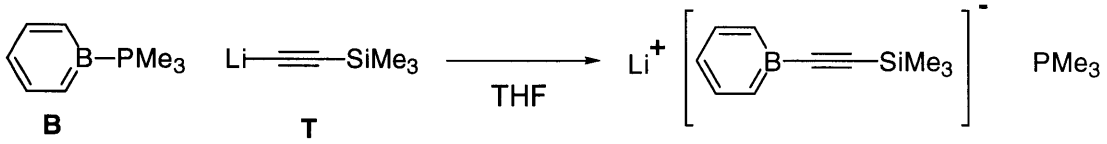

Figure 2.5. The model system chosen to study the mechanism of aromatic substitution reaction.

In analogy with the chemistry of benzene derivatives,[11] three of the most likely mechanisms for nucleophilic aromatic substitution of **B** are the dissociative, borabenzyne, and associative pathways (Figure 2.6).

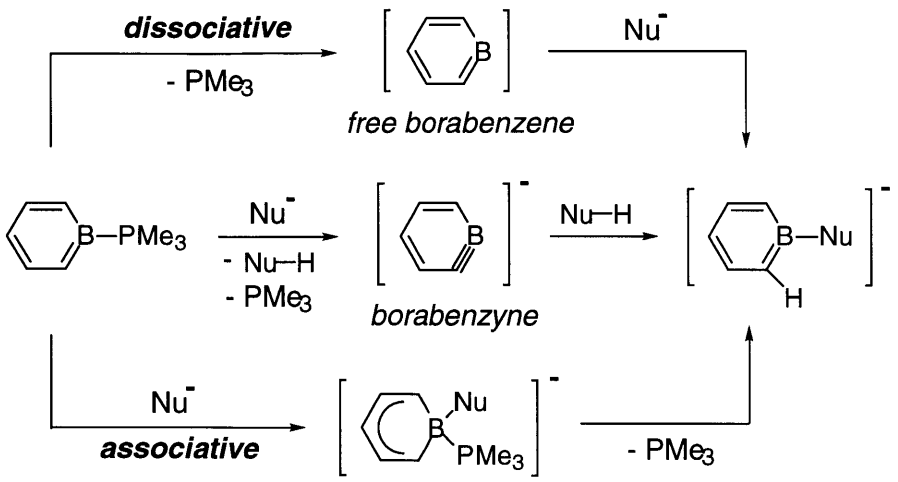

Figure 2.6. Three of the most likely mechanisms for nucleophilic aromatic substitution of borabenzene-PMe_3.

The dissociative pathway proceeds through free borabenzene, a species which has thus far eluded detection.[12-17] To test the validity of this proposal, we treated borabenzene-PMe_3 with 3 equivalents of PMe_3-d_9 (Figure 2.7). Under the assumption of a dissociative mechanism, exchange of borabenzene-PMe_3 with PMe_3-d_9 should occur. Dr. Kenneth E. Stockman first discovered that the exchange reaction does not occur in d_6-benzene. We repeated the reaction in d_8-THF to eliminate the possibility of solvent effects. As no exchange is observed in d_8-THF either, this mechanism is ruled out.

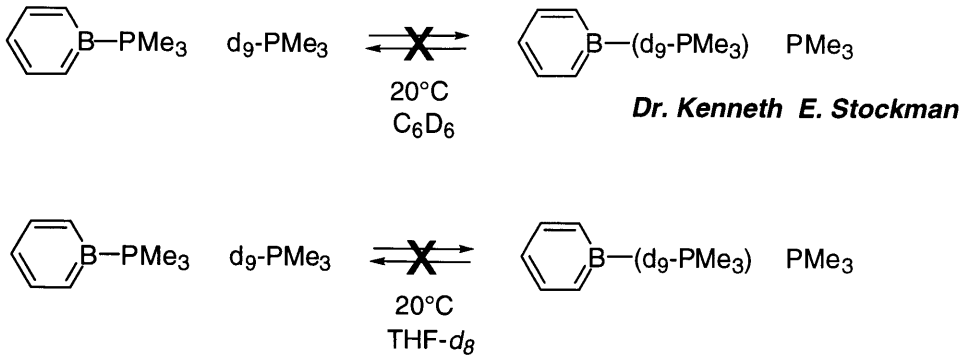

Figure 2.7. Disproof of the dissociative mechanism.

The borabenzyne pathway represents another mechanistic possibility for the substitution reaction as the nucleophiles such as lithium trimethylsilylacetylide (**T**) are fairly basic. To address this possibility, we ran the substitution reaction in the presence of 5 equivalents of 1-deuterio-2-trimethylsilylacetylene (Figure 2.8). Under the borabenzyne assumption, **T** will first act as a base to abstract the α-hydrogen from the borabenzene ring resulting in the formation of trimethylsilylacetylene and borabenzyne. The second step involves the addition of trimethylsilylacetylene to borabenzyne. It is reasonable to predict that under this mechanistic assumption, deuterium incorporation at the ortho position of the product would occur in the presence of an excess amount of 1-deuterio-2-trimethylsilylacetylene. However, we did not observe any deuterium incorporation by ^2H NMR which makes the borabenzyne mechanism highly unlikely.

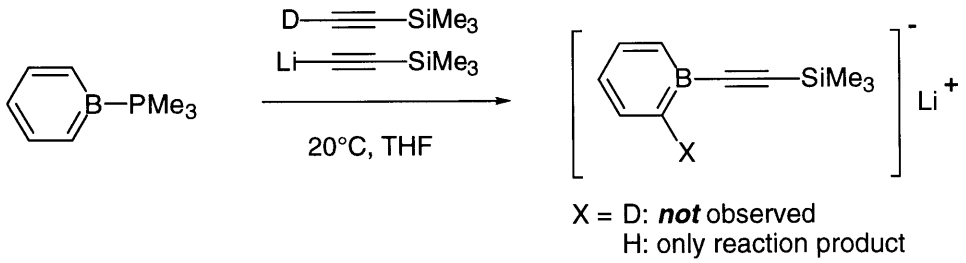

Figure 2.8. Disproof of the borabenzyne mechanism.

Only a very strong cage effect would make a borabenzyne mechanism compatible with the above results. In fact, we have not been able to design experiments to exclude this unusual case scenario. However, lithium trimethysilylacetylide has a much lower pKa than borabenzene (pKa for benzene is about 43). In addition, the hypothesized borabenzyne intermediate obviously suffers from an extremely high ring strain. Intuitively, it is the least likely of all three possible mechanisms. While the evidence against borabenzyne mechanism is not

definitive, it is sufficient in the absence of a highly unusual cage effect. In an additional labelling study, we have established that when borabenzene-(PMe_3-d_9) is treated with lithium trimethylsilylacetylide, all of the deuterium remains in the phosphine methyl groups. This finding further supports a mechanism which does not involve deprotonations.

Although the experimental results are inconsistent with two of the three most likely mechanisms, they are compatible with the presumed associative pathway. As the associative pathway implies rate dependence on both borabenzene-PMe_3 (**B**) and lithium trimethylsilylacetylide (**T**), we initiated a series of kinetic studies.

Pseudo-first-order kinetic experiments were conducted to determine the rate dependence on **T** (Figure 2.9). The concentration of **B** was held constant and in large excess while the starting concentration of **T** varied.

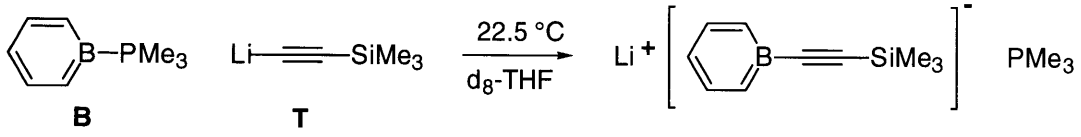

B **T**

$$\frac{dT}{dt} = -\,k\,B^{x}\,T^{y}$$

x, y, and k are constants
T = concentration of lithium trimethylsilylacetylide
B = concentration of borabenzene - PMe_3
$B \sim B_0$ throughout the reaction

Figure 2.9. Pseudo-first-order kinetic study of the rate dependence on **T**.

The conversion was determined by integrating the resonances corresponding to the TMS group of the reactant and the product in a single-pulse ^1H NMR spectrum. Observed rate constants (k_{obs}) were calculated based on a zero-, half-, and

first-order dependence on **T** (Figure 2.10 and Table 2.1). The results best fit (i.e., a constant k_{obs}) a kinetic scheme in which the substitution is half-order in **T**.

$$\frac{dT}{dt} = -k B^x T^y$$

x, y, and k are constants

T = concentration of lithium trimethylsilylacetylide

B = concentration of borabenzene - PMe_3

$B \sim B_0$ throughout the reaction

When y = 0.5, $\left(\frac{T}{T_0}\right)^{0.5} = \frac{-k B_0^{\,x}}{2\sqrt{T_0}} t + 1$

Plot $\left(\frac{T}{T_0}\right)^{0.5}$ versus t $\Rightarrow$ Slope = $-\frac{k B_0^{\,x}}{2\sqrt{T_0}} = \frac{-k_{obs}}{\sqrt{T_0}}$

When y = 1, $\ln\left(\frac{T}{T_0}\right) = -k B_0^{\,x} t$

Plot $\ln\left(\frac{T}{T_0}\right)$ versus t $\Rightarrow$ Slope = $-k B_0^{\,x} = -k_{obs}$

When y = 0, $\left(\frac{T}{T_0}\right) = -\left(\frac{k B_0^{\,x}}{T_0}\right) t + 1$

Plot $\left(\frac{T}{T_0}\right)$ versus t $\Rightarrow$ Slope = $-\left(\frac{k B_0^{\,x}}{T_0}\right) = -\frac{k_{obs}}{T_0}$

Figure 2.10. Derivation of rate equations under different assumptions of rate dependence on **T**.

	k(observed) if half order	k(observed) if first order	k(observed) if zero order
Run 1	1.2×10^{-5}	7.8×10^{-4}	8.1×10^{-7}
Run 2	1.3×10^{-5}	4.1×10^{-4}	1.8×10^{-6}
Run 3	1.4×10^{-5}	2.0×10^{-4}	3.8×10^{-6}

Table 2.1 Data analysis of the pseudo-first-order experiments.

The half-order rate dependence likely reflects a requirement for deaggregation prior to nucleophilic addition to borabenzene-PMe_3. Considering the copious amount of research on organo-lithium salts aggregation,[18-21] it is not surprising that lithium trimethysilylacetylide exists as an aggregate in THF.

Next, we performed the same type of pseudo-first-order kinetic experiments to study the rate dependence on **B**. The concentration of **T** was held constant and in large excess while the starting concentration of **B** varied (Figure 2.11).

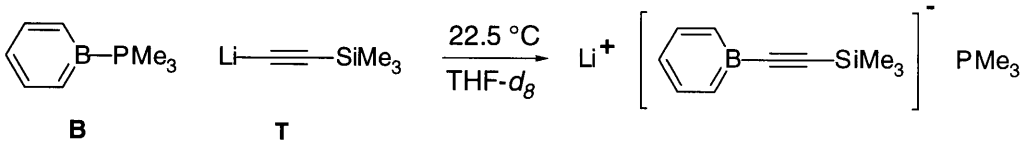

B **T**

$$\frac{dB}{dt} = -k\ B^x\ T^y$$

x, y, and k are constants

B = concentration of borabenzene - PMe_3

T = concentration of lithium trimethylsilylacetylide

$T \sim T_0$ throughout the reaction

Figure 2.11. Pseudo-first-order kinetic study of the rate dependence on **B**.

The conversion was determined by integrating the resonances corresponding to the PMe_3 group of the reactant and the product in a single-pulse ^1H NMR spectrum. Observed rate constants (k_{obs}) were calculated based on a zero-, first-, and

second-order dependence on **B** (Figure 2.12 and Table 2.2). The results best fit (i.e., a constant k_{obs}) a kinetic scheme in which the substitution is first-order in **B.**

$$\frac{dB}{dt} = -k\ B^x\ T^y$$

x, y, and k are constants

B = concentration of borabenzene - PMe_3

T = concentration of lithium trimethylsilylacetylide

T ~ T_0 throughout the reaction

When x = 1, $\ln\left(\frac{B}{B_0}\right) = -k\ T_0^{\ y}\ t$

Plot $\ln\left(\frac{B}{B_0}\right)$ versus t $\Rightarrow$ Slope $= -k\ T_0^{\ y} = -k_{obs}$

When x = 0, $\left(\frac{B}{B_0}\right) = -\left(\frac{k\ T_0^{\ y}}{B_0}\right) t + 1$

Plot $\left(\frac{B}{B_0}\right)$ versus t $\Rightarrow$ Slope $= -\left(\frac{k\ T_0^{\ y}}{B_0}\right) = -\frac{k_{obs}}{B_0}$

When x = 2, $\frac{1}{B} = k\ T_0^{\ y}\ t + \frac{1}{B_0}$

Plot $\frac{1}{B}$ versus t $\Rightarrow$ Slope $= k\ T_0^{\ y} = k_{obs}$

Figure 2.12. Derivation of rate equations under different assumptions of rate dependence on **B**.

	k(observed) if first order	k(observed) if zero order	k(observed) if second order
Run 4	9.6×10^{-5}	2.3×10^{-6}	4.2×10^{-3}
Run 5	9.7×10^{-5}	7.0×10^{-7}	1.4×10^{-2}
Run 6	9.1×10^{-5}	2.9×10^{-7}	2.8×10^{-2}

Table 2.2. Data analysis of the pseudo-first-order experiments.

Each set of pseudo-first-order kinetic studies were conducted with two separate batches of independently prepared borabenzene-PMe_3 and lithium trimethylsilylacetylide. With the order of the reaction in each of the two components in hand (half-order in lithium trimethylsilylacetylide and first-order in borabenzene-PMe_3), the data were analyzed to give the actual rate constant for the substitution reaction. The data, which involve significantly different concentrations of the two reactants, provide good agreement with respect to the value of the rate constant: $k \sim 4.4 \times 10^{-4}\ M^{-0.5}s^{-1}$ at 22.5 °C. All the experiments have been repeated twice, and the difference between sets is less than 5%. We did not pursue a rigorous least-square analysis of the kinetic data.

The kinetic data demonstrate that the rate of the substitution reaction is dependent on both borabenzene-PMe_3 and lithium trimethylsilylacetylide, which is consistent with the associative pathway. To provide additional support for this mechanism, we performed a competition experiment illustrated in Figure 2.13. $Cr(CO)_3$ is known to be a strong electron-withdrawing group which facilitates nucleophilic aromatic substitution reactions.[22] We confirmed that π-complexation of $Cr(CO)_3$ to borabenzene-PMe_3 greatly enhanced its reactivity towards substitution. This result is consistent with an associative mechanism.

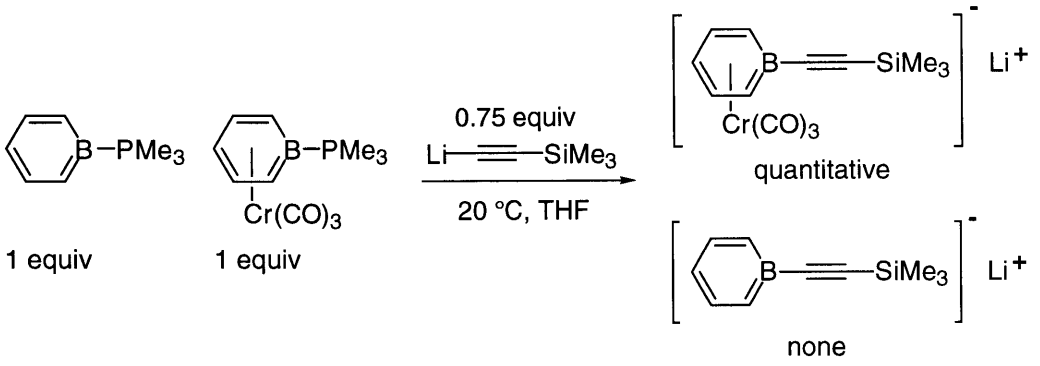

Figure 2.13. Additional support for the associative mechanism.

We briefly considered the possibility of a radical process involving electron transfer as an alternate to the dissociative, borabenzyne and associative mechanisms.[23] However, the highly reproducible kinetics that we observed for the reaction of borabenzene-PMe_3 with lithium trimethylsilylacetylide, essentially independent of the presence or absence of light or oxygen, suggests that a radical process is not operative.

Finally, variable temperature ^1H NMR was employed to determine the activation parameters for this exchange reaction. The activation parameters determined according to Figure 2.14 (Table 2.3) are:

$$Ea = 75.7 \text{ kJ/mol} = 18.1 \text{ kcal/mol}$$

$$\Delta H^{\neq} = 73.2 \text{ kJ/mol} = 17.5 \text{ kcal/mol}$$

$$\Delta S^{\neq} = -61.0 \text{ J K}^{-1} \text{ mol}^{-1} = -14.6 \text{ cal K}^{-1} \text{ mol}^{-1}$$

The negative $\Delta S^{\neq}$ indicates a more ordered transition state, which is consistent with an associative pathway.

Temp (K)	1/(RT) (mol/J)	k ($M^{-0.5}s^{-1}$)	ln k
271.3	4.44×10^{-4}	0.27×10^{-4}	-10.52
285.3	4.22×10^{-4}	1.7×10^{-4}	-8.68
296.0	4.07×10^{-4}	4.8×10^{-4}	-7.64
308.0	3.90×10^{-4}	17×10^{-4}	-6.38
318.0	3.78×10^{-4}	40×10^{-4}	-5.52

Table 2.3. Determination of activation parameters.

$$\ln k = \ln A - \frac{Ea}{RT}$$

Plot (ln k) versus $\frac{1}{RT}$

Slope $= -Ea$

$$\Delta H^{\neq} = Ea - RT$$

$$\frac{\Delta S^{\neq}}{19.15} = \log k - 10.753 - \log T + \frac{Ea}{19.15T}$$

Figure 2.14. Equations involved in determining the activation parameters.

In summary, we have performed a comprehensive series of experiments which strongly support an associative (addition-elimination) pathway for aromatic substitution (Figure 2.15).

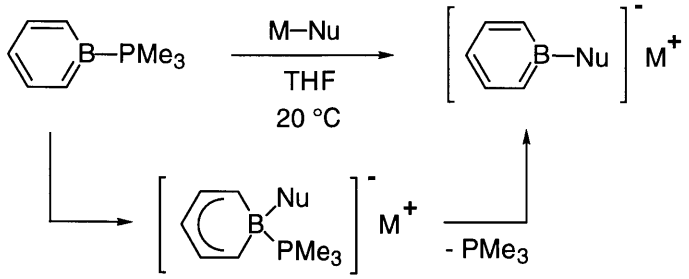

Figure 2.15. The strongly supported addition-elimination mechanism.

The mechanistic understanding we have gained will undoubtedly improve our grasp of borabenzene chemistry, thereby providing further insight into the design and synthesis of a chiral Lewis acid catalyst based on borabenzene.

Experimental

General

^1H nuclear magnetic resonance spectra were recorded on Varian XL-300, Unity 300, or VXR 500 NMR spectrometers at ambient temperature in d_8-THF and are referenced to residual solvent downfield from tetramethylsilane (δ 3.58 for THF), unless otherwise specified. ^1H NMR data are reported as follows: chemical shift (δ scale), multiplicity (br = broad, s = singlet, d = doublet, t = triplet, q = quartet, and m = multiplet), coupling constant (Hz), and integration. ^{13}C chemical shifts are reported in ppm downfield from tetramethylsilane (δ scale). All ^{13}C spectra were determined with complete proton decoupling. ^{11}B NMR spectra were obtained in d_8-THF on Varian Unity 300 MHz spectrometer (96 MHz) and are referenced to external BF_3-OEt_2 (δ 0). ^2H NMR spectra were obtained in THF on Varian XL-300 or Unity 300 NMR spectrometers (46 MHz) and are referenced to residual solvent downfield from tetramethylsilane (δ 3.58 for THF).

Lithium trimethylsilylacetylide was prepared by dropwise addition of 0.95 equivalents of *n*-butyllithium (Aldrich; 1.6 M in hexanes) to trimethylsilylacetylene (Aldrich) in hexanes at room temperature (exotherm), followed by drying. $LiNMe_2$, $LiNEt_2$ and LDA (Strem) were used as received. Borabenzene-PMe_3 and borabenzene-PMe_3-$Cr(CO)_3$ were prepared according to the literature procedure.[3,24] The materials used for mechanistic studies were purified by crystallization and then sublimation.

All reactions were set up under an atmosphere of nitrogen in oven-dried glassware inside a Vacuum Atmospheres HE-43-2 glove box.

Mechanistic Studies

Exchange between borabenzene-PMe_3 and d_9-PMe_3

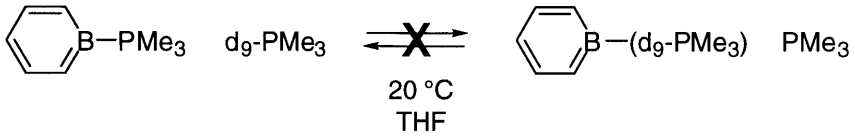

d_9-PMe_3 (45 μL, 0.44 mmol) was added to a solution of borabenzene-PMe_3 (22 mg, 0.14 mmol) in 0.7 mL of d_8-THF. The reaction was monitored by ^1H NMR for 20 hours, during which time no free PMe_3 was observed.

Reaction of borabenzene-PMe_3 with lithium trimethylsilylacetylide in the presence of 1-deuterio-2-trimethylsilylacetylene

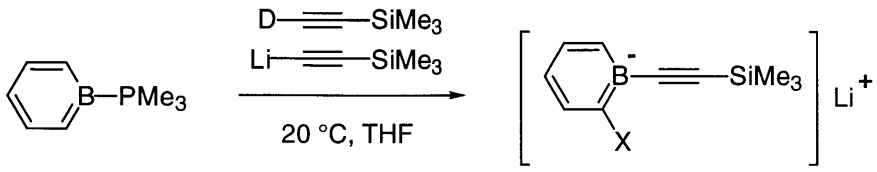

X = D: ***not*** observed
H: only reaction product

Synthesis of 1-deuterio-2-trimethylsilylacetylene. Lithium trimethylsilylacetylide (0.70 g, 6.7 mmol) was dissolved in 6 mL of THF. Deuterium oxide (72 μL, 4.0 mmol) was added slowly by syringe to the stirred solution. Following completion of the addition, the mixture was allowed to stir at room temperature for one hour. The

suspension was filtered, and the resulting solution was diluted to 10 mL to make the concentration of 1-deuterio-2-trimethylsilylacetylene approximately 0.4 mM.
^{2}H NMR: δ 2.68.

Reaction of borabenzene-PMe$_3$ with lithium trimethylsilylacetylide in the presence of 1-deuterio-2-trimethylsilylacetylene. Borabenzene-PMe$_3$ (18 mg, 0.12 mmol) and lithium trimethylsilylacetylide (18 mg, 0.17 mmol) were added at room temperature to a THF solution of 1-deuterio-2-trimethylsilylacetylene (2 mL, ~0.8 mmol; see above). The reaction mixture was then transferred to a J. Young NMR tube. The progress of the substitution reaction was monitored by ^{11}B NMR spectroscopy, and deuterium incorporation in the aromatic ring was monitored by ^{2}H NMR. No deuterium was detected (limits of detection: ~5%) in the aromatic region at any point during the reaction.

Synthesis of borabenzene-(d$_9$-PMe$_3$). Borabenzene-(d$_9$-PMe$_3$) was synthesized according to the procedure reported for the preparation of borabenzene-PMe$_3$.[3]

Reaction of borabenzene-(d$_9$-PMe$_3$) with lithium trimethylsilylacetylide. Borabenzene-(d$_9$-PMe$_3$) (19 mg, 0.12 mmol) and lithium trimethylsilylacetylide (19 mg, 0.18 mmol) were dissolved in 2 mL of THF at room temperature. The reaction mixture was then transferred to a J. Young NMR tube. The progress of the substitution reaction was monitored by ^{11}B NMR spectroscopy, and the location of the deuteria was monitored by ^{2}H NMR. No deuterium was lost from d$_9$-PMe$_3$ during the reaction.

Competition experiment between borabenzene-PMe_3 and (borabenzene-PMe_3)$Cr(CO)_3$ for lithium trimethylsilylacetylide

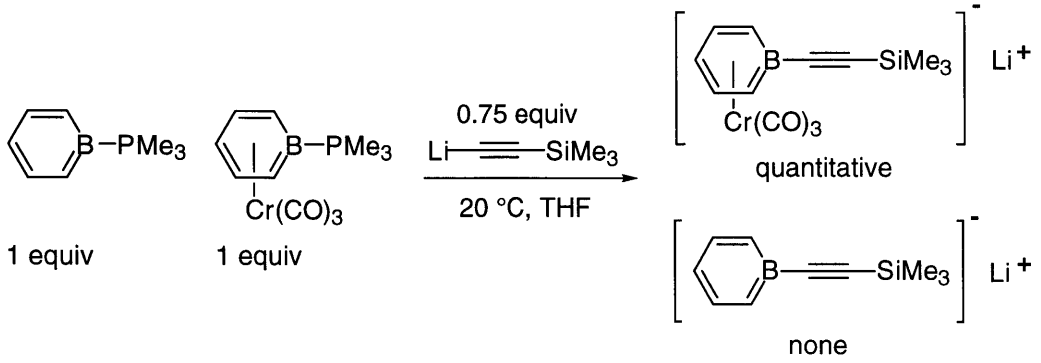

A solution of (borabenzene-PMe_3)$Cr(CO)_3$ (9.2 mg, 0.032 mmol) in 500 μL of d_8-THF and a solution of borabenzene-PMe_3 (7.5 mg, 0.049 mmol) in 760 μL of d_8-THF were prepared, and 250 μL of each solution (0.016 mmol) was added to a J. Young NMR tube. Lithium trimethylsilylacetylide (17 mg, 0.163 mmol) was dissolved in 1.0 mL of d_8-THF, and 75 μL (0.012 mmol) of this solution was added to the J. Young NMR tube (cooled to 0 °C). A ^1H NMR spectrum taken within ten minutes showed that all of the lithium trimethylsilylacetylide had been consumed. Li[($C_5H_5BCCSiMe_3$)$Cr(CO)_3$], (borabenzene-PMe_3)$Cr(CO)_3$, borabenzene-PMe_3, and PMe_3 were the only compounds present. No Li($C_5H_5BCCSiMe_3$) was produced.

Kinetic studies of the reaction of

borabenzene-PMe_3 with lithium trimethylsilylacetylide

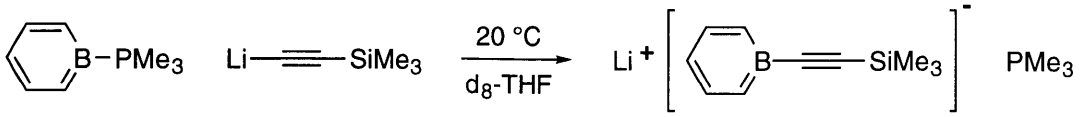

Each study was conducted with two separate batches of independently prepared borabenzene-PMe_3 and lithium trimethylsilylacetylide.

In the experiments in which the order in each reactant is determined, the concentrations of lithium trimethylsilylacetylide are calculated on the basis of a monomeric species although this species exists as an aggregate. The aggregation state of lithium trimethylsilylacetylide does not affect the conclusions of these experiments.

Order in lithium trimethylsilylacetylide.

^1H NMR experiments were conducted under pseudo-first-order conditions with borabenzene-PMe_3 in large excess. In experiments 1-3, borabenzene-PMe_3 (28.8 mg, 0.19 mmol) was dissolved in 1.0 mL of d_8-THF, thereby generating a 0.19 M solution. Lithium trimethylsilylacetylide (10.2 mg, 0.098 mmol) was dissolved in 2.0 mL of d_8-THF, providing a 0.049 M solution. The borabenzene-PMe_3 solution (300 μL, 0.057 mmol) was added to each of three J. Young NMR tubes labeled 1, 2, and 3. d_8-THF (320 μL, 240 μL, and 0 μL, respectively) was added to the three NMR tubes, followed by the lithium trimethylsilylacetylide solution [40 μL (0.0020 mmol), 120 μL (0.0059 mmol), and 360 μL (0.018 mmol), respectively]. The time of mixing of the two reactants was taken as time zero. The conversion of reactants to products was determined by integrating the resonances corresponding to the trimethylsilyl group of the reactant and the product in a single-pulse ^1H NMR spectrum (Table 2.4).

The study was repeated according to the same procedure with a second batch of independently prepared reactants, and similar results were observed.

Table 2.4. Order in lithium trimethylsilylacetylide: Data table (B = borabenzene-PMe_3; T = lithium trimethylsilylacetylide)

	time (min)	[B] (M)	[T] (M)
Run 1	0.00	0.0864	0.00300
	6.67	0.0858	0.00236
	11.67	0.0854	0.00196
	16.67	0.0849	0.00150
	21.67	0.0847	0.00126
	26.67	0.0844	0.000987
	31.67	0.0842	0.000831
	36.67	0.0841	0.000657
	41.67	0.0839	0.000477
	46.67	0.0837	0.000348
Run 2	0.00	0.0864	0.00890
	16.5	0.0845	0.00695
	19	0.0838	0.00635
	24	0.0833	0.00579
	29	0.0826	0.00506
	34	0.0821	0.00457
	39	0.0814	0.00392
	44	0.0810	0.00350
	49	0.0807	0.00318
	56.5	0.0801	0.00263
Run 3	0.00	0.0864	0.0270
	7.67	0.0834	0.0240
	12.67	0.0828	0.0234
	17.67	0.0808	0.0214
	22.67	0.0802	0.0208
	27.67	0.0784	0.0190
	32.67	0.0777	0.0183
	37.67	0.0765	0.0171
	42.67	0.0755	0.0161
	47.67	0.0747	0.0153

Observed rate constants (k_{obs}) were calculated for runs 1-3 based on a zero-, half-, and first-order dependence on lithium trimethylsilylacetylide concentration (Scheme 2.1 and Table 2.5). The results best fit (i.e., a constant k_{obs}) a kinetic scheme in which the substitution reaction is half-order in lithium trimethylsilylacetylide.

Scheme 2.1

$$\frac{dT}{dt} = - k B^x T^y$$

x, y, and k are constants

T = concentration of lithium trimethylsilylacetylide

B = concentration of borabenzene - PMe_3

$B \sim B_0$ throughout the reaction

When y = 0.5, $\left(\frac{T}{T_0}\right)^{0.5} = \frac{- k B_0^{\,x}}{2\sqrt{T_0}} t + 1$

Plot $\left(\frac{T}{T_0}\right)^{0.5}$ versus t $\Rightarrow$ Slope = $- \frac{k B_0^{\,x}}{2\sqrt{T_0}} = \frac{-k_{obs}}{\sqrt{T_0}}$

When y = 1, $\ln\left(\frac{T}{T_0}\right) = -k B_0^{\,x} t$

Plot $\ln\left(\frac{T}{T_0}\right)$ versus t $\Rightarrow$ Slope = $- k B_0^{\,x} = - k_{obs}$

When y = 0, $\left(\frac{T}{T_0}\right) = -\left(\frac{k B_0^{\,x}}{T_0}\right) t + 1$

Plot $\left(\frac{T}{T_0}\right)$ versus t $\Rightarrow$ Slope = $-\left(\frac{k B_0^{\,x}}{T_0}\right) = - \frac{k_{obs}}{T_0}$

Table 2.5. Order in lithium trimethylsilylacetylide: Data analysis

	k(observed) if half order	k(observed) if first order	k(observed) if zero order
Run 1	1.2×10^{-5}	7.8×10^{-4}	8.1×10^{-7}
Run 2	1.3×10^{-5}	4.1×10^{-4}	1.8×10^{-6}
Run 3	1.4×10^{-5}	2.0×10^{-4}	3.8×10^{-6}

Order in borabenzene-PMe_3.

^1H NMR experiments were conducted under pseudo-first-order conditions with lithium trimethylsilylacetylide in large excess. Borabenzene-PMe_3 (10.0 mg, 0.066 mmol) was dissolved in 0.95 mL of d_8-THF, thereby generating a 0.069 M solution. Lithium trimethylsilylacetylide (24.5 mg, 0.236 mmol) was dissolved in 1.0 mL of d_8-THF, producing a 0.236 M solution. The lithium trimethylsilylacetylide solution (250 μL) was added to each of three J. Young NMR tubes labeled 4, 5, and 6. d_8-THF (100 μL, 310 μL, and 360 μL) was added to NMR tubes 4, 5, and 6, respectively. The borabenzene-PMe_3 solution (300 μL) was added to NMR tube 4, and the reaction was monitored by NMR. The time of mixing of the two reactants was taken as time zero. The borabenzene solution (90 μL and 40 μL) was added to NMR tubes 5 and 6, respectively, and these reactions were also monitored by NMR. The conversion of reactants to products was determined by integrating the resonances corresponding to the PMe_3 group of the reactant and the product in a single-pulse ^1H NMR spectrum (Table 2.6).

Table 2.6. Order in borabenzene-PMe_3: Data table (B = borabenzene-PMe_3; T = lithium trimethylsilylacetylide)

	time (min)	[B] (M)	[T] (M)
Run 4	0	0.0320	0.0906
	12	0.0300	0.0886
	24	0.0276	0.0862
	36	0.0259	0.0845
	48	0.0240	0.0826
	60	0.0223	0.0809
	72	0.0209	0.0795
	84	0.0196	0.0782
	96	0.0183	0.0769
Run 5	0	0.00960	0.0906
	6	0.00914	0.0901
	12	0.00882	0.0898
	24	0.00830	0.0893
	36	0.00777	0.0888
	48	0.00714	0.0881
	60	0.00669	0.0877
	72	0.00625	0.0873
	84	0.00582	0.0868
	90	0.00558	0.0866
Run 6	0	0.00430	0.0906
	6	0.00411	0.0904
	12	0.00388	0.0902
	24	0.00362	0.0899
	36	0.00341	0.0897
	48	0.00320	0.0895
	60	0.00300	0.0893
	72	0.00285	0.0892
	84	0.00264	0.0889
	90	0.00255	0.0888

The study was repeated according to the same procedure with a second batch of independently prepared reactants, and similar results were observed.

Scheme 2.2

$$\frac{dB}{dt} = -\,k\ B^x\ T^y$$

x, y, and k are constants

B = concentration of borabenzene - PMe_3

T = concentration of lithium trimethylsilylacetylide

T ~ T_0 throughout the reaction

When x = 1, $\ln\left(\frac{B}{B_0}\right) = -k\ T_0{}^y\ t$

Plot $\ln\left(\frac{B}{B_0}\right)$ versus t $\Rightarrow$ Slope $= -k\ T_0{}^y = -k_{obs}$

When x = 0, $\left(\frac{B}{B_0}\right) = -\left(\frac{k\ T_0{}^y}{B_0}\right) t + 1$

Plot $\left(\frac{B}{B_0}\right)$ versus t $\Rightarrow$ Slope $= -\left(\frac{k\ T_0{}^y}{B_0}\right) = -\frac{k_{obs}}{B_0}$

When x = 2, $\frac{1}{B} = k\ T_0{}^y\ t + \frac{1}{B_0}$

Plot $\frac{1}{B}$ versus t $\Rightarrow$ Slope $= k\ T_0{}^y = k_{obs}$

Observed rate constants (k_{obs}) were calculated for runs 4-6 based on a zero-, first-, and second-order dependence on borabenzene-PMe_3 concentration (Scheme 2.2 and Table 2.7). The results best fit (i.e., a constant k_{obs}) a kinetic scheme in which the substitution reaction is first-order in borabenzene-PMe_3.

Table 2.7. Order in borabenzene-PMe_3: Data analysis

	k(observed) if first order	k(observed) if zero order	k(observed) if second order
Run 4	9.6×10^{-5}	2.3×10^{-6}	4.2×10^{-3}
Run 5	9.7×10^{-5}	7.0×10^{-7}	1.4×10^{-2}
Run 6	9.1×10^{-5}	2.9×10^{-7}	2.8×10^{-2}

Determination of the rate constant.

With the order of the reaction in each of the components in hand (half-order in lithium trimethylsilylacetylide and first-order in borabenzene-PMe_3), the data can be analyzed to give the actual rate constant for the substitution reaction. It should be noted that in the work described above, the concentration of lithium trimethylsilylacetylide was calculated based on a monomeric structure. In the following calculations, the half-order dependence of the reaction on lithium trimethylsilylacetylide is taken into account.

Scheme 2.3

$$\frac{dT}{dt} = -\frac{1}{2} k B T^{0.5}$$

$B = B_0$ throughout the reaction

$$\left(\frac{T}{T_0}\right)^{0.5} = \frac{-k B_0}{4\sqrt{T_0}} t + 1$$

Plot $\left(\frac{T}{T_0}\right)^{0.5}$ versus t

$$\text{Slope} = \frac{-k B_0}{4\sqrt{T_0}}$$

$$k = -\frac{\text{Slope} \times 4\sqrt{T_0}}{B_0}$$

Table 2.8. Rate constant from experiments 1-3

	B_0 (M)	T_0 (M)	Slope	k($M^{-0.5}s^{-1}$)
Run 1	8.6×10^{-2}	1.5×10^{-3}	-22×10^{-5}	4.0×10^{-4}
Run 2	8.6×10^{-2}	4.5×10^{-3}	-14×10^{-5}	4.4×10^{-4}
Run 3	8.6×10^{-2}	1.3×10^{-2}	-8.4×10^{-5}	4.5×10^{-4}

Tables 2.8 and 2.9 show that the six sets of data, which involve significantly different concentrations of the two reactants, provide good agreement with respect to the value of the rate constant: $k \sim 4.4 \times 10^{-4}\ M^{-0.5}s^{-1}$ at 22.5 °C.

Scheme 2.4

$$\frac{dB}{dt} = -k\,B\,T^{0.5}$$

$T = T_0$ throughout the reaction

$$\ln\left(\frac{B}{B_0}\right) = -k\sqrt{T_0}\,t$$

Plot $\ln\left(\frac{B}{B_0}\right)$ versus t

$$\text{Slope} = -k\sqrt{T_0}$$

$$k = -\frac{\text{Slope}}{\sqrt{T_0}}$$

Table 2.9. Rate constant from experiments 4-6

	B_0 (M)	T_0 (M)	Slope	$k(M^{-0.5}s^{-1})$
Run 4	3.2×10^{-2}	4.5×10^{-2}	-9.6×10^{-5}	4.5×10^{-4}
Run 5	9.6×10^{-3}	4.5×10^{-2}	-9.7×10^{-5}	4.5×10^{-4}
Run 6	4.3×10^{-3}	4.5×10^{-2}	-9.1×10^{-5}	4.3×10^{-4}

Determination of the activation parameters.

Variable temperature ^{1}H NMR was employed to determine the activation parameters for this exchange reaction. Borabenzene-PMe_3 (59.1 mg, 0.389 mmol) was dissolved in 2.0 mL of d_8-THF, affording a 0.195 M solution. Lithium trimethylsilylacetylide (44.0 mg, 0.423 mmol) was dissolved in 2.0 mL of d_8-THF to provide a solution which was 0.106 M in lithium trimethylsilylacetylide dimer. 350 μL of the borabenzene-PMe_3 solution and 300 μL of the lithium trimethylsilylacetylide solution were mixed in a J. Young NMR tube at 273 K, and the reaction was followed by ^{1}H NMR. The concentration of each reactant and each product was monitored by integrating the PMe_3 and $SiMe_3$ resonances in a single-pulse ^{1}H NMR spectrum (Table 7). The data were analyzed by numerical integration in Matlab (The Mathworks, Inc., Version 4.2c) to give the rate constant k. The reaction was repeated at five temperatures over a range of 47 K using the same concentrations of each reactant. For each experiment, the temperature of the thermostatted probe was measured by analyzing the spectrum of neat methanol.

The study was repeated according to the same procedure with a second batch of independently prepared reactants, and similar results were observed.

The activation parameters determined according to Scheme 2.5 (Tables 2.10 and 2.11 and Scheme 2.6) are:

$$Ea = 75.7 \text{ kJ/mol} = 18.1 \text{ kcal/mol}$$

$$\Delta H^{\neq} = 73.2 \text{ kJ/mol} = 17.5 \text{ kcal/mol}$$

$$\Delta S^{\neq} = -61.0 \text{ J K}^{-1} \text{ mol}^{-1} = -14.6 \text{ cal K}^{-1} \text{ mol}^{-1}$$

Scheme 2.5

$$\ln k = \ln A - \frac{Ea}{RT}$$

Plot $(\ln k)$ versus $\frac{1}{RT}$

Slope $= -Ea$

$\Delta H^{\neq} = Ea - RT$

$$\frac{\Delta S^{\neq}}{19.15} = \log k - 10.753 - \log T + \frac{Ea}{19.15T}$$

Table 2.10. Determination of activation parameters: Data table (B = borabenzene-PMe_3; T = lithium trimethylsilylacetylide)

Temperature (K)	time (min)	[B] (M)	[T] (M)
271.3	0	0.105	0.0487
	16.5	0.104	0.0478
	76.5	0.102	0.0462
	136.5	0.0998	0.0451
	196.5	0.0981	0.0440
	256.5	0.0964	0.0430
	316.5	0.0949	0.0420
	376.5	0.0933	0.0411
	436.5	0.0917	0.0401
	496.5	0.0902	0.0392
	556.5	0.0887	0.0383
	616.5	0.0873	0.0373
	676.5	0.0858	0.0366
285.3	0	0.105	0.0487
	10	0.103	0.0474
	50	0.0936	0.0422
	90	0.0861	0.0384
	130	0.0800	0.0354
	170	0.0740	0.0324
	210	0.0694	0.0296
	250	0.0653	0.0278
	290	0.0617	0.0260
	330	0.0585	0.0244
	370	0.0554	0.0229
	410	0.0526	0.0214
	450	0.0500	0.0200
296.0	0	0.105	0.0487
	8	0.102	0.0468
	18	0.0959	0.0436
	38	0.0850	0.0385
	58	0.0761	0.0335
	78	0.0687	0.0301
	98	0.0623	0.0268
	118	0.0571	0.0243
	138	0.0524	0.0218
	158	0.0485	0.0200
	178	0.0447	0.0182
308.0	0	0.105	0.0487
	6	0.101	0.0463
	16	0.0838	0.0363
	26	0.0706	0.0291
	36	0.0605	0.0238
	46	0.0526	0.0200
	56	0.0463	0.0169
	66	0.0410	0.0145
	76	0.0371	0.0126
	86	0.0335	0.0109
318.0	0	0.105	0.0487
	11	0.0802	0.0355
	16	0.0650	0.0277
	21	0.0539	0.0219
	26	0.0458	0.0178
	31	0.0394	0.0148
	36	0.0345	0.0121
	41	0.0306	0.0104
	46	0.0275	0.0089
	51	0.0250	0.0078

Table 2.11. Determination of activation parameters

Temp (K)	1/(RT) (mol/J)	k ($M^{-0.5}s^{-1}$)	ln k
271.3	4.44×10^{-4}	0.27×10^{-4}	-10.52
285.3	4.22×10^{-4}	1.7×10^{-4}	-8.68
296.0	4.07×10^{-4}	4.8×10^{-4}	-7.64
308.0	3.90×10^{-4}	17×10^{-4}	-6.38
318.0	3.78×10^{-4}	40×10^{-4}	-5.52

Scheme 2.6

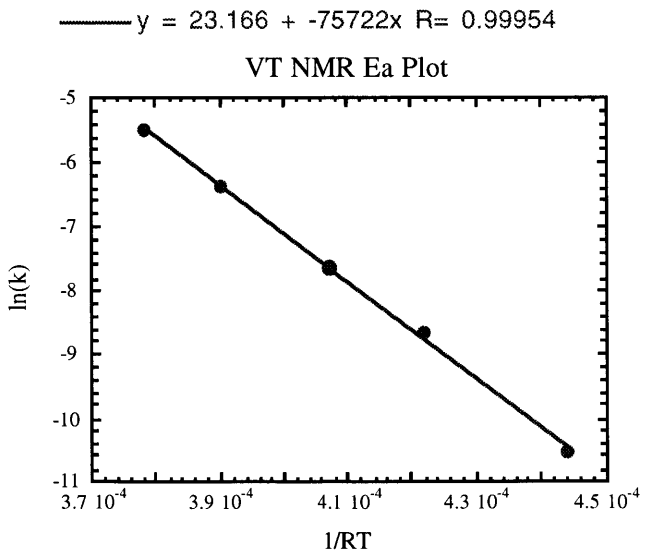

References

1 Boese, R.; Finke, N.; Keil, T.; Paetzold, P.; Schmid, G. *Z. Naturforsch., B* **1985**, *10*, 1327-32.
2 Boese, R.; Finke, N.; Henkelmann, J.; Maier, G.; Paetzold, P.; Reisenauer, H. P.; Schmid, G. *Chem. Ber.* **1985**, *118*, 1644-54.
3 Hoic, D. A.; Wolf, J. R.; Davis, W. M.; Fu, G. C. *Organometallics* **1996**, *15*, 1315-18.
4 Herberich, G. E.; Ohst, H. *Adv. Organomet. Chem.* **1986**, *25*, 199-236.
5 Ashe, A. J., III; Shu, P. *J. Am. Chem. Soc* **1971**, *93*, 1804-5.
6 Herberich, G. E.; Becker, H. J.; Carsten, K.; Engelke, C.; Koch, W. *Chem. Ber.* **1976**, *109*, 2382-8.
7 Herberich, G. E.; Greiss, G.; Heil, H. F.; Mueller, J. *J. Chem. Soc., Chem. Commun.* **1971**, *21*, 1328-9.
8 Herberich, G. E.; Schmidt, B.; Englert, U. *Organometallics* **1995**, *14*, 471-80.
9 Bazan, G. C.; Rodriguez, G.; Ashe, A. J., III; Al-Ahmad, S.; Muller, C. *J. Am. Chem. Soc.* **1996**, *118*, 2291-2.
10 Qiao, S.; Hoic, D. A.; Fu, G. C. *J. Am. Chem. Soc.* **1996**, *118*, 6329-6330.
11 March, J. *Advanced Organic Chemistry*; Wiley: New York, 1992.
12 Maier, G. *Pure Appl. Chem.* **1986**, *58*, 95-104.
13 Maier, G.; Reisenauer, H. P.; Henkelmann, J.; Kliche, C. *Angew. Chem., Int. Ed. Engl.* **1988**, *27*, 295-296.
14 Maier, G.; Wolf, H. J.; Boese, R. *Chem. Ber.* **1990**, *123*, 505-11.
15 Schulman, J. M.; Disch, R. L. *Organometallics* **1989**, *8*, 733-7.
16 Raabe, G.; Schleker, W.; Heyne, E.; Fleischhauer, J. *Z. Naturforsch., A* **1987**, *42*, 352-60.
17 Cioslowski, J.; Hay, P. J. *J. Am. Chem. Soc.* **1990**, *112*, 1707-10.
18 Fraenkel, G.; Pramanik, P. *J. Chem. Soc., Chem. Commun.* **1983**, 1527-1529.
19 Fraenkel, G. *Polym. Prepr., Am. Chem. Soc. Div. Polym. Chem.* **1986**, *27*, 132-133.
20 Bauer, W.; Seebach, D. *Helv. Chim. Acta.* **1984**, *67*, 1972-1988.
21 Geissler, M.; Kopf, J.; Schubert, B.; Weiss, E.; Neugebauer, W.; Schleyer, P. v. R. *Angew. Chem., Int. Ed. Engl.* **1987**, *26*, 587-588.
22 Semmelhack, M. F. In *Comprehensive Organometallic Chemistry II*; Abel, E. W., Stone, F. G. A. and Wilkinson, G., Eds.; Pergamon: New York, 1995.
23 Norris, R. K. In *Comprehensive Organic Chemistry*; Trost, B. M., Ed.; Pergamon: New York, 1991; Vol. 4, Chapter 2.2.
24 Hoic, D. A. Ph.D. Thesis, MIT, 1998.

Chapter 3
Fundamental Reactivity Studies of Borabenzene and Boratabenzene Complexes

Background

Our interest in developing a borabenzene-based chiral Lewis acid catalyst has since prompted us to pursue a deep understanding of this class of heterocycles. Many significant results have come out of the hard work of several people from our group.[1-3] Jennifer Tweddell was the first one to discover an asymmetric synthesis of a chiral borabenzene complex **3.1** and a chiral boratabenzene complex **3.2** (Figure 3.1)[4]. Unfortunately, the hydride **3.2** failed to generate any enantiomeric excesses in the reduction of aldehydes. Her valiant albeit unsuccessful efforts in making phosphidoboratabenzenes as chiral ligands (Figure 3.2)[3] have nonetheless contributed significantly to understanding the synthesis and reactivity of boratabenzenes in general. She determined the inversion barriers for a series of phosphidoboratabenzenes and found them to be low enough to result in racemization at room temperature. The great ease with which the phosphidoboratabenzenes racemizes makes them less than attractive as chiral ligands.

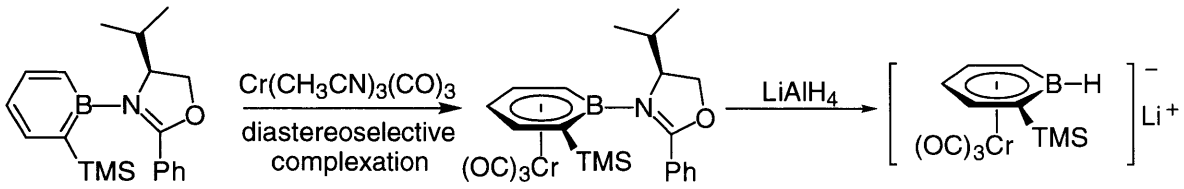

Figure 3.1. The first enantiopure synthesis of a chiral borabenzene and a chiral boratabenzene complex.

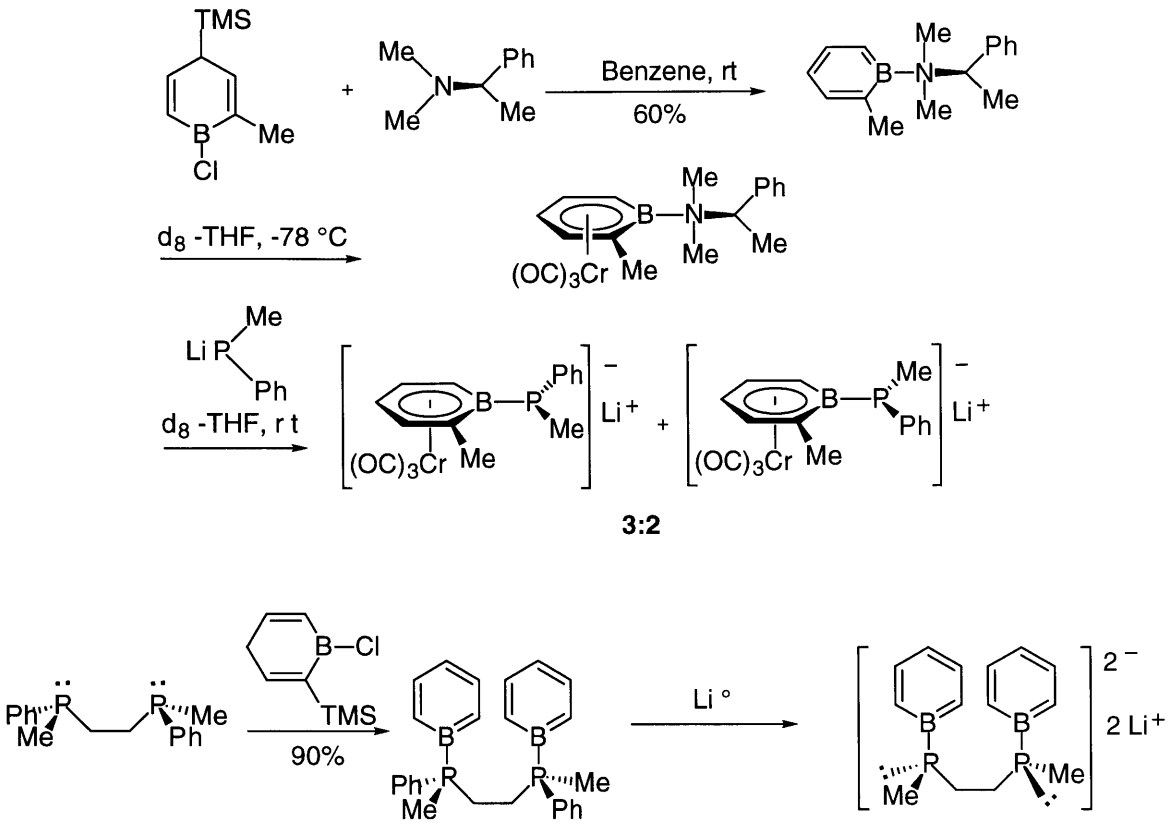

Figure 3.2. Synthesis of phosphidoboratabenzenes as potential chiral ligands.

Despite much progress in the field of borabenzenes, relatively little has been known about their chemistry in comparison with their carbon and nitrogen analogues, benzene and pyridine, respectively. Following the mechanistic study of nucleophilic aromatic substitution reaction (Chapter 2), we have since further explored the fundamental reactivity of borabenzene and boratabenzene complexes.

Results and Discussion

Synthesis and Structure of Borabenzene-(4-Phenylpyridine), a Heterocyclic Analogue of *p*-Terphenyl

Borabenzenes are frequently compared to their carbon and nitrogen analogues. 1*H*-boratabenzene, which is the third member of the isoelectronic series, pyridinium ion, benzene and 1*H*-boratabenzene (Figure 3.3), has been synthesized through a nucleophilic aromatic substitution reaction (see Figure 2.3 in Chapter 2).[5]

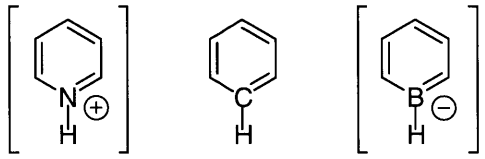

Figure 3.3. The isoelectronic series.

As part of our program in extending the chemistry discovered earlier in our group,[5-9] we then turned our attention to the synthesis of borabenzene-4-phenylpyridine **3.3**, an aesthetically pleasing, paralinked triaromatic compound which incorporates one unit of each of the first-row (hetero)cycles in Figure 3.3. As a zwitterionic analogue of *p*-terphenyl,[10] it may possess material properties which are similar to those of *p*-terphenyl which has interesting material properties.[11] The synthesis is illustrated in Figure 3.4.

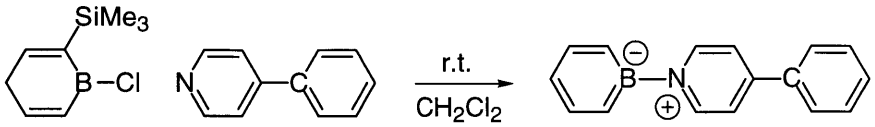

3.4 **3.3**

Figure 3.4. Synthesis of borabenzene-4-phenylpyridine.

Treatment of boracycle **3.4**[7] with 4-phenylpyridine in CH_2Cl_2 at room temperature affords borabenzene-4-phenylpyridine **3.3** in 76% yield. While it is fairly stable as an orange solid, it is extremely air-sensitive in solution. The UV/vis spectrum of **3.3** reveals absorptions at 280 nm ($\varepsilon = 2.0 \times 10^4$ $M^{-1}cm^{-1}$) and 484 nm ($\varepsilon = 6.7 \times 10^3$ $M^{-1}cm^{-1}$), compared with 170-175 nm and 190 nm for *p*-terphenyl.[12]

A crystal suitable for X-ray diffraction was grown by diffusion of hexane into a CH_2Cl_2 solution of **3.3** at room temperature. The structure was solved by Dr. Diego A. Hoic. The borabenzene ring and the phenyl ring are nearly coplanar (dihedral angle of 6°), with the central pyridine ring twisted by about 45° relative to each of the other rings (Figure 3.5). In the case of *p*-terphenyl, crystallographic studies reveal a similar coplanar relationship between the remote rings, with the central ring twisted by about 15°.[13-15] The 49° dihedral angle between the borabenzene and pyridine rings of **3.3** compares with a 43° angle for borabenzene-pyridine, a hetero-biphenyl analogue.[16] For compound **3.3**, the B-N and C8-C11 bond lengths are 1.551(3) Å and 1.480(3) Å, respectively, compared with a C-C (inter-ring) bond length of 1.50 Å for *p*-terphenyl[13-15] and a B-N bond distance of 1.56 Å for borabenzene-pyridine.[16]

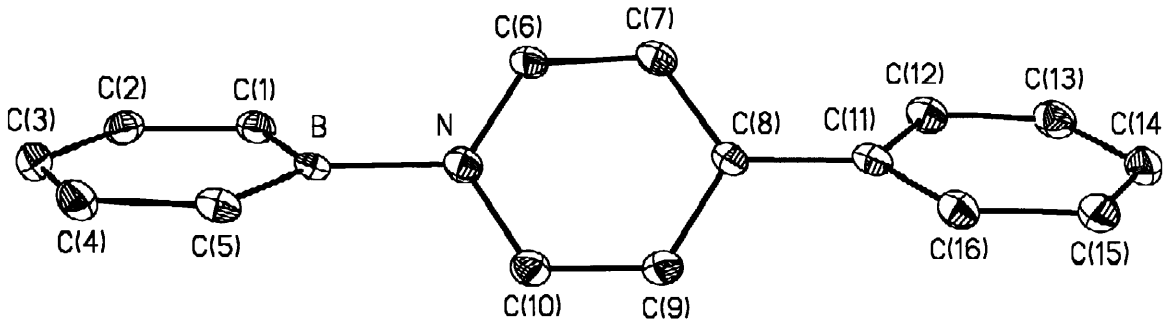

Figure 3.5. The ORTEP illustration of **3.3**.

Due to the sensitivity of **3.3**, we have not pursued the application of this compound as an analogue of *p*-terphenyl. However, the potential material properties of this compound remain open avenues for investigation.

Further study of nucleophilic aromatic substitution reactions in borabenzenes and boratabenzenes

Nucleophilic aromatic substitution of borabenzene complexes, which was demonstrated first in the case of the parent borabenzene-PMe_3,[6] continued to fascinate us. We found out that ortho-substituted borabenzene-PMe_3 can also undergo this reaction to generate the corresponding boratabenzene complexes in good yields (Figure 3.6). The addition of an ortho-trimethysilyl group to the borabenzene ring does not seem to affect the rate of the reaction very much.

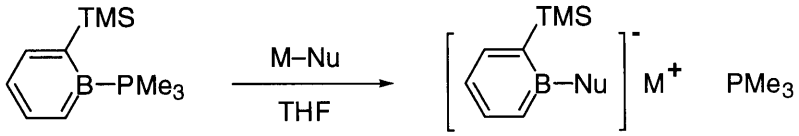

Nucleophile	Product	Yield (%)
Li–NMe_2	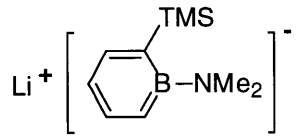	79
Na–OEt	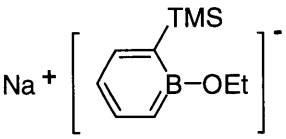	100
K–PPh_2	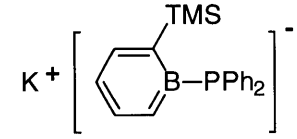	74

Figure 3.6. Synthesis of ortho-substituted boratabenzene complexes through nucleophilic aromatic substitutions.

As our mechanistic study from Chapter 2 strongly suggests an associative pathway, we were then interested in the possibility of applying nucleophilic

aromatic substitution to boratabenzene complexes. We demonstrated that a stronger anionic nucleophile can displace a relatively weak nucleophile leading to a new boratabenzene complex (Figure 3.7). The conversion of all the reactions is 100%. The NMR yield is calculated based on the internal standard hexamethylbenzene.

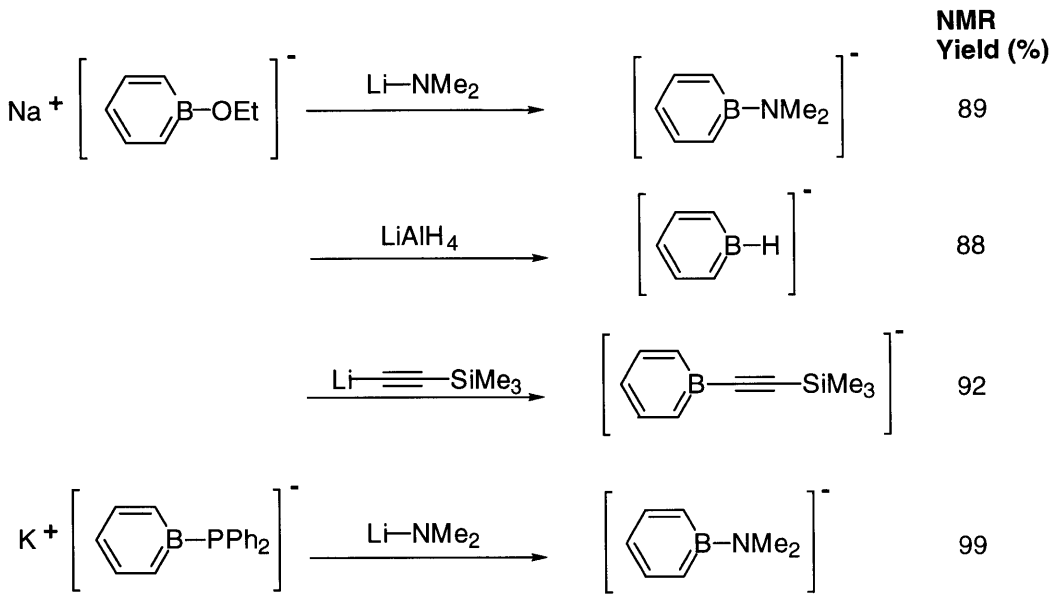

Figure 3.7. Nucleophilic aromatic substitutions of boratabenzene complexes. NMR yield is based on an internal standard of hexamethylbenzene.

We also briefly investigated the possibility of electrophilic aromatic substitution of borabenzene complexes. However, even the mildest reagents resulted in decomposition of the aromatic system. Other efforts to functionalize the borabenzene ring also resulted in failure.

In summary, we have demonstrated the utility of nucleophilic aromatic substitution reactions in borabenzene chemistry. The knowledge gained through the synthetic and mechanistic studies mentioned above will no doubt put us a few steps closer to achieving the goal of exploiting borabenzene derivatives in organic synthesis.

Experimental

Experimental

General

4-phenylpyridine, $LiAlH_4$ and $KPPh_2$ and NaOEt were purchased from Aldrich. $LiNMe_2$ was purchased from Strem. Lithium trimethylsilylacetylide[6] and ortho-trimethylsilyl borabenzene-PMe_3[1] were prepared by reported methods.

^1H and ^{13}C nuclear magnetic resonance spectra were recorded on a Varian XL-300 NMR spectrometer at ambient temperature. ^1H data are reported as follows: chemical shift in parts per million downfield from tetramethylsilane (δ scale), multiplicity (br = broad, s = singlet, d = doublet, t = triplet, q = quartet, and m = multiplet), integration, coupling constant (Hz), and assignment. ^{13}C chemical shifts are reported in ppm downfield from tetramethylsilane (δ scale). All ^{13}C spectra were determined with complete proton decoupling. Infrared spectra were obtained on a Perkin-Elmer Series 1600 FT-IR spectrophotometer. High resolution mass spectra were recorded on a Finnegan MAT System 8200 spectrometer. ^{11}B NMR spectra were obtained in d_8-THF on Varian Unity 300 MHz spectrometer (96 MHz) and are referenced to external BF_3-OEt_2 (δ 0).

All reactions were carried out under an atmosphere of nitrogen in oven-dried glassware with magnetic stirring.

Synthesis of Borabenzene - 4-phenylpyridine.

4-Phenylpyridine (0.67 g, 3.6 mmol) was dissolved in 6 ml of CH_2Cl_2. This solution was slowly added to boracycle (0.51 g, 3.3 mmol) in 2 ml CH_2Cl_2. Precipitation of a red solid was observed. The reaction mixture was stirred at room temperature for 12 hours. Evaporation of the solvent resulted in a red solid which

was then washed with CH_2Cl_2, affording the orange red product borabenzene - 4-phenylpyridine (0.58 g, 76%).

^1H NMR (300 MHz, CD_2Cl_2): δ 9.03 (d, 2H, J = 6.6), 7.93 (d, 3H, J = 6.9), 7.80 (m, 2H), 7.59 (m, 3H), 7.41 (t, 2H, J = 8.4), 6.68 (d, 2H, J = 9.9), 6.53 (t, 1H, J = 7.2); ^{13}C NMR (75 MHz, CD_2Cl_2): δ 152.1, 144.8, 135.8, 135.6, 131.7, 130.3, 127.9, 124.3, 119.6, 116.8; ^{11}B NMR (CD_2Cl_2, 96 MHz): 32.8; IR (KBr): 2990, 1624, 1530, 1479, 1411, 1292, 1137, 846, 773, 723, 698; HRMS: Calcd for $C_{16}H_{14}NB$: 231.1219; found: 231.1218.

UV/vis Study of Borabenzene - 4-phenylpyridine.

10 mg of borabenzene - 4-phenylpyridine was dissolved in 1000 ml of CH_2Cl_2 resulting in a red solution (0.043 mM). CH_2Cl_2 in the same cuvette was taken as the standard. The UV/vis spectrum shows one absorption in the UV region at 280 nm with an extinction coefficient of 2.0×10^4 M^{-1} cm^{-1} and one absorption in the visible region at 484 nm with an extinction coefficient of 6.7×10^3 M^{-1} cm^{-1}.

Cyclic Voltammetry Study of Borabenzene - 4-phenylpyridine.

Cyclic voltammetry was performed on the CH_2Cl_2 solution of borabenzene - 4-phenylpyridine in the dry box. The compound was irreversibly oxidized.

X-ray crystal structure of Borabenzene - 4-phenylpyridine.

See Appendix I for detailed X-ray data.

Synthesis of $Li(C_{10}H_{19}BNSi)$

A solution of *o*-trimethylsilylborabenzene-PMe_3 (235 mg, 1.05 mmol) in 10 ml of THF was added to $LiNMe_2$ (53.5 mg) in 2 ml of THF. After stirring for 30 minutes at room temperature, the mixture was filtered and then dried to a brown oil. It was

then treated with pentane and dried to provide a creamy white solid (164 mg, 79% yield).

^{1}H NMR (300 MHz): d 7.22 (d, *J* = 6.3, 1H), 6.99 (dd, *J* = 11.1 6.6, 1H), 5.65 (d, *J* = 11.1, 1H), 5.55 (t, *J* = 6.3, 1H), 2.75 (s, 6H), 0.18 (s, 9H); ^{13}C NMR: d 141.5, 135.6, 102.9, 43.1, 3.5; ^{11}B NMR: d 34.7 ; IR: 3008, 2954, 2893, 2790, 1613, 1519, 1381, 1252, 1128, 976, 844, 754; HRMS (EI, *m/e*) calcd for $C_{10}H_{20}BNSi$ (M+H-Li$^+$) 193.1458; found 193.1459.

Synthesis of Na($C_{10}H_{18}BOSi$)

A solution of *o*-trimethylsilylborabenzene-PMe_3 (148 mg, 0.66 mmol) in 8 ml of THF was added to NaOEt (45 mg, 0.66mmol). The reaction mixture was stirred at room temperature for four days. It was then filtered, dried, treated with hexane and dried again. A creamy white solid resulted (150 mg) resulted. The ^{1}H NMR spectrum of the product in THF - d_8 showed the presence of THF. Treating the solid with pentane followed by drying it *in vacuo* did not get rid of the residual THF. Integration of the corresponding peaks in ^{1}H NMR spectrum of the product in CD_2Cl_2 gave an adjusted yield of 100%.

^{1}H NMR (300 MHz): d 7.31 (d, *J* = 6.6, 1H), 7.23 (dd, *J* = 10.5, 6.6, 1H), 5.72 (t, *J* = 6.9, 1H), 5.67 (d, *J* = 10.8, 1H), 3.76 (q, *J* = 6.9, 2H), 1.20 (t, *J* = 6.9, 3H), 0.11 (s, 9H); ^{13}C NMR: d 140.4, 138.2, 119.2 (br), 107.4 (br), 104.6, 60.0, 18.7, 1.4; ^{11}B NMR: d 37.5; IR: 2961, 2892, 1609, 1521, 1427, 1372, 1240, 838, 748; HRMS (EI, *m/e*) calcd for $C_{10}H_{19}BOSi$ (M+H-Na$^+$) 194.1298; found 194.1299.

Synthesis of K($C_{20}H_{23}BPSi$)

A solution of potassium diphenylphosphide (0.5 M in THF; 2.2 ml, 1.1 mmol) was added to a solution of *o*-trimethylsilylborabenzene-PMe_3 in 6 ml of THF. The reaction mixture was stirred at room temperature for 18 hours before dried to a

yellow solid. Recrystalization in THF/hexane resulted in a white solid (299 mg, 74% yield).

^{1}H NMR (300 MHz): d 7.46 (t, J = 5.7, 1H), 7.34 (t, J = 6.6, 4H), 7.16 (dd, J = 9.9, 6.9, 1H), 7.01 (m, 6H), 6.34 (m, 2H), 0.18 (s, 9H); ^{13}C NMR: d 147.3 (d, $J_{C\text{-}P}$ = 17.9), 138.7 (d, $J_{C\text{-}P}$ = 15.5), 135.7 (d, $J_{C\text{-}P}$ = 16.7), 135.1 (d, $J_{C\text{-}P}$ = 4.1), 132.5 (br), 129.1(br), 127.9 (d, $J_{C\text{-}P}$ = 5.3), 125.7, 114.6, 3.0 (d, $J_{C\text{-}P}$ = 7.1); ^{11}B NMR: d 36.7; IR: 3050, 2949, 1648, 1578, 1521, 1475, 1432, 1354, 1241, 1091, 1026, 961, 831, 741, 700; HRMS (EI, *m/e*) calcd for $C_{20}H_{24}BPSi$ (M+H-K$^+$) 334.1478; found 334.1477.

References

1 Amendola, M. C. M.S. Thesis, MIT, 1995 and references therein.
2 Hoic, D. A. Ph.D. Thesis, MIT, 1998 and references therein.
3 Tweddell, J. M.S. Thesis, MIT, 1997 and references therein.
4 Tweddell, J.; Hoic, D. A.; Fu, G. C. *J. Org. Chem.* **1997**, *62*, 8286-8287.
5 Hoic, D. A.; Davis, W. M.; Fu, G. C. *J. Am. Chem. Soc.* **1995**, *117*, 8480-1.
6 Qiao, S.; Hoic, D. A.; Fu, G. C. *J. Am. Chem. Soc.* **1996**, *118*, 6329-6330.
7 Hoic, D. A.; Wolf, J. R.; Davis, W. M.; Fu, G. C. *Organometallics* **1996**, *15*, 1315-18.
8 Hoic, D. A.; Davis, W. M.; Fu, G. C. *J. Am. Chem. Soc.* **1996**, *118*, 8176-8177.
9 Amendola, M.; Stockman, K. E.; Hoic, D. A.; Davis, W. M.; Fu, G. C. *Angew. Chem., Int. Ed. Engl.* **1997**, *36*, 267-269.
10 Thompson, Q. E. In *Kirk-Othmer Encyclopedia of Chemical Technology*; 4th ed.; Wiley: New York, 1992; Vol. 4, pp 223-237.
11 Abe, J.; Shirai, Y. *J. Am. Chem. Soc.* **1996**, *118*, 4705-4706.
12 Milazzo, G.; Gasperis, P. *J. Chim. Phys. Phys.-Chim. Biol.* **1968**, *65*, 1171-1176.
13 Baudour, P. J. L.; Delugeard, Y.; Cailleau, H. *Acta. Crystallogr.* **1976**, *B32*, 150-154.
14 Baudour, P. J. L.; Cailleau, H.; Yelon, W. B. *Acta. Crystallogr.* **1977**, *B33*, 1773-1780.
15 Baudour, P. J. L.; Toupet, L.; Delugeard, Y.; Ghemid, S. *Acta. Crystallogr.* **1986**, *C42*, 1211-1217.
16 Boese, R.; Finke, N.; Henkelmann, J.; Maier, G.; Paetzold, P.; Reisenauer, H. P.; Schmid, G. *Chem. Ber.* **1985**, *118*, 1644-54.

Part II
Chiral Phosphaferrocenes and Their Applications in Asymmetric Catalysis

Chapter 1
Introduction

The past two decades have seen a phenomenal growth in the area of chiral ligands in asymmetric synthesis.[1] Discoveries and applications of a variety of nitrogen-based as well as phosphorus-based ligands have led to remarkably selective transition-metal catalyzed organic transformations which are useful in constructing complex molecules.

Many nitrogen-based chiral ligands have been demonstrated to effect asymmetry in various organic reactions. There are plenty of examples of both sp^2 and sp^3 hybridized nitrogen-based ligands. In the case of sp^2 nitrogen-based ligands, for example, bisoxazolines and Pybox ligands (Figure 1.1)[2] have shown great selectivity in cyclopropanations. In the case of sp^3 nitrogen-based ligands, DHQD and DHQ based molecules have been found to be superior ligands in dihydroxylations of olefins.[3]

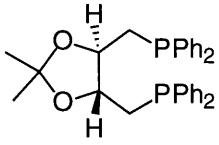

DIOP

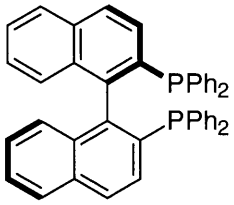

BINAP

All existing chiral phosphine ligands are based on sp^3 phosphorus.

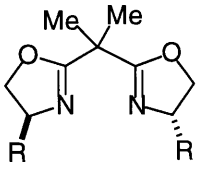

Bisoxazoline

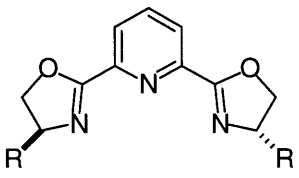

Pybox

Figure 1.1. Some well-known phosphorus-based and nitrogen-based ligands.

In the field of phosphine ligands, much progress has been made in sp^3 phosphorus-based ligands while little is known about the potential of sp^2 phosphorus-based compounds as ligands. Chiral chelating phosphines including

BINAP and DIOP (Figure 1.1) have shown remarkable selectivities in reactions such as hydrogenations,[4] allylic substitutions,[5] and allylamine isomerizations.[6] However, there had been no report of an sp^2 phosphorus-based chiral ligand, presumably because of the high reactivity of phospha-alkenes in general. Moreover, in our laboratory, planar chiral nitrogen heterocycles, namely azaferrocene derivatives, have been utilized as efficient ligands in cyclopropanations of terminal olefins[7] and diethylzinc additions to aldehydes (Figure 1.2).[8] Phosphaferrocenes as chiral ligands, on the other hand, had remained an unexplored territory.

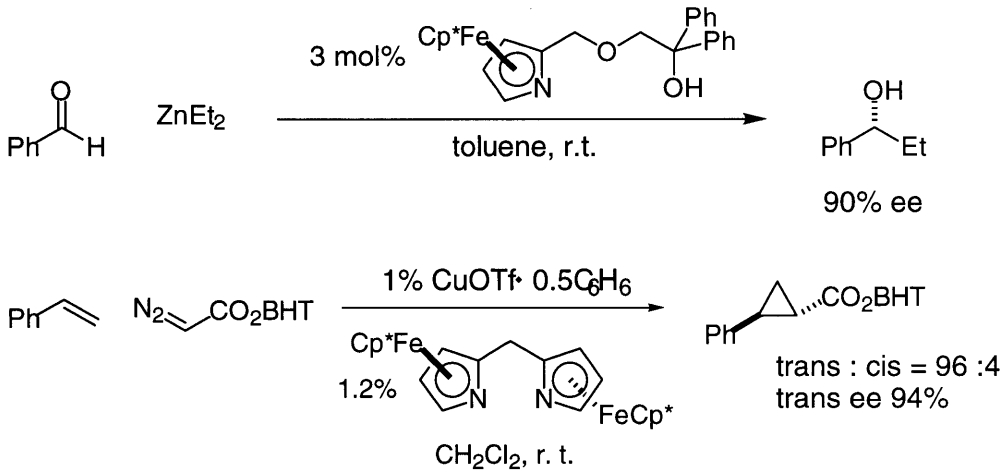

Figure 1.2. Applications of azaferrocenes in asymmetric catalysis.

Development of a chiral ligand bearing sp^2 hybridized phosphorus henceforth became the focus of our research interest. Despite the high reactivities of phospha-alkenes, the aromatic stabilization energy (ASE) of the phospholyl anion has been estimated to be approximately 90-100% of that of the cyclopentadienyl anion.[9,10] We therefore decided upon phosphaferrocene derivatives as our target molecules in search of an sp^2 hybridized phosphorus-based ligand. Our intention was to create a repertoire of phosphaferrocenes including both monodentate and bidentate ligands. In the case of bidentate phosphaferrocenes, we were interested in

exploring the potential of both C_2-symmetric molecules as well as those that bear no symmetry element at all.

Thus, in Chapter 2, the efforts to design, synthesize and resolve a series of phosphaferrocene derivatives are described. We first investigated the possibility of resolving some of the racemic phosphaferrocenes previously reported in literature. It was during this phase that we discovered the difficulty in handling this class of compounds. Many of them are extremely air-sensitive or too non-polar to be resolved by chiral HPLC. Functionalization of the phospholyl ring also proved to be quite problematic as the molecules usually cannot withstand harsh reaction conditions such as strong acid or base.[11] Nonetheless, we successfully synthesized and resolved a series of fairly stable phosphaferrocenes after experimenting with various reaction conditions.

The first reaction to which we attempted to apply one of our bidentate phosphaferrocenes was the asymmetric hydrogenation of dehydroamino acids. This undertaking is described in Chapter 3 (Section 3.2). As the current state of the art in hydrogenations of this class of substrates is near perfection, our endeavor was rather to demonstrate the potential of phosphaferrocenes as chiral ligands. The success we had in this reaction was the first application of a planar-chiral phosphorus heterocycle in asymmetric catalysis. To further explore the versatility of this phosphaferrocene, asymmetric hydrogenations of aryl enamides were then investigated. In Section 3.3 of Chapter 3, a detailed discussion of this reaction is presented. The key finding in the process is the use of an additive which enhances the enantioselectivities to over 90% which essentially match or surpass the best reported in literature (Figure 1.3). Further applications of phosphaferrocenes in asymmetric catalysis such as isomerization of allylic alcohols are discussed in Section 3.4.

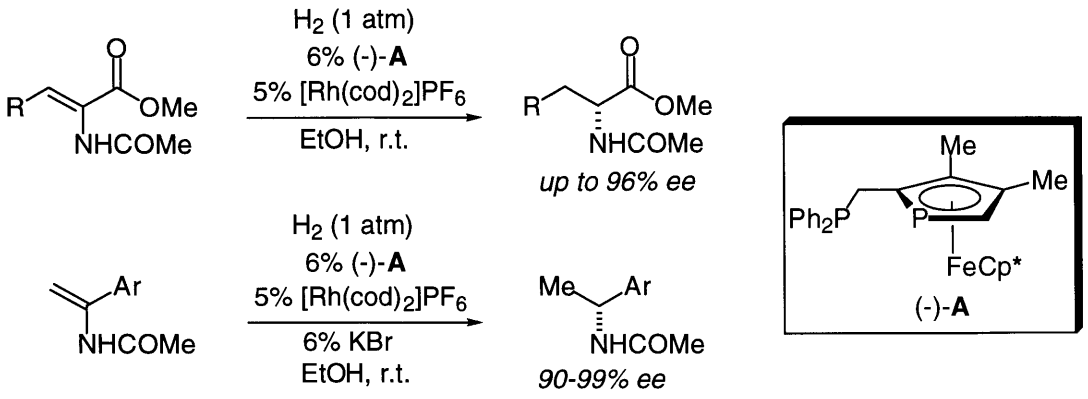

Figure 1.3. The first applications of phosphaferrocenes in asymmetric catalysis.

The goal of this work was to address the possibility of developing planar-chiral phosphorus heterocycles as ligands and to investigate the utility of this class of compounds in asymmetric synthesis. The success of this work raises the possibility that phosphaferrocenes of unprecedented reactivity and selectivity be discovered in the future.

References

1 Ojima, I. *Catalytic Asymmetric Synthesis*; Wiley-VCH: New York, 1993 and references therein.
2 Doyle, M. P. In *Catalytic Asymmetric Synthesis*; Ojima, I., Ed.; Wiley-VCH: New York, 1993; Chapter 3 and references therein.
3 Johnson, R. A.; Sharpless, K. B. In *Catalytic Asymmetric Synthesis*; Ojima,I., Ed.; Wiley-VCH: New York, 1993; Chapter 4.4 and references therein.
4 Takaya, H.; Ohta, T.; Noyori, R. In *Catalytic Asymmetric Synthesis*; Ojima,I., Ed.; Wiley-VCH: New York, 1993; Chapter 1 and references therein.
5 Hayashi, T. In *Catalytic Asymmetric Synthesis*; Ojima,I., Ed.; Wiley-VCH: New York, 1993; Chapter 7.1 and references therein.
6 Akutagawa, S.; Tani, K. In *Catalytic Asymmetric Synthesis*; Ojima,I., Ed.; Wiley-VCH: New York, 1993; Chapter 2 and references therein.
7 Lo, M. M.-C.; Fu, G. C. *J. Am. Chem. Soc.* **1998**, *120*, 10270-10271.
8 Dosa, P. I.; Fu, G. C. *J. Org. Chem.* **1997**, *62*, 444-445.
9 Guimon, C.; Gonbeau, D.; Pfister-Guillouzo, G.; De Lauzon, G.; Mathey, F. *Chem. Phys. Lett.* **1984**, *104*, 560-7.
10 Kostic, N. M.; Fenske, R. F. *Organometallics* **1983**, *2*, 1008-13.
11 Garrett, G. C. Personal Communication.

Chapter 2
Design, Synthesis and Resolution of Chiral Phosphaferrocenes

Background

Chiral phosphines have continued to fascinate organic chemists. Starting from the early 1970s, there have been numerous discoveries of new phosphine ligands in asymmetric catalysis.[1] However, it is important to note that there had been no report of an sp^2 hybridized phosphine as a chiral ligand despite the abundance of sp^3 hybridized phosphine ligands.

Our efforts as well as literature precedents[2] in the research area of phosphabenzenes led us to believe that phosphabenzenes were too sensitive and hard to handle to be of practical value in catalysis. Phosphaferrocenes then attracted our attention as they in general were reputed to be less sensitive and hence easier to handle. Much of the research effort in this area had been focused on fundamental reactivity and coordination chemistry studies.[3-13] Mathey and others have synthesized a series of structurally interesting and aesthetically pleasing phosphaferrocenes in racemic form only (See Figure 2.1 for examples). The synthesis is either conducted under rather harsh reaction conditions (the synthesis of **2.1** for example)[14] or tedious and hard to generalize in making a series of derivatives (the syntheses of **2.2** and **2.3** for examples).[9,12] In other words, no attention had been dedicated to find the synthetic utilities of this class of compounds prior to our efforts.

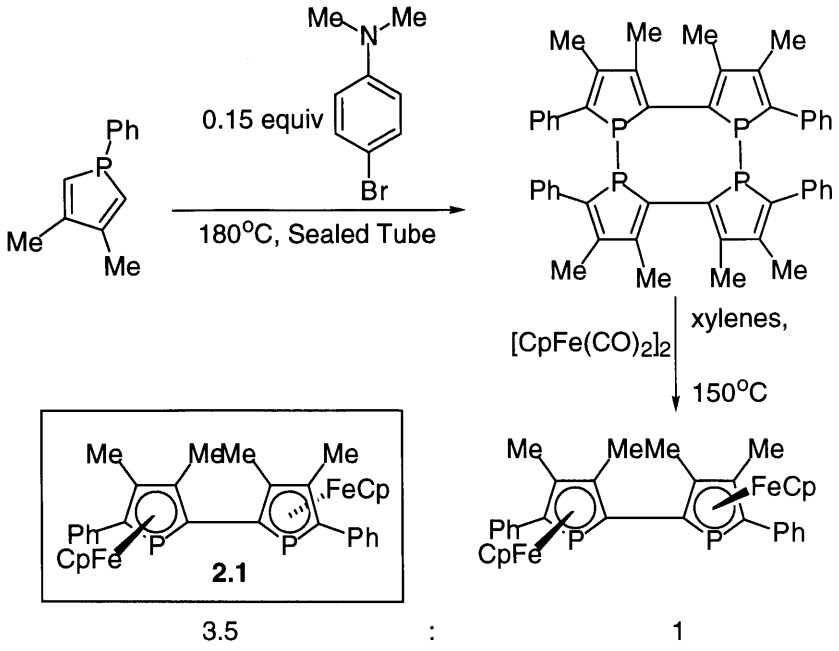

Synthesis of 2.1.

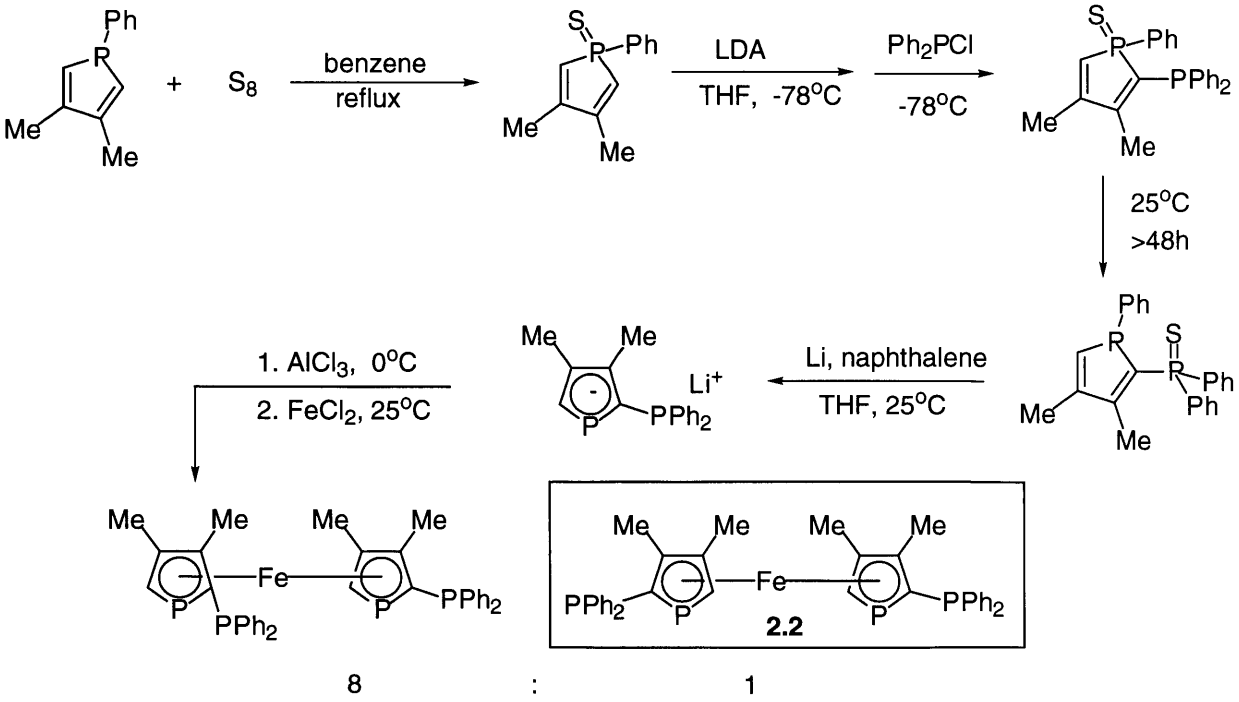

Synthesis of 2.2.

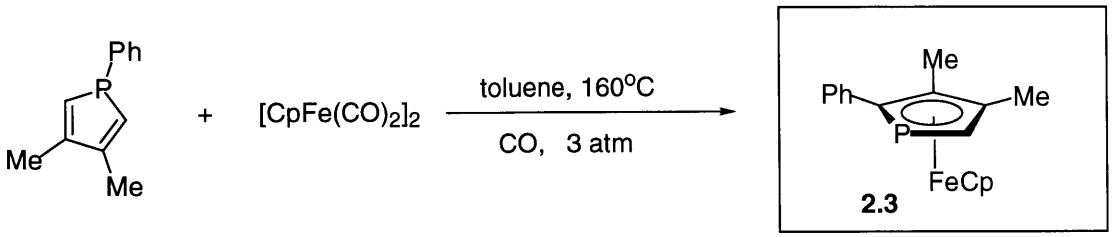

Synthesis of 2.3.

Figure 2.1. Racemic synthesis of some phosphaferrocenes.

Concurrently with our group's effort, Christian Ganter and his group have independently carried out research endeavors in designing and synthesizing phosphaferrocenes as potential ligands for transition metals.[15-18] Most notably, they reported the first straightforward access to enantiomerically pure phosphaferrocenes (Figure 2.2).[16] However, to the best of our knowledge, there had been no reports of synthetic applications of phosphaferrocenes prior to my work in this area which will be discussed in Chapter 3. It is worth mentioning that Christian Ganter and his group reported phosphaferrocene derivatives in allylic alkylation with up to 19% ee[18b] during the preparation of this thesis.

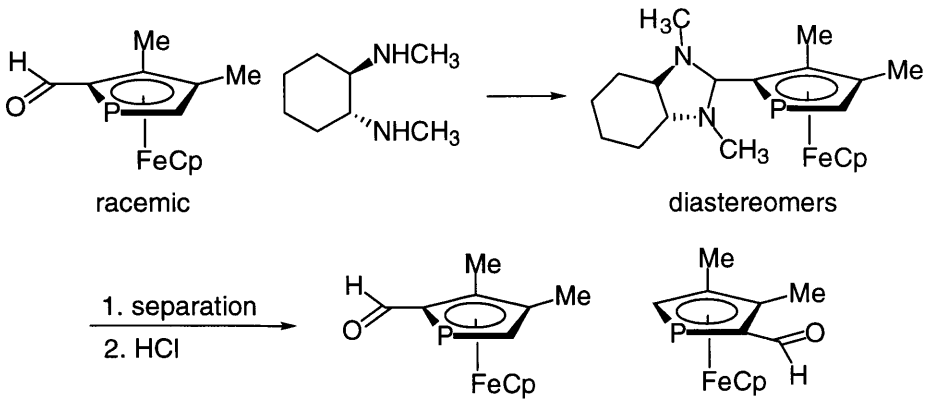

Figure 2.2. Enantiomerically pure phosphaferrocenes prepared by resolution of racemate via column chromatography on silica gel of diastereomeric aminals.

Moreover, it is worth noting that achiral phosphaferrocenes have been established to function as nucleophilic catalysts. For example, Dr. Christine E. Garrett in our laboratory demonstrated the utility of achiral phosphaferrocenes in ring-opening of epoxides in the presence of TMSCl (Figure 2.3).[19] Our goal to find asymmetric applications for this class of molecules naturally depended on the design, synthesis and resolution of phosphaferrrocene derivatives.

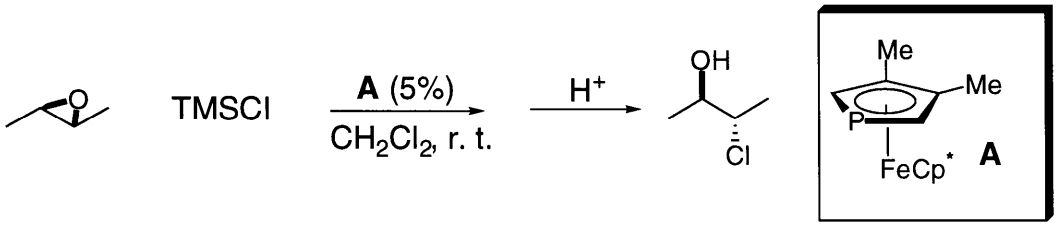

Figure 2.3. Achiral phosphaferrocenes as catalysts in ring opening of epoxides with TMSCl.

Results and Discussion

We began our efforts to obtain enantiomerically pure ligands by trying to resolve some previously reported racemic phosphaferrocenes on chiral HPLC. Illustrated in Figure 2.4 are some of the racemic phosphaferrocenes we intended to explore as ligands after resolution. The syntheses of these phosphaferrocenes are shown in Figure 2.1.

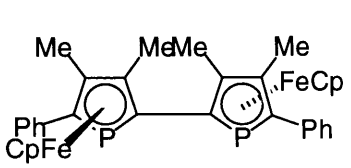

2.1

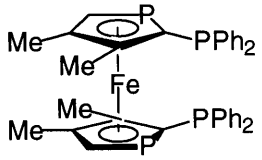

2.2

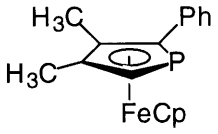

2.3

Figure 2.4. Target phosphaferrocenes which have been previously synthesized in racemic form.

The C_2-symmetric compound **2.1** which could potentially serve as a chelating phosphine was highly air-sensitive and decomposed readily upon exposure to air. Efforts to make the Cp^* analog resulted in failure. The C_2-symmetric bis-diphenylphosphino diphosphaferrocene **2.2** was an interesting target due to the presence of one pair of sp^2 and one pair of sp^3 hybridized phosphorus. However, we failed to resolve the racemate. The synthesis itself so far does not allow resolution by reversible chemical modification to be accomplished. Lastly, the putative monodentate phosphine **2.3** also proved to be too unstable to be useful for our purpose. Any efforts to make the Cp^* analog of **2.3** failed.

As we encountered little luck in the existing pool of racemic phosphaferrocenes, we ventured out into the design, synthesis and resolution of phosphaferrocenes of novel structural and electronic properties. In light of Cowley's report that 1,1'-diphosphaferrocenes can serve as chelating ligands for transition metals,[20] we prepared an enantiopure C_2-symmetric diphosphaferrocene **2.4**. As the phospholide anion **2.5** is readily available by a two-step procedure developed by Mathey,[21] the synthesis of the complex **2.4** is fairly straightforward (Figure 2.5). Treatment of the anion **2.5** with $FeCl_2$ provides the desired racemic diphosphaferrocene **2.4** and the meso isomer in 73% overall yield. The diastereomers can be separated by HPLC on silica gel. The enantiomers can then be separated by chiral HPLC.

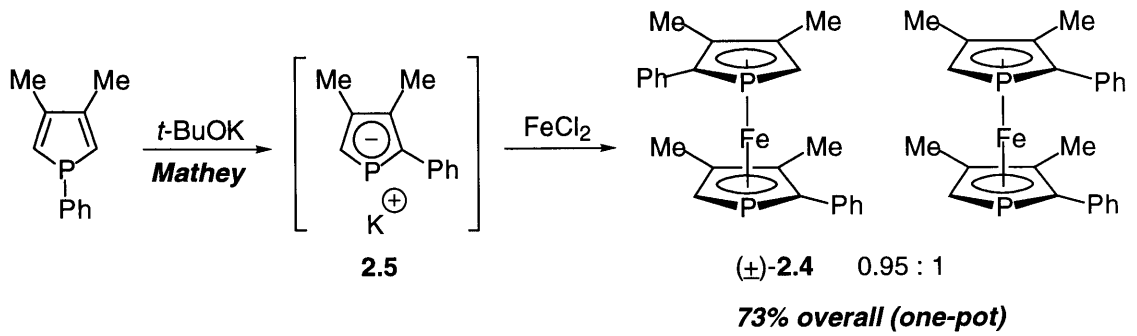

Figure 2.5. Synthesis and resolution of diphosphaferrocene **2.4.**

Crystals of (-)-**2.4** grown from CH_2Cl_2/pentane were suitable for an X-ray diffraction study (Figure 2.6). The crystal structure was solved by Dr. Diego A. Hoic. The absolute configuration of this enantiomer was also thus established. The structure resembles that of 3,3',4,4'-tetramethyl-1,1'-diphosphaferrocene.[5] The two phospholyl rings are nearly parallel to each other with a 6° deviation from coplanarity. They adopt an eclipsed geometry relative to one another. The Fe-centroid distance is 1.67Å.

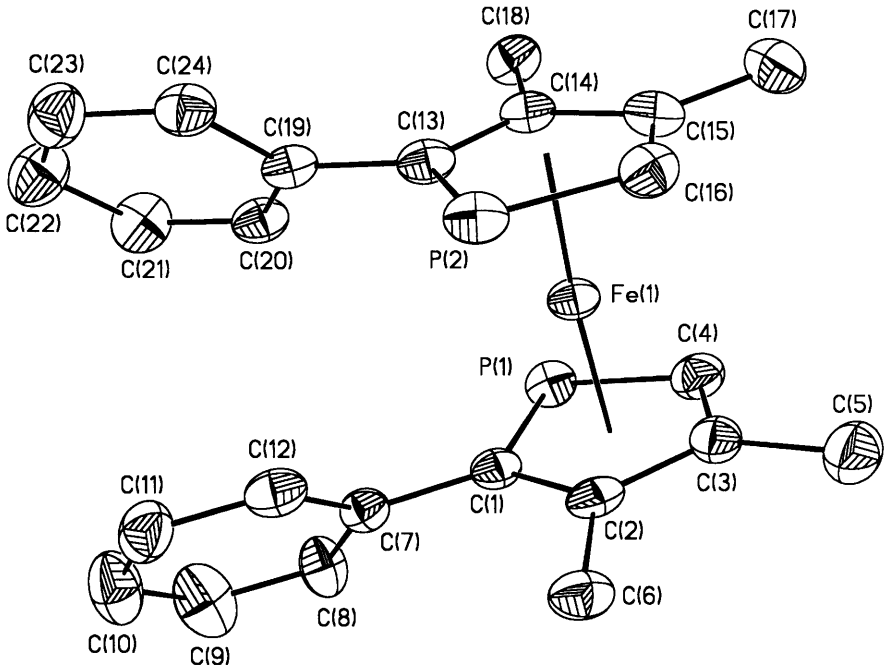

Figure 2.6. ORTEP illustration of the X-ray crystallographic study of (-)-**2.4**, with thermal ellipsoids drawn at the 35% probability level.

Compound **2.4** which incorporates two sp^2 phosphorus could potentially be a bidentate ligand although the near-coplanarity of the two phospholyl rings renders it unlikely to accomodate bidentate binding to commonly used transition metals such as Rh, Ru and Pd. For example, mixing $[Rh(cod)Cl]_2$ and **2.4** results in a mixture of complexes which is indicative of oligomeric binding. However, we could probably use it as a chiral nucleophilic catalyst in reactions utilizing mono-phosphines.

While we were delighted to have obtained the first C_2-symmetric phosphaferrocene in enantiopure form, we were more interested in developing a more general synthetic route that could lead to more than one interesting candidate. With the achiral 3,4-dimethyl-pentamethyl-phosphaferrocene first synthesized by Mathey,[19,22] functionalization of the phospholyl ring by alkylation proved to be problematic.[23] Vilsmeyer-Haack formylation turns out to be a mild method which is compatible with the phosphaferrocene framework.[5] The formylation is fairly facile with an average yield of 70% (Figure 2.7). Reduction of the aldehyde **2.6** with $LiAlH_4$ then affords the phosphaferrocene alcohol **2.7** in 98% yield. Treatment of the alcohol **2.7** with oxalyl chloride and a catalytic amount of DMF then generates the phosphaferrocene chloride which is then in situ displaced by $KPPh_2$ yielding the desired diphenylphosphino phosphaferrocene **2.8**.[24] Christian Ganter and his group independently developed a different synthetic route leading to the Cp analog of **2.8.**[15] Noting that this molecule **2.8** incorporates both an sp^2 and sp^3 hybridized phosphorus, we anticipated that it could be a potential chelating ligand for transition metals. It was then imperative to resolve the racemate.

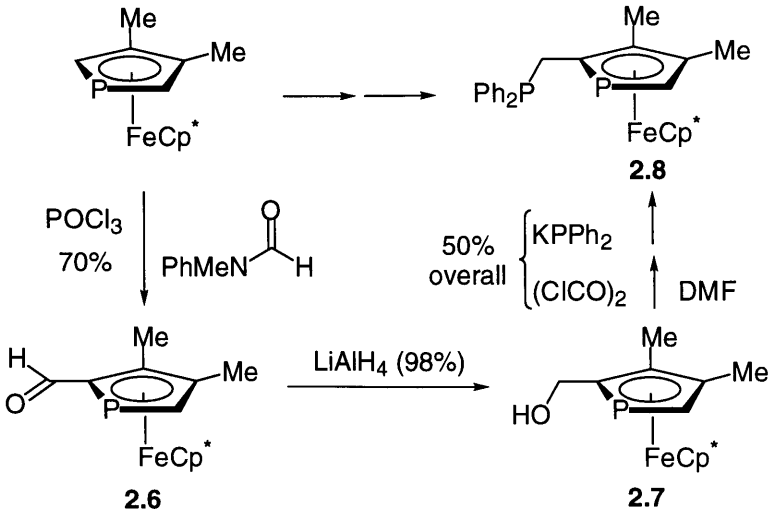

Figure 2.7. Synthesis of a diphenylphosphino phosphaferrocene **2.8**.

Attempts of resolution at the aldehyde stage by formation of diastereomeric chiral aminals or chiral acetals resulted in failure. There could be two rationalizations. One, the aldehyde is an unusually stable compound which does not react with chiral diamines or chiral diols. Two, the chiral aminals or acetals formed are very unstable, so the reverse reaction predominates. It is interesting to point out that the resolution of the Cp analogue of **2.6** by forming diastereomeric aminals has been reported by Christian Ganter and his group (Figure 2.2).[16] In the case of **2.6**, it is possible that the Cp* fragment poses too much steric hindrance for the formation of aminals.

Resolution of the aldehyde **2.6** by making diastereomeric transition metal complexes was another viable option (Figure 2.8). By ^{31}P NMR, when **2.6** was treated with the Pd complex, a complexation did occur. However, the resulting diastereomeric mixture could not be separated by either chromatography or crystallization. When this strategy was applied to resolve **2.7** and **2.8**, we encountered no success again.

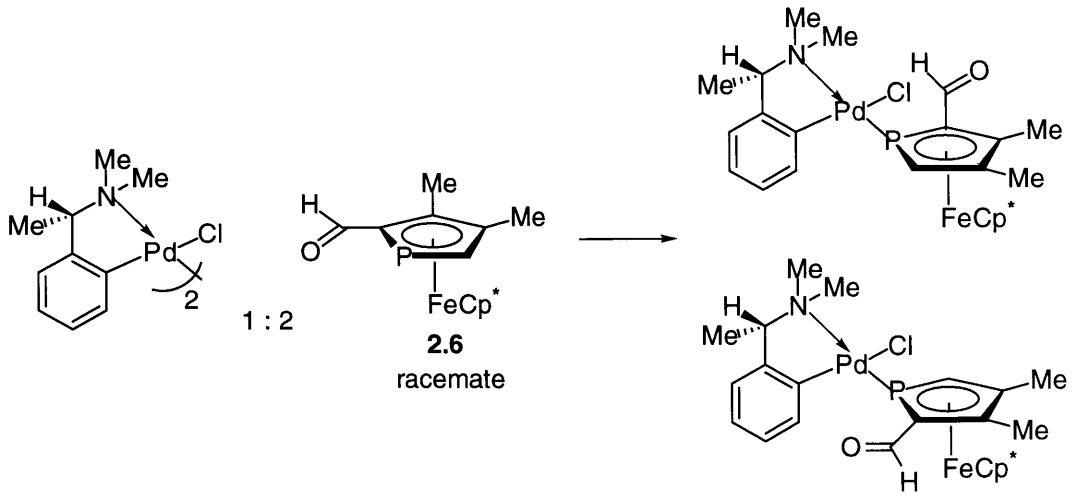

Figure 2.8. Attempts of resolution by forming diastereomeric Pd-complexes.

Chiral HPLC failed to resolve either **2.6** or **2.8**. Fortunately, the alcohol **2.7** can be resolved by Chiral HPLC (Chiracel OD). The disadvantages of chiral HPLC are very obvious. The method is time consuming and presents great difficulty in scaling up. As we were still in the ligand development stage, we decided to settle on this strategy for the time being. Our rationale was that we would thoroughly investigate the possibility of classical resolution if the compound **2.8** or any other derivative resulting from **2.7** proved to be a superb chiral ligand in high demand in future studies.

There are both advantages and disadvantages in resolving at the early stage of the alcohol **2.7**. As semi-preparative chiral HPLC is a painstaking procedure, it is not ideal to resolve at the intermediate alcohol stage as we lose materials by further transformations. The advantage is not as obvious. There is some generality to the synthetic route illustrated in Figure 2.7. Nucleophiles other than $KPPh_2$ could be employed to displace the chloride generated *in situ* to give rise to other phosphaferrocene derivatives. Therefore, having a pure enantiomer at the alcohol **2.7** stage would eliminate the necessity to resolve each new derivative resulting from the alcohol which in itself is an advantage.

In analogy with the synthesis illustrated in Figure 2.7, a series of phosphaferrocene derivatives were obtained (Figure 2.9). Compounds **2.9** and **2.10** are interesting because they both have two modes of chirality - planar chirality and a chiral phosphorus center. **2.9** and **2.10** identified by ^{1}H NMR and ^{31}P NMR were obtained as diastereomeric mixtures. Unfortunately, efforts to separate the diastereomers have so far met with no success.

The dicyclohexylphosphino phosphaferrocene **2.11** is a potential chelating ligand in much the same way as **2.8**. It would be interesting to compare their reactivities and selectivities in metal-catalyzed reactions utilizing bidentate phosphine ligands.

The methoxyether **2.12** can be regarded as a potential monodentate ligand. While there is a surplus of chiral bisphosphines in literature, very few monodentate phosphines have been reported to be useful in asymmetric processes.[25] Generally, monophosphines have been relatively under-investigated.

Our interest in having a P,N mixed ligand led us to the efforts to obtain the dimethylamino phosphaferrocene **2.13**. By crude ^{1}H NMR, the compound was formed briefly. However, it is too unstable to be fully characterized or to be useful for our purpose.

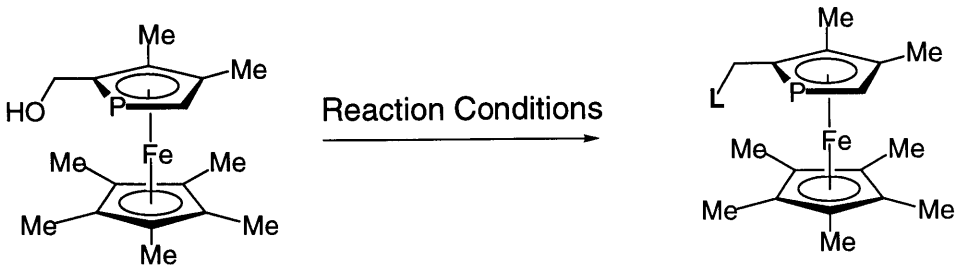

Reaction Conditions	Yield (%)	Product
1. a) $(COCl)_2$, DMF b) KPPhMe	61	**L** = PPhMe (**2.9**)
2. a) $(COCl)_2$, DMF b) KPPhCy	60	**L** = PPhCy (**2.10**)
3. a) $(COCl)_2$, DMF b) $LiPCy_2$, TMEDA	67	**L** = PCy_2 (**2.11**)
4. NaH, MeI	70	**L** = OMe (**2.12**)
5. a) $(COCl)_2$, DMF b) $LiNMe_2$, TMEDA	N/A	**L** = NMe_2 (**2.13**)

Figure 2.9. Syntheses of some related phosphaferrocene derivatives.

In summary, a variety of phosphaferrocenes have been designed, synthesized and resolved. While the reaction and resolving conditions are not ideal at the moment and no effort has been taken to achieve asymmetric syntheses of the phosphaferrocenes mentioned above, the author is optimistic that future efforts in optimization would result in success should the need arise.

Experimental

General

^1H nuclear magnetic resonance spectra were recorded on a Varian Unity 300 NMR spectrometer at ambient temperature and are referenced to residual solvent downfield from tetramethylsilane. ^1H NMR data are reported as follows: chemical shift (δ scale), multiplicity (br = broad, s = singlet, d = doublet, t = triplet, q = quartet, and m = multiplet), coupling constant (Hz), and integration.

All ^{13}C NMR spectra were obtained with complete proton decoupling on a Varian Unity 300 NMR spectrometer and are referenced to solvent downfield from tetramethylsilane.

^{31}P NMR spectra were obtained on a Varian Unity 300 NMR spectrometer (121 MHz) and are referenced to external 85% H_3PO_4 (δ 0).

Infrared spectra were obtained on a Perkin-Elmer 1600 FT-IR spectrophotometer (cm^{-1}). Analytical chiral HPLC was performed on a Daicel CHIRALCEL OD column (4.6 mm x 25 cm). Analytical achiral HPLC was performed on a Alltech ECONOSPHERE SILICA 5μ column (250mm x 4.6mm). Optical rotations were obtained using a Perkin Elmer Model 241 polarimeter.

THF, hexane, and pentane were distilled from sodium-benzophenone ketyl. CH_2Cl_2 was distilled from CaH_2.

$FeCl_2$ and $LiNMe_2$ were purchased from Strem. All reagents were purchased from Aldrich without further purification unless otherwise noted. $KPPh_2$ was purchased from Aldrich as a 0.5 M solution in THF. $LiPCy_2$ was prepared by treating $HPCy_2$ with n-BuLi. KPPhCy was prepared by treating HPPhCy with KH. KPPhMe was prepared by treating HPPhMe with KH.

All reactions were performed under nitrogen using either a dry box or standard Schlenk techniques.

Preparation of Phosphaferrocenes

Synthesis of 2.4.

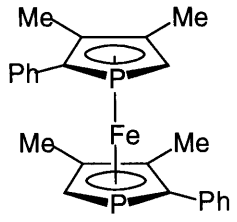

(±)-**2.4**

A mixture of 3,4 - dimethyl - 1 - phenylphosphole (1.88g, 10.0mmol) and ^{t}BuOK (1.35g, 12.0mmol) in THF (10ml) in a closed Schlenk tube was heated and stirred at 140 °C for 12 hours. The resulting yellow solution was then cannula transferred into a stirred slurry of $FeCl_2$ (0.89g, 7.0mmol) in THF (20ml) at 25 °C, immediately providing a dark red mixture. The reaction was then stirred at 25 °C for 12 hours. Solvents were then removed in vacuo. The dark brown residue was purified by column chromatography (silica gel, 20% benzene/hexane) affording 1.58g (73%) of the product (meso/*dl* 1.05 : 1.00) as a red solid. The diastereomers of the product were separated using preparative HPLC (Alltech ECONOSPHERE SILICA 10u, 250mm x 22mm, methylene chloride/hexane 8 : 92, 20ml/min). The racemates were collected from 11.5 to 12.6 minutes.

^{1}H NMR (300 MHz, CD_2Cl_2): δ 7.30 (m, 4H), 7.14 (m, 6H), 3.44 (m, 2H), 2.15 (s, 3H), 2.09 (s, 3H); ^{13}C NMR (75 MHz, CD_2Cl_2): δ 139.6 (t, $J_{c\text{-}p}$ = 8.6), 131.0 (t, $J_{c\text{-}p}$ = 4.8), 128,1, 126.5, 100.8, 94.5, 83.4 (d, $J_{c\text{-}p}$ = 6.1), 82.6 (d, $J_{c\text{-}p}$ = 6.2), 15.5, 13.9; ^{31}P NMR (CD_2Cl_2, 122 MHz): - 63.7; IR (KBr): 3448, 3043, 2922, 1595, 1492, 1441, 1374, 1028, 839, 749; Anal. Calcd for $C_{24}H_{24}P_2Fe$: C, 67.00; H, 5.62. Found: C, 67.27; H, 5.69.

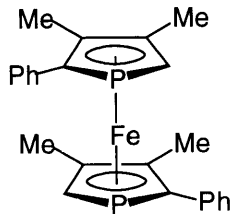

(-)-**2.4**

The enantiomers of the product were separated using semi-preparative HPLC (Daicel CHIRACEL OD, 1cm x 25cm, chloroform/hexane 14 : 86, 2.5 ml/min). Enantiomer (+)-1a ($[\alpha]^{20}_D$ = +441°, c = 0.10, THF) was collected from 5.8 to 6.8 minutes. Enantiomer (-)-1b was collected from 7.6 to 10.0 minutes.

Synthesis of 2.6.

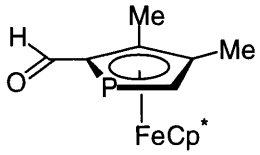

(±)-**2.6**

A mixture of 3,4-dimethyl-pentamenthylphosphaferrocene (2.20 g, 7.30 mmol), $POCl_3$ (1.40 mL, 15.0 mmol), and *N*-methylformanilide (1.70 mL, 13.8 mmol) in CH_2Cl_2 (10 mL) was heated and stirred in a closed Schlenk tube at 54 °C for 12 h. The resulting dark-red solution was then diluted with CH_2Cl_2 and neutralized with saturated aqueous Na_2CO_3. The aqueous layer was extracted with CH_2Cl_2, and the combined organic layers were washed with brine, dried ($MgSO_4$), and concentrated. The resulting black residue was purified by column chromatography (benzene, followed by CH_2Cl_2), which afforded 1.68 g (70%) of the desired product as a red solid.

^{1}H NMR (300 MHz, CD_2Cl_2): δ 9.71 (d, $J_{H\text{-}P}$ = 5.4, 1H), 3.83 (d, $J_{H\text{-}P}$ = 36.3, 1H), 2.21 (s, 3H), 2.05 (s, 3H), 1.74 (s, 15H); ^{13}C NMR (75 MHz, CD_2Cl_2): δ 197.3 (d, $J_{C\text{-}P}$ = 26.6), 101.3 (d, $J_{C\text{-}P}$ = 8.4), 92.4 (d, $J_{C\text{-}P}$ = 4.1), 90.0 (d, $J_{C\text{-}P}$ = 55.0), 87.8 (d, $J_{C\text{-}P}$ = 57.5),

85.0, 13.9, 11.5, 10.8; ^{31}P NMR (121 MHz, CD_2Cl_2): -46.9; IR (KBr): 2972, 2905, 2745, 1646, 1478, 1448, 1375, 1320, 1227, 1031. HRMS: Calcd for $C_{17}H_{23}OPFe$: 330.0836; found: 330.0836.

Synthesis of 2.7.

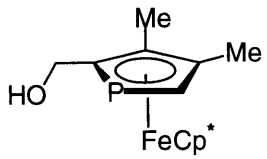

(±)-**2.7**

A solution of **2.6** (700 mg, 2.13 mmol) in 20 mL of Et_2O was added dropwise to a suspension of $LiAlH_4$ (162 mg, 4.27 mmol) in Et_2O (20 mL) at 0 °C. After this mixture had been stirred for 15 min, water (0.77 mL, 43 mmol) was added. The resulting yellow suspension was dried ($MgSO_4$), and the solvents were removed to furnish 690 mg (98%) of **4** as a yellow solid.

^1H NMR (300 MHz, CD_2Cl_2): δ 4.10 (m, 2H), 3.30 (d, J_{H-P} = 36.3, 1H), 2.02 (s, 3H), 1.96 (s, 3H), 1.79 (s, 15H), 1.24 (br s, 1H); ^{13}C NMR (75 MHz, CD_2Cl_2): δ 97.2 (d, J_{C-P} = 56.6), 96.4 (d, J_{C-P} = 6.9), 91.0 (d, J_{C-P} = 4.5), 83.1, 81.7 (d, J_{C-P} = 56.8), 61.2 (d, J_{C-P} = 23.1), 14.4, 11.0, 10.7; ^{31}P NMR (121 MHz, CD_2Cl_2): δ - 62.5; IR (KBr): 3276, 2946, 2902, 2857, 1451, 1425, 1376, 1235, 1022, 999. HRMS: Calcd for $C_{17}H_{25}OPFe$: 332.0992; found: 332.0993.

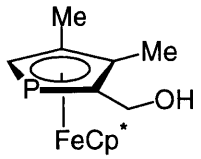

(+)-2.7

The enantiomers of **2.7** were separated using semi-preparative HPLC (Daicel CHIRALCEL OD; 1 cm x 25 cm; isopropanol/hexane 10 : 90; 2.5 mL/min). Enantiomer (+)-**2.7** ($[\alpha]^{20}_D$ = +41°, c = 1.0, THF) was collected from 10.0 to 11.5

minutes. Enantiomer (-)-**2.7** was collected from 12.0 to 13.5 minutes. The absolute configuration of (+)-**2.7** was established by X-ray crystallographic studies.

Synthesis of (-)-2.8.

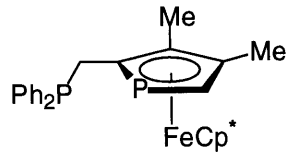

(-)-2.8

Oxalyl chloride (1.00 mL, 11.5 mmol) was added dropwise to a -20 °C solution of (-)-**2.7** (220 mg, 0.660 mmol) in THF (20 mL) containing a catalytic amount of DMF (2 drops). After gas evolution and precipitation of solids had ceased, the reaction mixture was concentrated. The resulting solid was taken up in THF and filtered through an acrodisc (0.2 μm), providing a dark-red solution. $KPPh_2$ (0.5 M in THF; 2.6 mL, 1.3 mmol) was added dropwise to the cooled (-78 °C), dark-red solution. After the addition was complete, the solution was warmed to r.t. and stirred for 2 h. The solvents were then evaporated, and the resulting black residue was extracted with CH_2Cl_2 (3x). The combined organic layers were dried ($MgSO_4$) and concentrated. The product was then purified by chromatography (benzene/hexane 20 : 80), which furnished 180 mg (54%) of (-)-**2.8** as an orange-yellow oil.

^1H NMR (300 MHz, CD_2Cl_2): δ 7.36 (m, 10H), 3.17 (d, J_{H-P} = 36.3, 1H), 2.84 (m, 2H), 1.98 (s, 3H), 1.79 (s, 15H), 1.76 (s, 3H); ^{13}C NMR (75 MHz, CD_2Cl_2): δ 140.1 (d, J_{C-P} = 17.0), 138.6 (d, J_{C-P} = 15.9), 134.2 (dd, J_{C-P} = 19.2, 1.8), 133.0 (d, J_{C-P} = 17.9), 128.8 (d, J_{C-P} = 6.3), 94.8 (m), 90.8 (dd, J_{C-P} = 5.1, 2.4), 82.6, 81.1 (d, J_{C-P} = 57.2), 29.4 (dd, J_{C-P} = 19.5, 14.3), 14.7, 11.3, 10.9; ^{31}P NMR (121 MHz, CD_2Cl_2): δ -11.6 (d, J_{P-P} = 26.7), -61.4 (d, J_{P-P} = 26.7); IR (KBr): 3448, 2969, 2901, 2345, 1477, 1432, 1374, 1028, 739, 696; HRMS: Calcd for $C_{29}H_{34}P_2Fe$: 500.1485; found: 500.1483. $[\alpha]^{20}_D$ = -42° (c = 0.77, THF).

Synthesis of 2.9.

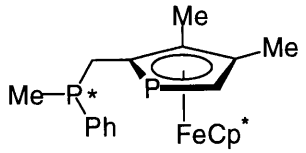

2.9

The procedure is the same as that of synthesis of **2.8** except that KPPhMe is used in place of $KPPh_2$. The diastereomers cannot be not separated. See Appendix II for ^1H and ^{31}P NMR spectra.

Synthesis of 2.10.

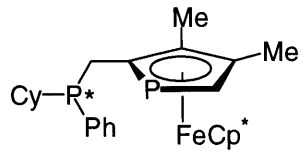

2.10

The procedure is the same as that of synthesis of **2.8** except that KPPhCy is used in place of $KPPh_2$. The diastereomers cannot not separated. See Appendix II for ^1H and ^{31}P NMR spectra.

Synthesis of (+)-2.11.

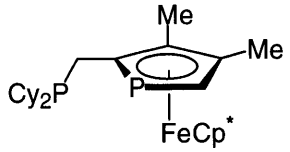

(+)-2.11

Oxalyl chloride (1.0 ml, 11.5 mmol) was added dropwise to a -20 °C solution of (-)-**2.7** (62 mg, 0.19 mmol) in THF (20 ml) containing a catalytic amount of DMF (2 drops). After gas evolution and precipitation of solids had ceased, the reaction mixture was concentrated. The resulting solid was taken up in THF and filtered

through an acrodisc (0.2 μm), providing a dark-red solution. A THF solution of TMEDA (87 mg, 0.75 mmol) and $LiPCy_2$ (76 mg, 0.37 mmol) was added dropwise to the cooled (-78 °C), dark-red solution. After the addition was complete, the solution was warmed to r.t. and stirred for 2 h. The solvents were then evaporated, and the resulting black residue was extracted with CH_2Cl_2 (3x). The combined organic layers were dried ($MgSO_4$) and concentrated. The product was then purified by chromatography (benzene/hexane 20 : 80), which furnished 64 mg (67%) of (+)-**2.11** as an orange-yellow oil.

^1H NMR (300 MHz, CD_2Cl_2): δ 3.17 (d, J_{H-P} = 36.0, 1H), 2.20 (m, 2H), 2.01 (s, 3H), 1.93 (s, 1H), 1.78 (s, 15H), 1.74-1.23 (m, 22H); ^{13}C NMR (75 MHz, CD_2Cl_2): δ 82.4, 80.4 (d, J_{C-P} = 57.0), 34.1 (d, J_{C-P} = 16.0), 33.7 (d, J_{C-P} = 17.3), 31.1 (t, J_{C-P} = 12.0), 30.3 (d, J_{C-P} = 10.4), 29.6 (d, J_{C-P} = 8.2), 28.2 (t, J_{C-P} = 9.8), 27.8 (m), 27.2 (d, J_{C-P} = 3.7), 22.3 (t, J_{C-P} = 20.0), 14.7, 10.8; ^{31}P NMR (121 MHz, CD_2Cl_2): δ 1.0 (d, J_{P-P} = 18.4), -59.6 (d, J_{P-P} = 18.3); IR (neat on KBr): 3442, 2968, 2849, 1447, 1374, 1071, 1029; HRMS: Calcd for $C_{29}H_{44}P_2Fe$: 510.2268; found: 510.2279. $[\alpha]^{20}_D$ = +119° (c = 5.1, THF).

Synthesis of (+)-**2.12**.

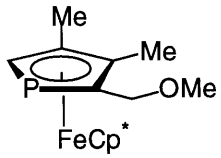

(+)-**2.12**

NaH (21 mg, 0.90 mmol) and MeI (113 μl, 1.81 mmol) were stirred in THF in a schlenk flask at room temperature. The THF solution of (+)-**2.7** was then added dropwise to the flask. The solution was stirred overnight. Upon evaporation of the solvents, the residue was taken up in Et_2O and a drop of water was added. The solution was then dried ($MgSO_4$) and concentrated. The product was then purified by chromatography on basic alumina (benzene/hexane 20 : 80), which furnished 71

mg (70%) of (-)-**2.12** as a yellow solid. ^{1}H NMR (500 MHz, CD_2Cl_2): δ 4.01 (dd, J_{H-P} = 16.5, J_{H-H} = 11.0, 1H), 3.77 (dd, J_{H-P} = 6.5, J_{H-H} = 11.0, 1H), 3.29 (d, J_{H-P} = 34.5, 1H), 2.01 (s, 3H), 1.92 (s, 3H), 1.78 (s, 15H); ^{13}C NMR (75 MHz, CD_2Cl_2): δ 96.1 (d, J_{C-P} = 6.5), 93.1 (d, J_{C-P} = 55.7), 91.4 (d, J_{C-P} = 4.8), 82.9, 81.9 (d, J_{C-P} = 56.6), 70.8 (d, J_{C-P} = 21.4), 57.8, 14.4, 10.9, 10.8; ^{31}P NMR (121 MHz, CD_2Cl_2): δ - 60.2; IR (KBr): 2919, 1478, 1449, 1373, 1185, 1096, 1026, 943, 867. HRMS: Calcd for $C_{18}H_{27}OPFe$: 346.1149; found: 346.1151. $[\alpha]^{20}_D$ = +188° (c = 0.16, THF).

X-ray Crystallographic Studies

Crystal Structure of (-)-2.4

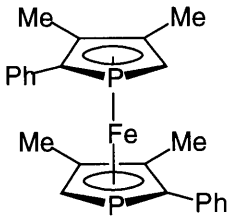

(-)-**2.4**

See **Figure 2.6** for the ORTEP illustration. (-)-**2.4** was dissolved in CH_2Cl_2. Crystals suitable for X-ray structural analysis were obtained by diffusing pentane into this solution at room temperature.

See Appendix I for detailed crystallographic data (Tables **1-5**).

Crystal Structure of (+)-2.7

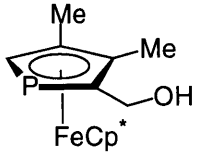

(+)-2.7

(+) **2.7** was dissolved in CH_2Cl_2. Crystals suitable for X-ray structural analysis were obtained by diffusing pentane into this solution at room temperature.

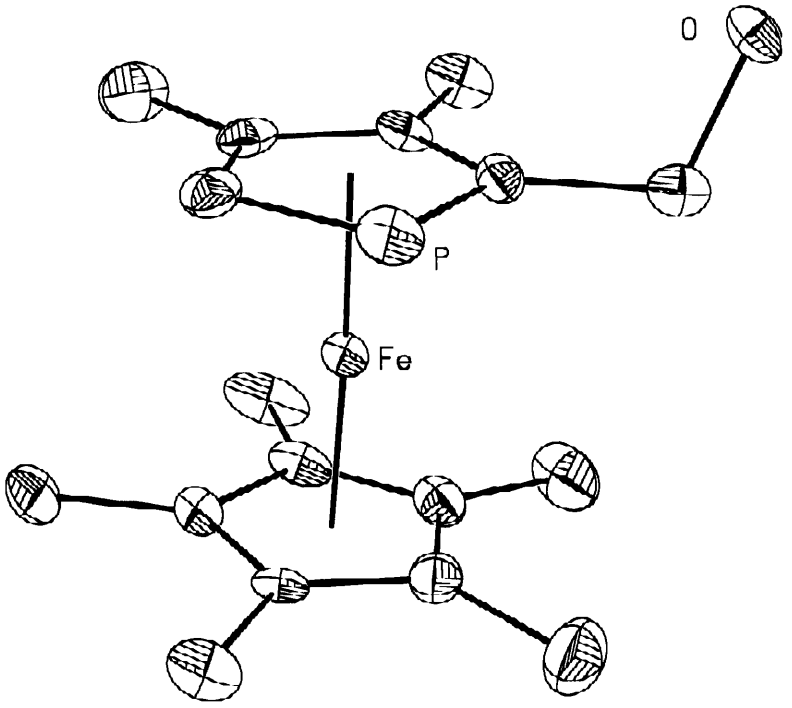

See Appendix I for detailed crystallographic data (Tables **1-5**).

References

1 Ojima, I. *Catalytic Asymmetric Synthesis*; Wiley-VCH: New York, 1993.
2 Le Floch, P.; Mathey, F. *Coord. Chem. Rev.* **1998**, 771-791.
3 De Lauzon, G.; Mathey, F.; Simalty, M. *J. Organomet. Chem.* **1978**, *156*, C33-C36.
4 De Lauzon, G.; Deschamps, B.; Mathey, F. *Nouv. J. Chim.* **1980**, *4*, 683-5.
5 De Lauzon, G.; Deschamps, B.; Fischer, J.; Mathey, F.; Mitschler, A. *J. Am. Chem. Soc.* **1980**, *102*, 994-1000.
6 Deschamps, B.; Fischer, J.; Mathey, F.; Mitschler, A. *Inorg. Chem.* **1981**, *20*, 3252-9.
7 Deschamps, B.; Fischer, J.; Mathey, F.; Mitschler, A.; Ricard, L. *Organometallics* **1982**, *1*, 312-16.
8 Deschamps, B.; Mathey, F.; Fischer, J.; Nelson, J. H. *Inorg. Chem.* **1984**, *23*, 3455-62.
9 Deschamps, B.; Mathey, F. *Organometallics* **1992**, *11*, 1411-1413.
10 Deschamps, B.; Ricard, L.; Mathey, F. *J. Organomet. Chem.* **1997**, *548*, 17-22.
11 Mathey, F.; Mitschler, A.; Weiss, R. *J. Am. Chem. Soc.* **1977**, *99*, 3537-8.
12 Mathey, F.; Mercier, F.; Charrier, C.; Fischer, J.; Mitschler, A. *J. Am. Chem. Soc.* **1981**, *1981*, 4595.
13 Mathey, F. *Coord. Chem. Rev.* **1994**, 1-52.
14 Mathey, F.; Mercier, F.; Nief, F.; Fischer, J.; A., M. *J. Am. Chem. Soc.* **1982**, *104*, 2077-2079.

15 Ganter, C.; Brassat, L.; Ganter, B. *Chem. Ber.* **1997**, *130*, 1771-1776.
16 Ganter, C.; Brassat, L.; Ganter, B. *Tetrahedron: Asymmetry* **1997**, *8*, 2607-2611.
17 Ganter, C.; Brassat, L.; Glinsboeckel, C.; Ganter, B. *Organometallics* **1997**, *16*, 2862-2867.
18 a). Brassat, L.; Ganter, B.; Ganter, C. *Chem. Eur. J.* **1998**, 2148-2153.
b). Ganter, C.; Glinsböckel, C.; Ganter, B. *Eur. J. Inorg. Chem.* **1998**, 1163-1168.
19 Garrett, C. E.; Fu, G. C. *J. Org. Chem.* **1997**, *62*, 4534-4535.
20 Atwood, D. A.; Cowley, A. H.; Dennis, S. M. *Inorg. Chem.* **1993**, *32*, 1527-8.
21 Holand, S.; Jeanjean, M.; Mathey, F. *Angew. Chem.., Int. Ed. Engl.* **1997**, *36*, 98-100.
22 Roman, E.; Leiva, A. M.; Casasempere, M. A.; Charrier, C.; Mathey, F.; Garland, M. T.; Le Marouille, J. Y. *J. Organomet. Chem.* **1986**, *309*, 323-32.
23 Garrett, C. E., personal communication.
24 Liang, J., personal communication.
25 Hayashi, T.; Hayashizaki, K.; Kiyoi, T.; Ito, Y. *J. Am. Chem. Soc.* **1988**, *110*, 8153-8156.

Chapter 3
The First Applications of Chiral Phosphaferrocenes in Asymmetric Catalysis

3.1 Introduction

As mentioned in Chapter 1, no application of an sp^2 phosphorus compound had ever been reported in asymmetric catalysis prior to our work. With some relatively stable chiral phosphaferrocenes synthesized and resolved in Chapter 2, we were ready to screen their reactivities as well as selectivities in transition metal catalyzed reactions.

Chelating phosphine ligands play an important role in many well-known asymmetric processes.[1] Figure 3.1.1 shows some well-established bisphosphines. An interesting phenomenon is that an overwhelming majority of reported chiral bisphosphines bear C_2-symmetry. Whether C_2-symmetry is actually essential in a chelating ligand or not was a question we were interested in addressing as some of the chiral phosphaferrocenes we obtained in Chapter 2 do not bear any symmetry element at all.

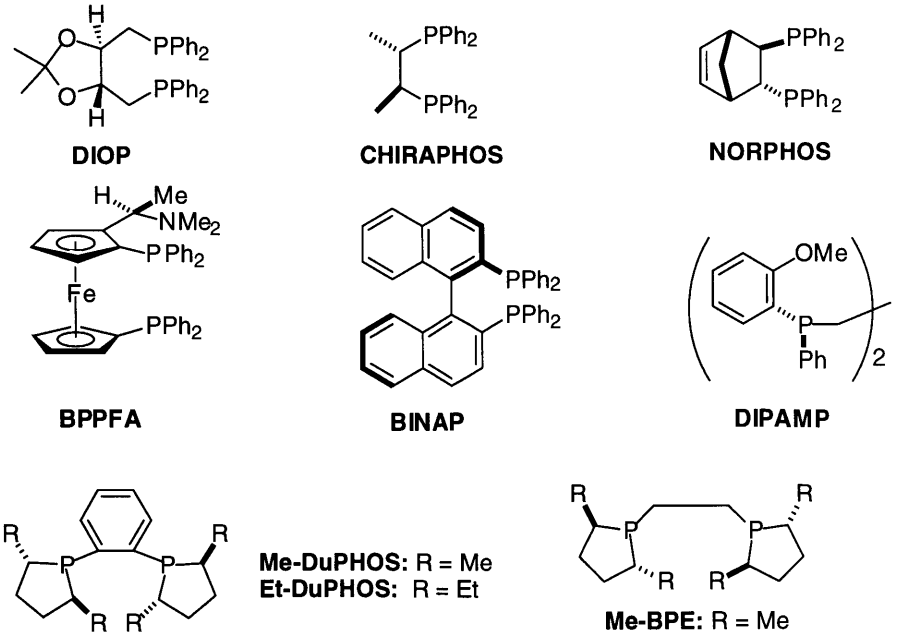

Figure 3.1.1. Some well-known chiral bisphosphines utilized in asymmetric catalysis.

Of all the reactions involving chiral bisphosphines, asymmetric hydrogenation of olefins is one of the most mature fields.[2] Kagan, Knowles and others developed Rh (I) complexes of chiral chelating phosphines, DIOP and DIPAMP, respectively.[3,4] Their pioneering success in the asymmetric hydrogenation of dehydroamino acids has led to the discovery of numerous optically pure diphosphines (Figure 3.1.2).[2] Dehydroamino acids were chosen as substrates in the early studies on the asymmetric hydrogenation of olefins partly because of the significance of the products α-amino acids. They are also highly functionalized olefins which have been revealed to be better substrates for Rh (I) catalyzed hydrogenations than less functionalized olefins. As it turned out, we chose this reaction as a testing ground for some of our phosphaferrocenes. In Section 3.2, the state of the art of this reaction as well as our successful effort in utilizing a chiral phosphaferrocene in that reaction will be discussed in more detail.

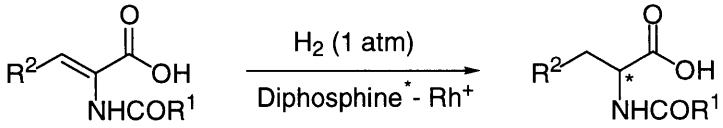

	Chiral Diphosphine					
	(*R*,*R*)-DIOP	(*R*,*R*)-DIPAMP	(*S*,*S*)-NORPHOS	(*S*,*S*)-CHIRAPHOS	(*S*)-BINAP[a]	(*S*,*R*)-BPPFA
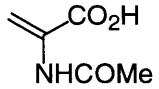	73 (*R*)	90 (*S*)	95 (*R*)	91 (*R*)	[98] (*R*)	76 (*S*)
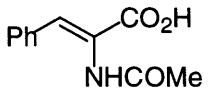	85 (*R*)	96 (*S*)	95 (*R*)	89 (*R*)	[100] (*R*)	93 (*S*)

[a] Figures in brackets indicate the results for *N*-benzoyl derivatives.

Figure 3.1.2. Asymmetric Hydrogenation of dehydroamino acids catalyzed by some well-known chiral bisphosphines.

Aryl enamides are a class of substrates which have not been as thoroughly investigated as dehydroamino acids in hydrogenation reactions.[5-7] In Section 3.3, we will discuss the general background for this reaction and the demonstrated versatility of our phosphaferrocene in that reaction as well. Lastly, in Section 3.4, a brief overview of our continuing efforts in applying phosphaferrocenes in catalysis will be presented. Preliminary studies of asymmetric isomerization of allylic alcohols will be discussed.

In addition to hydrogenations of olefinic substrates, bisphosphines have also been demonstrated to be effective ligands in hydrogenations of ketones. Optically active secondary alcohols with a neighboring functional group are extremely useful starting materials for the synthesis of various biologically active compounds. Consequently, the asymmetric hydrogenation of functionalized ketones has attracted much attention. In the case of functionalized ketones, the levels of enantioselectivities are quite impressive (Figure 3.1.3).[2]

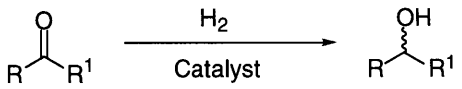

			Product	
R	R^1	Catalyst	% ee	Config.
Me	CH_2NMe_2	$RuBr_2$(*S*)-BINAP	95	*S*
Me	CH_2OH	$RuCl_2$(*R*)-BINAP	92	*R*
Me	CH_2CO_2Me	$RuCl_2$(*R*)-BINAP	>99	*R*
Me	COMe	$RuBr_2$(*S*)-BINAP	100[a]	*S,S*
Me	CH_2COMe	$RuCl_2$(*R*)-BINAP	100[b]	*R,R*

[a] dl/meso = 26/76
[b] dl/meso = 99/1

Figure 3.1.3. Asymmetric hydrogenation of functionalized ketones ($RCOR^1$) catalyzed by Ru-BINAP complexes.

High enantioselectivity in the hydrogenation of simple ketones has been difficult to attain with conventional chiral diphosphine complexes. Great results have been achieved with alkenyl, cyclopropyl and aryl ketones with a mixture of a Ru(II)-BINAP complex, a chiral diamine and base.[8] In this catalytic system, the chelating chiral diamine is as important a stereochemistry-controlling element as the chiral BINAP ligand. The recently discovered Rh(I)-PennPhos system, however, marked a breakthrough in obtaining optically active secondary alcohols by hydrogenation catalyzed by a simple metal-bisphosphine complex (Figure 3.1.4).[9]

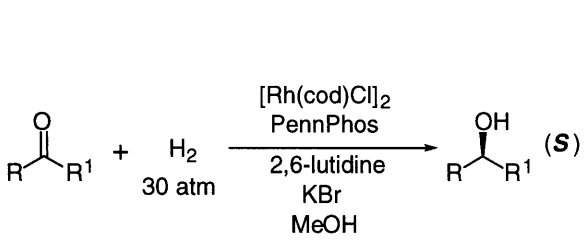

Entry	Ketone	Yield (%)	ee (%)
1[a]	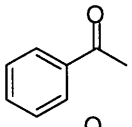	97	95
2	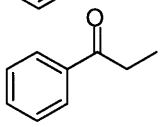	95	93
3	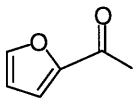	99	96
4	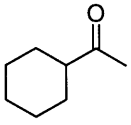	90	92
5	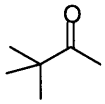	51	94

[a] No KBr added.

Figure 3.1.4. Asymmetric hydrogenation of simple ketones catalyzed by a Rh-PennPhos complex.

Aside from hydrogenation reactions, the success and versatility of chelating phosphines have also been demonstrated in the Pd-catalyzed allylic substitution[10] and the Rh-catalyzed allylamine isomerization[11] and so on. Asymmetric hydroboration of olefins, on the other hand, has shown limited success. The only substrates which show excellent enantioselectivities are styrene derivatives (Figure 3.1.5).[12]

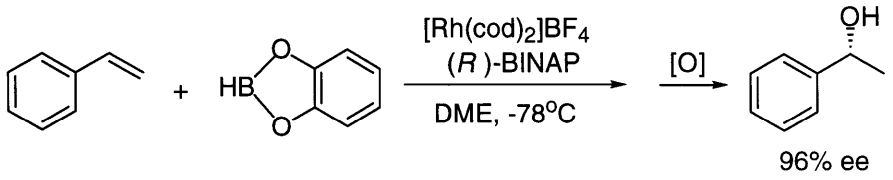

Figure 3.1.5. Asymmetric hydroboration catalyzed by Rh(I)-BINAP complex.

It is indeed impossible to cover all types of reactions which utilize bisphosphines. However, it is clear that there is a continuing need for discovering novel chiral bisphosphines. While some of the reactions such as the hydrogenation of dehydroamino acids have reached near perfection with certain phosphines, there is not one bisphosphine which is truly versatile. The search for efficient ligands for any given reaction is still largely Edisonian in character. As new metal-catalyzed reactions are discovered at a fast pace nowadays, there is a clear incentive to enlarge the pool of chiral bisphosphines and to enrich the design features as well. In doing so, it will also enable us to better understand the origin of selectivity and to eventually achieve the ultimate goal of "rational design of ligands and catalysts" in asymmetric catalysis.

In comparison with chelating phosphines, much less has been accomplished in the case of monophosphines. Accordingly, fewer chiral monodentate phosphines

have been discovered. One of the most successful applications of monodentate phosphines is asymmetric hydrosilylation (Figure 3.1.6).[13]

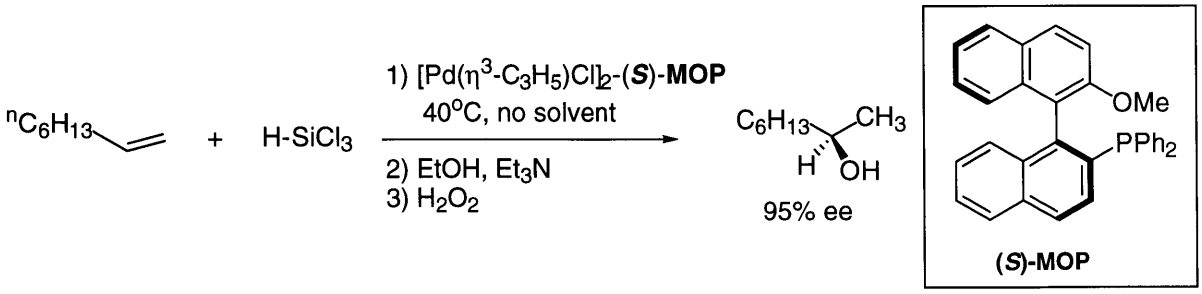

Figure 3.1.6. Asymmetric hydrosilylation catalyzed by Pd-MOP complex.

There is undoubtedly great potential in the seemingly mature field of chiral phosphine ligands. With sp^2 hybridized nitrogen-based chiral ligands extensively utilized, we were enthusiastic about investigating the potential of sp^2 hybridized phosphorus-based compounds as chiral ligands. The design is by nature fundamentally different from those of all previously reported phosphine ligands. From an academic point of view, this intellectual pursuit was exciting due to the nature of its novelty. From a practical point of view, a planar-chiral phosphorus is sterically and electronically different from a sp^3 phosphorus which might present advantages in certain reactions which have not been studied well. In Sections 3.2 and 3.3, the successful applications of chiral phosphaferrocenes in the asymmetric hydrogenations of dehydroamino acids and aryl enamides will be discussed.

3.2. Enantioselective Hydrogenation of Dehydroamino Acids Catalyzed by a Rh(I)-Phosphaferrocene - The First Application of a Planar-Chiral Phosphorus Heterocycle in Asymmetric Catalysis.

Background

Dehydroamino acids were the first olefinic substrates successfully used in the homogeneous asymmetric hydrogenation. Kagan reported enantioselective hydrogenation of (*Z*)-α-acetamidocinnamic acid with DIOP-Rh^+ complexes, giving *N*-acetylphenylalanine as the product with 72% ee.[3] The Monsanto group led by Knowles developed DIPAMP and achieved very high enantioselectivities (>90% ee) in this reaction.[4] Since then, many chiral phosphine ligand-metal complexes have been discovered to be efficient catalysts for this reaction (see Figure 3.1.1 and Figure 3.1.2).

The mechanism of the reaction has been elucidated by detailed studies on the catalytic cycle.[14-17] Halpern and coworkers determined the structure of a key intermediate, the catalyst-substrate adduct [Rh((*S*,*S*)-CHIRAPHOS)(EAC)]$^+$, in the hydrogenation of ethyl-2-acetamidocinnamate (EAC) by X-ray analysis and demonstrated that the minor diastereomeric catalyst-substrate adduct is more reactive towards H_2 than the major one and thus gives the corresponding enantiomer as the predominant product (Figure 3.2.1).

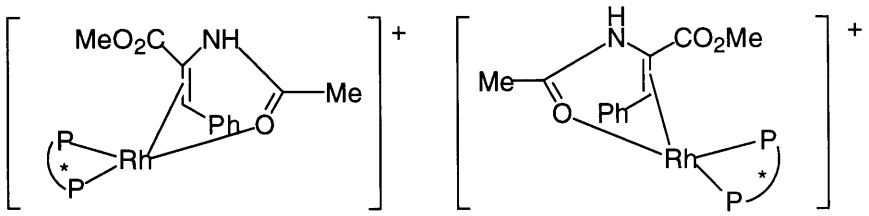

Minor diastereomeric adduct Major diastereomeric adduct

[Rh(*S*,*S*)-CHIRAPHOS)(EAC)]$^+$
EAC = ethyl (*Z*)-α-acetamidocinnamate

Figure 3.2.1. Mechanistic studies by Halpern and coworkers.

In recent years, this reaction has been a testing ground for newly discovered bisphosphines. There have been reports of ingeniously designed bisphosphines which generate extremely high levels of enantioselectivities with ee's approaching 100%.[18-22] When we decided to test phosphaferrocenes on this reaction, our intention was not to beat the unbeatable current state of the art. It was rather to quickly assess the possibility of a planar-chiral phosphorus heterocycle as a chelating ligand. With this goal in mind, we started to explore the utility of phosphaferrocenes in this reaction.

Results and Discussion

The chelating phosphine we first decided to investigate is the diphenylphosphino phosphaferrocene **A** (Figure 3.2.2). We proposed that the flexible methylene linker could adopt a geometry most compatible with a five-membered metallocycle formation. Under the initial reaction conditions (Figure 3.2.2), We were delighted to observe enantioselectivities. However, we were perplexed by irreproducible ee's ranging from 20% to 80% for a long time. After numerous repetitions and many changes of variables, we discovered two things that we were not aware of due to our initial lack of expertise in the field of

hydrogenation. First, while many reported Rh(I) catalyzed asymmetric hydrogenations are not moisture sensitive, our Rh(I)-**A** system is quite susceptible to water. In the presence of a trace amount of water, the reaction mixtures were sometimes suspensions rather than bright red solutions of Rh(I)-**A**. This phenomenon led us to the realization that our phosphaferrocene-Rh(I) system easily falls apart in the presence of water. It is possible that the phospholyl P to Rh bond is weaker than a tertiary P to Rh bond which results in the increase of sensitivity to moisture. Second, we were initially running the hydrogenation reactions by bubbling H_2 into the reaction mixture followed by setting up a H_2 balloon during the rest of the reaction. Had we known the importance of keeping oxygen away from the reaction mixture, we would have switched to running the reaction in a schlenk tube much earlier on. As the phosphaferrocene has an sp^2 phosphorus which undergoes oxidation faster than generic tertiary phosphines, keeping the reaction mixture oxygen-free is especially crucial in getting reproducible results.

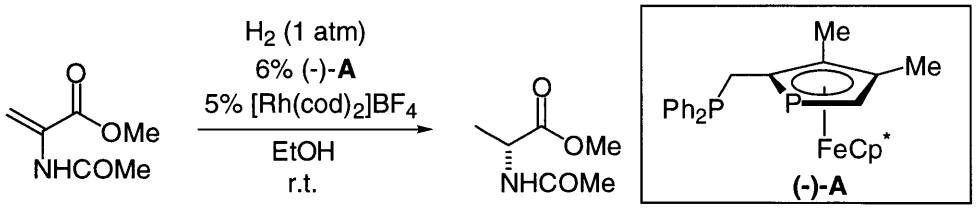

Figure 3.2.2. Initial reaction conditions for the hydrogenation of dehydroamino acids catalyzed by Rh(I)-(-)-**A** complex.

Once the origin of irreproducibility was found, the optimization effort became quite straightforward. In order to find the best reaction condition, we first changed the counterion of the cationic Rh(I) species (Figure 3.2.3). Earlier studies have demonstrated that $[Rh(cod)Cl]_2$ is not reactive enough for hydrogenations of α-acetamidocinnamic acids. As illustrated in Figure 3.2.3, while $Rh(cod)_2PF_6$ proves to

be the best in terms of enantioselectivity, there is essentially not a dramatic counterion effect. There is also not a dramatic rate difference as all the reactions are complete within 12 hours.

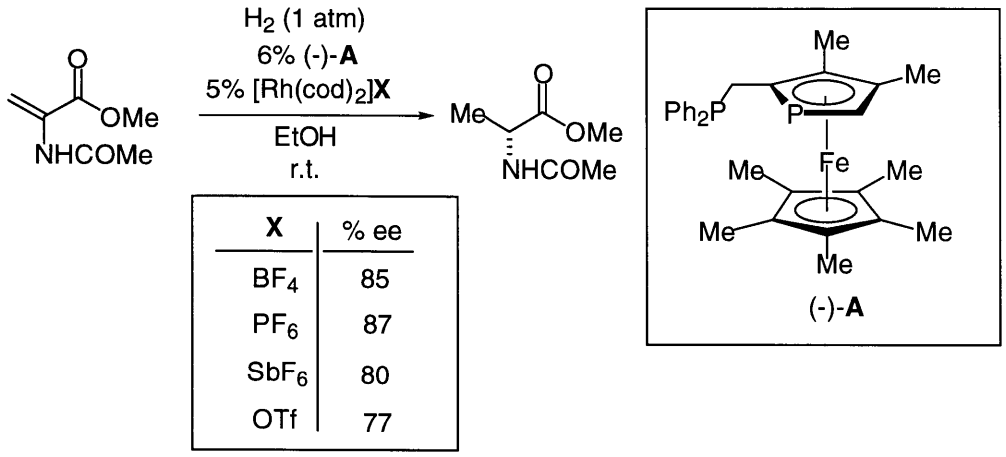

X	% ee
BF_4	85
PF_6	87
SbF_6	80
OTf	77

Figure 3.2.3. Counterion effects on asymmetric hydrogenation.

Next, we looked into the solvent effects. Not surprisingly, our results corroborate part of the catalytic cycle which has been elucidated by Halpern and others in their mechanistic studies (Figure 3.2.4).[2] According to their studies, prior to complexation of the substrate to Rh(I), two solvent molecules were coordinated to Rh(I) after initial hydrogenation of cyclooctadiene.

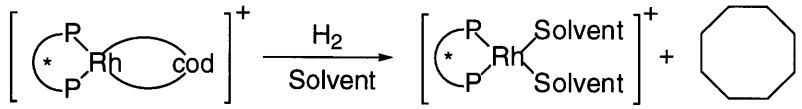

Figure 3.2.4. Solvent complexation prior to substrate complexation.

In our studies (Figure 3.2.5), coordinating solvents such as THF and EtOH are preferred over non-coordinating solvents such as CH_2Cl_2. We chose EtOH in the end for its benign environmental effects as well as its relatively low costs of

production. Et_2O and benzene as solvents do not dissolve the catalyst complex and hence are not included in the solvent study.

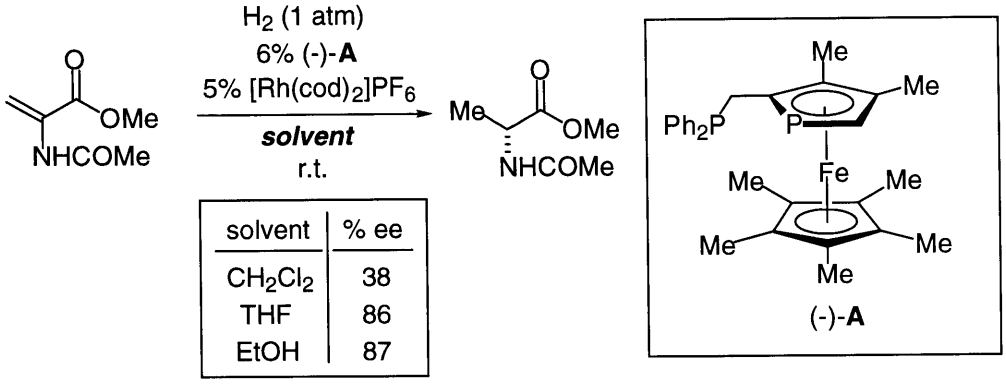

solvent	% ee
CH_2Cl_2	38
THF	86
EtOH	87

Figure 3.2.5. Solvent effects on asymmetric hydrogenation.

We briefly investigated the effects of pressure and temperature on the enantioselectivity. The levels of enantioselectivity remain essentially constant within the temperature range 0-50 °C. Increasing the pressure does not affect the ee very much either. Therefore, we have decided on the most convenient pressure and temperature which are 1atm H_2 pressure and room temperature, respectively.

Under the optimized reaction condition (1 atm of H_2, 5% $Rh(cod)_2PF_6$, 6% (-)-**A**, anhydrous EtOH as the solvent, room temperature, 12 hours reaction time), a wide range of substrates are reduced enantioselectively with good to excellent ee's and quantitative yields (Figure 3.2.6).

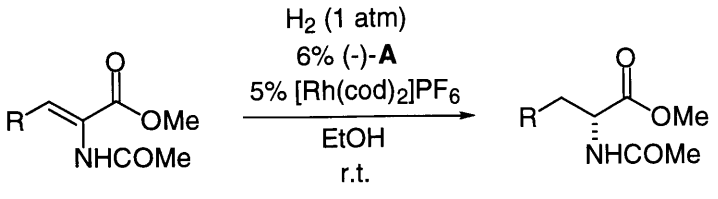

entry	R	% ee	yield
1	H	87	99
2	Ph	87	95
3	4-OMe-C_6H_4	87	96
4	4-Cl-C_6H_4	85	95
5	4-NO_2-C_6H_4	79	100
6	Me	88	96
7	Et	96	92
8	*i*-Pr	90	96

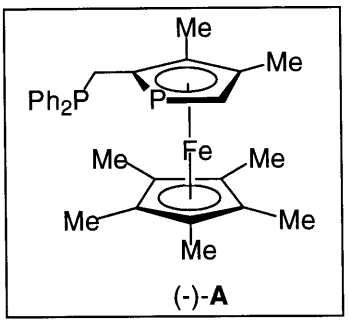

Figure 3.2.6. The table of substrates.

An investigation of the cinnamate derivatives (Entries 2-5) reveals a slight electronic effect. It seems that more electron rich systems furnish slightly higher ee's than electron poor systems. β-alkyl substituted esters are also reduced enantioselectively. The ee's in general are slightly higher than those of the cinnamate derivatives. α-acetamidocrotonate (Entry 7) gives the highest ee (96%). One major difference in terms of electronic property between phosphaferrocene **A** and other well-known bisphosphines is that the phospholyl phosphorus is less electron rich than tertiary phosphorus. Hence it is possible that our Rh(I)-(-)-**A** works better with relatively more electron rich substrates (alkyl substituted esters versus aryl substituted esters, electron-donating groups versus electron-withdrawing groups on the aryl ring, etc). When (+)-**A** is used instead of (-)-**A**, we obtain the opposite enantiomer of the substrates. As both enantiomers of the ligands are available, we have access to the synthesis of a variety of both D- and L-amino acids.

Since we always mixed $Rh(cod)_2PF_6$ and **A** in situ to generate the catalyst, we were interested in finding out whether **A** which incorporates both an sp^2 and an sp^2 phosphorus indeed acts as a bidentate ligand to Rh(I) or not. First, we undertook a ^{31}P NMR study of the complexation of $Rh(cod)_2PF_6$ and **A** (Figure 3.2.7).

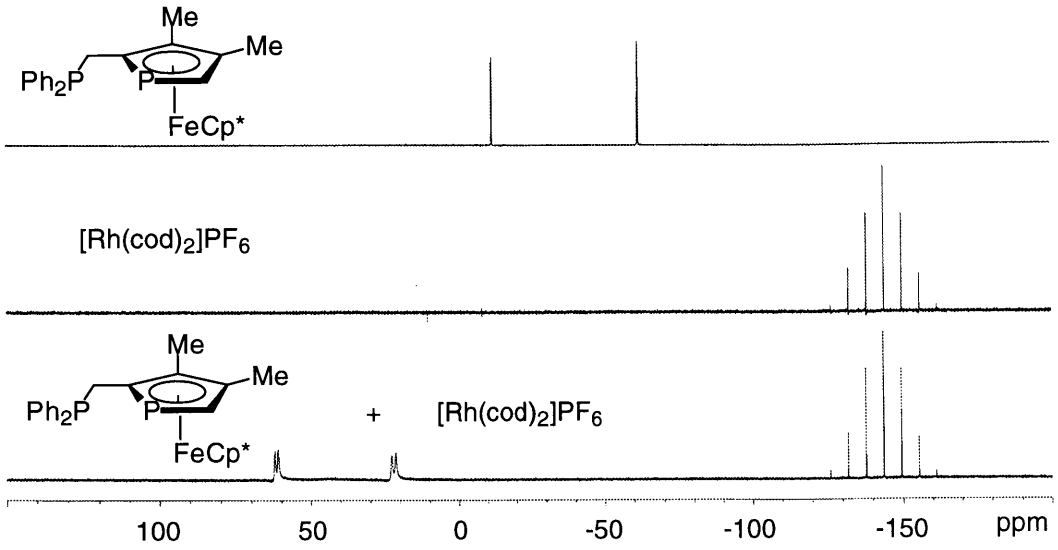

Figure 3.2.7. ^{31}P NMR study of the complexation of $Rh(cod)_2PF_6$ and (-)-**A.**

^{31}P NMR of the phosphaferrocene itself in CD_2Cl_2 shows two doublets as the two P atoms are coupled to each other. The resonance of phospholyl phosphorus is at -61.4 ppm while the tertiary phosphorus has a resonance of -11.6 ppm. The P-P coupling constant is 27 Hz. ^{31}P NMR of $Rh(cod)_2PF_6$ in CD_2Cl_2 shows a characteristic septuplet as P is coupled to six fluorines. Upon mixing the two at 1:1 ratio, we observed immediate downfield shifting of both phosphorus atoms of the phosphaferrocene whereas the phosphorus of PF_6^- stays put. The resonance of the phospholyl phosphorus moved from -61.7 ppm to 22.6 ppm. The resonance of the tertiary phosphorus moved from -11.6 ppm to 61.8 ppm. In addition, both resonances are doublets of doublets which indicates that the two phosphorus atoms are not only coupled to each other but also coupled to Rh. The phospholyl P-Rh

coupling constant is approximately 172 Hz. The tertiary P-Rh coupling constant is about 141 Hz. The P-P coupling constant remains essentially unchanged at 28 Hz. ^{31}P NMR study of the complexation of $Rh(cod)_2PF_6$ and (-)-**A** thus offers compelling evidence for the bidendate binding of (-)-**A** to Rh(I).

This binding fashion was then further supported by an X-ray crystal structural study of the complex. Equimolar amounts of (+)-**A** and $Rh(cod)_2PF_6$ were dissolved in CH_2Cl_2. Crystals suitable for X-ray structural analysis were obtained by diffusing pentane into this solution at room temperature (Figure 3.2.8). The crystal structure was solved by Michael M-C. Lo.

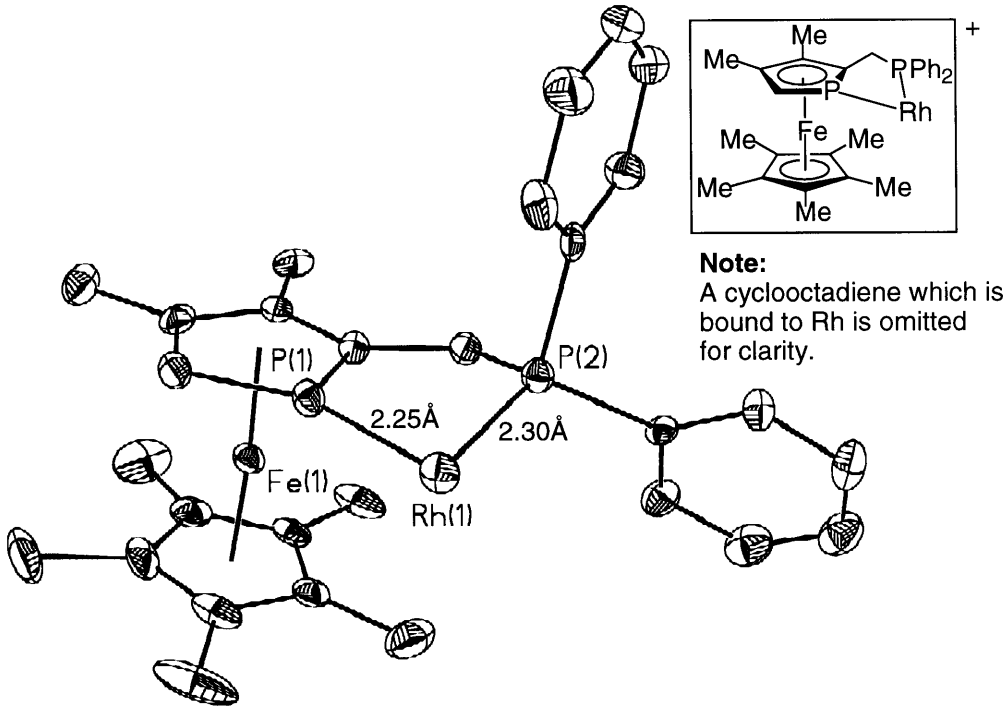

Figure 3.2.8. ORTEP illustration of the X-ray crystal structure of the complex.

The ORTEP illustration of the X-ray crystal structure unambiguously corroborates the bidentate binding mode of the phosphaferrocene **A**. The Rh-P(1) distance is 2.25 Å. The Rh-P(2) distance is 2.30 Å. The shorter bond between Rh and the sp^2 phosphorus indicates that this sp^2 phosphorus is a very strong binding atom.

We propose that this shorter bond is partially due to this phosphorus' capacity for π back bonding from Rh.

Although the crystallographic information itself does not offer much insight into the mechanism of the reaction or the origin of selectivity, it does give us enough evidence to state that the phosphaferrocene **A** is acting as a chelating ligand to Rh. As our primary research focus is not mechanistic study, we speculate that the mechanism of this reaction is analogous to Halpern's finding.

In summary, we have demonstrated that phosphaferrocenes incorporating both an sp^2 and sp^3 hybridized phosphorus can act as effective chiral ligands in the enantioselective hydrogenation of dehydroamino acids. Although the enantioselectivities of our system are somewhat worse than the best reported in the literature, it is by far the first example of applying planar-chiral phosphorus heterocycles to asymmetric catalysis. The phosphaferrocene **A** has only one kind of chirality — planar chirality. Moreover, it does not bear the ubiquitous C_2 symmetry. Our success marks the beginning of active research in discovering novel and versatile phosphine ligands in the pool of planar-chiral phosphorus heterocycles such as phosphaferrocenes.

As mentioned in Chapter 2, phosphaferrocene **A** is only one of the chelating phosphines we have synthesized in enantiopure form. Dicyclohexylphosphino phosphaferrocene **B** resembles **A** structurally. With the phenyl groups of **A** replaced by bulkier and more electron rich cyclohexyl groups, we anticipated seeing different levels of enantioselectivity in the hydrogenation reactions. **B** turns out to be a worse ligand than **A** in this reaction (Figure 3.2.9). However, the difference in enantioselectivity is very small.

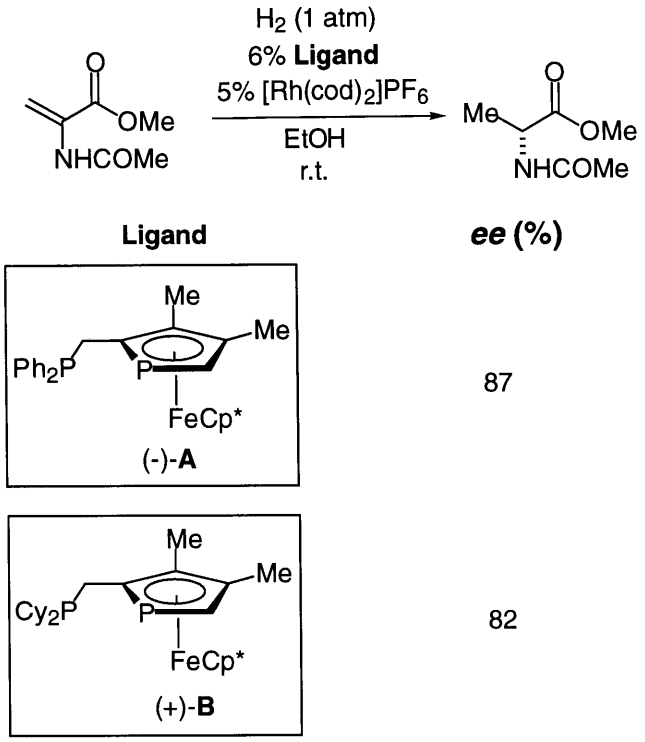

Figure 3.2.9. Comparison of two phosphaferrocenes **A** and **B** in the asymmetric hydrogenation.

In the asymmetric hydrogenation of dehydroamino acids alone, we could have continued to investigate (*E*)-acyldehydroamino acids as well as β,β-disubstituted dehydroamino acids as another two potential classes of substrates. Relatively little success has been reported in these two cases.[20,22] However, as our mission was not to perfect this reaction but rather to use this reaction as a initial test, we were less inclined to perfect this reaction with our system than to investigate the versatility and generality of this type of ligands in other less investigated reactions.[23] The next reaction we explored was Rh(I) catalyzed hydrogenation of aryl enamides. The remarkable success of **A** in hydrogenation of enamides will be discussed in Section 3.3.

Experimental

General

^1H nuclear magnetic resonance spectra were recorded on a Varian Unity 300 NMR spectrometer at ambient temperature and are referenced to residual solvent downfield from tetramethylsilane. ^1H NMR data are reported as follows: chemical shift (δ scale), multiplicity (br = broad, s = singlet, d = doublet, t = triplet, q = quartet, quint = quintet, and m = multiplet), coupling constant (Hz), and integration.

^{31}P NMR spectra were obtained on a Varian Unity 300 NMR spectrometer (121 MHz) and are referenced to external 85% H_3PO_4 (δ 0).

THF, Et_2O, and benzene were distilled from sodium-benzophenone ketyl. CH_2Cl_2 was distilled from CaH_2. Anhydrous EtOH (Aldrich) was used as received.

Grade V hydrogen (Middlesex Gases Technologies, Inc.) was used as received. All reagents were purchased from commercial suppliers and used as received, unless otherwise noted. All dehydroamino acids were purchased or prepared by literature procedures.[24-26]

All reactions were performed under nitrogen using either a dry box or standard Schlenk techniques.

Hydrogenation of Olefins

All yields and enantiomeric excesses reported are the average of ≥2 runs.

General Procedure for Asymmetric Hydrogenation. A 100 mL Schlenk tube was charged with substrate (0.22 mmol), (-)-**A** (6.7 mg, 0.013 mmol), $Rh(cod)_2PF_6$[27] (5.1 mg, 0.011 mmol), and anhydrous EtOH (6.0 mL). After three vacuum/H_2-refill

cycles, the valve to the Schlenk tube was closed. The reaction mixture was then stirred for 12 hours at r.t., at which time TLC indicated that all of the starting material had been consumed. The reaction mixture was concentrated and then passed through a short column (50:50 EtOAc:hexane). The ee was determined by chiral GC.

Determination of Enantiomeric Excess. Alltech Chirasil-VAL GC column (25 m x 0.25 mm; R enantiomers elute faster than S enantiomers). Racemic products were prepared by catalytic hydrogenation.

***N*-acetylalanine methyl ester** (90 °C isothermal for 4 min, followed by an increase of 4 °C/min to 180 °C) t(*R*) = 9.63 min; t(*S*) = 10.23 min.

***N*-acetylphenylalanine methyl ester** (160 °C, isothermal) t(*R*) = 12.38 min; t(*S*) = 12.86 min.

***N*-acetyl-*p*-methoxyphenylalanine methyl ester** (190 °C, isothermal) t(*R*) = 10.65 min; t(*S*) = 10.84 min.

***N*-acetyl-*p*-chlorophenylalanine methyl ester** (190 °C, isothermal) t(*R*) = 8.45 min; t(*S*) = 8.64 min.

***N*-acetyl-*p*-nitrophenylalanine methyl ester** (200 °C, isothermal) t(*R*) = 13.08 min; t(*S*) = 13.31 min.

Methyl 2-(*N*-acetylamino)butanoate (90 °C isothermal for 4 min, followed by an increase of 4 °C/min to 180 °C) t(*R*) = 11.95 min; t(*S*) = 12.50 min.

Methyl 2-(*N*-acetylamino)pentanoate (90 °C isothermal for 4 min, followed by an increase of 4 °C/min to 180 °C) t(*R*) = 14.64 min; t(*S*) = 15.14 min.

***N*-Acetylleucine methyl ester** (90 °C isothermal for 4 min, followed by an increase of 4 °C/min to 180 °C) t(*R*) = 15.98 min; t(*S*) = 16.57 min.

Assignment of Absolute Configuration. The absolute configurations were established through comparison of the sign of the optical rotation of our reaction products with rotations reported in the literature. On the Alltech Chirasil-VAL GC column, R enantiomers elute faster than S.

(*S*)-*N*-Acetylalanine methyl ester: $[\alpha]^{23}_D$ = -91.7° (c = 2.0, H_2O).[28]

(*S*)-*N*-Acetylphenylalanine methyl ester: $[\alpha]^{20}_D$ = +16.4° (c = 2.0, MeOH).[29]

(*S*)-*N*-Acetyl-*p*-methoxyphenylalanine methyl ester: $[\alpha]_D$ = +26.3° (c = 0.50, EtOH).[30]

(*S*)-*N*-Acetyl-*p*-chlorophenylalanine methyl ester: assigned by analogy.

(*S*)-*N*-Acetyl-*p*-nitrophenylalanine methyl ester: assigned by analogy.

(*S*)-Methyl 2-(*N*-acetylamino) butanoate: $[\alpha]^{25}_D$ = -75.1° (c = 2.2, H_2O).[31]

(*R*)-Methyl 2-(*N*-acetylamino)pentanoate: $[\alpha]^{25}_D$ = -19.0° (c = 1.0, $CHCl_3$).[22]

(*S*)-*N*-Acetylleucine methyl ester: $[\alpha]^{17}_D$ = -42.0° (c = 3.3, MeOH).[32]

X-Ray Crystallographic Study

X-ray Crystal Structure of Rh(I)-(+)-A Complex.

See Figure 3.2.8 for its ORTEP representation.

Equimolar amounts of (+)-**A** and $Rh(cod)_2PF_6$ were dissolved in CH_2Cl_2. Crystals suitable for X-ray structural analysis were obtained by diffusing pentane into this solution at room temperature.

Tables **1-5** (See Appendix I) provide the full crystallographic data for the X-ray structure.

3.3. Highly Enantioselective Hydrogenation of Aryl Enamides Catalyzed by a Rh(I)-Phosphaferrocene Complex.

Background

Asymmetric hydrogenation of aryl enamides has not been as thoroughly investigated as that of dehydroamino acids. The products of this reaction - optically active aryl-alkyl amines - constitute an important class of compounds which have frequently been employed as chiral auxiliaries, resolving agents and intermediates in natural product synthesis.[33] The broad utility of α-1-alkylaryl amine derivatives has stimulated relentless pursuit of practical asymmetric routes to these compounds. In this regard, catalytic asymmetric reduction of C=N or C=C double bonds potentially could provide an efficient and convenient route to many chiral amines. Yet only limited success has been achieved along these lines of research.[2] While very high enantioselectivities have been attained in the hydrogenation of dehydroamino acids, the development of similarly effective catalysts for asymmetric hydrogenation of aryl enamides has remained a challenging objective. In 1996, Burk and coworkers reported an important breakthrough on this reaction with Rh catalysts containing DuPHOS and BPE ligands (Figure 3.3.1).[5]

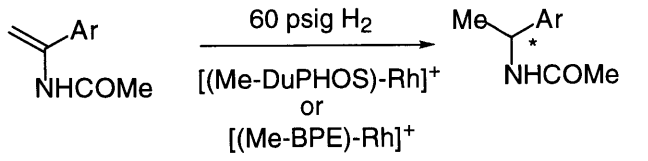

Ar	optimum ligand	% ee (confign)
C_6H_5	(*R, R*)-Me-BPE	95.2 (*R*)
p- CH_3-C_6H_4	(*R, R*)-Me-BPE	96.5 (*R*)
p- CH_3O-C_6H_4	(*R, R*)-Me-BPE	95.3 (*R*)
2,6-$F_2C_6H_3$	(*R, R*)-Me-BPE	97.8 (*R*)
m- CH_3-C_6H_4	(*S,S*)-DuPHOS	94.9 (*S*)

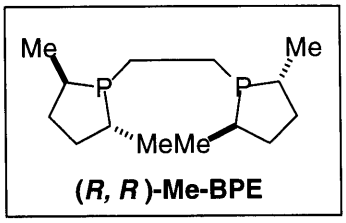

(*R, R*)-Me-BPE

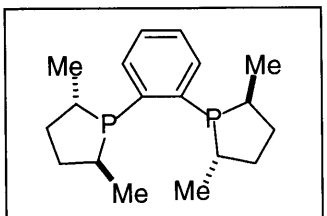

(*S,S*)-Me-DuPHOS

Figure 3.3.1. Asymmetric hydrogenation catalyzed by Rh(I)-Me-DuPHOS or Rh(I)-Me-BPE complexes.

The Me-DuPHOS-Rh and Me-BPE-Rh catalysts are capable of tolerating β-substituents on the aryl enamides. They have also been reported to possess the unique feature of hydrogenating mixtures of (*E*)- and (*Z*)-enamides. However, during the course of our investigation, we discovered that their presumed mixtures of (*E*)- and (*Z*)-enamides were actually rotamers of (*Z*)-enamides only. Therefore, there has been essentially no report of hydrogenation of mixtures of (*E*)- and (*Z*)-enamides.

Since then, several groups have reported significant success in this reaction. For example, Albert S. C. Chan's chiral bisaminophosphine ligands work very well with unsubstituted aryl enamides (Figure 3.3.2).[6]

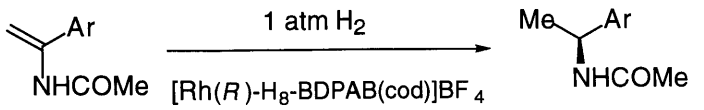

Ar	% ee
C_6H_5	96.8
p- CH_3-C_6H_4	97.0
p- CF_3-C_6H_4	99.0
m- CH_3-C_6H_4	94.9

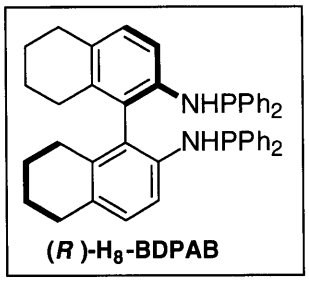

Figure 3.3.2. Asymmetric hydrogenation catalyzed by Rh-H_8-BDPAB complexes.

Most recently, Xumu Zhang and his group reported not only a highly enantioselective hydrogenation of simple aryl enamides but also practical syntheses of β-amino alcohols by hydrogenation of aryl enamides bearing a MOM-protected β-hydroxy group (Figure 3.3.3).[7,34]

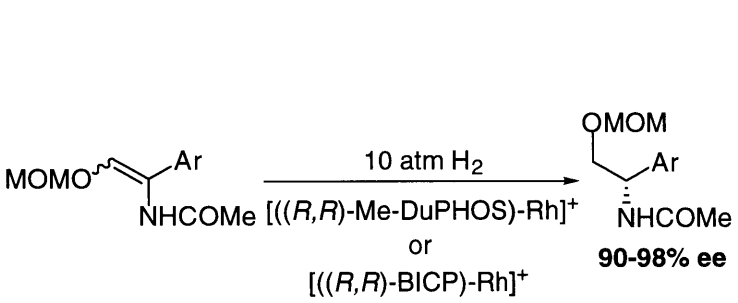

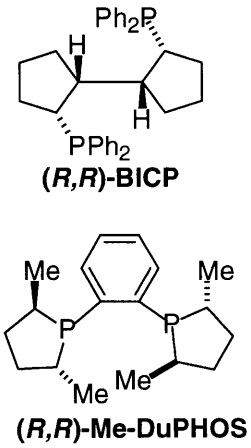

Figure 3.3.3. Practical syntheses of β-amino alcohols by hydrogenation of aryl enamides bearing a MOM-protected β-hydroxy group.

The overall success of chiral bisphosphines in the hydrogenation of aryl enamides is still quite limited. Many chelating phosphines which work well in the hydrogenation of dehydroamino acids give poor or mediocre performances in the

hydrogenation of enamides (for example, BINAP).[5] There are still drawbacks with reported catalyst systems (limited substrate scope, high hydrogen pressure, etc). There has been essentially no mechanistic study to elucidate the origin of enantioselectivity. It is clearly a reaction worth investigating and perfecting as there is plenty of room for improvement.

Aryl enamides are fairly electron-rich substrates compared to dehydroamino acids. As phosphaferrocenes in general are less electron-rich than generic tertiary phosphines, we speculated that they might prove to be superior to conventional phosphines for the hydrogenation of aryl enamides.

Results and Discussion

The phosphaferrocene we initially chose to study was again **A** due to its success detailed in the previous section (Section 3.2). As the reaction is also a Rh(I) catalyzed hydrogenation, our initial test reaction was run under the same condition optimized for hydrogenation of dehydroamino acids (Section 3.2). We were delighted to observe a moderate 75% ee. Inspired by the highly enantioselective hydrogenation of simple ketones catalyzed by Rh-PennPhos complex in the presence of additives (Figure 3.1.4),[9] we decided to screen the effects of some additives (Figure 3.3.4).

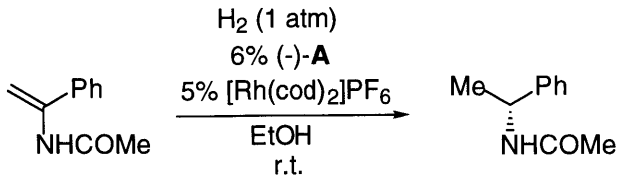

Additive

Additive	% ee
KBr	**96**
Et_3N	10
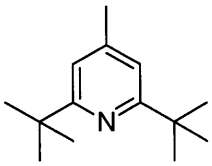	68
NaOMe	~ 0
No additive	75

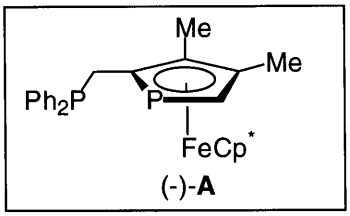

Figure 3.3.4. The effects of additives on enantioselectivity.

We discovered that while most additives decreased the enantiomeric excess, KBr as an additive greatly enhanced the ee to 96%. It is possible that the addition of KBr results in a new catalytic species which is more selective or more reactive. The role of KBr in the reaction will be further discussed later in this section. Coordinating solvents again proved to be the solvents of choice (Figure 3.3.5). In the presence of KBr, the levels of enantioselectivity are essentially comparable in solvents such as THF, EtOH and MeOH. Lower ee was also observed in THF in the absence than in the presence of KBr.

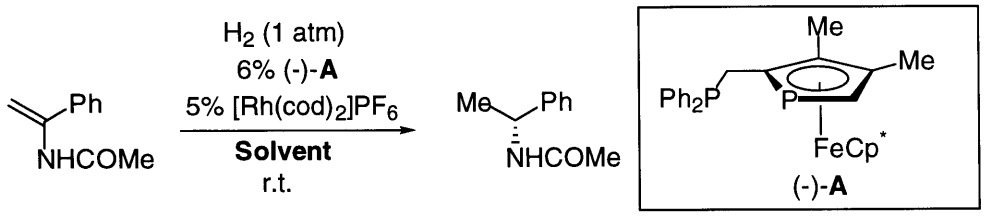

In the presence of KBr		In the absence of KBr	
Solvent	% ee	**Solvent**	% ee
EtOH	**96**	EtOH	75
MeOH	93	THF	78
THF	92		

Figure 3.3.5. Solvent effects on enantioselectivity.

The effects of counterions were investigated briefly (Figure 3.3.6). In the absence of KBr, $Rh(cod)_2BF_4$ is clearly a better choice than $Rh(cod)_2PF_6$. However, in the presence of KBr, they are equally selective. As the addition of KBr apparently eliminated the difference between the two Rh(I) species, we speculated that there might be some counterion-bromide exchange. This hypothesis could help explain the elimination of difference between the two Rh(I) sources in the hydrogenation reactions. More detailed discussion on KBr will follow later in this section.

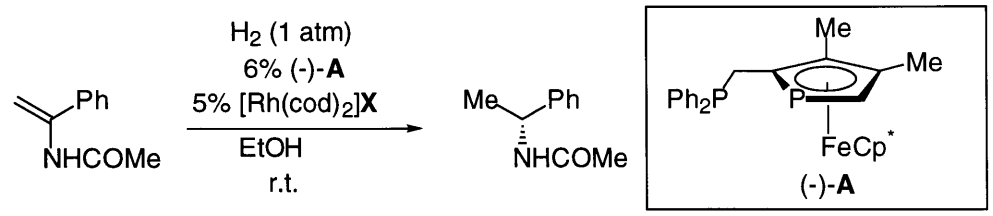

In the presence of KBr		In the absence of KBr	
X	% ee	**X**	% ee
PF_6	96	PF_6	75
BF_4	95	BF_4	85

Figure 3.3.6. Counterion effects both in the presence and in the absence of KBr.

Continuing the optimization effort, we varied the reaction temperature from 0 to 50 °C and observed essentially the same levels of enantioselectivity during the whole temperature range. We did not observe any dramatic effects of temperature change either in the hydrogenation of dehydroamino acids (see Section 3.2). Increasing the H_2 pressure, however, resulted in worse selectivity. In Section 3.2, the H_2 pressure does not play an important role in the hydrogenation of dehydroamino acids. Finally, we ran the hydrogenation of dehydroamino acids in the presence of KBr and observed no change in enantiomeric excesses. KBr which is the key to high selectivity in hydrogenation of aryl enamides proved to be utterly useless in hydrogenation of dehydroamino acids. Overall, there is some similarity between the two types of hydrogenations utilizing our Rh-phosphaferrocene system. On the other hand, the phenomena mentioned above indicate that the hydrogenation of aryl enamides is fundamentally different enough not to be a mere natural extension of that of dehydroamino acids.

To render the reaction more practical and economical, we experimented with lowering the catalyst loading. We found out that a catalyst loading as low as 2.5% still generates the same level of enantioselectivity. For experimental ease and accuracy, we still ran all the substrates under 5% catalyst loading.

Under the optimized reaction condition, a wide array of substrates are reduced with excellent enantioselectivities and quantitative yields (Figure 3.3.7).

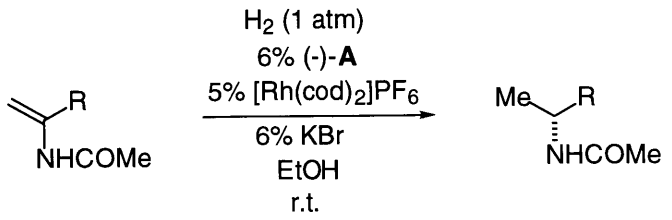

entry	R	% ee	Yield (%)
1	Ph	96	93
2	2,6-F_2-C_6H_3	99	98
3	*p*-CF_3-C_6H_4	95	95
4	*p*-CH_3-C_6H_4	95	97
5	*p*-CH_3O-C_6H_4	92	92
6	2-thienyl	95	96
7	2-furanyl	90	93

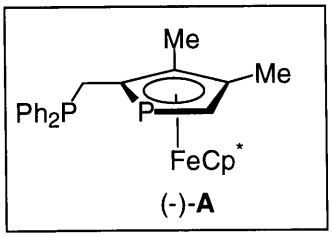

Figure 3.3.7. Enantioselective hydrogenation of unsubstituted aryl enamides catalyzed by Rh-(-)-**A**.

As illustrated in Figure 3.3.7, the enantioselectivities are uniformly very high. Thus, our hydrogenation process provides a convenient route to a variety of highly enantiomerically-enriched ring-substituted α-phenethylamine derivatives. Substitution at the para position of the parent enamide (Entries 2-5) does not greatly influence the enantioselectivity. However, a slight substituent electronic effect on the ee's was observed. It seems that electron-poor systems furnish slightly higher ee's than electron-rich systems. It is important to mention that this slight electronic effect is exactly the opposite of what was observed in the hydrogenation of dehydroamino acids. Dehydroamino acids in general are much less electron-rich than enamides. The fact that we observed best results with electron-poor enamides and electron-rich dehydroamino acids indicates that electronic effects play an important role in the enantioselectivity. The phosphaferrocene **A** is less electron-

rich than most generic chelating phosphines such as DuPHOS and BINAP. It is reasonable to predict that **A** works better with electron-rich substrates in general. This prediction is fairly consistent with our finding in the hydrogenations of dehydroamino acids and enamides. Enamides which are more electron-rich are much better substrates than dehydroamino acids. In the case of electron-poor dehydroamino acids, more electron-rich substrates are better substrates. However, it is not easy to rationalize why we observed the opposite substituent effect in the enamide reduction. It is possible that the best electronic match between substrate and catalyst complex is found at the electron-poor aryl enamide such as entry 2 in Figure 3.3.7.

Heteroaryl enamides (Entries 6 and 7) are also reduced with high enantioselectivities. All the reactions proceed smoothly at room temperature. Within 12 hours, the conversion is complete with all substrates. When (+)-**A** is used, we obtain the (*S*)-enantiomer.

Efforts were taken to understand the role of KBr. we found out that as long as the loading of KBr is equal to or higher than 6%, the enantioselectivies are essentially the same. This finding eliminated the possibilities that KBr might be binding to the substrates or the aggregation states of the substrates might be affected by the presence of KBr directly leading to higher selectivities.

In order to confirm our belief that it is the bromide rather than the potassium ion which is the reactive component in changing the enantioselectivity, we ran the hydrogenations of *N*-Acetyl-1-(2-furyl)ethenamine in the presence of KCl and KI as well (Figure 3.3.8). While the addition of KCl increased the ee to approximately the same level, the presence of KI essentially shut down the reactivity. This gave us further proof that the halides probably react with the catalyst complex to some extent to generate a new species.

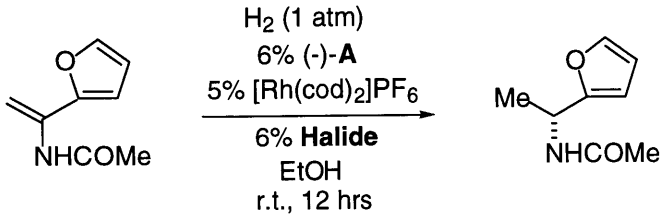

Entry	Halide	% ee	Conversion (%)
1	KCl	88	100
2	KBr	90	100
3	KI	N/A	trace

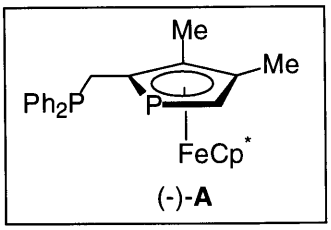

Figure 3.3.8. Halide effects on the enantioselectivity.

^{31}P NMR study was then undertaken to verify the assumption. When KBr was added to [Rh(cod)(**A**)]$^{+}PF_6^{-}$ (see Figure 3.2.8 for its X-ray structure), we observed some new species as well as the old resonances corresponding to [Rh(cod)(**A**)]$^{+}PF_6^{-}$. This implies that it would be almost impossible to obtain a crystal structure of this new species as the solution is a mixture of both the new species and [Rh(cod)(**A**)]$^{+}PF_6^{-}$. The ^{31}P NMR of the new species resembles that of the 1:2 mixture of $[Rh(cod)Cl]_2$ and **A**. This led us to speculate that the new species might be a dimeric Rh species (Figure 3.3.9). One way to rationalize the increase of ee in the cases of KCl and KBr is that the dimeric species formed are much more reactive and selective than the cationic Rh species. In the case of KI, maybe the new species is completely inactive.

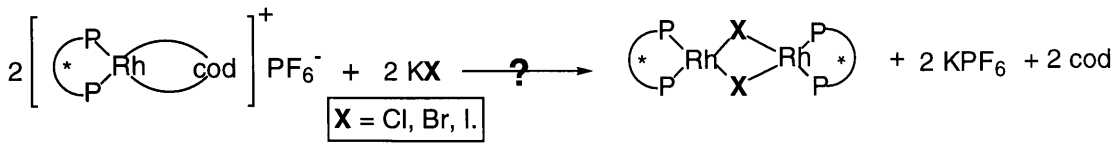

Figure 3.3.9. One tentative hypothesis about the role of KBr.

If the hypothesis were correct, we should have been able to observe the same level of enantioselectivity using $[Rh(cod)Cl]_2$ instead of $Rh(cod)_2PF_6$ as the Rh source. However, the poor enantioselectivities demonstrated by $[Rh(cod)Cl]_2$ and $[Rh(cod)Cl]_2$/KBr (Figure 3.3.10) indicate that the new catalytic species is after all not the dimeric species hypothesized in Figure 3.3.9 despite the similarity between their ^{31}P NMR spectra. It is clear that the halide reacts with the catalyst complex to generate a new species which might involve halide bridges. Yet the exact nature of the new catalytic species is still unclear. As detailed mechanistic study is not the focus of our research interest, we have not pursued any further in elucidating the mechanism for the time being. We are confident that given enough time a better understanding of the role of KBr will be attained should the need arise.

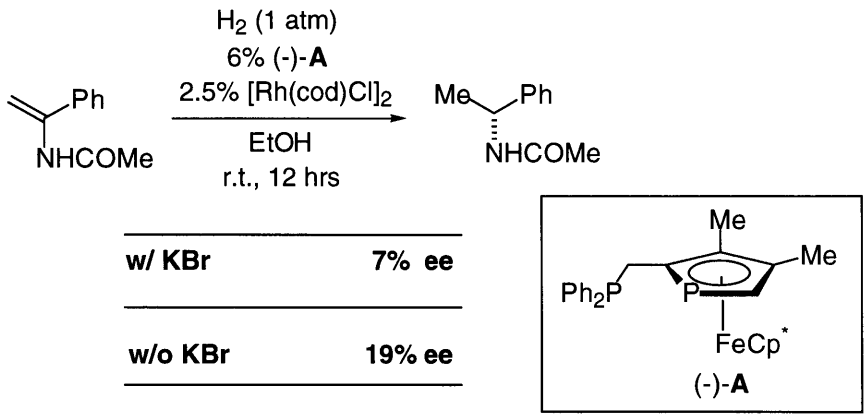

Figure 3.3.10. Disproof of the hypothesis of the dimeric Rh species as the new catalytic species.

β-substituted aryl enamides represent a natural expansion of the substrate scope. As mentioned earlier, Mark Burk and his group followed by Xumu Zhang and his group reported the hydrogenation of mixtures of (*Z*)- and (*E*)-β-substituted aryl enamides with excellent enantioselectivities.[5,7] However, during the course of our study, we discovered that the supposed mixture of (*Z*)- and (*E*)-isomers were the

two rotamers of only (Z)-isomers (Figure 3.3.11). This conclusion was corroborated by literature[35] as well as our variable temperature NMR and NOE studies.[36] Following literature procedures,[5] we obtained both (*Z*)- and (*E*)-isomers which were separated by column chromatography (with the exception of the synthesis of *N*-acetyl-1-(2-thienyl)propenamine in which we only isolated the (*Z*)-isomer. The (*E*)-isomers were then fully characterized and hydrogenated to give exactly the same product as the hydrogenation product of the (*Z*)-isomers.

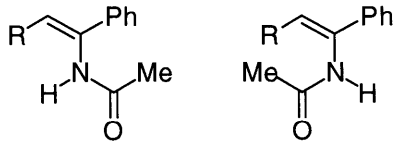

Figure 3.3.11. The two rotamers of a (*Z*)-β-substituted aryl enamide.

The results of our hydrogenation of β-substituted aryl enamides are illustrated in Figure 3.3.12. As the substrates are more sterically hindered substrates, the reactions are run at elevated temperatures (55-60°C) to ensure 100% conversion over 12 hours. The enantioselectivities are excellent. Both (*Z*)- and (*E*)-isomers are hydrogenated with similarly high ee's which marks the first time that both isomers have been hydrogenated to the same enantiomer with excellent enantioselectivity. This finding is particularly important in that it obviates the need to separate the isomers prior to hydrogenation.

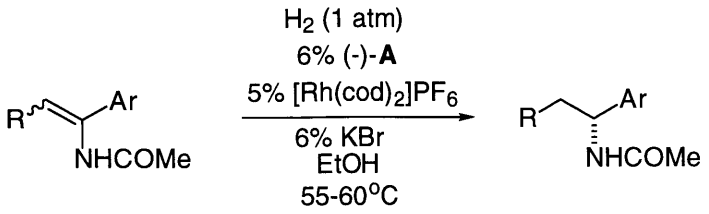

Substrate		% ee	Yield (%)
Me, Ph, NHCOMe	Z-isomer	89	100
	E-isomer	91	100
Et, Ph, NHCOMe	Z-isomer	90	92
	E-isomer	92	98
Me, S, NHCOMe		95	95

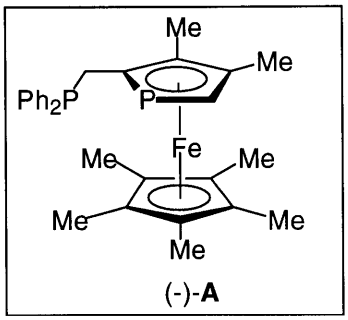

Figure 3.3.12. Asymmetric hydrogenation of β-substituted aryl enamides.

There are some limitations of our system in the hydrogenation of β-substituted aryl enamides (Figure 3.3.13). For example, when the substituent at the β-position is as bulky as isopropyl, we observe incomplete reaction (even at elevated temperatures) as well as low ee's. When the substituent is a phenyl group which is bulky as well as deactivating, we observe no reactivity whatsoever.

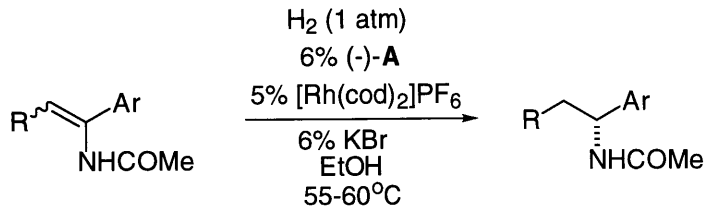

Substrate		% ee	conv.(%)
i-Pr, Ph, NHCOMe	*Z*-isomer	22	20
	E-isomer	45	18
Ph, Ph, NHCOMe		N/A	0

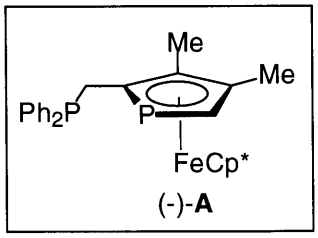

Figure 3.3.13. Limitations of our asymmetric hydrogenation of β-substituted aryl enamides.

The acetyl groups of the hydrogenated products need to be cleaved as optically aryl-alkyl amines are in essence the desired products of the hydrogenation reactions. It generally requires a strongly acidic condition to cleave the acetyl group. Knowing that there has been no literature precedent of hydrogenations of enamides bearing protecting groups other than the acetyl group, we attempted to synthesize some enamides with relatively labile protecting groups such as ^{t}Boc, Cbz, Fmoc and CF_3CO. However, we did not encounter any success using the generic method of preparation of aryl enamides (Figure 3.3.14). In all the reactions, we obtained acetophenone indicating that either the protected imines did not form or hydrolysis (resulting in acetophenone) was much more facile than tautomerization (resulting in the protected enamides).

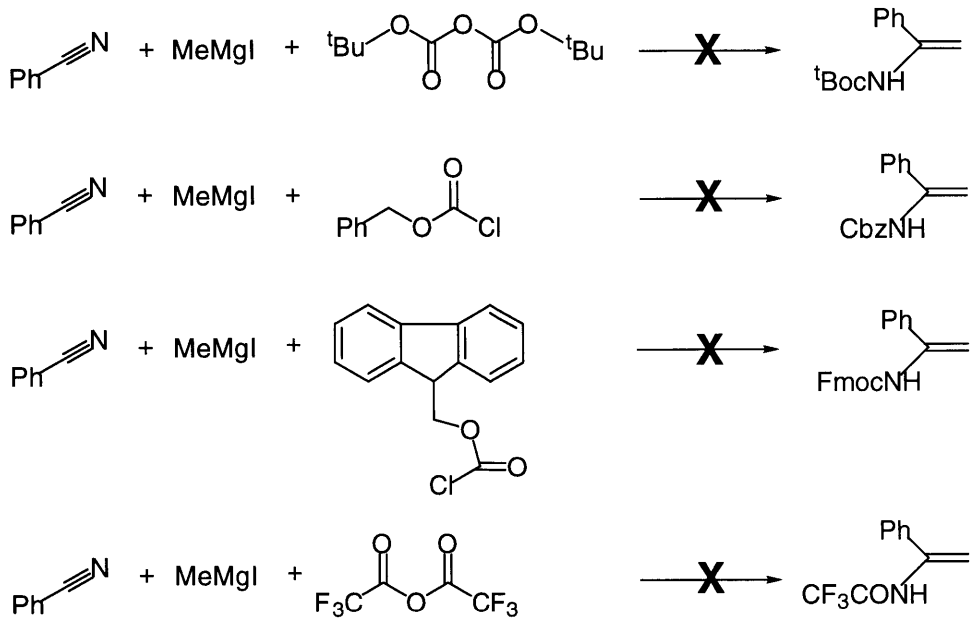

Figure 3.3.14. Failed syntheses of aryl enamides bearing labile protecting groups using the generic preparative method.

Moreover, using a recently reported procedure in synthesizing protected enamides,[37] we again failed to obtain the desired products (Figure 3.3.15). We henceforth speculate that aryl enamides bearing labile protecting groups are not stable for practical purpose. *N*-trifluoroacetyl-1-phenylethenamine has been reported to undergo facile hydrolysis to generate acetophenone.[38] Therefore it has not been isolated or fully characterized. It is possible that the other aryl enamides I attempted to synthesize in Figure 3.3.14 have the same problem with stability.

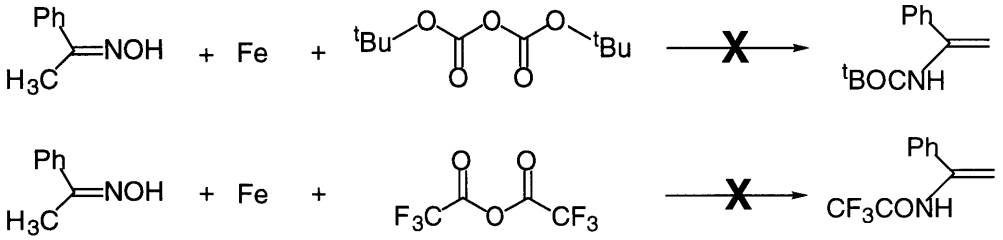

Figure 3.3.15. Failed syntheses of aryl enamides bearing labile protecting groups using the recently reported method.

We were also interested in aryl enamides bearing a MOM-protected β-hydroxy group. The products are β–amino alcohols which have been extensively used in asymmetric synthesis. Figure 3.3.3 illustrates the first enantioselective hydrogenation of this type of substrates by Xumu Zhang and his group.[34] However, our catalyst complex proved to be inactive for the hydrogenation of these enamides. We speculate that the additional oxygens in the substrate could bind to Rh which would result in an inactive metal complex. As sp^2 hybridized P-Rh bond is probably weaker than the sp^3 hybridized P-Rh bond, it is reasonable that our catalyst system has less tolerance for substrates with additional binding atoms than BICP and DuPHOS.

When another chelating phosphaferrocene **B** was used, we observed essentially racemates in the hydrogenation (Figure 3.3.16). The difference between **A** and **B** in this reaction is much bigger than that in the hydrogenation of dehydroamino acids (see Figure 3.2.9 for comparison).

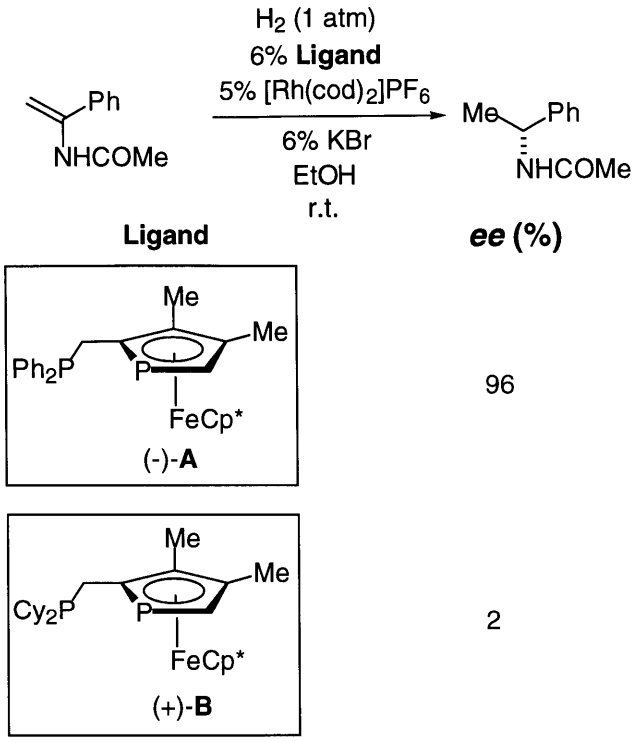

Figure 3.3.16. Comparison of **A** and **B** in the hydrogenation of aryl enamides.

In summary, our Rh-**A** complex has proved to be a remarkable catalytic system for the enantioselective hydrogenation of aryl enamides. While our ee's from the hydrogenation of dehydroamino acids are somewhat worse than the best reported in literature, our results in the hydrogenation of aryl enamides essentially match or exceed the state of the art. Although several groups claimed to have investigated hydrogenation of isomeric mixtures of β-substituted aryl enamides, we have been the first to report high enantioselectivities in the hydrogenation of both (*Z*)- and (*E*)-isomers which have been unambiguously identified. Despite some limitations of our catalyst system, it is still one of the best in obtaining optically active aryl-alkyl amines by hydrogenation. Of all the bisphosphines utilized in hydrogenations of enamides, **A** is the only phosphine that incorporates an sp^2 phosphorus and the only one that does not bear C_2-symmetry. This finding strongly suggests that sp^2 phosphorus-based compounds can act as superb ligands in metal-

catalyzed reactions. In certain reactions such as hydrogenation of enamides, they prove to be superior to generic tertiary phosphines. In addition, our finding suggests that C_2-symmetry is not necessary for high enantioselectivities in Rh(I) catalyzed hydrogenations.

Experimental

General

^1H nuclear magnetic resonance spectra were recorded on a Varian Unity 300 NMR spectrometer at ambient temperature and are referenced to residual solvent downfield from tetramethylsilane. ^1H NMR data are reported as follows: chemical shift (δ scale), multiplicity (br = broad, s = singlet, d = doublet, t = triplet, q = quartet, quint = quintet, and m = multiplet), coupling constant (Hz), and integration.

All ^{13}C NMR spectra were obtained with complete proton decoupling on a Varian Unity 300 NMR spectrometer and are referenced to solvent downfield from tetramethylsilane.

Infrared spectra were obtained on a Perkin-Elmer 1600 FT-IR spectrophotometer (cm^{-1}). Optical rotations were obtained using a Perkin Elmer Model 241 polarimeter.

Anhydrous EtOH (Aldrich) and KBr (Mallinkrodt) were used as received.

Grade V hydrogen (Middlesex Gases Technologies, Inc.) was used as received. All reagents were purchased from commercial suppliers and used as received, unless otherwise noted. All aryl enamides substrates were prepared by reacting the arylnitrile with a *Grignard* reagent, then acetylating the imine intermediate and treating with methanol. Chiral phosferrocene ligand was prepared as previously described.

Synthesis of Aryl Enamide Substrates

All the unsubstituted aryl enamide substrates were prepared according to literature procedures.[5] The β-substituted aryl enamides reported by Mark J. Burk *et al* to be E/Z mixtures are rotamers of the *Z* isomers only.[35] The *E* isomers of *N*-acetyl-1-phenylpropenamine and *N*-acetyl-1-phenylbutenamine were obtained together with the *Z* isomers in the synthesis procedure reported by Mark J. Burk *et al* [22]and were purified by column chromatography. They eluted prior to the *Z* isomers.

(*E*)-*N*-Acetyl-1-phenylpropenamine.

^{1}H NMR (300 MHz, $CDCl_3$): δ 1.70 (d, *J* = 7.2, 3H), 2.03 (s, 3H), 6.33 (q, *J* = 7.2, 1H), 6.62 (s, 1H), 7.35 (m, 5H); ^{13}C NMR (75 MHz, $CDCl_3$): δ 13.8, 23.7, 115.4, 127.7, 128.1, 128.7, 134.3, 136.6, 169.3; IR (KBr): 3274, 3182, 3060, 2967, 1660, 1600, 1558, 1440, 1378, 1282; HRMS: Calcd for $C_{11}H_{13}NO$: 175.0997; found: 175.0995.

(*E*)-*N*-Acetyl-1-phenylbutenamine.

^{1}H NMR (300 MHz, $CDCl_3$): δ 0.97 (t, *J* = 7.5, 3H), 1.89 (s, 3H), 2.04 (quint, *J* = 7.5, 2H), 6.16 (t, *J* = 7.8, 1H), 6.85 (s, 1H), 7.29 (m, 5H); ^{13}C NMR (75 MHz, $CDCl_3$): δ 15.0, 21.7, 24.2, 122.1, 127.9, 128.2, 128.6, 133.2, 136.9, 168.9; IR (KBr): 3243, 3166, 3052, 2960, 2871, 1655, 1553, 1492, 1435, 1374; HRMS: Calcd for $C_{12}H_{15}NO$: 189.1154; found: 189.1158.

(*E*)-*N*-Acetyl-1-phenyl-3-methyl-butenamine.

^{1}H NMR (300 MHz, $CDCl_3$): δ 7.31 (m, 5H), 6.71 (s, 1H), 6.16 (d, *J* = 10.5, 1H), 2.35 (m, 1H), 1.99 (s, 3H), 1.00 (d, *J* = 6.6, 6H); ^{13}C NMR (75 MHz, $CDCl_3$): δ 168.6, 137.4, 132.0, 128.7, 128.5, 128.1, 127.0, 27.8, 24.7, 23.9; IR (KBr): 3268, 3178, 3077, 2949,

2863, 1650, 1552, 1371, 1277, 1071; HRMS: Calcd for $C_{13}H_{17}NO$: 203.1310; found: 203.1308.

(*E*)-*N*-Acetyl-1,2-diphenylethenamine.

^1H NMR (300 MHz, DMF-d_7): δ 9.30 (s, 1H), 7.49 (s, 1H), 7.36 (m, 5H), 7.09 (m, 3H), 6.93 (m, 2H), 2.14 (s, 3H); ^{13}C NMR (75 MHz, DMF-d_7): δ 170.1, 138.5, 138.4, 138.1, 130.7, 129.9, 129.6, 129.4, 129.0, 126.7, 116.7, 24.7; IR (KBr): 3260, 3190, 3025, 1658, 1533, 1282, 1196, 1101, 1073, 1028; HRMS: Calcd for $C_{16}H_{15}NO$: 237.1154; found: 237.1148.

Asymmetric Hydrogenation of Aryl Enamides

All yields and enantiomeric excesses reported are the average of ≥2 runs.

General Procedures for Asymmetric Hydrogenation of Aryl Enamides. A 100 mL Schlenk tube was charged with substrate (0.22 mmol), (-)-**A** (6.7 mg, 0.013 mmol), $Rh(cod)_2PF_6$[27] (5.1 mg, 0.011 mmol), and anhydrous EtOH (6.0 mL). After three vacuum/H_2-refill cycles, the valve to the Schlenk tube was closed. The reaction mixture was then stirred for 12 hours at r.t. (55-60 °C for the β-substituted aryl enamides), at which time TLC indicated that all of the starting material had been consumed. The reaction mixture was concentrated and then passed through a short column (50:50 EtOAc:hexane). The ee was determined by chiral GC.

Determination of Enantiomeric Excess. Alltech Chirasil-VAL GC column (25 m x 0.25 mm; *R* enantiomers elute faster than *S* enantiomers). Racemic products were prepared by hydrogenation catalyzed by Pd-C.

***N*-Acetyl-1-phenylethylamine** (130 °C isothermal) t(*R*) = 16.14 min; t(*S*) = 16.65 min.

***N*-Acetyl-1-tolylethylamine** (140 °C, isothermal) t(*R*) = 16.69 min; t(*S*) = 17.24 min.

***N*-Acetyl-1-(4'-trifluoromethylphenyl)ethylamine** (140 °C, isothermal) t(*R*) = 12.20 min; t(*S*) = 12.67 min.

***N*-Acetyl-1-(4'-methoxyphenyl)ethylamine** (150 °C, isothermal) t(*R*) = 25.09 min; t(*S*) = 25.79 min.

***N*-Acetyl-1-(2-furyl)ethylamine** (95 °C, isothermal) t(*R*) = 21.83 min; t(*S*) = 22.60 min.

***N*-Acetyl-1-(2-thienyl)ethylamine** (120 °C, isothermal) t(*R*) = 22.02 min; t(*S*) = 22.81 min.

***N*-Acetyl-1-(2',6'-difluorophenyl)ethylamine** (120 °C, isothermal) t(*R*) = 12.77 min; t(*S*) = 13.18 min.

***N*-Acetyl-1-phenylpropylamine** (130 °C, isothermal) t(*R*) = 23.20 min; t(*S*) = 24.13 min.

***N*-Acetyl-1-phenylbutylamine** (130 °C, isothermal) t(*R*) = 34.27 min; t(*S*) = 35.32 min.

***N*-Acetyl-1-(2-thienyl)propylamine** (120 °C, isothermal) t(*R*) = 31.33 min; t(*S*) = 32.41 min.

Assignment of Absolute Configuration. The absolute configurations were established through comparison of the sign of the optical rotation of our reaction products with rotations reported in the literature. On the Alltech Chirasil-VAL GC column, *R* enantiomers elute faster than *S*.

(*R*)-*N*-Acetyl-1-tolylethylamine: $[\alpha]^{25}_D$ = +148° (c = 0.38, $CHCl_3$).[5]
(*S*)-*N*-Acetyl-1-phenylethylamine: $[\alpha]^{25}_D$ = -140° (c = 0.96, $CHCl_3$).[5]
(*R*)-*N*-Acetyl-1-phenylpropylamine: $[\alpha]^{25}_D$ = -138° (c = 0.11, MeOH).[5]
(*S*)-*N*-Acetyl-1-(4'-trifluoromethylphenyl)ethylamine: $[\alpha]^{25}_D$ = -75° (c = 0.12, $CHCl_3$).[5]
(*R*)-*N*-Acetyl-1-(4'-methoxyphenyl)ethylamine: $[\alpha]^{25}_D$ = +51.2° (c = 0.11, $CHCl_3$).[5]
(*S*)-*N*-Acetyl-1-(2-furyl)ethylamine: $[\alpha]^{25}_D$ = -195° (c = 0.11, $CHCl_3$).[5]
(*S*)-*N*-Acetyl-1-(2-thienyl)ethylamine: $[\alpha]^{25}_D$ = -144° (c = 0.36, $CHCl_3$).[5]
(*S*)-*N*-Acetyl-1-(2',6'-difluorophenyl)ethylamine: $[\alpha]^{20}_D$ = -88.1° (c = 0.29, $CHCl_3$).[5]
(*S*)-*N*-Acetyl-1-phenylbutylamine: $[\alpha]^{25}_D$ = -106° (c = 1.01, $CHCl_3$).[5]
(*S*)-*N*-Acetyl-1-(2-thienyl)propylamine: $[\alpha]^{25}_D$ = -148° (c = 0.14, $CHCl_3$).[5]

3.4. Further Applications of Phosphaferrocenes in Asymmetric Catalysis: Preliminary Study of Asymmetric Isomerization of Allylic Alcohols.

Background

In Sections 3.2 and 3.3, the first two successful applications of a bidendate phosphaferrocene **A** in asymmetric catalysis were discussed. While pursuing further applications of chelating phosphaferrocenes **A** and **B**, we are also interested in exploring the versatility of other phosphaferrocene derivatives synthesized in Chapter 2 (Figure 3.4.1).

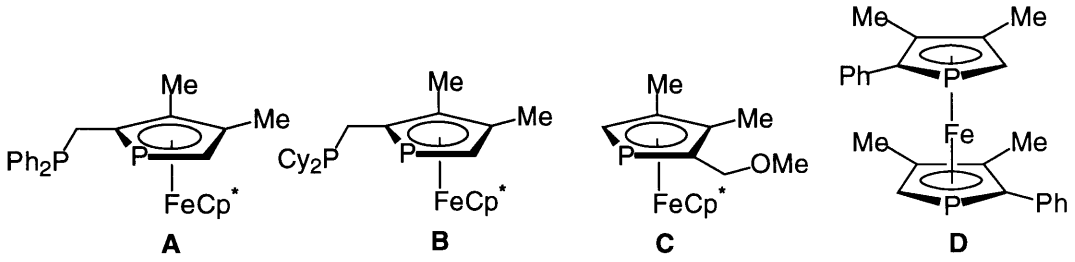

Figure 3.4.1. Optically pure phosphaferrocenes under investigation for asymmetric applications.

Both **C** and **D** were tested as catalysts in the ring-opening of epoxides in the presence of TMSCl. They were both efficient catalysts but no enantiomeric excess was observed. They both failed to behave as effective ligands in Pd-catalyzed hydrosilylation of olefins. **C** was also tried as a ligand in the Ni-catalyzed cross coupling[39] but showed no reactivity whatsoever. **A** showed 20% ee in the Rh-catalyzed hydroboration of styrenes with catecholborane.[12]

Although many reactions catalyzed by transition metal-bisphosphine complexes have reached very high enantioselectivities with certain bisphosphines, there are still some basic transformations which have yet to reach higher than 60%

ee. For example, isomerization of allylic alcohols catalyzed by Rh-BINAP has been reported with only up to 53% ee[11] (Figure 3.4.2). Optically active citronellal is a useful intermediate for the synthesis of many optically active natural products. Thus, the discovery of efficient asymmetric isomerization of allylic alcohols would open the door to the synthesis of active terpenoids.

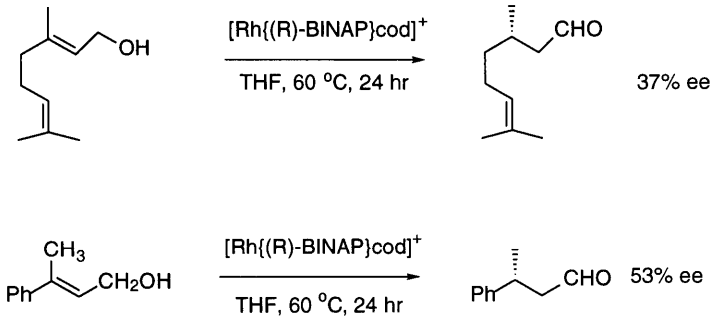

Figure 3.4.2. Best reported asymmetric isomerization of allylic alcohols.

Contrary to the dismal state of isomerization of allylic alcohols, asymmetric isomerization of allyl amines has been applied on an industrial scale to generate highly enantiopure enamines (Figure 3.4.3).[11] As hydrolysis of the enamines proceeds without racemization and produces the aldehydes, isomerization of allyl amines has been the method of choice in industry to generate the desired optically active aldehydes.

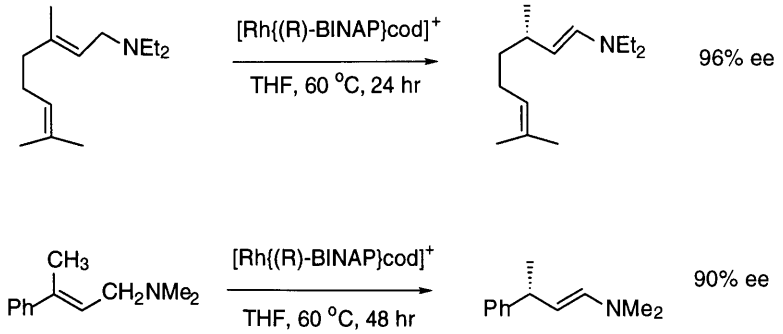

Figure 3.4.3. Asymmetric isomerization of allyl amines catalyzed by $[Rh(BINAP)L_n]ClO_4$.

Since the desired products from asymmetric isomerization of allyl amines are actually aldehydes, there is a strong incentive to improve the unsatisfactory state of the art of asymmetric isomerization of allylic alcohols. As chiral phosphaferrocenes are electronically and sterically different from generic bisphosphines such as BINAP, it is possible that reactions which fail to behave well with generic bisphosphines might meet with better success with phosphaferrocenes. The proposed mechanism of isomerization of allylic alcohols is illustrated in Figure 3.4.4.[40]

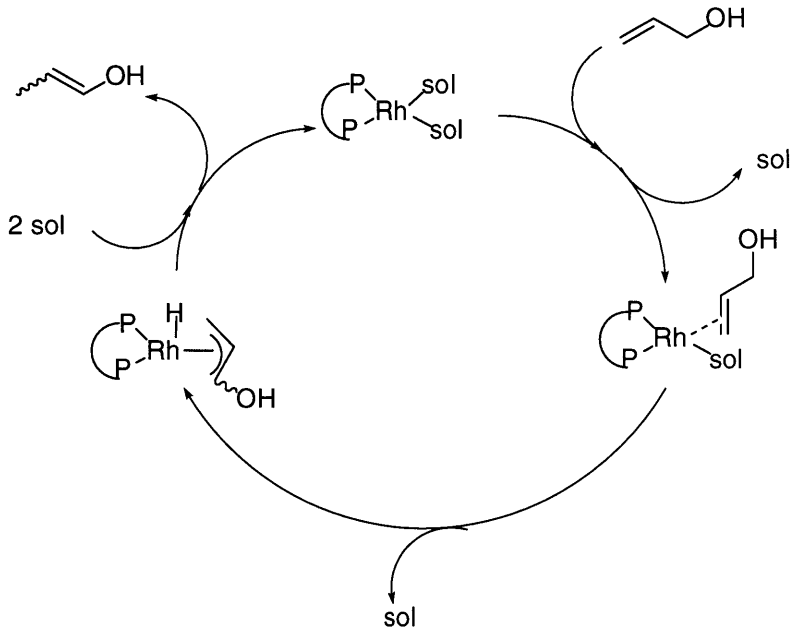

Figure 3.4.4. Postulated mechanism of double-bond migration in the formation of enols from allylic alcohols (sol = solvent).

Results and Discussion

Our initial test of phosphaferrocene **A** yielded very disappointing results. No reaction was observed after 24 hours of heating (Figure 3.4.5). We postulated that in our catalyst system cyclooctadienes could be too competitive as ligands to Rh in the

presence of allylic alcohols. Our hypothesis turned out to be correct. When we first hydrogenated the cyclooctadienes to make the $[Rh(solvent)_2$**(-)-A**$]^+$, we observed a fairly clean reaction and a promising enantiomeric excess of 58% (Figure 3.4.5).

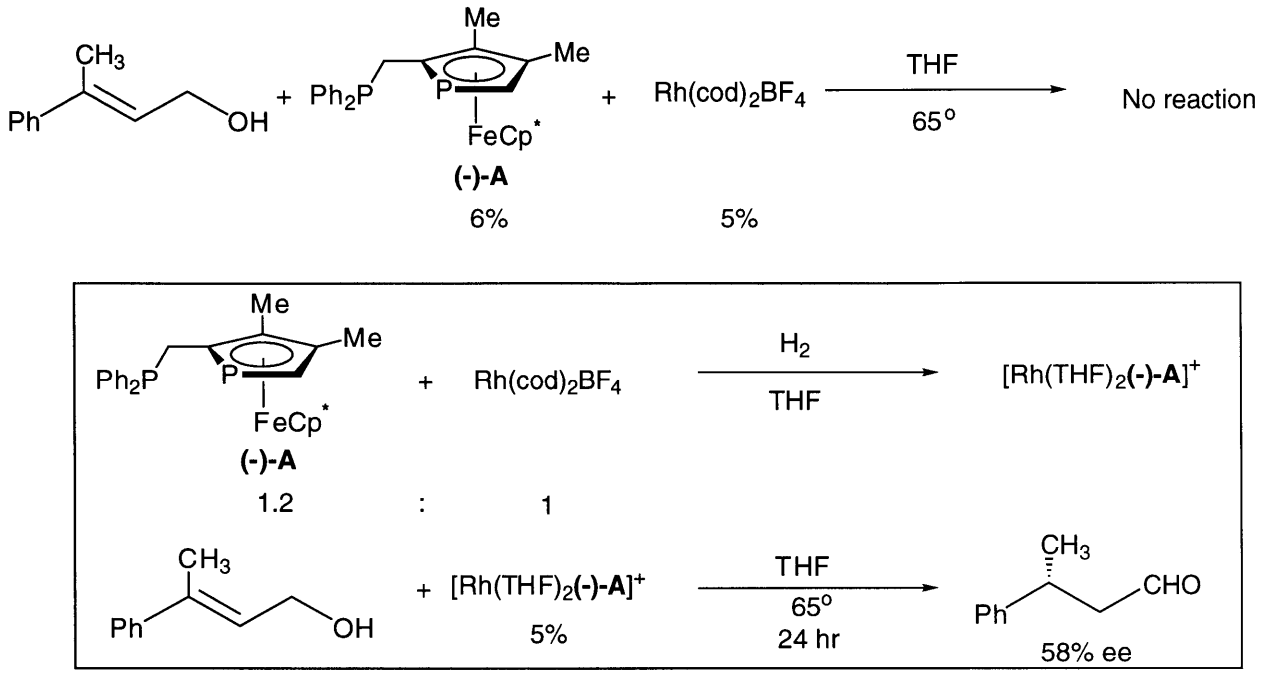

Figure 3.4.5. Preliminary Studies of Asymmetric Isomerization of Allylic Alcohols Catalyzed by Rh-**(-)-A** Complexes.

Efforts to optimize the reaction conditions have included varying temperatures, catalyst loadings, concentrations, metal to ligand ratios, solvents and counterions. The optimized reaction conditions are as follows: $Rh(cod)_2BF_4$ as the source of Rh, EtOH or THF as the solvent in hydrogenation, THF as the solvent in isomerization, 65°C for 24 hours at 5% catalyst loading, 0.1 M in substrates and a 1:1.2 metal to ligand ratio. An initial screening of substrates has also been conducted. Our phosphaferrocene **A** presents a distinctive advantage over BINAP (Figure 3.4.6).

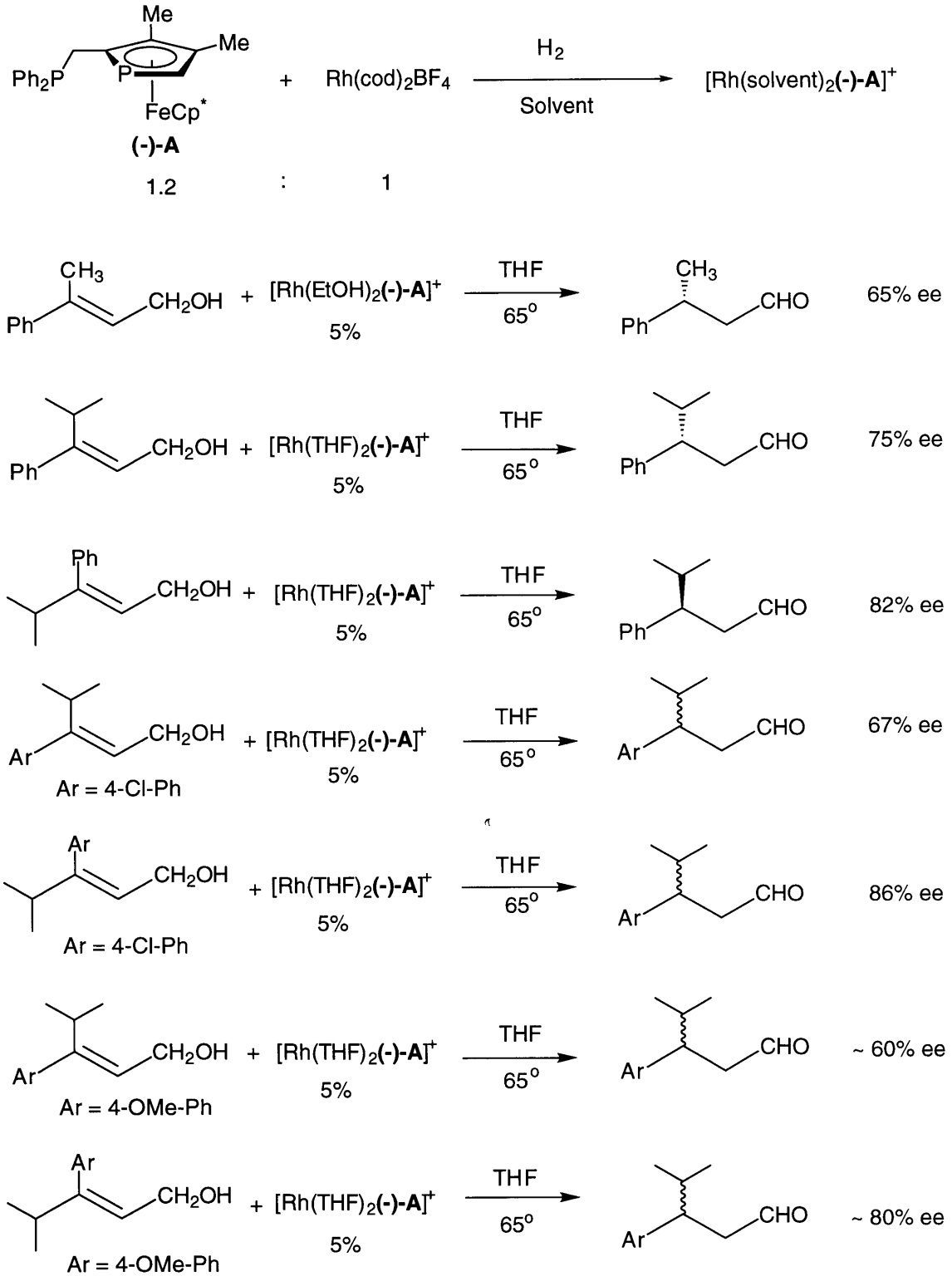

Figure 3.4.6. Asymmetric Isomerization of Allylic Alcohols Catalyzed by Rh-**(-)-A** Complexes.

Overall, the remarkable success we have had with **A** demonstrates the great potential of this class of heterocycles in catalysis. It marks the beginning rather than the end of active research in discovering new phosphaferrocenes or new reactions for phosphaferrocenes. The finding in this area will undoubtedly have a profound impact on how phosphine ligands will be designed in the future. The author is pleased to have contributed to the breakthrough in applying phosphaferrocenes to asymmetric synthesis and is confident that future efforts in this area will meet with even more impressive success.

Experimental

^1H nuclear magnetic resonance spectra were recorded on a Varian Unity 300 NMR spectrometer at ambient temperature and are referenced to residual solvent downfield from tetramethylsilane. ^1H NMR data are reported as follows: chemical shift (δ scale), multiplicity (br = broad, s = singlet, d = doublet, t = triplet, q = quartet, quint = quintet, and m = multiplet), coupling constant (Hz), and integration.

All ^{13}C NMR spectra were obtained with complete proton decoupling on a Varian Unity 300 NMR spectrometer and are referenced to solvent downfield from tetramethylsilane.

Infrared spectra were obtained on a Perkin-Elmer 1600 FT-IR spectrophotometer (cm^{-1}). Optical rotations were obtained using a Perkin Elmer Model 241 polarimeter.

Grade V hydrogen (Middlesex Gases Technologies, Inc.) was used as received. All reagents were purchased from commercial suppliers and used as received, unless otherwise noted. All allylic alcohols were prepared by reduction of the corresponding esters by $LiAlH_4$. The esters which are not commercially available were prepared by Horner-Emmons-Wadsworth coupling of the corresponding

ketones and triethylphosphono acetate. The *E* isomers of these esters were obtained together with the *Z* isomers in the synthesis. The *E* isomers of the esters elute prior to the *Z* isomers of the esters on silica gel. In the case of *para* substituted esters, alcohols and the corresponding products aldehydes, the assignment of structures and absolute configuration is by analogy and tentative.

(*E*)-3-phenyl-4-methyl-2-pentenol

^{1}H NMR (300 MHz, $CDCl_3$): δ 1.07 (d, *J* = 6.9, 6H), 1.40 (s, 1H), 3.04 (quint, *J* = 6.9, 1H), 4.38 (t, *J* = 6.9, 2H), 5.50 (t, *J* = 6.9, 1H), 7.17-7.31 (m, 5H); ^{13}C NMR (75 MHz, $CDCl_3$): δ 22.2, 30.0, 59.2, 126.8, 127.5, 127.8, 128.6, 142.4, 150.2; IR (KBr): 3316, 2963, 2930, 2871, 1492, 1460, 1362, 1014, 763, 701; HRMS: Calcd for $C_{12}H_{16}O$: 176.1201; found: 176.1203.

(*Z*)-3-phenyl-4-methyl-2-pentenol

^{1}H NMR (300 MHz, $CDCl_3$): δ 1.04 (d, *J* = 6.9, 6H), 1.35 (s, 1H), 2.60 (quint, *J* = 6.9, 1H),3.97 (d, *J* = 6.9, 2H), 5.65 (t, *J* = 6.9, 1H), 7.07-7.34 (m, 5H); ^{13}C NMR (75 MHz, $CDCl_3$): δ 21.8, 35.9, 60.7, 123.3, 127.1, 128.2, 128.7, 140.4, 151.1; IR (KBr): 3315, 2960, 2870, 1493, 1024, 985, 769, 702; HRMS: Calcd for $C_{12}H_{16}O$: 176.1201; found: 176.1205.

(*E*)-3-(4'-chloro)-phenyl-4-methyl-2-pentenol

^{1}H NMR (300 MHz, $CDCl_3$): δ 1.05 (d, *J* = 7.2, 6H), 1.41 (s, 1H), 3.02 (quint, *J* = 7.2, 1H),4.37 (d, *J* = 6.6, 2H), 5.47 (t, *J* = 6.6, 1H), 7.27 (d, *J* = 8.7, 2H), 7.11 (d, *J* = 8.7, 2H).

(*Z*)-3-(4'-chloro)-phenyl-4-methyl-2-pentenol

^{1}H NMR (300 MHz, $CDCl_3$): δ 1.03 (d, *J* = 6.9, 6H), 1.25 (s, 1H), 2.57 (quint, *J* = 6.9, 1H),3.96 (d, *J* = 6.9, 2H), 5.66 (t, *J* = 6.9, 1H), 7.03 (d, *J* = 8.4, 2H), 7.30 (d, *J* = 8.4, 2H).

(*E*)-3-(4'-methoxy)-phenyl-4-methyl-2-pentenol

^{1}H NMR (300 MHz, $CDCl_3$): δ 1.06 (d, *J* = 7.2, 6H), 1.33 (s, 1H), 3.02 (quint, *J* = 6.9, 1H),3.82 (s, 3H), 4.36 (d, *J* = 6.6, 2H), 5.48 (t, *J* = 6.6, 1H), 6.84 (d, *J* = 8.7, 2H), 7.13 (d, *J* = 8.9, 2H)).

(*Z*)-3-(4'-methoxy)-phenyl-4-methyl-2-pentenol

^{1}H NMR (300 MHz, $CDCl_3$): δ 1.04 (d, *J* = 6.6, 6H), 1.19 (s, 1H), 2.58 (quint, *J* = 6.3, 1H),3.83 (s, 3H), 3.99 (d, *J* = 6.9, 2H), 5.63 (t, *J* = 6.9, 1H), 6.89 (d, *J* = 8.7 2H), 7.02 (d, *J* = 8.7, 2H).

General Procedure for Asymmetric Isomerization of Allylic Alcohols. A 100 mL Schlenk tube was charged with (-)-**A** (6.7 mg, 0.013 mmol), $Rh(cod)_2PF_6$[27] (5.1 mg, 0.011 mmol), and anhydrous EtOH or THF (6.0 mL). After three vacuum/H_2-refill cycles, the valve to the Schlenk tube was closed. The reaction mixture was then stirred for 2 hours at r.t., at which time the solvents were evacuated. THF (3ml) and the substrate (0.22 mmol) were then added. The reaction mixture was heated at 65° for 24 hours. The reaction mixture was concentrated and then passed through a short column (25:75 EtOAc:hexane). The ee was determined by chiral GC.

Determination of Enantiomeric Excess. Analytical GC was performed on a Chiraldex G-TA column (20 m x 0.25 mm). Racemic products were prepared by isomerization of the allylic alcohols catalyzed by Rh-BINAP complexes.

3-phenyl-butanal (90 °C isothermal) t(*S*) = 14.86 min; t(*R*) = 15.74 min.

3-phenyl-4-methyl-pentanal (105 °C isothermal) t(*R*) = 14.04 min; t(*S*) = 16.19 min.

The para-substituted products cannot be assayed on G-TA column. Analytical GC was performed on Chiraldex B-PH column (20 m x 0.25 mm).

3-(4'-chloro)-phenyl-4-methyl-pentanal (120 °C isothermal) t(*fast enantiomer*) = 21.51 min; t(*slow enantiomer*) = 22.02 min.

3-(4'-methoxy)-phenyl-4-methyl-pentanal (100 °C isothermal) t(*fast enantiomer*) = 91.93 min; t(*slow enantiomer*) = 93.31 min. The two enantiomers are not perfectly separated. Hence the enantiomeric excesses are approximations.

Assignment of Absolute Configuration. The absolute configurations were established through comparison of the sign of the optical rotation of our reaction products with rotations reported in the literature. The rest were assigned by analogy.

(*S*)-3-phenyl-butanal $[\alpha]^{20}_D = 39^o$ (Et_2O)[41]

References

1 Ojima, I. *Catalytic Asymmetric Synthesis*; Wiley-VCH: New York, 1993.
2 Takaya, H.; Ohta, T.; Noyori, R. In *Catalytic Asymmetric Synthesis*; Ojima, I., Ed.; Wiley-VCH: New York, 1993; Chapter 1 and references therein.
3 Kagan, H. B.; Dang, T. P. *J. Am. Chem. Soc.* **1972**, *94*, 6429.
4 Knowles, W. S. *Acc. Chem. Res.* **1983**, *16*, 106-12.
5 Burk, M. J.; Wang, Y. M.; Lee, J. R. *J. Am. Chem. Soc.* **1996**, *118*, 5142-5143.
6 Zhang, F.-Y.; Pai, C.-C.; Chan, A. S. C. *J. Am. Chem. Soc.* **1998**, *120*, 5808-5809.
7 Zhu, G.; Zhang, X. *J. Org. Chem.* **1998**, *63*, 9590-9593.
8 Ohkuma, T.; Koizumi, M.; Doucet, H.; Pham, T.; Kozawa, M.; Murata, K.; Katayama, E.; Yokozawa, T.; Ikariya, T.; Noyori, R. *J. Am. Chem. Soc.* **1998**, *120*, 13529-13530.
9 Jiang, Q.; Jiang, Y.; Xiao, D.; Cao, P.; Zhang, X. *Angew. Chem., Int. Ed. Engl.* **1998**, *37*, 1100-1103.
10 Hayashi, T. In *Catalytic Asymmetric Synthesis*; Ojima, I., Ed.; Wiley-VCH: New York, 1993; Chapter 7.1.
11 Akutagawa, S.; Tani, K. In *Catalytic Asymmetric Synthesis*; Ojima, I., Ed.; Wiley-VCH: New York, 1993; Chapter 2 and references therein.
12 For example, see: Hayashi, T.; Matsumoto, Y.; Ito, Y. *Tetrahedron: Asymmetry* **1991**, *2*, 601-612.
13 Brunner, H.; Nishiyama, H.; Itoh, K. In *Catalytic Asymmetric Synthesis*; Ojima, I., Ed.; Wiley-VCH: New York, 1993; Chapter 6.
14 Halpern, J. *Pure Appl. Chem.* **1983**, *55*, 99.
15 Landis, C. R.; Halpern, J. *J. Am. Chem. Soc.* **1987**, *109*, 1746.
16 Brown, J. M.; Chaloner, P. A.; Morris, G. A. *J. Chem. Soc., Chem. Commun* **1983**, *12*, 664-6.
17 Brown, J. M.; Evans, P. L. *Tetrahedron* **1988**, *44*, 4905-16.
18 Zhu, G.; Cao, P.; Jiang, Q.; Zhang, X. *J. Am. Chem. Soc.* **1997**, *119*, 1799-1800.
19 Zhu, G.; Zhang, X. *J. Org. Chem.* **1998**, *63*, 3133-3136.

20 Sawamura, M.; Kuwano, R.; Ito, Y. *J. Am. Chem. Soc.* **1995**, *117*, 9602-9603.
21 Chan, A. S. C.; Hu, W.; Pai, C.-C.; Lau, C.-P. *J. Am. Chem. Soc.* **1997**, *119*, 9570-9571.
22 Burk, M. J.; Feaster, J. E.; Nugent, W. A.; Harlow, R. L. *J. Am. Chem. Soc.* **1993**, *115*, 10125-38.
23 We were interested in applying the the phosphaferrocene to reactions in which generic phosphines (such as BINAP) are not able to effect high ee's.
24 Herbst, R. M.; Shemin, D. In *Organic Synthesis*; Blatt, A.H., Ed.; John Wiley & Sons, Inc.: New York, 1943; Vol. 2; pp 1-3.
25 Schmidt, U.; Lieberknecht, A.; Wild, J. *Synthesis* **1988**, 159-172.
26 Schmidt, U.; Griesser, H.; Leitenberger, V.; Lieberknecht, A.; Mangold, R.; Meyer, R.; Riedl, B. *Synthesis* **1992**, 487-490.
27 Schrock, R. R.; Osborn, J. A. *J. Am. Chem. Soc.* **1971**, *93*, 2397-2407.
28 Wolf, J. P. I.; Neimann, C. *Biochemistry* **1963**, *2*, 493.
29 Vineyard, B. D.; Knowles, W. S.; Sabacky, M. J.; Bachman, G. L.; Weinkauff, D. J. *J. Am. Chem. Soc.* **1977**, *99*, 5946-52.
30 Hebel, D.; Lerman, O.; Rozen, S. *Bull. Soc. Chim. Fr.* **1986**, 861-863.
31 Jones, J. B.; Kunitake, T.; Niemann, C.; Hein, G. E. *J. Am. Chem. Soc.* **1965**, *87*, 1777.
32 Smart, N. A.; Young, G. T.; Williams, M. W. *J. Chem. Soc.* **1960**, 3902.
33 Nogradi, M. *Stereoselective Synthesis,* 2nd ed.; VCH: Weinheim, Germany, 1995.
34 Zhu, G.; Casalnuovo, A. L.; Zhang, X. *J. Org. Chem.* **1998**, *63*, 8100-8101.
35 Brettle, R.; Shibb, S. M.; Wheeler, K. J. *J. Chem. Soc., Perkin Trans. 1* **1985**, 831-836.
36 I observed coalescence of peaks in my variable temperature NMR studies of (*Z*)-enamides which indicates that the sample contains one isomer rather than a mixture of both (*Z*) and (*E*) isomers. My NOE studies also helped prove the identity of both (*Z*) and (*E*)-isomers.
37 Burk, M. J.; Casy, G.; Johnson, N. B. *J. Org. Chem.* **1998**, *63*, 6084-6085.
38 Johnson, M. R.; Sousa, L. R. *J. Org. Chem.* **1977**, *42*, 2439-2443.
39 Hayashi, T.; Hayashizaki, K.; Kiyoi, T.; Ito, Y. *J. Am. Chem. Soc.* **1988**, *110*, 8153-8156.
40 Bergens, S. H.; Bosnich, B. *J. Am. Chem. Soc.* **1991**, *113*, 958-967.
41 Berlan, J.; Besace, Y., Prat, D.; Pourcelot, G. *J. Organomet. Chem.* **1984**, *264*, 399-408.

Appendix I

X-ray Structural Data

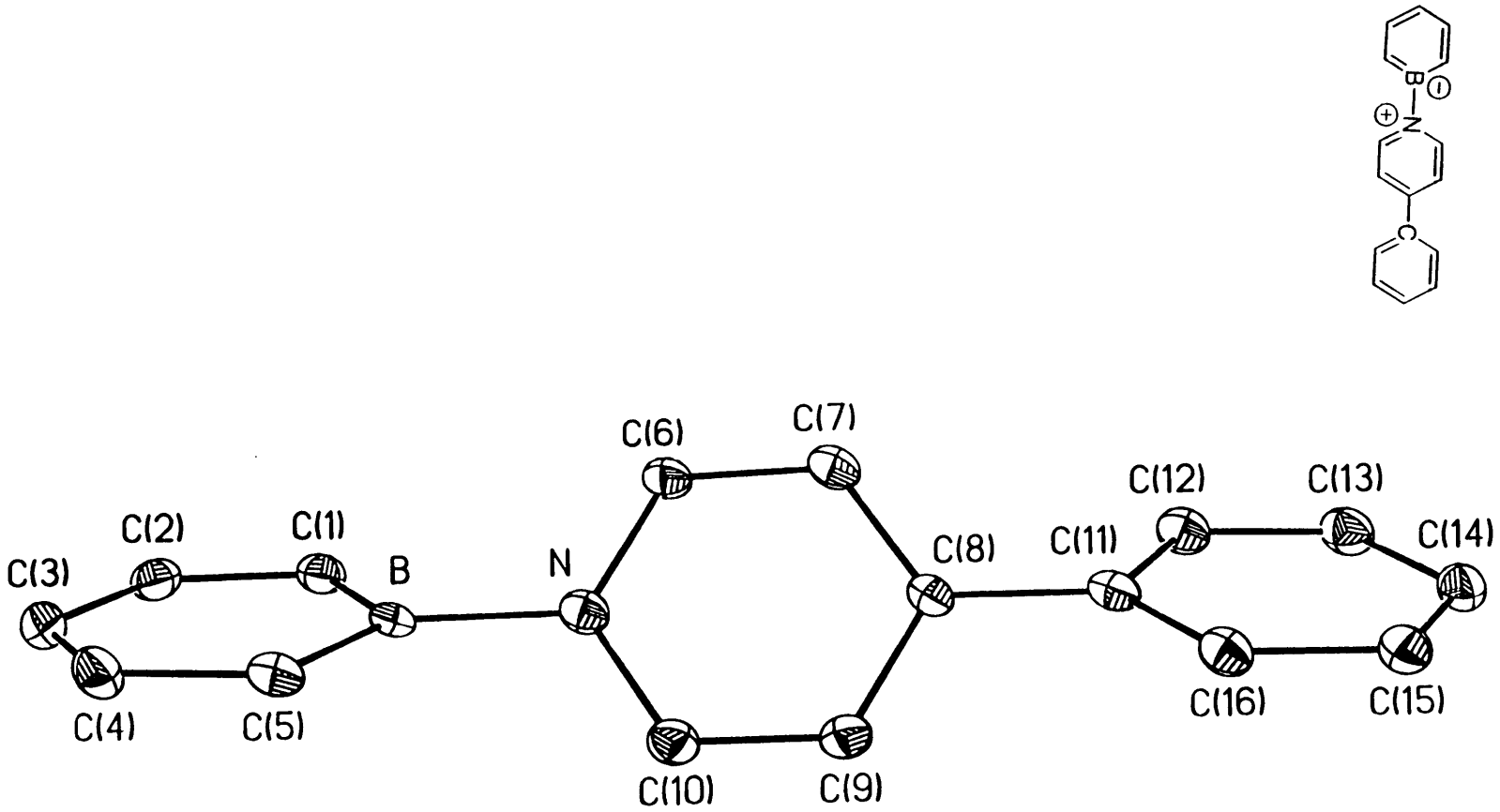
C(6)
C(7)
C(12)
C(13)
C(2)
C(1)
C(8)
C(11)
C(14)
C(3)
B
N
C(16)
C(15)
C(4)
C(5)
C(10)
C(9)

Table 1. Crystal data and structure refinement for 1.

A. Crystal Data

Identification code	96101
Empirical formula	$C_{16}H_{14}BN$
Formula weight	231.09
Temperature	293(2) K
Wavelength	0.71073 Å
Crystal morphology	orange plate
Crystal size	0.78 x 0.24 x 0.08 mm
Crystal system	Monoclinic
Space group	$P2_1/c$
Unit cell dimensions	a = 7.04920(10) Å alpha = 90° b = 16.4895(6) Å beta = 95.672(2)° c = 10.4136(4) Å gamma = 90°
Volume, Z	1204.53(7) $Å^3$, 4
Density (calculated)	1.274 Mg/m^3
Absorption coefficient	0.073 mm^{-1}
F(000)	488

B. Data Collection and Reduction

Diffractometer	Siemens SMART/CCD
Scan Type	ω Scans
Scan angle	0.30°
θ range for data collection	2.32 to 23.30°
Limiting indices	$-7 \le h \le 4$, $-18 \le k \le 17$, $-9 \le l \le 11$

Reflections collected	4727
Independent reflections	1731 (R_{int} = 0.0749)
Absorption correction	None

C. Solution and Refinement

Refinement method	Full-matrix least-squares on F^2
Data / restraints / parameters	1730 / 0 / 220
Goodness-of-fit on F^2	1.153
Final R indices [$I>2\sigma(I)$]	R1 = 0.0544, wR2 = 0.1323
R indices (all data)	R1 = 0.0768, wR2 = 0.1540
Extinction coefficient	0.009(3)
Largest diff. peak and hole	0.204 and -0.271 $eÅ^{-3}$

Table 2. Atomic coordinates [x 10^4] and equivalent isotropic displacement parameters [$Å^2$ x 10^3] for 1. U(eq) is defined as one third of the trace of the orthogonalized U_{ij} tensor.

	x	y	z	U(eq)
N	1125(3)	4539(1)	2816(2)	22(1)
C(1)	-852(3)	3958(2)	4623(2)	23(1)
C(2)	-2338(3)	3470(2)	4953(2)	25(1)
C(3)	-3496(4)	3036(2)	4022(3)	29(1)
C(4)	-3209(3)	3079(2)	2717(3)	29(1)
C(5)	-1802(3)	3555(2)	2270(3)	25(1)
C(6)	2904(3)	4468(2)	3435(2)	22(1)
C(7)	4401(4)	4920(2)	3094(2)	24(1)
C(8)	4137(3)	5471(1)	2083(2)	20(1)
C(9)	2301(3)	5532(2)	1449(2)	24(1)
C(10)	854(4)	5071(2)	1825(2)	23(1)
C(11)	5704(3)	5978(2)	1677(2)	22(1)
C(12)	7000(3)	6354(2)	2609(3)	26(1)
C(13)	8424(4)	6850(2)	2238(3)	28(1)
C(14)	8631(3)	6976(2)	946(3)	28(1)
C(15)	7375(3)	6596(2)	12(3)	26(1)
C(16)	5925(3)	6107(2)	377(2)	23(1)
B	-536(4)	4017(2)	3238(3)	20(1)

Table 3. Bond lengths [Å] and angles [°] for 1.

N-C(10)	1.354(3)	N-C(6)	1.358(3)
N-B	1.551(3)	C(1)-C(2)	1.391(4)
C(1)-B	1.484(4)	C(1)-H(1A)	1.00(3)
C(2)-C(3)	1.401(4)	C(2)-H(2A)	1.02(3)
C(3)-C(4)	1.395(4)	C(3)-H(3A)	0.98(3)
C(4)-C(5)	1.381(4)	C(4)-H(4A)	1.01(3)
C(5)-B	1.488(4)	C(5)-H(5A)	1.00(3)
C(6)-C(7)	1.367(4)	C(6)-H(6A)	0.99(3)
C(7)-C(8)	1.390(3)	C(7)-H(7A)	0.91(3)
C(8)-C(9)	1.397(3)	C(8)-C(11)	1.480(3)
C(9)-C(10)	1.360(4)	C(9)-H(9A)	0.92(3)
C(10)-H(10A)	1.00(3)	C(11)-C(16)	1.394(3)
C(11)-C(12)	1.409(4)	C(12)-C(13)	1.379(4)
C(12)-H(12A)	0.98(3)	C(13)-C(14)	1.384(4)
C(13)-H(13A)	1.01(3)	C(14)-C(15)	1.398(4)
C(14)-H(14A)	1.03(3)	C(15)-C(16)	1.385(4)
C(15)-H(15A)	0.99(3)	C(16)-H(16A)	0.97(3)

C(10)-N-C(6)	118.1(2)	C(10)-N-B	121.5(2)
C(6)-N-B	120.4(2)	C(2)-C(1)-B	117.9(2)
C(2)-C(1)-H(1A)	119(2)	B-C(1)-H(1A)	123(2)
C(1)-C(2)-C(3)	121.7(2)	C(1)-C(2)-H(2A)	120.0(14)
C(3)-C(2)-H(2A)	118.3(14)	C(4)-C(3)-C(2)	121.2(2)
C(4)-C(3)-H(3A)	120(2)	C(2)-C(3)-H(3A)	119(2)
C(5)-C(4)-C(3)	122.4(2)	C(5)-C(4)-H(4A)	120(2)
C(3)-C(4)-H(4A)	117(2)	C(4)-C(5)-B	117.7(2)
C(4)-C(5)-H(5A)	120(2)	B-C(5)-H(5A)	122(2)
N-C(6)-C(7)	122.1(2)	N-C(6)-H(6A)	115(2)
C(7)-C(6)-H(6A)	123(2)	C(8)-C(7)-C(6)	120.3(2)
C(8)-C(7)-H(7A)	119(2)	C(6)-C(7)-H(7A)	121(2)
C(7)-C(8)-C(9)	117.0(2)	C(7)-C(8)-C(11)	122.6(2)
C(9)-C(8)-C(11)	120.4(2)	C(10)-C(9)-C(8)	120.6(2)
C(10)-C(9)-H(9A)	122(2)	C(8)-C(9)-H(9A)	118(2)
N-C(10)-C(9)	121.9(2)	N-C(10)-H(10A)	115(2)
C(9)-C(10)-H(10A)	123(2)	C(16)-C(11)-C(12)	118.4(2)
C(16)-C(11)-C(8)	121.4(2)	C(12)-C(11)-C(8)	120.2(2)
C(13)-C(12)-C(11)	120.6(2)	C(13)-C(12)-H(12A)	121(2)
C(11)-C(12)-H(12A)	118(2)	C(14)-C(13)-C(12)	120.7(2)
C(14)-C(13)-H(13A)	120(2)	C(12)-C(13)-H(13A)	120(2)
C(13)-C(14)-C(15)	119.3(2)	C(13)-C(14)-H(14A)	121(2)
C(15)-C(14)-H(14A)	120(2)	C(16)-C(15)-C(14)	120.3(2)
C(16)-C(15)-H(15A)	121(2)	C(14)-C(15)-H(15A)	119(2)
C(15)-C(16)-C(11)	120.8(2)	C(15)-C(16)-H(16A)	120(2)
C(11)-C(16)-H(16A)	119(2)	C(1)-B-C(5)	119.2(2)
C(1)-B-N	120.1(2)	C(5)-B-N	120.7(2)

Symmetry transformations used to generate equivalent atoms:

Table 4. Anisotropic displacement parameters [$Å^2$ x 10^3] for 1.

The anisotropic displacement factor exponent takes the form:

$-2\pi^2$ [$(ha^*)^2U_{11}$ + ... + $2hka^*b^*U_{12}$]

	U11	U22	U33	U23	U13	U12
N	20(1)	24(1)	20(1)	-1(1)	-2(1)	1(1)
C(1)	20(1)	22(1)	28(2)	-1(1)	-1(1)	4(1)
C(2)	26(1)	21(1)	27(2)	4(1)	4(1)	5(1)
C(3)	20(1)	23(2)	43(2)	5(1)	4(1)	0(1)
C(4)	20(1)	28(2)	37(2)	-2(1)	-5(1)	-2(1)
C(5)	20(1)	28(2)	25(2)	2(1)	-3(1)	4(1)
C(6)	18(1)	27(2)	21(1)	4(1)	-3(1)	2(1)
C(7)	18(1)	28(2)	24(1)	-1(1)	-4(1)	2(1)
C(8)	15(1)	21(1)	23(1)	-2(1)	1(1)	2(1)
C(9)	23(1)	26(2)	22(1)	6(1)	0(1)	3(1)
C(10)	21(1)	26(2)	22(1)	1(1)	-2(1)	1(1)
C(11)	17(1)	22(1)	25(1)	-2(1)	-2(1)	4(1)
C(12)	22(1)	29(2)	26(2)	-1(1)	-2(1)	1(1)
C(13)	21(1)	27(2)	35(2)	-2(1)	-4(1)	-1(1)
C(14)	20(1)	21(2)	42(2)	4(1)	5(1)	0(1)
C(15)	24(1)	27(2)	28(2)	2(1)	6(1)	5(1)
C(16)	19(1)	24(1)	25(1)	-4(1)	0(1)	1(1)
B	13(2)	20(2)	27(2)	3(1)	-1(1)	4(1)

Table 5. Hydrogen coordinates (x 10^4) and isotropic displacement parameters ($Å^2$ x 10^3) for 1.

	x	y	z	U(eq)
H(3A)	-4531(38)	2703(17)	4293(26)	35(7)
H(14A)	9690(37)	7349(16)	671(25)	34(7)
H(2A)	-2602(32)	3418(15)	5893(25)	24(6)
H(6A)	3022(35)	4064(16)	4136(25)	26(7)
H(15A)	7545(35)	6675(16)	-913(27)	33(7)
H(16A)	5051(36)	5846(16)	-279(25)	30(7)
H(1A)	-86(39)	4266(18)	5316(27)	43(8)
H(13A)	9292(37)	7142(16)	2917(27)	36(7)
H(7A)	5589(36)	4855(15)	3499(24)	25(7)
H(5A)	-1613(39)	3558(17)	1327(28)	42(8)
H(9A)	2103(35)	5907(16)	793(25)	26(7)
H(12A)	6809(37)	6284(16)	3520(27)	31(7)
H(10A)	-480(38)	5113(16)	1417(25)	33(7)
H(4A)	-4088(39)	2752(17)	2097(28)	41(8)

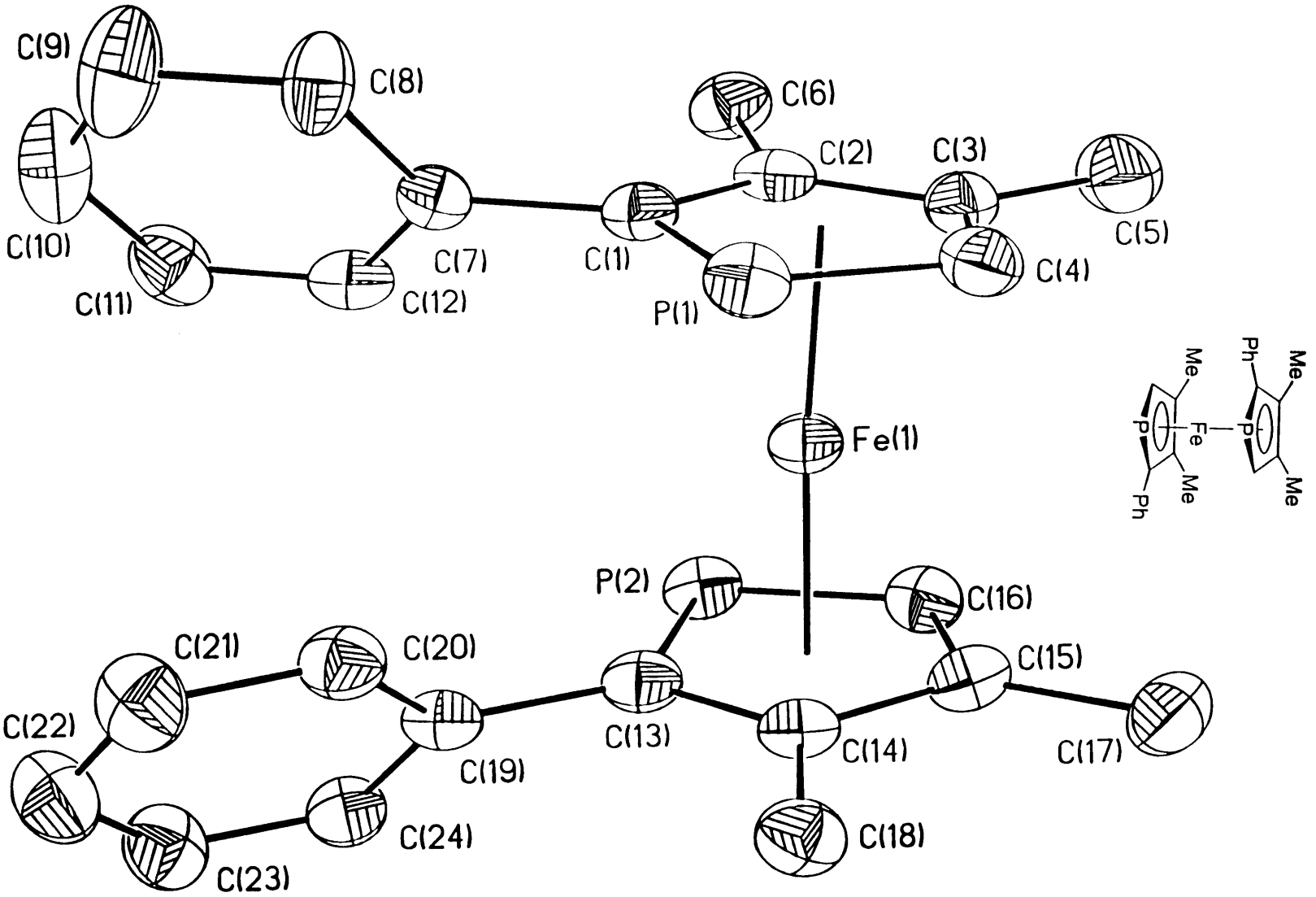
C(9)
C(8)
C(6)
C(2)
C(3)
C(5)
C(10)
C(7)
C(1)
C(4)
C(11)
C(12)
P(1)
Fe(1)
P(2)
C(16)
C(21)
C(20)
C(15)
C(22)
C(19)
C(13)
C(14)
C(17)
C(24)
C(18)
C(23)
Me
Ph
Fe
Me
Ph
Me
Ph
Me

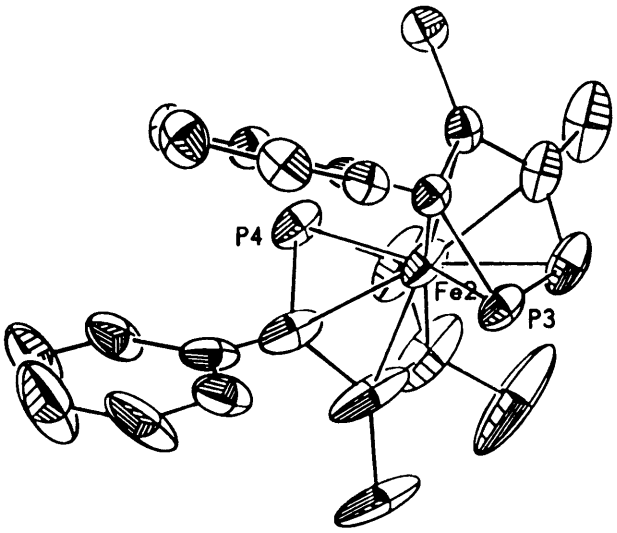
P4
Fe2
P3

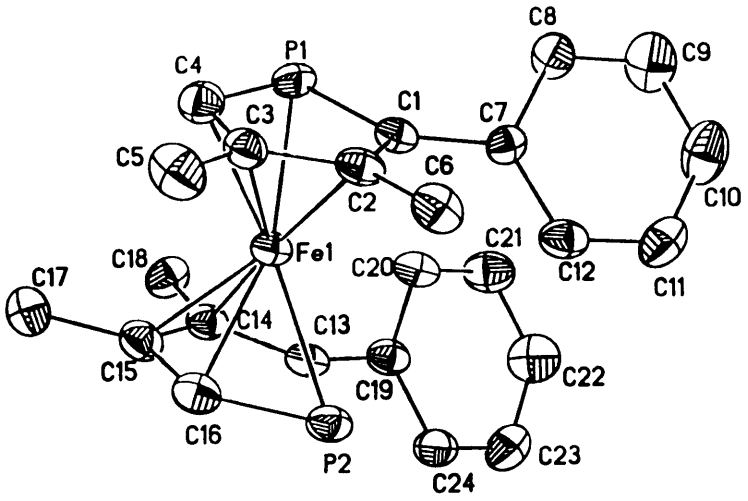
C8
C9
P1
C4
C1
C7
C3
C5
C6
C2
C10
C21
Fe1
C18
C20
C12
C17
C14
C13
C11
C15
C19
C22
C16
P2
C24
C23

Table 1. Crystal data and structure refinement for 1.

A. Crystal Data

Identification code	97133a
Empirical formula	$C_{24}H_{24}FeP_2$
Formula weight	430.22
Temperature	183(2) K
Wavelength	0.71073 Å
Crystal morphology	block
Crystal size	0.45 x 0.27 x 0.15 mm
Crystal system	Monoclinic
Space group	C2
Unit cell dimensions	a = 22.9303(8) Å alpha = 90°
	b = 11.3262(4) Å beta = 105.5510(10)°
	c = 16.6256(8) Å gamma = 90°
Volume, Z	4159.8(3) Å^3, 8
Density (calculated)	1.374 Mg/m^3
Absorption coefficient	0.885 mm^{-1}
F(000)	1792

B. Data Collection and Reduction

Diffractometer	Siemens SMART/CCD
Scan Type	ω Scans
Scan angle	0.30°
θ range for data collection	1.27 to 23.23°
Limiting indices	$-19 \le h \le 25$, $-11 \le k \le 12$, $-17 \le l \le 18$

Reflections collected	8372
Independent reflections	5422 (R_{int} = 0.0342)
Absorption correction	Semi-empirical from psi-scans
Max. and min. transmission	0.6199 and 0.5557

C. Solution and Refinement

Refinement method	Full-matrix least-squares on F^2
Data / restraints / parameters	5415 / 1 / 488
Goodness-of-fit on F^2	1.057
Final R indices [I>2σ(I)]	R1 = 0.0396, wR2 = 0.1020
R indices (all data)	R1 = 0.0432, wR2 = 0.1143
Absolute structure parameter	-0.01(2)
Extinction coefficient	0.0007(2)
Largest diff. peak and hole	0.348 and -0.559 $eÅ^{-3}$

Table 2. Atomic coordinates [x 10^4] and equivalent isotropic displacement parameters [$Å^2$ x 10^3] for 1. U(eq) is defined as one third of the trace of the orthogonalized U_{ij} tensor.

	x	y	z	U(eq)
Fe(1)	-1270(1)	-4369(1)	-3983(1)	35(1)
Fe(2)	-1250(1)	-6946(1)	-8846(1)	56(1)
P(1)	-2235(1)	-3694(1)	-4562(1)	41(1)
P(2)	-284(1)	-4000(1)	-3272(1)	41(1)
P(3)	-970(1)	-7139(1)	-7424(1)	53(1)
P(4)	-1522(1)	-7665(2)	-10185(1)	62(1)
C(1)	-1889(2)	-3463(4)	-3478(3)	36(1)
C(2)	-1704(2)	-4542(5)	-3035(3)	40(1)
C(3)	-1820(2)	-5548(5)	-3571(3)	42(1)
C(4)	-2099(2)	-5226(5)	-4410(3)	47(1)
C(5)	-1691(3)	-6809(5)	-3295(4)	63(2)
C(6)	-1459(2)	-4634(5)	-2095(3)	48(1)
C(7)	-1824(2)	-2260(4)	-3110(3)	35(1)
C(8)	-2332(2)	-1539(4)	-3263(3)	49(1)
C(9)	-2292(3)	-394(6)	-2958(4)	72(2)
C(10)	-1761(3)	25(6)	-2482(4)	70(2)
C(11)	-1250(3)	-667(5)	-2309(3)	58(2)
C(12)	-1281(2)	-1806(5)	-2619(3)	46(1)
C(13)	-615(2)	-3214(4)	-4211(3)	39(1)
C(14)	-847(2)	-3957(4)	-4911(3)	38(1)
C(15)	-762(2)	-5201(5)	-4686(3)	45(1)
C(16)	-476(2)	-5340(5)	-3822(3)	45(1)
C(17)	-944(3)	-6197(5)	-5287(4)	57(1)
C(18)	-1115(2)	-3570(5)	-5794(3)	47(1)
C(19)	-607(2)	-1890(5)	-4231(3)	39(1)
C(20)	-1123(2)	-1210(5)	-4560(3)	46(1)
C(21)	-1092(2)	10(5)	-4553(4)	59(2)
C(22)	-553(2)	578(6)	-4226(4)	65(2)
C(23)	-34(3)	-88(5)	-3904(4)	59(2)
C(24)	-64(2)	-1297(5)	-3920(3)	46(1)
C(31)	-1659(2)	-7790(5)	-8012(3)	40(1)
C(32)	-2066(2)	-6957(5)	-8523(3)	47(1)
C(33)	-1805(3)	-5804(5)	-8436(4)	65(2)
C(34)	-1226(3)	-5764(6)	-7890(3)	73(2)
C(35)	-2128(4)	-4733(6)	-8892(4)	106(3)
C(36)	-2702(2)	-7241(6)	-9016(3)	58(1)
C(49)	-1792(2)	-9060(5)	-7926(3)	37(1)
C(50)	-1964(2)	-9824(5)	-8608(3)	45(1)
C(51)	-2064(3)	-11005(5)	-8497(4)	54(1)
C(52)	-1986(3)	-11465(5)	-7698(4)	64(2)
C(53)	-1822(3)	-10724(5)	-7021(4)	56(1)
C(54)	-1720(2)	-9533(5)	-7135(3)	43(1)
C(65)	-672(5)	-6127(10)	-9441(5)	122(5)
C(66)	-1248(4)	-6217(8)	-9988(4)	103(3)
C(67)	-350(6)	-4945(12)	-9173(5)	220(9)
C(69)	-728(2)	-9446(9)	-9290(3)	72(2)
C(70)	-500(3)	-9889(8)	-8486(4)	81(2)
C(64)	-433(3)	-7228(12)	-9128(4)	116(4)

C(63)	-843(3)	-8186(8)	-9463(3)	75(2)
C(71)	-379(4)	-11066(10)	-8332(5)	129(4)
C(68)	208(3)	-7425(11)	-8557(4)	140(5)
C(72)	-499(5)	-11795(11)	-9000(7)	168(6)
C(73)	-744(4)	-11422(11)	-9805(6)	150(5)
C(74)	-850(3)	-10261(9)	-9947(4)	98(3)

Table 3. Bond lengths [Å] and angles [°] for 1.

Fe(1)-C(3)	2.074(5)	Fe(1)-C(16)	2.082(5)
Fe(1)-C(15)	2.082(5)	Fe(1)-C(14)	2.083(4)
Fe(1)-C(4)	2.082(5)	Fe(1)-C(2)	2.086(4)
Fe(1)-C(1)	2.101(5)	Fe(1)-C(13)	2.101(5)
Fe(1)-P(2)	2.2908(13)	Fe(1)-P(1)	2.2954(13)
Fe(2)-C(33)	2.055(7)	Fe(2)-C(34)	2.069(6)
Fe(2)-C(66)	2.070(6)	Fe(2)-C(64)	2.073(8)
Fe(2)-C(65)	2.074(7)	Fe(2)-C(32)	2.081(5)
Fe(2)-C(31)	2.101(5)	Fe(2)-C(63)	2.100(8)
Fe(2)-P(3)	2.2890(14)	Fe(2)-P(4)	2.294(2)
P(1)-C(4)	1.769(5)	P(1)-C(1)	1.783(5)
P(2)-C(16)	1.766(5)	P(2)-C(13)	1.780(5)
P(3)-C(34)	1.769(7)	P(3)-C(31)	1.780(5)
P(4)-C(66)	1.755(7)	P(4)-C(63)	1.793(8)
C(1)-C(2)	1.431(7)	C(1)-C(7)	1.484(7)
C(2)-C(3)	1.427(7)	C(2)-C(6)	1.516(6)
C(3)-C(4)	1.417(7)	C(3)-C(5)	1.506(8)
C(7)-C(8)	1.390(7)	C(7)-C(12)	1.390(7)
C(8)-C(9)	1.386(8)	C(9)-C(10)	1.349(9)
C(10)-C(11)	1.373(9)	C(11)-C(12)	1.384(8)
C(13)-C(14)	1.420(7)	C(13)-C(19)	1.500(7)
C(14)-C(15)	1.457(7)	C(14)-C(18)	1.497(6)
C(15)-C(16)	1.420(7)	C(15)-C(17)	1.492(8)
C(19)-C(24)	1.388(7)	C(19)-C(20)	1.395(7)
C(20)-C(21)	1.383(8)	C(21)-C(22)	1.370(8)
C(22)-C(23)	1.388(8)	C(23)-C(24)	1.371(8)
C(31)-C(32)	1.435(7)	C(31)-C(49)	1.485(7)
C(32)-C(33)	1.428(8)	C(32)-C(36)	1.503(7)
C(33)-C(34)	1.394(9)	C(33)-C(35)	1.514(9)
C(49)-C(54)	1.387(6)	C(49)-C(50)	1.396(7)
C(50)-C(51)	1.378(8)	C(51)-C(52)	1.394(8)
C(52)-C(53)	1.373(8)	C(53)-C(54)	1.391(8)
C(65)-C(66)	1.392(13)	C(65)-C(64)	1.40(2)
C(65)-C(67)	1.537(12)	C(69)-C(70)	1.391(9)
C(69)-C(74)	1.401(10)	C(69)-C(63)	1.465(11)
C(70)-C(71)	1.372(13)	C(64)-C(63)	1.445(11)
C(64)-C(68)	1.537(12)	C(71)-C(72)	1.351(13)
C(72)-C(73)	1.371(14)	C(73)-C(74)	1.346(14)

C(3)-Fe(1)-C(16)	101.8(2)	C(3)-Fe(1)-C(15)	112.0(2)
C(16)-Fe(1)-C(15)	39.9(2)	C(3)-Fe(1)-C(14)	146.4(2)
C(16)-Fe(1)-C(14)	69.5(2)	C(15)-Fe(1)-C(14)	40.9(2)
C(3)-Fe(1)-C(4)	39.9(2)	C(16)-Fe(1)-C(4)	119.0(2)
C(15)-Fe(1)-C(4)	101.2(2)	C(14)-Fe(1)-C(4)	114.5(2)
C(3)-Fe(1)-C(2)	40.1(2)	C(16)-Fe(1)-C(2)	115.5(2)
C(15)-Fe(1)-C(2)	146.4(2)	C(14)-Fe(1)-C(2)	172.4(2)
C(4)-Fe(1)-C(2)	68.7(2)	C(3)-Fe(1)-C(1)	69.3(2)
C(16)-Fe(1)-C(1)	150.2(2)	C(15)-Fe(1)-C(1)	169.9(2)
C(14)-Fe(1)-C(1)	133.2(2)	C(4)-Fe(1)-C(1)	73.2(2)
C(2)-Fe(1)-C(1)	40.0(2)	C(3)-Fe(1)-C(13)	170.8(2)
C(16)-Fe(1)-C(13)	73.1(2)	C(15)-Fe(1)-C(13)	69.3(2)
C(14)-Fe(1)-C(13)	39.7(2)	C(4)-Fe(1)-C(13)	149.3(2)
C(2)-Fe(1)-C(13)	134.7(2)	C(1)-Fe(1)-C(13)	111.1(2)
C(3)-Fe(1)-P(2)	123.4(2)	C(16)-Fe(1)-P(2)	47.3(2)
C(15)-Fe(1)-P(2)	75.52(14)	C(14)-Fe(1)-P(2)	75.58(12)

C(4)-Fe(1)-P(2)	160.9(2)	C(2)-Fe(1)-P(2)	103.40(13)
C(1)-Fe(1)-P(2)	112.56(13)	C(13)-Fe(1)-P(2)	47.59(13)
C(3)-Fe(1)-P(1)	75.49(14)	C(16)-Fe(1)-P(1)	160.3(2)
C(15)-Fe(1)-P(1)	122.43(14)	C(14)-Fe(1)-P(1)	101.69(13)
C(4)-Fe(1)-P(1)	47.4(2)	C(2)-Fe(1)-P(1)	75.30(13)
C(1)-Fe(1)-P(1)	47.60(13)	C(13)-Fe(1)-P(1)	111.87(13)
P(2)-Fe(1)-P(1)	149.63(6)	C(33)-Fe(2)-C(34)	39.5(3)
C(33)-Fe(2)-C(66)	101.9(3)	C(34)-Fe(2)-C(66)	116.1(3)
C(33)-Fe(2)-C(64)	148.1(4)	C(34)-Fe(2)-C(64)	115.7(3)
C(66)-Fe(2)-C(64)	68.3(4)	C(33)-Fe(2)-C(65)	114.1(4)
C(34)-Fe(2)-C(65)	100.9(3)	C(66)-Fe(2)-C(65)	39.3(3)
C(64)-Fe(2)-C(65)	39.6(5)	C(33)-Fe(2)-C(32)	40.4(2)
C(34)-Fe(2)-C(32)	69.3(2)	C(66)-Fe(2)-C(32)	117.5(3)
C(64)-Fe(2)-C(32)	170.6(4)	C(65)-Fe(2)-C(32)	149.4(4)
C(33)-Fe(2)-C(31)	69.0(2)	C(34)-Fe(2)-C(31)	73.2(2)
C(66)-Fe(2)-C(31)	153.8(3)	C(64)-Fe(2)-C(31)	132.0(4)
C(65)-Fe(2)-C(31)	166.9(3)	C(32)-Fe(2)-C(31)	40.1(2)
C(33)-Fe(2)-C(63)	168.3(2)	C(34)-Fe(2)-C(63)	152.2(3)
C(66)-Fe(2)-C(63)	73.1(4)	C(64)-Fe(2)-C(63)	40.5(3)
C(65)-Fe(2)-C(63)	69.0(4)	C(32)-Fe(2)-C(63)	132.1(2)
C(31)-Fe(2)-C(63)	110.7(2)	C(33)-Fe(2)-P(3)	75.2(2)
C(34)-Fe(2)-P(3)	47.6(2)	C(66)-Fe(2)-P(3)	156.4(2)
C(64)-Fe(2)-P(3)	101.4(2)	C(65)-Fe(2)-P(3)	119.8(2)
C(32)-Fe(2)-P(3)	75.84(13)	C(31)-Fe(2)-P(3)	47.60(13)
C(63)-Fe(2)-P(3)	113.7(2)	C(33)-Fe(2)-P(4)	120.9(2)
C(34)-Fe(2)-P(4)	156.9(2)	C(66)-Fe(2)-P(4)	47.1(2)
C(64)-Fe(2)-P(4)	75.7(2)	C(65)-Fe(2)-P(4)	74.8(2)
C(32)-Fe(2)-P(4)	102.64(13)	C(31)-Fe(2)-P(4)	115.20(14)
C(63)-Fe(2)-P(4)	47.9(2)	P(3)-Fe(2)-P(4)	153.73(8)
C(4)-P(1)-C(1)	89.2(2)	C(4)-P(1)-Fe(1)	60.0(2)
C(1)-P(1)-Fe(1)	60.5(2)	C(16)-P(2)-C(13)	89.3(2)
C(16)-P(2)-Fe(1)	60.1(2)	C(13)-P(2)-Fe(1)	60.6(2)
C(34)-P(3)-C(31)	89.0(3)	C(34)-P(3)-Fe(2)	59.7(2)
C(31)-P(3)-Fe(2)	60.7(2)	C(66)-P(4)-C(63)	88.8(4)
C(66)-P(4)-Fe(2)	59.8(2)	C(63)-P(4)-Fe(2)	60.4(2)
C(2)-C(1)-C(7)	126.0(4)	C(2)-C(1)-P(1)	112.6(4)
C(7)-C(1)-P(1)	121.4(3)	C(2)-C(1)-Fe(1)	69.5(2)
C(7)-C(1)-Fe(1)	127.5(3)	P(1)-C(1)-Fe(1)	71.9(2)
C(1)-C(2)-C(3)	112.4(4)	C(1)-C(2)-C(6)	124.5(5)
C(3)-C(2)-C(6)	123.0(4)	C(1)-C(2)-Fe(1)	70.5(3)
C(3)-C(2)-Fe(1)	69.5(3)	C(6)-C(2)-Fe(1)	131.7(3)
C(4)-C(3)-C(2)	111.6(5)	C(4)-C(3)-C(5)	123.0(5)
C(2)-C(3)-C(5)	125.4(5)	C(4)-C(3)-Fe(1)	70.4(3)
C(2)-C(3)-Fe(1)	70.4(3)	C(5)-C(3)-Fe(1)	128.6(4)
C(3)-C(4)-P(1)	114.1(4)	C(3)-C(4)-Fe(1)	69.8(3)
P(1)-C(4)-Fe(1)	72.6(2)	C(8)-C(7)-C(12)	117.7(5)
C(8)-C(7)-C(1)	118.5(4)	C(12)-C(7)-C(1)	123.9(4)
C(7)-C(8)-C(9)	120.8(5)	C(10)-C(9)-C(8)	120.3(6)
C(9)-C(10)-C(11)	120.5(6)	C(10)-C(11)-C(12)	119.9(5)
C(11)-C(12)-C(7)	120.8(5)	C(14)-C(13)-C(19)	125.3(4)
C(14)-C(13)-P(2)	113.6(4)	C(19)-C(13)-P(2)	121.0(4)
C(14)-C(13)-Fe(1)	69.5(3)	C(19)-C(13)-Fe(1)	129.8(3)
P(2)-C(13)-Fe(1)	71.8(2)	C(13)-C(14)-C(15)	111.6(4)
C(13)-C(14)-C(18)	126.5(5)	C(15)-C(14)-C(18)	121.8(4)
C(13)-C(14)-Fe(1)	70.8(3)	C(15)-C(14)-Fe(1)	69.5(3)
C(18)-C(14)-Fe(1)	129.9(3)	C(16)-C(15)-C(14)	111.2(5)
C(16)-C(15)-C(17)	124.4(5)	C(14)-C(15)-C(17)	124.4(5)
C(16)-C(15)-Fe(1)	70.1(3)	C(14)-C(15)-Fe(1)	69.6(3)
C(17)-C(15)-Fe(1)	128.4(4)	C(15)-C(16)-P(2)	114.3(4)

C(15)-C(16)-Fe(1)	70.1(3)	P(2)-C(16)-Fe(1)	72.5(2)
C(24)-C(19)-C(20)	117.5(5)	C(24)-C(19)-C(13)	119.3(4)
C(20)-C(19)-C(13)	123.2(4)	C(21)-C(20)-C(19)	120.8(5)
C(22)-C(21)-C(20)	120.7(5)	C(21)-C(22)-C(23)	119.1(6)
C(24)-C(23)-C(22)	120.1(5)	C(23)-C(24)-C(19)	121.7(5)
C(32)-C(31)-C(49)	125.2(4)	C(32)-C(31)-P(3)	113.2(4)
C(49)-C(31)-P(3)	121.5(3)	C(32)-C(31)-Fe(2)	69.2(3)
C(49)-C(31)-Fe(2)	130.1(3)	P(3)-C(31)-Fe(2)	71.7(2)
C(33)-C(32)-C(31)	110.7(5)	C(33)-C(32)-C(36)	124.7(5)

C(31)-C(32)-C(36)	124.4(5)	C(33)-C(32)-Fe(2)	68.8(4)
C(31)-C(32)-Fe(2)	70.7(3)	C(36)-C(32)-Fe(2)	131.9(3)
C(34)-C(33)-C(32)	113.3(5)	C(34)-C(33)-C(35)	123.5(6)
C(32)-C(33)-C(35)	123.2(6)	C(34)-C(33)-Fe(2)	70.8(4)
C(32)-C(33)-Fe(2)	70.8(3)	C(35)-C(33)-Fe(2)	127.0(5)
C(33)-C(34)-P(3)	113.8(5)	C(33)-C(34)-Fe(2)	69.7(4)
P(3)-C(34)-Fe(2)	72.8(3)	C(54)-C(49)-C(50)	117.8(5)
C(54)-C(49)-C(31)	119.3(4)	C(50)-C(49)-C(31)	122.9(4)
C(51)-C(50)-C(49)	120.9(5)	C(50)-C(51)-C(52)	120.5(5)
C(53)-C(52)-C(51)	119.3(5)	C(52)-C(53)-C(54)	120.0(5)
C(49)-C(54)-C(53)	121.5(5)	C(66)-C(65)-C(64)	112.6(7)
C(66)-C(65)-C(67)	123.4(12)	C(64)-C(65)-C(67)	123.9(10)
C(66)-C(65)-Fe(2)	70.2(4)	C(64)-C(65)-Fe(2)	70.2(4)
C(67)-C(65)-Fe(2)	124.8(7)	C(65)-C(66)-P(4)	114.8(8)
C(65)-C(66)-Fe(2)	70.5(4)	P(4)-C(66)-Fe(2)	73.2(2)
C(70)-C(69)-C(74)	117.2(9)	C(70)-C(69)-C(63)	122.8(6)
C(74)-C(69)-C(63)	120.1(7)	C(71)-C(70)-C(69)	122.3(7)
C(65)-C(64)-C(63)	112.1(7)	C(65)-C(64)-C(68)	124.8(9)
C(63)-C(64)-C(68)	122.9(12)	C(65)-C(64)-Fe(2)	70.2(6)
C(63)-C(64)-Fe(2)	70.7(4)	C(68)-C(64)-Fe(2)	130.9(4)
C(69)-C(63)-C(64)	126.3(8)	C(69)-C(63)-P(4)	122.0(5)
C(64)-C(63)-P(4)	111.6(8)	C(69)-C(63)-Fe(2)	129.4(4)
C(64)-C(63)-Fe(2)	68.8(5)	P(4)-C(63)-Fe(2)	71.7(3)
C(72)-C(71)-C(70)	117.0(9)	C(71)-C(72)-C(73)	123.7(11)
C(74)-C(73)-C(72)	118.6(9)	C(73)-C(74)-C(69)	121.2(8)

Symmetry transformations used to generate equivalent atoms:

Table 4. Anisotropic displacement parameters [$Å^2$ x 10^3] for 1.

The anisotropic displacement factor exponent takes the form:

$-2\pi^2 [(ha^*)^2 U_{11} + ... + 2hka^* b^* U_{12}]$

	U11	U22	U33	U23	U13	U12
Fe(1)	28(1)	43(1)	34(1)	4(1)	10(1)	3(1)
Fe(2)	70(1)	69(1)	26(1)	0(1)	9(1)	-32(1)
P(1)	29(1)	50(1)	39(1)	3(1)	3(1)	0(1)
P(2)	30(1)	56(1)	36(1)	6(1)	6(1)	7(1)
P(3)	56(1)	70(1)	28(1)	-4(1)	6(1)	-18(1)
P(4)	69(1)	87(1)	26(1)	-2(1)	8(1)	-27(1)
C(1)	30(2)	43(3)	38(2)	5(2)	13(2)	4(2)
C(2)	32(2)	51(3)	42(3)	11(3)	19(2)	3(2)
C(3)	37(3)	42(3)	50(3)	1(2)	17(2)	1(2)
C(4)	41(3)	52(3)	51(3)	-1(3)	18(2)	-8(2)
C(5)	69(4)	49(3)	80(4)	11(3)	33(3)	6(3)
C(6)	52(3)	58(3)	39(3)	12(2)	20(2)	9(2)
C(7)	35(2)	43(3)	27(2)	4(2)	6(2)	-2(2)
C(8)	53(3)	37(3)	50(3)	1(2)	0(2)	12(2)
C(9)	88(5)	53(4)	61(4)	9(3)	-4(3)	30(3)
C(10)	100(5)	43(3)	58(4)	-1(3)	6(4)	3(3)
C(11)	60(3)	60(4)	51(3)	-4(3)	9(3)	-20(3)
C(12)	36(2)	62(4)	43(3)	8(3)	14(2)	1(2)
C(13)	27(2)	51(3)	39(3)	6(2)	10(2)	5(2)
C(14)	31(2)	50(3)	33(2)	4(2)	11(2)	1(2)
C(15)	40(3)	56(3)	40(3)	1(2)	16(2)	7(2)
C(16)	38(3)	47(3)	50(3)	10(2)	13(2)	7(2)
C(17)	59(3)	60(4)	55(3)	-9(3)	20(3)	4(3)
C(18)	47(3)	58(3)	35(3)	2(2)	9(2)	-7(2)
C(19)	32(2)	50(3)	35(2)	8(2)	12(2)	3(2)
C(20)	34(2)	54(3)	50(3)	8(3)	14(2)	6(2)
C(21)	48(3)	57(4)	66(4)	15(3)	7(3)	11(3)
C(22)	62(3)	56(4)	76(4)	13(4)	16(3)	-2(3)
C(23)	54(3)	60(4)	59(4)	-7(3)	8(3)	-13(3)
C(24)	35(3)	56(3)	47(3)	1(2)	9(2)	3(2)
C(31)	45(3)	47(3)	29(2)	-1(2)	12(2)	-3(2)
C(32)	60(3)	45(3)	32(2)	0(2)	7(2)	7(2)
C(33)	104(5)	45(3)	42(3)	2(3)	11(3)	-9(3)
C(34)	111(5)	64(4)	36(3)	-3(3)	8(3)	-33(4)
C(35)	189(9)	56(4)	56(4)	10(3)	2(5)	0(5)
C(36)	58(3)	64(4)	45(3)	5(3)	5(3)	11(3)
C(49)	26(2)	52(3)	34(2)	3(2)	11(2)	4(2)
C(50)	45(3)	56(3)	34(3)	-1(2)	11(2)	-4(2)
C(51)	66(4)	46(3)	52(3)	-4(3)	21(3)	-1(3)
C(52)	78(4)	42(3)	76(4)	12(3)	27(3)	5(3)
C(53)	64(3)	56(4)	52(3)	17(3)	22(3)	11(3)
C(54)	45(2)	51(3)	33(2)	6(2)	11(2)	3(2)
C(65)	167(10)	167(10)	39(4)	-8(5)	40(5)	-119(8)
C(66)	176(8)	102(6)	31(3)	3(3)	28(4)	-76(6)
C(67)	343(17)	247(14)	76(6)	-37(7)	63(9)	-256(15)
C(69)	28(2)	147(7)	39(3)	-17(4)	3(2)	11(4)
C(70)	45(3)	143(7)	52(4)	-22(4)	10(3)	22(4)
C(64)	76(5)	247(13)	31(3)	-20(5)	24(3)	-102(7)

C(63)	52(4)	150(8)	26(3)	-11(4)	18(3)	-38(4)
C(71)	97(6)	199(11)	75(5)	-14(6)	-3(4)	108(7)
C(68)	62(4)	303(14)	59(4)	-43(6)	22(3)	-100(7)
C(72)	180(11)	170(11)	112(8)	-50(8)	-32(7)	126(10)
C(73)	135(8)	183(11)	101(7)	-73(7)	-24(6)	103(8)
C(74)	67(4)	162(9)	55(4)	-42(5)	0(3)	48(5)

Table 5. Hydrogen coordinates (x 10^4) and isotropic displacement parameters ($Å^2$ x 10^3) for 1.

	x	y	z	U(eq)
H(4A)	-2184(2)	-5806(5)	-4881(3)	56
H(5A)	-1498(3)	-6831(5)	-2693(4)	95
H(5B)	-1420(3)	-7164(5)	-3594(4)	95
H(5C)	-2071(3)	-7254(5)	-3418(4)	95
H(6A)	-1364(2)	-5460(5)	-1939(3)	73
H(6B)	-1764(2)	-4345(5)	-1828(3)	73
H(6C)	-1091(2)	-4156(5)	-1911(3)	73
H(8A)	-2712(2)	-1835(4)	-3580(3)	59
H(9A)	-2640(3)	97(6)	-3086(4)	86
H(10A)	-1739(3)	803(6)	-2264(4)	84
H(11A)	-876(3)	-364(5)	-1979(3)	69
H(12A)	-928(2)	-2284(5)	-2494(3)	56
H(16A)	-414(2)	-6129(5)	-3541(3)	54
H(17A)	-1132(3)	-5883(5)	-5846(4)	85
H(17B)	-1235(3)	-6703(5)	-5112(4)	85
H(17C)	-586(3)	-6661(5)	-5299(4)	85
H(18A)	-1239(2)	-4265(5)	-6150(3)	70
H(18B)	-814(2)	-3121(5)	-5988(3)	70
H(18C)	-1469(2)	-3070(5)	-5822(3)	70
H(20A)	-1500(2)	-1589(5)	-4793(3)	55
H(21A)	-1449(2)	459(5)	-4777(4)	70
H(22A)	-534(2)	1416(6)	-4219(4)	78
H(23A)	342(3)	295(5)	-3674(4)	71
H(24A)	297(2)	-1740(5)	-3711(3)	55
H(34A)	-970(3)	-5036(6)	-7797(3)	87
H(35A)	-2527(4)	-4966(6)	-9240(4)	160
H(35B)	-1889(4)	-4398(6)	-9245(4)	160
H(35C)	-2176(4)	-4140(6)	-8485(4)	160
H(36A)	-2774(2)	-8090(6)	-8983(3)	86
H(36B)	-2757(2)	-7016(6)	-9601(3)	86
H(36C)	-2989(2)	-6802(6)	-8786(3)	86
H(50A)	-2013(2)	-9525(5)	-9156(3)	54
H(51A)	-2187(3)	-11509(5)	-8969(4)	65
H(52A)	-2046(3)	-12283(5)	-7622(4)	77
H(53A)	-1777(3)	-11025(5)	-6474(4)	67
H(54A)	-1599(2)	-9031(5)	-6661(3)	51
H(66A)	-1496(4)	-5509(8)	-10223(4)	124
H(67A)	50(6)	-5092(12)	-8791(5)	331
H(67B)	-591(6)	-4466(12)	-8890(5)	331
H(67C)	-303(6)	-4523(12)	-9667(5)	331
H(70A)	-426(3)	-9358(8)	-8028(4)	97
H(71A)	-217(4)	-11356(10)	-7781(5)	154
H(68A)	267(3)	-8267(11)	-8422(4)	210
H(68B)	258(3)	-6971(11)	-8041(4)	210
H(68C)	507(3)	-7165(11)	-8844(4)	210
H(72A)	-409(5)	-12610(11)	-8907(7)	201
H(73A)	-836(4)	-11972(11)	-10253(6)	180
H(74A)	-1010(3)	-9990(9)	-10504(4)	117

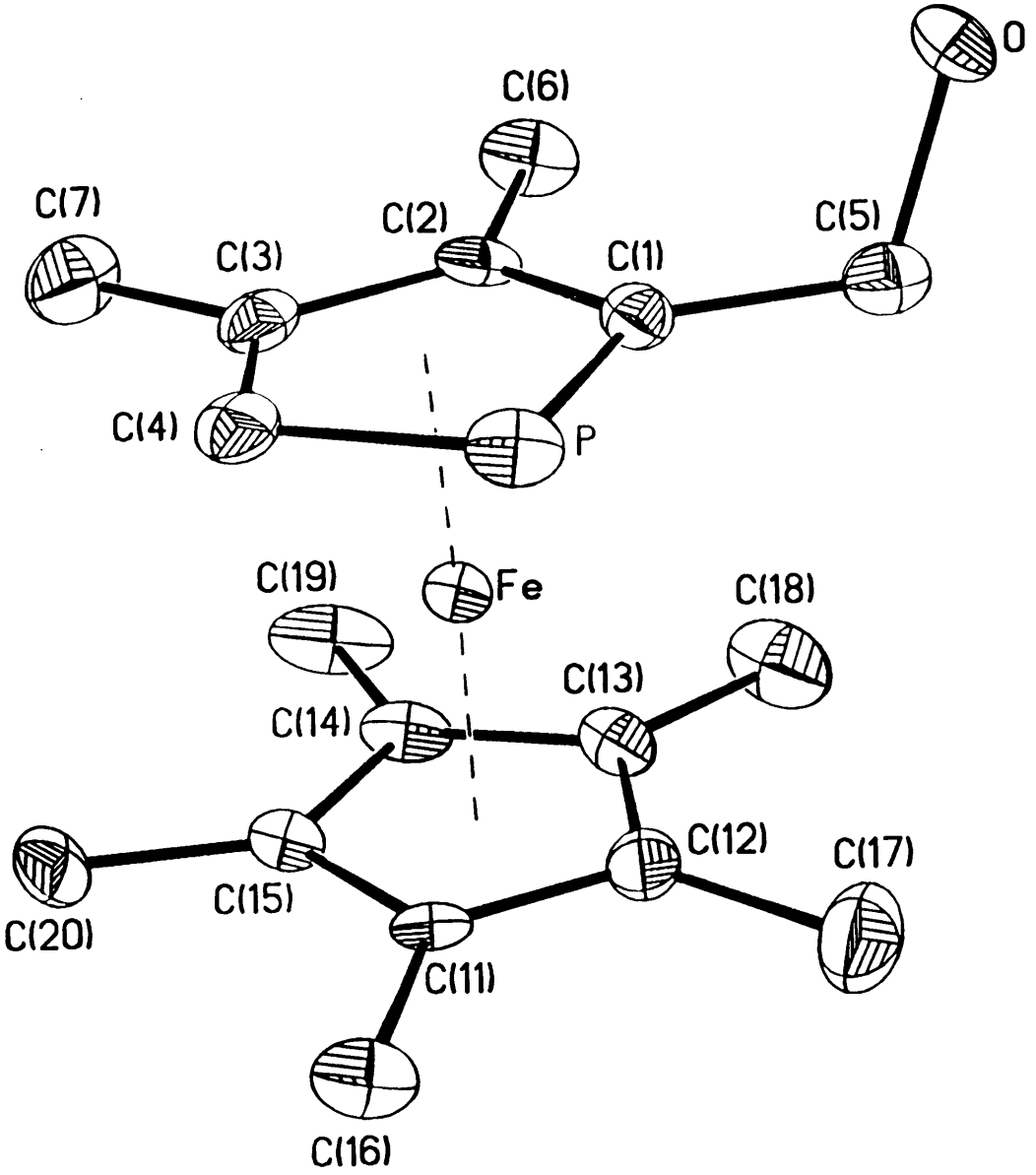
O
C(6)
C(7)
C(2)
C(5)
C(3)
C(1)
C(4)
P
Fe
C(19)
C(18)
C(13)
C(14)
C(12)
C(17)
C(15)
C(20)
C(11)
C(16)

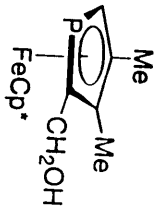
Me
P
FeCp*
CH2OH
Me

Table 1. Crystal data and structure refinement for 98027.

A. Crystal Data

Identification code	98027
Empirical formula	$C_{17}H_{25}FeOP$
Formula weight	332.19
Temperature	183(2) K
Wavelength	0.71073 Å
Crystal morphology	block
Crystal size	0.3 x 0.33 x 0.42 mm
Crystal system	Tetragonal
Space group	$I4_1$
Unit cell dimensions	a = 20.1248(9) Å alpha = 90°
	b = 20.1248(9) Å beta = 90°
	c = 8.2114(5) Å gamma = 90°
Volume, Z	3325.7(3) $Å^3$, 8
Density (calculated)	1.327 Mg/m^3
Absorption coefficient	0.997 mm^{-1}
F(000)	1408

B. Data Collection and Reduction

Diffractometer	Siemens SMART/CCD
Scan Type	ω Scans
Scan angle	0.30°
θ range for data collection	1.43 to 23.27°
Limiting indices	$-18 \le h \le 22$, $-22 \le k \le 21$, $-6 \le l \le 9$

Reflections collected	6891
Independent reflections	2232 (R_{int} = 0.0694)
Absorption correction	Semi-empirical from psi-scans
Max. and min. transmission	0.9940 and 0.6042

C. Solution and Refinement

Refinement method	Full-matrix least-squares on F^2
Data / restraints / parameters	2232 / 1 / 181
Goodness-of-fit on F^2	1.166
Final R indices [$I>2\sigma(I)$]	R1 = 0.0469, wR2 = 0.1133
R indices (all data)	R1 = 0.0529, wR2 = 0.1198
Absolute structure parameter	0.02(4)
Largest diff. peak and hole	0.329 and -0.285 $e\text{Å}^{-3}$

Table 2. Atomic coordinates [x 10^4] and equivalent isotropic displacement parameters [$Å^2$ x 10^3] for 98027. U(eq) is defined as one third of the trace of the orthogonalized U_{ij} tensor.

	x	y	z	U(eq)
Fe	5083(1)	2398(1)	1711(1)	22(1)
P	4686(1)	2850(1)	-634(2)	33(1)
O	3005(2)	2097(2)	89(5)	31(1)
C(1)	4128(3)	2473(3)	757(8)	28(2)
C(2)	4154(3)	2753(3)	2339(8)	29(2)
C(3)	4638(3)	3275(3)	2447(8)	32(2)
C(4)	4976(4)	3372(3)	953(9)	34(2)
C(5)	3681(3)	1894(3)	300(9)	36(2)
C(6)	3713(3)	2552(4)	3727(8)	41(2)
C(7)	4767(4)	3678(4)	3941(10)	52(2)
C(11)	6008(3)	2052(3)	1162(7)	24(2)
C(12)	5553(3)	1520(3)	1144(9)	33(2)
C(13)	5264(3)	1479(3)	2725(9)	33(2)
C(14)	5547(3)	1983(4)	3711(8)	33(2)
C(15)	6010(3)	2342(3)	2746(8)	26(2)
C(16)	6444(3)	2275(4)	-236(9)	40(2)
C(17)	5437(4)	1047(4)	-256(10)	57(2)
C(18)	4771(4)	970(4)	3293(12)	62(3)
C(19)	5400(4)	2100(5)	5471(9)	56(2)
C(20)	6422(3)	2911(4)	3284(10)	41(2)

Table 3. Bond lengths [Å] and angles [°] for 98027.

Fe-C(11)	2.037(6)	Fe-C(15)	2.052(6)
Fe-C(13)	2.061(7)	Fe-C(12)	2.058(6)
Fe-C(14)	2.065(6)	Fe-C(3)	2.069(6)
Fe-C(4)	2.068(6)	Fe-C(2)	2.068(6)
Fe-C(1)	2.082(6)	Fe-P	2.275(2)
P-C(1)	1.772(7)	P-C(4)	1.773(8)
O-C(5)	1.432(8)	C(1)-C(2)	1.416(9)
C(1)-C(5)	1.520(9)	C(2)-C(3)	1.435(9)
C(2)-C(6)	1.499(9)	C(3)-C(4)	1.417(9)
C(3)-C(7)	1.495(10)	C(11)-C(12)	1.409(9)
C(11)-C(15)	1.425(9)	C(11)-C(16)	1.513(9)
C(12)-C(13)	1.425(10)	C(12)-C(17)	1.510(10)
C(13)-C(14)	1.418(11)	C(13)-C(18)	1.500(10)
C(14)-C(15)	1.420(9)	C(14)-C(19)	1.494(10)
C(15)-C(20)	1.482(9)		

C(11)-Fe-C(15)	40.8(3)	C(11)-Fe-C(13)	67.8(3)
C(15)-Fe-C(13)	67.9(3)	C(11)-Fe-C(12)	40.2(3)
C(15)-Fe-C(12)	68.2(3)	C(13)-Fe-C(12)	40.5(3)
C(11)-Fe-C(14)	68.0(3)	C(15)-Fe-C(14)	40.4(3)
C(13)-Fe-C(14)	40.2(3)	C(12)-Fe-C(14)	68.0(3)
C(11)-Fe-C(3)	138.8(3)	C(15)-Fe-C(3)	108.7(3)
C(13)-Fe-C(3)	136.4(3)	C(12)-Fe-C(3)	175.9(3)
C(14)-Fe-C(3)	108.0(3)	C(11)-Fe-C(4)	110.6(3)
C(15)-Fe-C(4)	105.8(3)	C(13)-Fe-C(4)	172.3(3)
C(12)-Fe-C(4)	142.5(3)	C(14)-Fe-C(4)	132.1(3)
C(3)-Fe-C(4)	40.1(3)	C(11)-Fe-C(2)	178.3(3)
C(15)-Fe-C(2)	137.6(3)	C(13)-Fe-C(2)	111.6(3)
C(12)-Fe-C(2)	140.2(3)	C(14)-Fe-C(2)	110.5(3)
C(3)-Fe-C(2)	40.6(3)	C(4)-Fe-C(2)	69.7(3)
C(11)-Fe-C(1)	141.7(3)	C(15)-Fe-C(1)	177.5(3)
C(13)-Fe-C(1)	112.3(3)	C(12)-Fe-C(1)	113.7(3)
C(14)-Fe-C(1)	138.2(3)	C(3)-Fe-C(1)	69.4(3)
C(4)-Fe-C(1)	73.8(3)	C(2)-Fe-C(1)	39.9(3)
C(11)-Fe-P	105.7(2)	C(15)-Fe-P	133.8(2)
C(13)-Fe-P	139.7(2)	C(12)-Fe-P	108.3(2)
C(14)-Fe-P	173.6(2)	C(3)-Fe-P	75.7(2)
C(4)-Fe-P	47.9(2)	C(2)-Fe-P	75.8(2)
C(1)-Fe-P	47.7(2)	C(1)-P-C(4)	89.4(3)
C(1)-P-Fe	60.4(2)	C(4)-P-Fe	59.9(2)
C(2)-C(1)-C(5)	123.6(6)	C(2)-C(1)-P	113.5(5)
C(5)-C(1)-P	123.0(5)	C(2)-C(1)-Fe	69.5(4)
C(5)-C(1)-Fe	125.7(5)	P-C(1)-Fe	71.9(2)
C(1)-C(2)-C(3)	111.8(6)	C(1)-C(2)-C(6)	124.7(6)
C(3)-C(2)-C(6)	123.4(6)	C(1)-C(2)-Fe	70.6(4)
C(3)-C(2)-Fe	69.7(4)	C(6)-C(2)-Fe	129.2(5)
C(4)-C(3)-C(2)	112.0(6)	C(4)-C(3)-C(7)	123.5(6)
C(2)-C(3)-C(7)	124.5(7)	C(4)-C(3)-Fe	69.9(4)
C(2)-C(3)-Fe	69.6(4)	C(7)-C(3)-Fe	128.9(5)
C(3)-C(4)-P	113.3(5)	C(3)-C(4)-Fe	70.0(4)
P-C(4)-Fe	72.2(2)	O-C(5)-C(1)	111.9(5)
C(12)-C(11)-C(15)	108.8(5)	C(12)-C(11)-C(16)	126.5(6)
C(15)-C(11)-C(16)	124.7(6)	C(12)-C(11)-Fe	70.7(3)
C(15)-C(11)-Fe	70.2(3)	C(16)-C(11)-Fe	126.6(4)
C(11)-C(12)-C(13)	107.5(6)	C(11)-C(12)-C(17)	125.9(6)

C(13)-C(12)-C(17)	126.4(6)	C(11)-C(12)-Fe	69.1(3)
C(13)-C(12)-Fe	69.9(4)	C(17)-C(12)-Fe	130.0(5)
C(14)-C(13)-C(12)	108.3(6)	C(14)-C(13)-C(18)	125.2(7)
C(12)-C(13)-C(18)	126.4(7)	C(14)-C(13)-Fe	70.1(4)
C(12)-C(13)-Fe	69.6(4)	C(18)-C(13)-Fe	128.4(5)
C(15)-C(14)-C(13)	108.0(6)	C(15)-C(14)-C(19)	126.1(8)
C(13)-C(14)-C(19)	125.8(7)	C(15)-C(14)-Fe	69.3(4)
C(13)-C(14)-Fe	69.8(4)	C(19)-C(14)-Fe	128.0(5)
C(14)-C(15)-C(11)	107.4(6)	C(14)-C(15)-C(20)	126.4(6)
C(11)-C(15)-C(20)	126.2(6)	C(14)-C(15)-Fe	70.3(4)
C(11)-C(15)-Fe	69.0(4)	C(20)-C(15)-Fe	126.2(5)

Symmetry transformations used to generate equivalent atoms:

Table 4. Anisotropic displacement parameters [$Å^2$ x 10^3] for 98027.

The anisotropic displacement factor exponent takes the form:

$-2\pi^2 [(ha^*)^2 U_{11} + ... + 2hka^* b^* U_{12}]$

	U11	U22	U33	U23	U13	U12
Fe	21(1)	25(1)	20(1)	3(1)	0(1)	2(1)
P	33(1)	40(1)	24(1)	9(1)	0(1)	6(1)
O	24(2)	41(3)	29(3)	9(2)	-5(2)	-2(2)
C(1)	23(3)	32(4)	29(4)	-7(3)	-2(3)	1(3)
C(2)	20(3)	39(4)	27(4)	2(3)	-1(3)	9(3)
C(3)	36(4)	28(4)	34(4)	0(3)	-5(3)	15(3)
C(4)	36(4)	25(4)	42(5)	9(3)	0(3)	8(3)
C(5)	34(4)	39(4)	34(4)	2(3)	1(3)	9(3)
C(6)	38(4)	60(5)	25(5)	5(3)	5(3)	9(3)
C(7)	57(5)	55(5)	44(6)	-14(4)	-16(4)	12(4)
C(11)	20(3)	31(4)	22(4)	2(3)	7(2)	10(3)
C(12)	31(4)	28(4)	39(5)	1(3)	-6(3)	5(3)
C(13)	27(4)	30(4)	42(4)	12(3)	-2(3)	1(3)
C(14)	27(3)	48(4)	23(4)	16(3)	-2(3)	13(3)
C(15)	24(3)	30(4)	24(4)	6(3)	0(3)	1(3)
C(16)	36(4)	56(5)	28(4)	6(3)	3(3)	8(3)
C(17)	65(5)	48(5)	58(6)	-15(4)	-13(4)	0(4)
C(18)	44(5)	45(5)	98(7)	35(5)	2(5)	-7(4)
C(19)	45(5)	106(7)	16(4)	17(4)	6(3)	30(4)
C(20)	27(4)	47(5)	48(5)	-1(4)	-17(3)	0(3)

Table 5. Hydrogen coordinates (x 10^4) and isotropic displacement parameters ($Å^2$ x 10^3) for 98027.

	x	y	z	U(eq)
H(0A)	2983(2)	2383(2)	-654(5)	47
H(4A)	5358(4)	3685(3)	823(9)	41
H(5A)	3844(3)	1691(3)	-724(9)	43
H(5B)	3704(3)	1551(3)	1164(9)	43
H(6A)	3823(3)	2817(4)	4690(8)	61
H(6B)	3781(3)	2080(4)	3969(8)	61
H(6C)	3248(3)	2627(4)	3429(8)	61
H(7A)	4479(4)	3523(4)	4826(10)	78
H(7B)	4672(4)	4147(4)	3714(10)	78
H(7C)	5233(4)	3630(4)	4264(10)	78
H(16A)	6713(3)	2656(4)	109(9)	60
H(16B)	6164(3)	2404(4)	-1160(9)	60
H(16C)	6737(3)	1909(4)	-561(9)	60
H(17A)	5094(4)	724(4)	46(10)	85
H(17B)	5851(4)	813(4)	-509(10)	85
H(17C)	5291(4)	1298(4)	-1214(10)	85
H(18A)	4648(4)	682(4)	2380(12)	94
H(18B)	4373(4)	1195(4)	3707(12)	94
H(18C)	4969(4)	702(4)	4163(12)	94
H(19A)	5060(4)	1785(5)	5837(9)	84
H(19B)	5237(4)	2555(5)	5619(9)	84
H(19C)	5806(4)	2037(5)	6112(9)	84
H(20A)	6700(3)	3063(4)	2376(10)	62
H(20B)	6708(3)	2772(4)	4190(10)	62
H(20C)	6133(3)	3275(4)	3642(10)	62

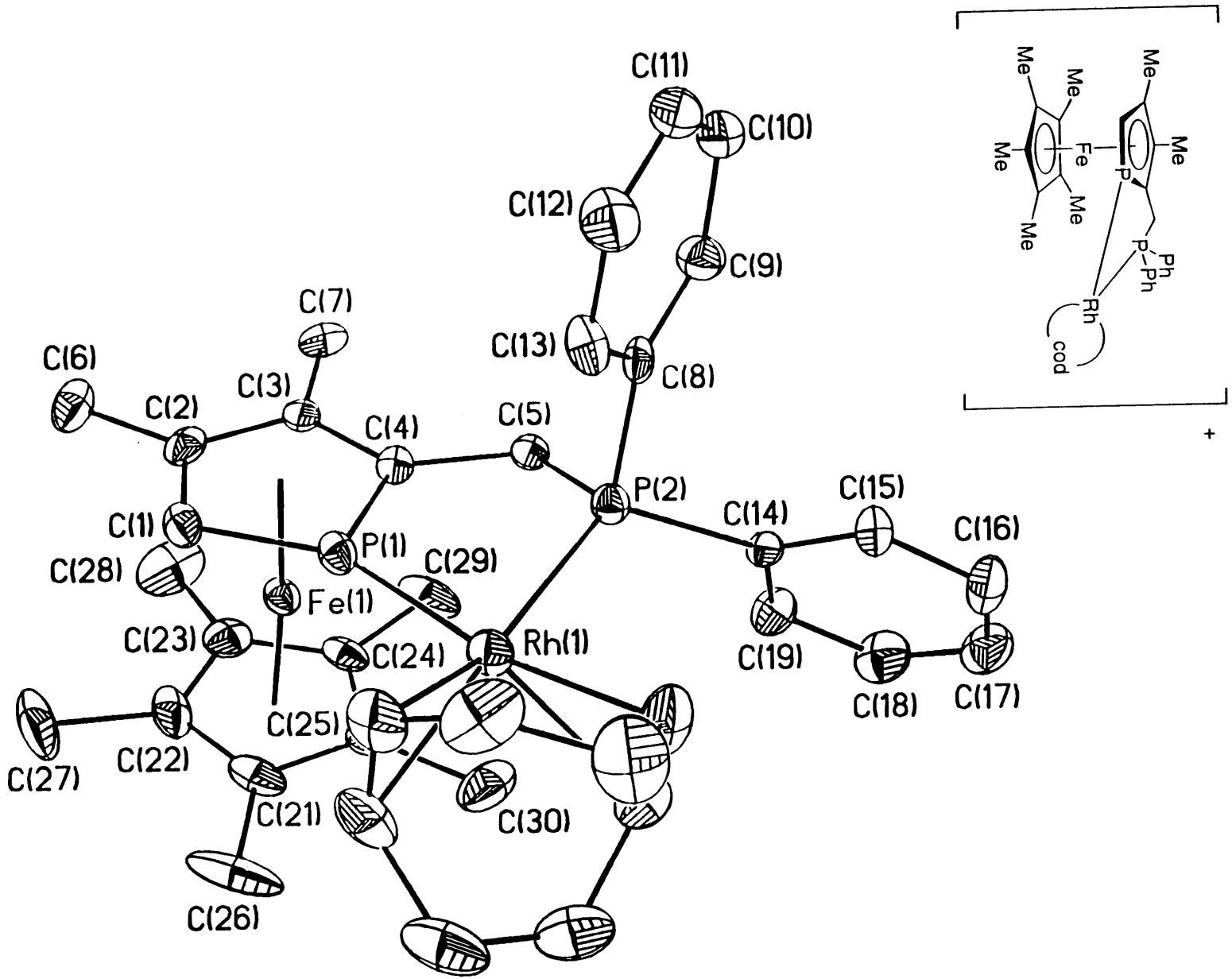
C(11)
C(10)
C(12)
C(9)
C(7)
C(13)
C(8)
C(6)
C(3)
C(2)
C(4)
C(5)
P(2)
C(15)
C(14)
C(1)
P(1)
C(29)
C(16)
C(28)
Fe(1)
C(23)
C(24)
Rh(1)
C(19)
C(18)
C(17)
C(25)
C(27)
C(22)
C(21)
C(30)
C(26)
Me
Me
Me
Fe
Me
Me
Me
Me
P
P
Ph
Ph
Rh
cod
+

Table 1. Crystal data and structure refinement for 1.

A. Crystal Data

Identification code	98090
Empirical formula	$C_{37}H_{46}F_6FeP_3Rh$
Formula weight	856.41
Temperature	183(2) K
Wavelength	0.71073 Å
Crystal morphology	block
Crystal size	0.09 x 0.12 x 0.15 mm
Crystal system	Orthorhombic
Space group	$P2_12_12_1$
Unit cell dimensions	a = 13.5363(2) Å alpha = 90°
	b = 15.3220(2) Å beta = 90°
	c = 17.8722(3) Å gamma = 90°
Volume, Z	3706.75(10) $Å^3$, 4
Density (calculated)	1.535 Mg/m^3
Absorption coefficient	1.022 mm^{-1}
F(000)	1752

B. Data Collection and Reduction

Diffractometer	Siemens SMART/CCD
Scan Type	ω Scans
Scan angle	0.30°
θ range for data collection	1.75 to 23.32°
Limiting indices	$-14 \le h \le 15$, $-17 \le k \le 16$, $-7 \le l \le 19$

Reflections collected	14889
Independent reflections	5320 (R_{int} = 0.0505)
Absorption correction	None

C. Solution and Refinement

Refinement method	Full-matrix least-squares on F^2
Data / restraints / parameters	5316 / 0 / 434
Goodness-of-fit on F^2	1.127
Final R indices [I>2σ(I)]	R1 = 0.0463, wR2 = 0.0911
R indices (all data)	R1 = 0.0596, wR2 = 0.1357
Absolute structure parameter	-0.02(3)
Extinction coefficient	0.00041(10)
Largest diff. peak and hole	0.542 and -0.528 eÅ^{-3}

Table 2. Atomic coordinates [x 10^4] and equivalent isotropic displacement parameters [$Å^2$ x 10^3] for 98090. U(eq) is defined as one third of the trace of the orthogonalized U_{ij} tensor.

	x	y	z	U(eq)
Rh(1)	7659(1)	4279(1)	652(1)	33(1)
Fe(1)	6405(1)	6637(1)	294(1)	27(1)
P(1)	7655(1)	5749(1)	605(1)	29(1)
P(2)	8037(1)	4481(1)	-592(1)	27(1)
P(3)	1424(2)	5339(1)	2326(1)	52(1)
F(1)	2109(5)	4609(3)	2655(4)	103(2)
F(2)	1803(6)	5152(5)	1520(3)	112(3)
F(3)	782(5)	6110(4)	2017(5)	115(3)
F(4)	2308(5)	6029(3)	2423(3)	83(2)
F(5)	1064(7)	5555(5)	3133(4)	131(3)
F(6)	581(5)	4654(4)	2222(5)	120(3)
C(1)	7591(5)	6800(5)	1010(4)	33(2)
C(2)	7611(5)	7451(4)	448(4)	34(2)
C(3)	7616(5)	7116(4)	-294(4)	29(2)
C(4)	7621(5)	6190(4)	-302(4)	25(1)
C(5)	7662(5)	5567(4)	-955(3)	27(2)
C(6)	7613(5)	8412(4)	633(5)	48(2)
C(7)	7632(6)	7673(4)	-983(4)	36(2)
C(8)	9375(5)	4458(4)	-711(4)	27(2)
C(9)	9804(6)	4608(5)	-1405(5)	37(2)
C(10)	10825(6)	4614(5)	-1485(5)	43(2)
C(11)	11412(6)	4466(5)	-868(5)	55(2)
C(12)	11010(6)	4321(6)	-183(5)	51(2)
C(13)	9983(6)	4338(5)	-87(4)	39(2)
C(14)	7567(5)	3685(4)	-1269(3)	26(2)
C(15)	8109(6)	2930(5)	-1412(4)	34(2)
C(16)	7686(7)	2262(5)	-1823(4)	45(2)
C(17)	6761(7)	2343(6)	-2108(5)	49(2)
C(18)	6254(7)	3103(6)	-2001(5)	50(2)
C(19)	6643(6)	3767(5)	-1568(4)	38(2)
C(21)	5137(5)	6257(6)	825(4)	43(2)
C(22)	5213(5)	7178(6)	821(5)	45(2)
C(23)	5241(6)	7469(6)	78(5)	40(2)
C(24)	5182(5)	6722(5)	-388(4)	32(2)
C(25)	5121(5)	5969(5)	70(4)	32(2)
C(26)	5034(7)	5690(9)	1504(5)	90(4)
C(27)	5255(7)	7763(8)	1516(6)	89(4)
C(28)	5245(6)	8404(6)	-163(7)	75(3)
C(29)	5146(6)	6746(7)	-1227(4)	58(3)
C(30)	4979(6)	5052(6)	-202(6)	65(3)
C(31)	8139(7)	4035(6)	1825(4)	49(2)
C(32)	7131(7)	4096(7)	1830(5)	58(3)
C(33)	6431(8)	3327(8)	1870(5)	78(3)
C(34)	6114(9)	2964(7)	1104(6)	86(4)
C(35)	6910(7)	3025(5)	506(6)	60(3)
C(36)	7898(8)	2862(5)	576(6)	59(3)
C(37)	8370(10)	2515(7)	1277(6)	83(4)
C(38)	8741(8)	3202(6)	1809(5)	66(3)

Table 3. Bond lengths [Å] and angles [°] for 98090.

Rh(1)-C(35)	2.188(8)	Rh(1)-C(36)	2.198(8)
Rh(1)-C(31)	2.226(7)	Rh(1)-C(32)	2.240(8)
Rh(1)-P(1)	2.254(2)	Rh(1)-P(2)	2.302(2)
Fe(1)-C(22)	2.044(7)	Fe(1)-C(21)	2.045(7)
Fe(1)-C(25)	2.056(7)	Fe(1)-C(24)	2.060(7)
Fe(1)-C(23)	2.063(8)	Fe(1)-C(1)	2.069(7)
Fe(1)-C(2)	2.073(7)	Fe(1)-C(4)	2.077(7)
Fe(1)-C(3)	2.081(7)	Fe(1)-P(1)	2.242(2)
P(1)-C(4)	1.756(7)	P(1)-C(1)	1.767(7)
P(2)-C(8)	1.825(7)	P(2)-C(14)	1.832(6)
P(2)-C(5)	1.856(6)	P(3)-F(2)	1.555(6)
P(3)-F(5)	1.559(6)	P(3)-F(6)	1.561(6)
P(3)-F(3)	1.567(6)	P(3)-F(1)	1.568(6)
P(3)-F(4)	1.606(6)	C(1)-C(2)	1.416(9)
C(2)-C(3)	1.422(9)	C(2)-C(6)	1.510(9)
C(3)-C(4)	1.418(8)	C(3)-C(7)	1.498(9)
C(4)-C(5)	1.509(8)	C(8)-C(9)	1.388(10)
C(8)-C(13)	1.399(10)	C(9)-C(10)	1.389(10)
C(10)-C(11)	1.379(12)	C(11)-C(12)	1.359(11)
C(12)-C(13)	1.400(10)	C(14)-C(19)	1.366(10)
C(14)-C(15)	1.394(9)	C(15)-C(16)	1.384(10)
C(16)-C(17)	1.358(12)	C(17)-C(18)	1.365(12)
C(18)-C(19)	1.383(11)	C(21)-C(22)	1.415(11)
C(21)-C(25)	1.418(11)	C(21)-C(26)	1.499(11)
C(22)-C(23)	1.402(13)	C(22)-C(27)	1.532(12)
C(23)-C(24)	1.418(11)	C(23)-C(28)	1.497(12)
C(24)-C(25)	1.418(10)	C(24)-C(29)	1.500(11)
C(25)-C(30)	1.500(11)	C(31)-C(32)	1.367(11)
C(31)-C(38)	1.516(12)	C(32)-C(33)	1.515(14)
C(33)-C(34)	1.538(14)	C(34)-C(35)	1.521(13)
C(35)-C(36)	1.366(12)	C(36)-C(37)	1.504(13)
C(37)-C(38)	1.505(13)		

C(35)-Rh(1)-C(36)	36.3(3)	C(35)-Rh(1)-C(31)	95.8(4)
C(36)-Rh(1)-C(31)	81.4(4)	C(35)-Rh(1)-C(32)	81.7(4)
C(36)-Rh(1)-C(32)	89.0(4)	C(31)-Rh(1)-C(32)	35.6(3)
C(35)-Rh(1)-P(1)	150.7(3)	C(36)-Rh(1)-P(1)	169.9(3)
C(31)-Rh(1)-P(1)	101.8(3)	C(32)-Rh(1)-P(1)	99.2(3)
C(35)-Rh(1)-P(2)	96.0(3)	C(36)-Rh(1)-P(2)	92.3(3)
C(31)-Rh(1)-P(2)	150.2(2)	C(32)-Rh(1)-P(2)	174.2(3)
P(1)-Rh(1)-P(2)	80.18(6)	C(22)-Fe(1)-C(21)	40.5(3)
C(22)-Fe(1)-C(25)	67.9(3)	C(21)-Fe(1)-C(25)	40.5(3)
C(22)-Fe(1)-C(24)	67.2(3)	C(21)-Fe(1)-C(24)	67.6(3)
C(25)-Fe(1)-C(24)	40.3(3)	C(22)-Fe(1)-C(23)	39.9(4)
C(21)-Fe(1)-C(23)	67.8(3)	C(25)-Fe(1)-C(23)	68.0(3)
C(24)-Fe(1)-C(23)	40.2(3)	C(22)-Fe(1)-C(1)	106.2(3)
C(21)-Fe(1)-C(1)	113.5(3)	C(25)-Fe(1)-C(1)	146.7(3)
C(24)-Fe(1)-C(1)	169.2(3)	C(23)-Fe(1)-C(1)	129.4(3)
C(22)-Fe(1)-C(2)	108.5(3)	C(21)-Fe(1)-C(2)	140.4(3)
C(25)-Fe(1)-C(2)	172.3(3)	C(24)-Fe(1)-C(2)	132.4(3)
C(23)-Fe(1)-C(2)	104.8(3)	C(1)-Fe(1)-C(2)	40.0(3)
C(22)-Fe(1)-C(4)	174.8(3)	C(21)-Fe(1)-C(4)	144.0(3)
C(25)-Fe(1)-C(4)	114.0(3)	C(24)-Fe(1)-C(4)	110.8(3)
C(23)-Fe(1)-C(4)	135.5(3)	C(1)-Fe(1)-C(4)	75.0(3)
C(2)-Fe(1)-C(4)	69.0(3)	C(22)-Fe(1)-C(3)	135.4(3)

C(21)-Fe(1)-C(3)	174.6(3)	C(25)-Fe(1)-C(3)	138.0(3)
C(24)-Fe(1)-C(3)	108.2(3)	C(23)-Fe(1)-C(3)	106.9(3)
C(1)-Fe(1)-C(3)	70.0(3)	C(2)-Fe(1)-C(3)	40.0(3)
C(4)-Fe(1)-C(3)	39.9(2)	C(22)-Fe(1)-P(1)	136.7(3)
C(21)-Fe(1)-P(1)	110.2(2)	C(25)-Fe(1)-P(1)	112.6(2)
C(24)-Fe(1)-P(1)	142.4(2)	C(23)-Fe(1)-P(1)	176.4(3)
C(1)-Fe(1)-P(1)	48.2(2)	C(2)-Fe(1)-P(1)	74.8(2)
C(4)-Fe(1)-P(1)	47.8(2)	C(3)-Fe(1)-P(1)	75.2(2)
C(4)-P(1)-C(1)	91.5(3)	C(4)-P(1)-Fe(1)	61.2(2)
C(1)-P(1)-Fe(1)	60.8(2)	C(4)-P(1)-Rh(1)	114.8(2)
C(1)-P(1)-Rh(1)	153.5(3)	Fe(1)-P(1)-Rh(1)	128.15(9)
C(8)-P(2)-C(14)	104.7(3)	C(8)-P(2)-C(5)	104.4(3)
C(14)-P(2)-C(5)	105.7(3)	C(8)-P(2)-Rh(1)	109.3(3)
C(14)-P(2)-Rh(1)	118.1(2)	C(5)-P(2)-Rh(1)	113.4(2)
F(2)-P(3)-F(5)	178.1(4)	F(2)-P(3)-F(6)	90.4(5)
F(5)-P(3)-F(6)	91.4(5)	F(2)-P(3)-F(3)	89.8(4)
F(5)-P(3)-F(3)	89.6(5)	F(6)-P(3)-F(3)	93.5(4)
F(2)-P(3)-F(1)	91.2(4)	F(5)-P(3)-F(1)	89.3(4)
F(6)-P(3)-F(1)	89.8(4)	F(3)-P(3)-F(1)	176.5(4)
F(2)-P(3)-F(4)	88.7(4)	F(5)-P(3)-F(4)	89.6(4)
F(6)-P(3)-F(4)	178.7(4)	F(3)-P(3)-F(4)	87.4(4)
F(1)-P(3)-F(4)	89.3(3)	C(2)-C(1)-P(1)	110.5(5)
C(2)-C(1)-Fe(1)	70.2(4)	P(1)-C(1)-Fe(1)	71.0(2)
C(1)-C(2)-C(3)	114.1(6)	C(1)-C(2)-C(6)	122.2(6)
C(3)-C(2)-C(6)	123.8(7)	C(1)-C(2)-Fe(1)	69.9(4)
C(3)-C(2)-Fe(1)	70.3(4)	C(6)-C(2)-Fe(1)	128.1(5)
C(4)-C(3)-C(2)	111.7(6)	C(4)-C(3)-C(7)	124.1(6)
C(2)-C(3)-C(7)	124.1(6)	C(4)-C(3)-Fe(1)	69.9(4)
C(2)-C(3)-Fe(1)	69.7(4)	C(7)-C(3)-Fe(1)	128.8(5)
C(3)-C(4)-C(5)	129.9(6)	C(3)-C(4)-P(1)	112.1(5)
C(5)-C(4)-P(1)	118.0(4)	C(3)-C(4)-Fe(1)	70.2(4)
C(5)-C(4)-Fe(1)	129.3(5)	P(1)-C(4)-Fe(1)	71.0(2)
C(4)-C(5)-P(2)	107.8(4)	C(9)-C(8)-C(13)	119.2(6)
C(9)-C(8)-P(2)	121.1(6)	C(13)-C(8)-P(2)	119.6(6)
C(8)-C(9)-C(10)	120.6(8)	C(11)-C(10)-C(9)	119.4(8)
C(12)-C(11)-C(10)	121.1(8)	C(11)-C(12)-C(13)	120.3(8)
C(8)-C(13)-C(12)	119.3(7)	C(19)-C(14)-C(15)	119.1(6)
C(19)-C(14)-P(2)	121.0(5)	C(15)-C(14)-P(2)	119.4(5)
C(16)-C(15)-C(14)	119.6(7)	C(17)-C(16)-C(15)	120.9(8)
C(16)-C(17)-C(18)	119.3(8)	C(17)-C(18)-C(19)	121.0(8)
C(14)-C(19)-C(18)	120.0(8)	C(22)-C(21)-C(25)	107.9(7)
C(22)-C(21)-C(26)	126.0(9)	C(25)-C(21)-C(26)	126.1(9)
C(22)-C(21)-Fe(1)	69.7(5)	C(25)-C(21)-Fe(1)	70.2(4)
C(26)-C(21)-Fe(1)	128.2(6)	C(23)-C(22)-C(21)	108.9(7)
C(23)-C(22)-C(27)	125.5(9)	C(21)-C(22)-C(27)	125.6(9)
C(23)-C(22)-Fe(1)	70.8(5)	C(21)-C(22)-Fe(1)	69.8(4)
C(27)-C(22)-Fe(1)	125.5(6)	C(22)-C(23)-C(24)	107.4(7)
C(22)-C(23)-C(28)	125.3(9)	C(24)-C(23)-C(28)	127.1(9)
C(22)-C(23)-Fe(1)	69.3(5)	C(24)-C(23)-Fe(1)	69.8(4)
C(28)-C(23)-Fe(1)	130.0(6)	C(25)-C(24)-C(23)	108.6(6)
C(25)-C(24)-C(29)	126.6(8)	C(23)-C(24)-C(29)	124.7(8)
C(25)-C(24)-Fe(1)	69.7(4)	C(23)-C(24)-Fe(1)	70.0(4)
C(29)-C(24)-Fe(1)	128.2(5)	C(24)-C(25)-C(21)	107.2(7)
C(24)-C(25)-C(30)	125.6(7)	C(21)-C(25)-C(30)	127.0(8)
C(24)-C(25)-Fe(1)	70.0(4)	C(21)-C(25)-Fe(1)	69.4(4)
C(30)-C(25)-Fe(1)	129.6(5)	C(32)-C(31)-C(38)	126.5(10)
C(32)-C(31)-Rh(1)	72.7(5)	C(38)-C(31)-Rh(1)	106.3(6)
C(31)-C(32)-C(33)	124.8(10)	C(31)-C(32)-Rh(1)	71.6(5)
C(33)-C(32)-Rh(1)	110.0(6)	C(32)-C(33)-C(34)	114.4(8)

C(35)-C(34)-C(33)	114.0(9)	C(36)-C(35)-C(34)	128.1(11)
C(36)-C(35)-Rh(1)	72.3(5)	C(34)-C(35)-Rh(1)	107.3(7)
C(35)-C(36)-C(37)	123.9(11)	C(35)-C(36)-Rh(1)	71.5(5)
C(37)-C(36)-Rh(1)	111.1(7)	C(36)-C(37)-C(38)	114.9(8)
C(37)-C(38)-C(31)	115.0(8)		

Symmetry transformations used to generate equivalent atoms:

Table 4. Anisotropic displacement parameters [$Å^2$ x 10^3] for 98090.

The anisotropic displacement factor exponent takes the form:

$-2\pi^2 [(ha^*)^2 U_{11} + ... + 2hka^* b^* U_{12}]$

	U11	U22	U33	U23	U13	U12
Rh(1)	42(1)	33(1)	23(1)	6(1)	1(1)	0(1)
Fe(1)	20(1)	35(1)	25(1)	-4(1)	1(1)	2(1)
P(1)	29(1)	35(1)	22(1)	-4(1)	-2(1)	2(1)
P(2)	30(1)	27(1)	24(1)	-1(1)	-1(1)	1(1)
P(3)	72(2)	35(1)	50(1)	2(1)	-4(1)	4(1)
F(1)	126(6)	50(3)	133(5)	10(3)	-68(5)	4(3)
F(2)	160(7)	125(6)	52(3)	-32(4)	11(4)	6(5)
F(3)	102(5)	86(5)	157(7)	53(5)	15(5)	43(4)
F(4)	98(4)	60(3)	91(4)	1(3)	-8(4)	-18(3)
F(5)	218(9)	99(6)	77(4)	-4(4)	71(5)	-27(6)
F(6)	89(5)	95(5)	176(8)	24(5)	-58(5)	-38(4)
C(1)	22(4)	48(4)	30(4)	-12(3)	-3(3)	1(4)
C(2)	19(4)	32(4)	50(5)	-8(3)	-3(4)	-3(3)
C(3)	17(3)	32(4)	38(4)	-7(3)	4(3)	-1(3)
C(4)	22(4)	26(3)	27(3)	-1(3)	-4(3)	3(3)
C(5)	31(4)	28(4)	23(3)	2(3)	3(3)	-2(4)
C(6)	30(4)	40(4)	75(5)	-24(5)	-8(5)	7(4)
C(7)	30(4)	33(4)	45(4)	11(3)	1(4)	-7(4)
C(8)	31(4)	19(4)	32(4)	-9(3)	-1(3)	4(3)
C(9)	33(5)	41(4)	37(5)	0(4)	1(4)	0(4)
C(10)	36(5)	48(5)	43(5)	-11(4)	6(4)	-8(4)
C(11)	31(4)	57(6)	76(7)	-24(5)	12(5)	-5(5)
C(12)	34(5)	64(6)	55(6)	-10(5)	-8(4)	9(5)
C(13)	47(5)	42(5)	28(4)	-8(4)	-2(4)	10(4)
C(14)	25(4)	34(4)	18(3)	-5(3)	-2(3)	-11(3)
C(15)	40(5)	31(4)	32(4)	-8(4)	0(4)	3(4)
C(16)	65(6)	29(4)	40(5)	-7(3)	-3(5)	0(4)
C(17)	60(6)	50(6)	37(5)	-3(4)	-3(4)	-18(5)
C(18)	48(6)	61(6)	41(5)	0(4)	-12(4)	-12(5)
C(19)	33(5)	43(5)	39(5)	-5(4)	-10(4)	-7(4)
C(21)	24(4)	75(6)	29(5)	13(4)	3(3)	6(4)
C(22)	24(4)	61(6)	51(6)	-25(5)	2(4)	12(4)
C(23)	18(4)	44(5)	58(6)	2(4)	5(4)	3(3)
C(24)	16(4)	58(5)	22(4)	5(4)	0(3)	0(4)
C(25)	18(4)	37(4)	42(5)	1(4)	6(3)	3(3)
C(26)	49(6)	162(12)	58(6)	63(8)	20(5)	8(8)
C(27)	42(6)	152(11)	73(8)	-76(8)	11(6)	4(7)
C(28)	40(6)	46(6)	140(11)	9(6)	-2(6)	15(5)
C(29)	26(5)	115(9)	34(5)	8(6)	3(4)	0(5)
C(30)	38(5)	45(5)	112(8)	-7(6)	3(5)	-7(5)
C(31)	68(7)	62(6)	17(4)	10(4)	-7(4)	2(5)
C(32)	73(7)	71(7)	32(5)	7(5)	15(5)	13(6)
C(33)	70(7)	120(10)	44(6)	30(7)	14(6)	-3(8)
C(34)	101(10)	70(8)	87(9)	24(7)	22(7)	-23(7)
C(35)	73(7)	41(5)	66(7)	-1(5)	11(6)	-11(5)
C(36)	110(9)	28(4)	40(5)	10(4)	-7(6)	2(5)
C(37)	124(10)	67(7)	58(7)	17(6)	-7(7)	19(7)
C(38)	77(7)	64(7)	57(6)	30(5)	-30(5)	-7(6)

Table 5. Hydrogen coordinates (x 10^4) and isotropic displacement parameters ($Å^2$ x 10^3) for 98090.

	x	y	z	U(eq)
H(1A)	7535(5)	6917(5)	1559(4)	40
H(5A)	8145(5)	5774(4)	-1330(3)	33
H(5B)	7006(5)	5527(4)	-1197(3)	33
H(6A)	7628(5)	8752(4)	168(5)	72
H(6B)	8197(5)	8551(4)	934(5)	72
H(6C)	7015(5)	8558(4)	915(5)	72
H(7A)	7625(6)	8290(4)	-839(4)	54
H(7B)	7050(6)	7544(4)	-1289(4)	54
H(7C)	8232(6)	7549(4)	-1271(4)	54
H(9A)	9396(6)	4707(5)	-1829(5)	44
H(10A)	11115(6)	4719(5)	-1961(5)	51
H(11A)	12110(6)	4466(5)	-923(5)	66
H(12A)	11427(6)	4207(6)	234(5)	61
H(13A)	9703(6)	4269(5)	397(4)	47
H(15A)	8765(6)	2874(5)	-1229(4)	41
H(16A)	8048(7)	1740(5)	-1906(4)	53
H(17A)	6469(7)	1876(6)	-2378(5)	59
H(18A)	5625(7)	3177(6)	-2228(5)	60
H(19A)	6267(6)	4281(5)	-1478(4)	46
H(26A)	4996(7)	5077(9)	1351(5)	134
H(26B)	4431(7)	5849(9)	1775(5)	134
H(26C)	5607(7)	5774(9)	1831(5)	134
H(27A)	5222(7)	7401(8)	1967(6)	134
H(27B)	4695(7)	8169(8)	1510(6)	134
H(27C)	5874(7)	8094(8)	1515(6)	134
H(28A)	5267(6)	8435(6)	-710(7)	113
H(28B)	5827(6)	8698(6)	45(7)	113
H(28C)	4645(6)	8693(6)	18(7)	113
H(29A)	5206(6)	7351(7)	-1399(4)	88
H(29B)	4517(6)	6502(7)	-1400(4)	88
H(29C)	5693(6)	6401(7)	-1430(4)	88
H(30A)	4961(6)	4654(6)	227(6)	97
H(30B)	5529(6)	4892(6)	-532(6)	97
H(30C)	4356(6)	5011(6)	-479(6)	97
H(31A)	8483(7)	4540(6)	2065(4)	59
H(32A)	6873(7)	4640(7)	2069(5)	70
H(33A)	5832(8)	3506(8)	2149(5)	93
H(33B)	6753(8)	2853(8)	2158(5)	93
H(34A)	5921(9)	2345(7)	1165(6)	103
H(34B)	5524(9)	3289(7)	931(6)	103
H(35A)	6654(7)	2931(5)	-13(6)	72
H(36A)	8226(8)	2669(5)	103(6)	71
H(37A)	8932(10)	2136(7)	1133(6)	99
H(37B)	7883(10)	2146(7)	1543(6)	99
H(38A)	9429(8)	3350(6)	1672(5)	79
H(38B)	8753(8)	2951(6)	2320(5)	79

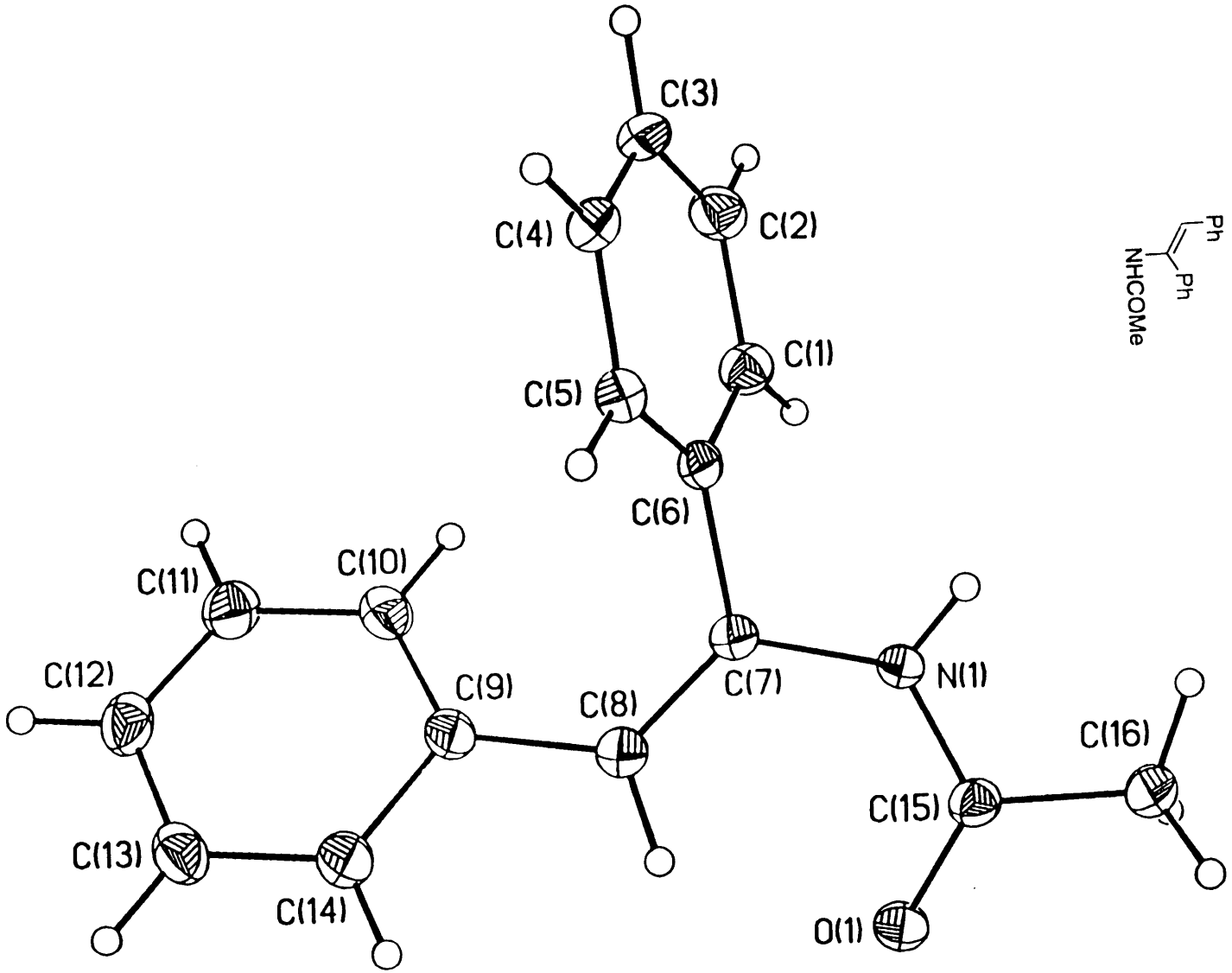
C(3)
C(4)
C(2)
C(1)
C(5)
C(6)
C(11)
C(10)
C(12)
C(9)
C(8)
C(7)
N(1)
C(16)
C(15)
C(13)
C(14)
O(1)
Ph
Ph
NHCOMe

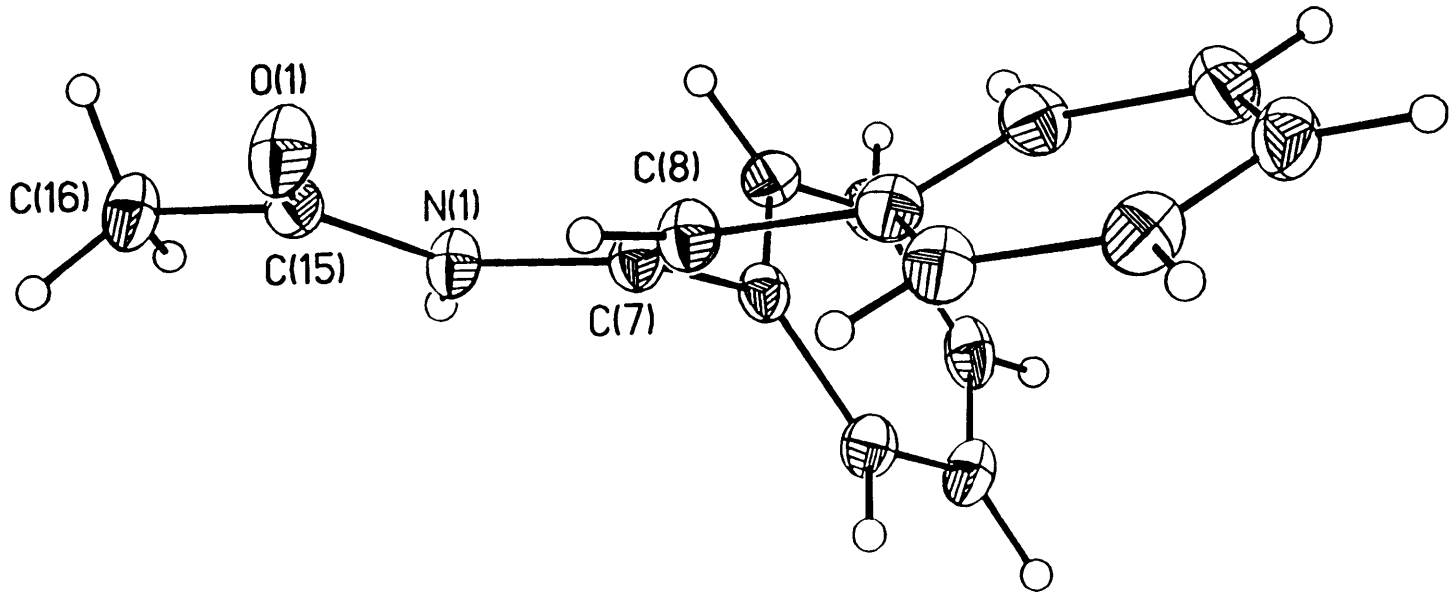
O(1)
C(16)
C(15)
N(1)
C(8)
C(7)

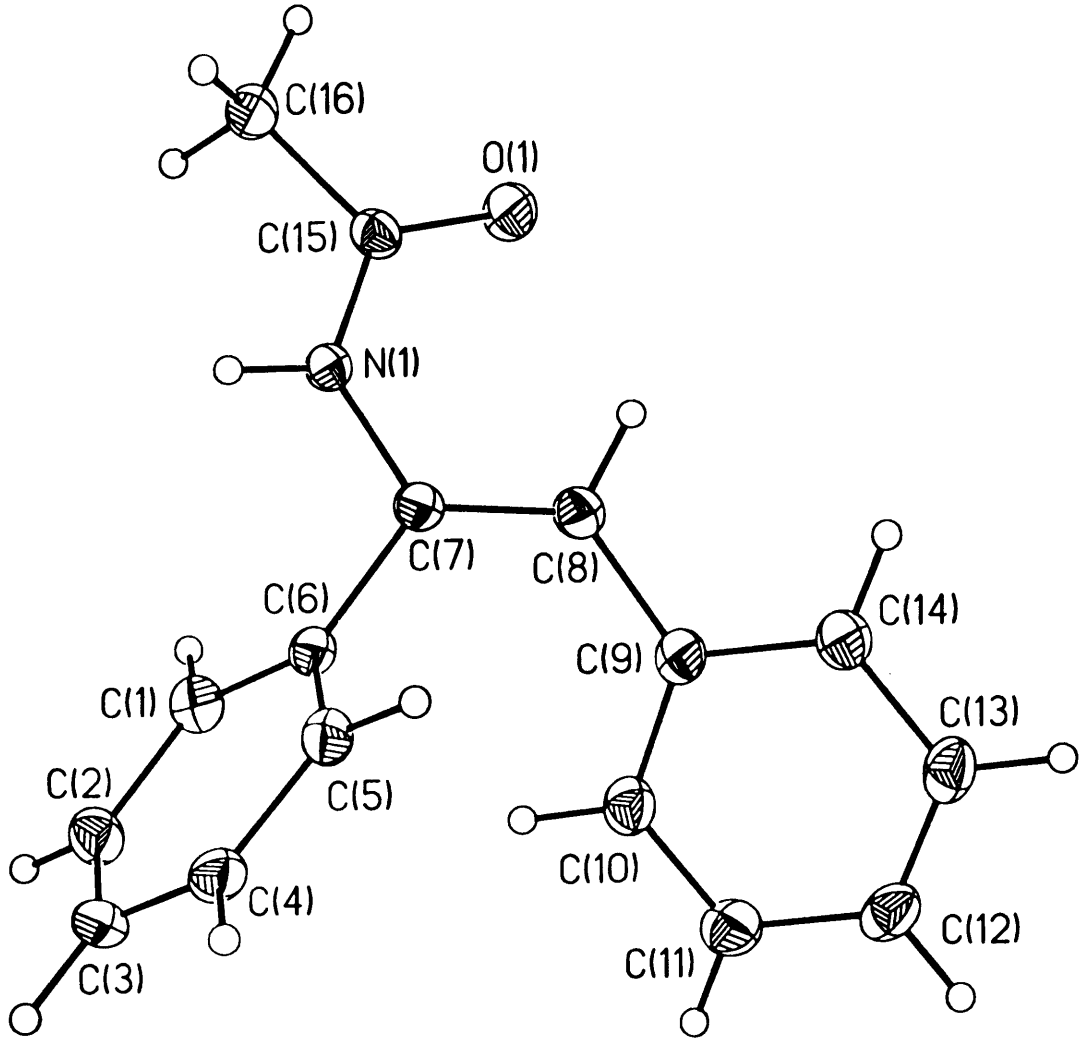
C(16)
O(1)
C(15)
N(1)
C(7)
C(8)
C(6)
C(14)
C(9)
C(1)
C(13)
C(2)
C(5)
C(10)
C(4)
C(12)
C(3)
C(11)

Table 1. Crystal data and structure refinement for 98222.

A. Crystal Data

Identification code	98222
Empirical formula	$C_{16}H_{15}NO$
Formula weight	237.29
Temperature	167(2) K
Wavelength	0.71073 Å
Crystal morphology	block
Crystal size	0.15 x 0.15 x 0.33 mm
Crystal system	Monoclinic
Space group	$P2_1/c$
Unit cell dimensions	a = 11.5679(11) Å alpha = 90°
	b = 9.4117(8) Å beta = 99.104(2)°
	c = 11.9124(11) Å gamma = 90°
Volume, Z	1280.6(2) $Å^3$, 4
Density (calculated)	1.231 Mg/m^3
Absorption coefficient	0.077 mm^{-1}
F(000)	504

B. Data Collection and Reduction

Diffractometer	Siemens SMART/CCD
Scan Type	ω Scans
Scan angle	0.30°
θ range for data collection	1.78 to 23.26°
Limiting indices	$-11 \le h \le 12$, $-10 \le k \le 10$, $-13 \le l \le 10$

Reflections collected	5031
Independent reflections	1831 (R_{int} = 0.0381)
Absorption correction	None

C. Solution and Refinement

Refinement method	Full-matrix least-squares on F^2
Data / restraints / parameters	1829 / 0 / 164
Goodness-of-fit on F^2	1.182
Final R indices [$I>2\sigma(I)$]	R1 = 0.0453, wR2 = 0.1037
R indices (all data)	R1 = 0.0655, wR2 = 0.1172
Extinction coefficient	0.017(3)
Largest diff. peak and hole	0.368 and -0.334 $e\text{Å}^{-3}$

Table 2. Atomic coordinates [x 10^4] and equivalent isotropic displacement parameters [$Å^2$ x 10^3] for 98222. U(eq) is defined as one third of the trace of the orthogonalized U_{ij} tensor.

	x	y	z	U(eq)
O(1)	4853(2)	1307(2)	7299(1)	42(1)
N(1)	4306(2)	-954(2)	6794(2)	29(1)
C(1)	2123(2)	-2729(2)	6099(2)	31(1)
C(2)	1533(2)	-3967(3)	5751(2)	36(1)
C(3)	1659(2)	-4581(3)	4724(2)	36(1)
C(4)	2363(2)	-3935(2)	4039(2)	33(1)
C(5)	2933(2)	-2671(2)	4374(2)	30(1)
C(6)	2826(2)	-2057(2)	5415(2)	25(1)
C(7)	3480(2)	-727(2)	5792(2)	26(1)
C(8)	3337(2)	526(2)	5247(2)	31(1)
C(9)	2427(2)	925(2)	4291(2)	29(1)
C(10)	1292(2)	369(3)	4116(2)	35(1)
C(11)	455(2)	856(3)	3241(2)	41(1)
C(12)	730(2)	1897(3)	2509(2)	40(1)
C(13)	1845(2)	2457(3)	2659(2)	38(1)
C(14)	2676(2)	1987(3)	3551(2)	34(1)
C(15)	4904(2)	23(2)	7497(2)	28(1)
C(16)	5629(2)	-553(3)	8552(2)	36(1)

Table 3. Bond lengths [Å] and angles [°] for 98222.

O(1)-C(15)	1.231(3)	N(1)-C(15)	1.357(3)
N(1)-C(7)	1.423(3)	C(1)-C(2)	1.381(3)
C(1)-C(6)	1.391(3)	C(2)-C(3)	1.381(3)
C(3)-C(4)	1.382(4)	C(4)-C(5)	1.387(3)
C(5)-C(6)	1.391(3)	C(6)-C(7)	1.494(3)
C(7)-C(8)	1.343(3)	C(8)-C(9)	1.472(3)
C(9)-C(14)	1.392(3)	C(9)-C(10)	1.399(3)
C(10)-C(11)	1.383(3)	C(11)-C(12)	1.381(4)
C(12)-C(13)	1.379(4)	C(13)-C(14)	1.388(3)
C(15)-C(16)	1.498(3)		

C(15)-N(1)-C(7)	128.7(2)	C(2)-C(1)-C(6)	121.0(2)
C(3)-C(2)-C(1)	120.2(2)	C(2)-C(3)-C(4)	119.6(2)
C(3)-C(4)-C(5)	120.3(2)	C(4)-C(5)-C(6)	120.5(2)
C(1)-C(6)-C(5)	118.4(2)	C(1)-C(6)-C(7)	121.3(2)
C(5)-C(6)-C(7)	120.2(2)	C(8)-C(7)-N(1)	123.5(2)
C(8)-C(7)-C(6)	124.9(2)	N(1)-C(7)-C(6)	111.5(2)
C(7)-C(8)-C(9)	128.0(2)	C(14)-C(9)-C(10)	117.2(2)
C(14)-C(9)-C(8)	118.6(2)	C(10)-C(9)-C(8)	124.0(2)
C(11)-C(10)-C(9)	121.2(2)	C(10)-C(11)-C(12)	120.4(3)
C(13)-C(12)-C(11)	119.6(2)	C(12)-C(13)-C(14)	119.8(2)
C(13)-C(14)-C(9)	121.8(2)	O(1)-C(15)-N(1)	122.9(2)
O(1)-C(15)-C(16)	121.3(2)	N(1)-C(15)-C(16)	115.9(2)

Symmetry transformations used to generate equivalent atoms:

Table 4. Anisotropic displacement parameters [$Å^2$ x 10^3] for 98222.

The anisotropic displacement factor exponent takes the form:

$-2\pi^2 [(ha^*)^2 U_{11} + ... + 2hka^* b^* U_{12}]$

	U11	U22	U33	U23	U13	U12
O(1)	53(1)	20(1)	47(1)	-3(1)	-12(1)	-1(1)
N(1)	34(1)	18(1)	31(1)	-1(1)	-5(1)	0(1)
C(1)	32(1)	30(1)	32(1)	-4(1)	5(1)	1(1)
C(2)	30(1)	34(2)	43(2)	5(1)	6(1)	-3(1)
C(3)	32(1)	28(1)	42(2)	-2(1)	-8(1)	-5(1)
C(4)	40(2)	30(1)	27(1)	-3(1)	-3(1)	-1(1)
C(5)	32(1)	28(1)	27(1)	3(1)	2(1)	0(1)
C(6)	24(1)	22(1)	28(1)	0(1)	-2(1)	3(1)
C(7)	27(1)	24(1)	27(1)	-1(1)	2(1)	-1(1)
C(8)	33(1)	26(1)	33(1)	0(1)	-1(1)	-1(1)
C(9)	35(2)	21(1)	32(1)	-1(1)	2(1)	4(1)
C(10)	37(2)	30(1)	38(2)	4(1)	4(1)	4(1)
C(11)	33(2)	39(2)	48(2)	0(1)	-2(1)	5(1)
C(12)	45(2)	34(2)	37(2)	-2(1)	-6(1)	9(1)
C(13)	52(2)	28(1)	34(2)	3(1)	5(1)	6(1)
C(14)	38(2)	28(1)	36(1)	0(1)	2(1)	2(1)
C(15)	28(1)	24(1)	30(1)	-4(1)	3(1)	-1(1)
C(16)	41(2)	28(1)	34(1)	-3(1)	-6(1)	-3(1)

Table 5. Hydrogen coordinates (x 10^4) and isotropic displacement parameters ($Å^2$ x 10^3) for 98222.

	x	y	z	U(eq)
H(1A)	4448(2)	-1848(2)	6985(2)	34
H(1B)	2048(2)	-2330(2)	6817(2)	38
H(2A)	1038(2)	-4397(3)	6218(2)	43
H(3A)	1264(2)	-5442(3)	4490(2)	43
H(4A)	2457(2)	-4357(2)	3335(2)	40
H(5A)	3400(2)	-2222(2)	3889(2)	35
H(8A)	3891(2)	1243(2)	5512(2)	37
H(10A)	1092(2)	-355(3)	4607(2)	42
H(11A)	-314(2)	471(3)	3143(2)	49
H(12A)	154(2)	2224(3)	1906(2)	48
H(13A)	2044(2)	3164(3)	2153(2)	46
H(14A)	3435(2)	2399(3)	3659(2)	41
H(16A)	5562(2)	-1590(3)	8560(2)	54
H(16B)	5351(2)	-157(3)	9222(2)	54
H(16C)	6450(2)	-287(3)	8565(2)	54

Appendix II

Selected NMR Spectra

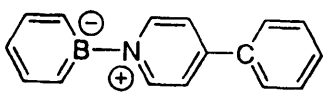

^{13}C NMR CD_2Cl_2

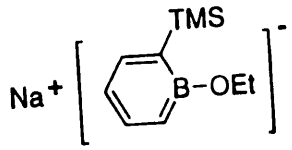

^{1}H NMR THF-d_8

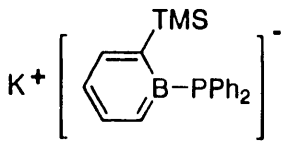

^{1}H NMR THF-d_8

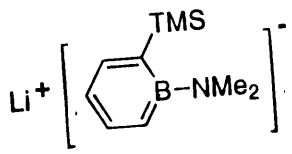

^{1}H NMR THF-d_8

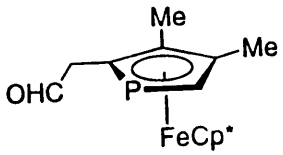

^{13}C NMR CD_2Cl_2

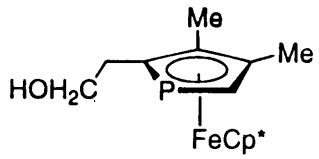

^{1}H NMR CD_2Cl_2

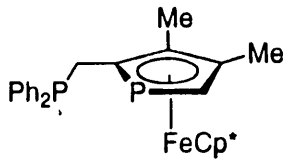

^{1}H NMR CD_2Cl_2

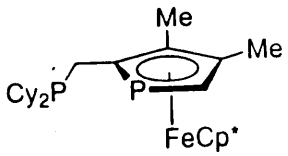

^{1}H NMR CD_2Cl_2

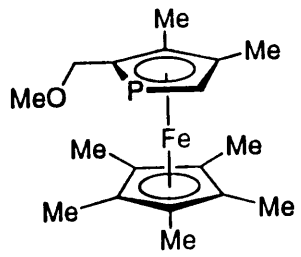

^1H NMR CD_2Cl_2

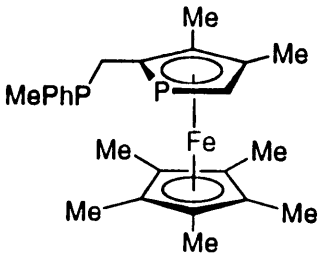

^{1}H NMR CD_2Cl_2
diastereomers

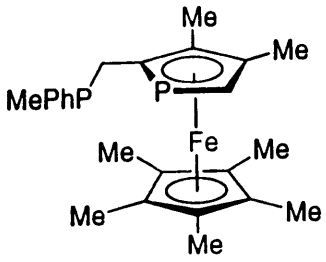

^{31}P NMR CD_2Cl_2
diastereomers

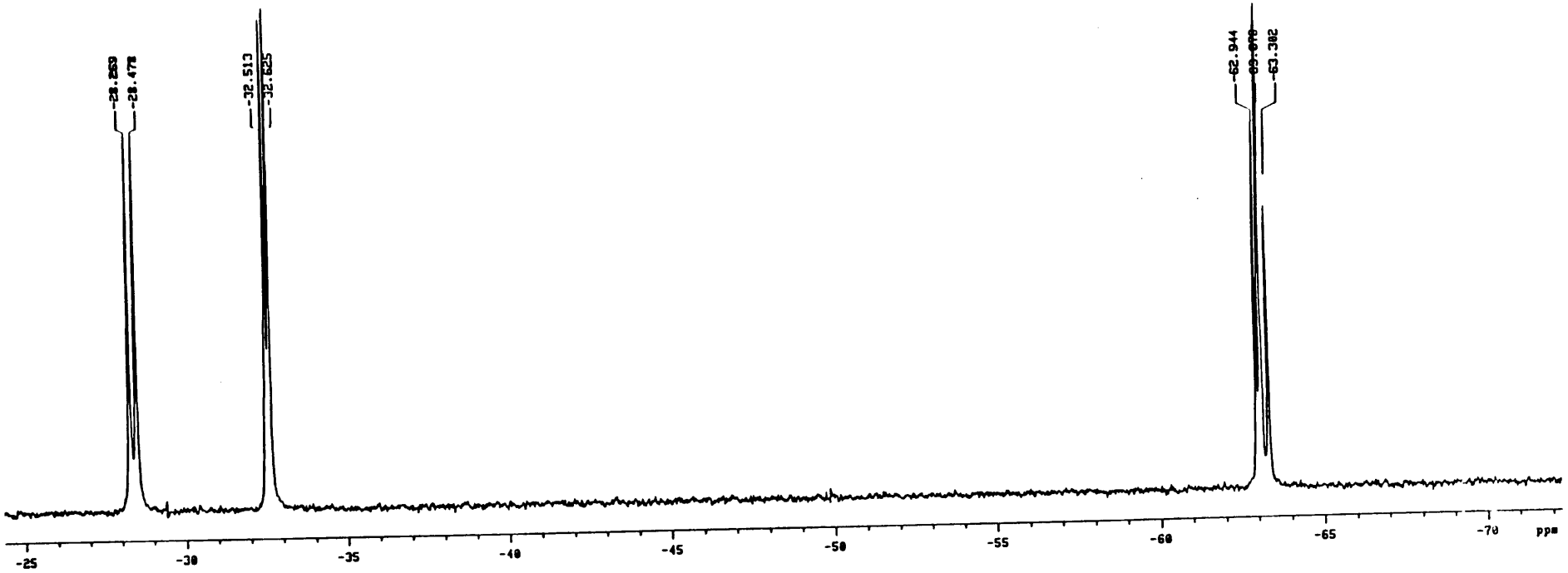

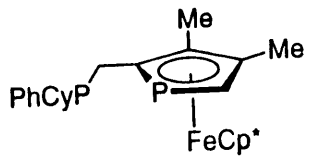

^{1}H NMR CD_2Cl_2
diastereomers

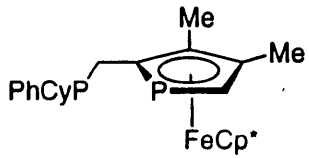

^{31}P NMR CD_2Cl_2
diastereomers

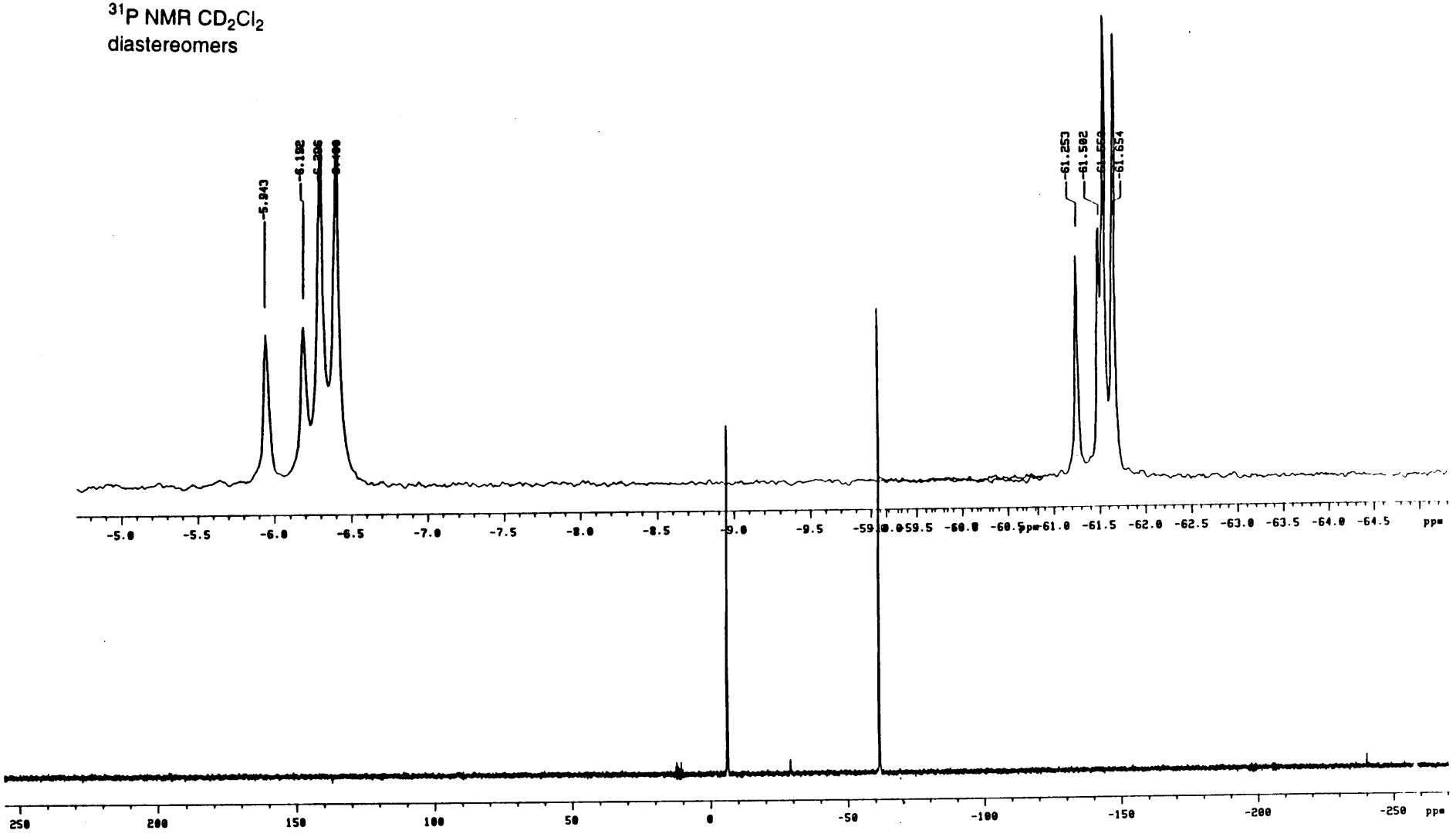

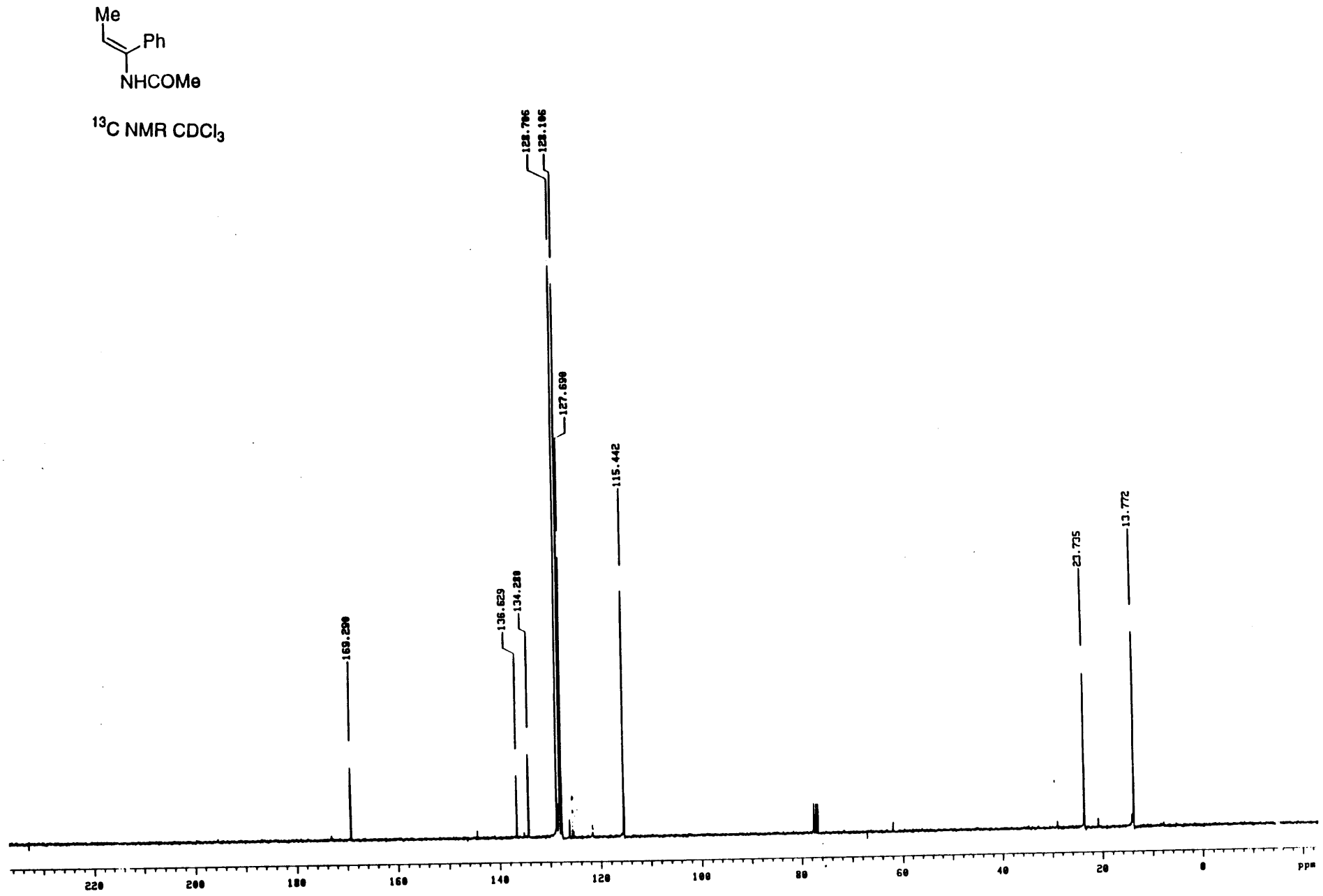
Me
Ph
NHCOMe
^{13}C NMR $CDCl_3$
169.290
136.629
134.280
128.706
128.186
127.698
115.442
23.735
13.772
220
200
180
160
140
120
100
80
60
40
20
0
ppm

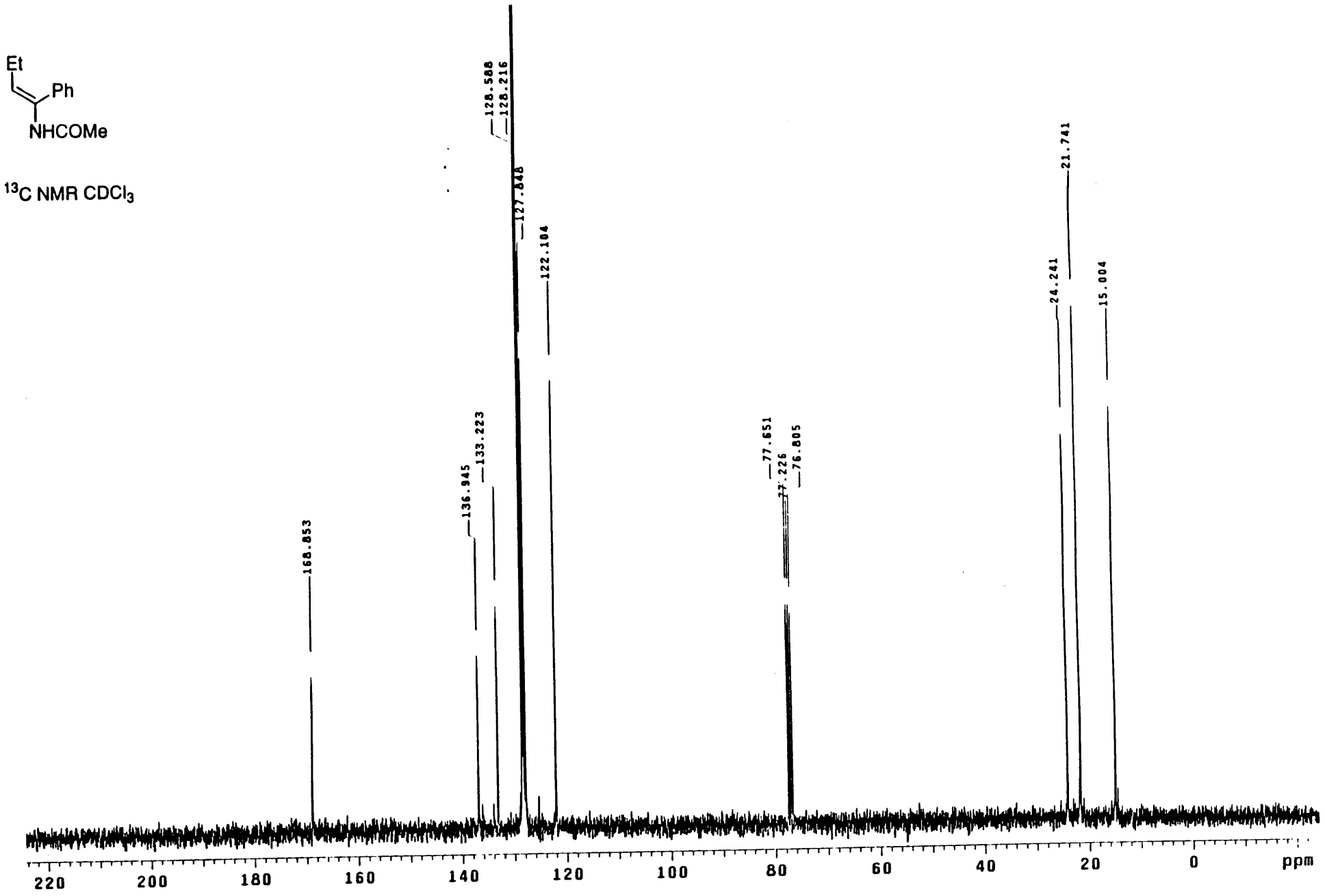
Et
Ph
NHCOMe
^{13}C NMR $CDCl_3$
168.853
136.945
133.223
128.588
128.216
127.848
122.104
77.651
77.226
76.805
24.241
21.741
15.004
220
200
180
160
140
120
100
80
60
40
20
0
ppm

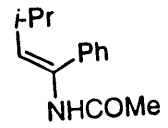

^{1}H NMR $CDCl_3$

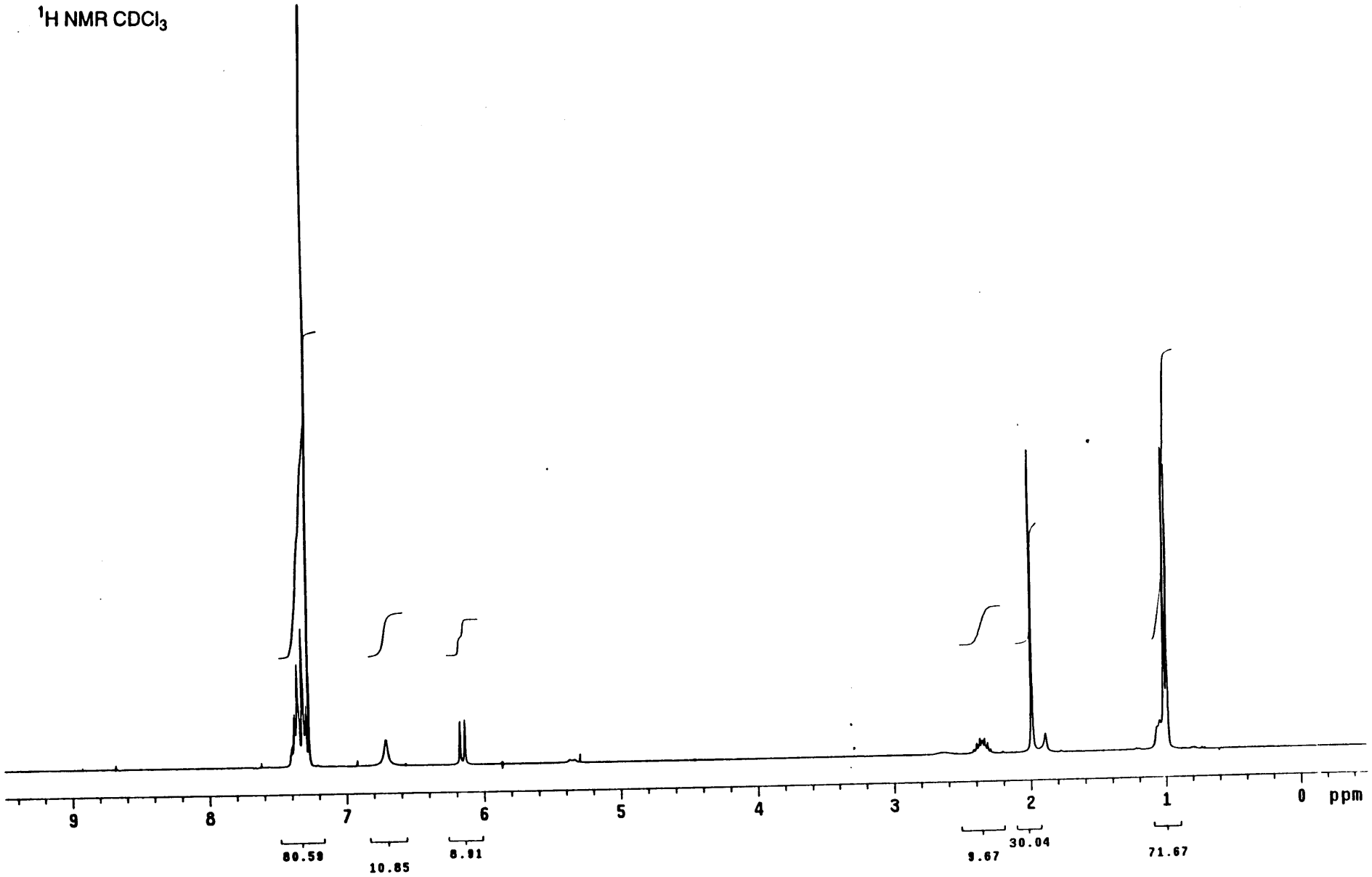

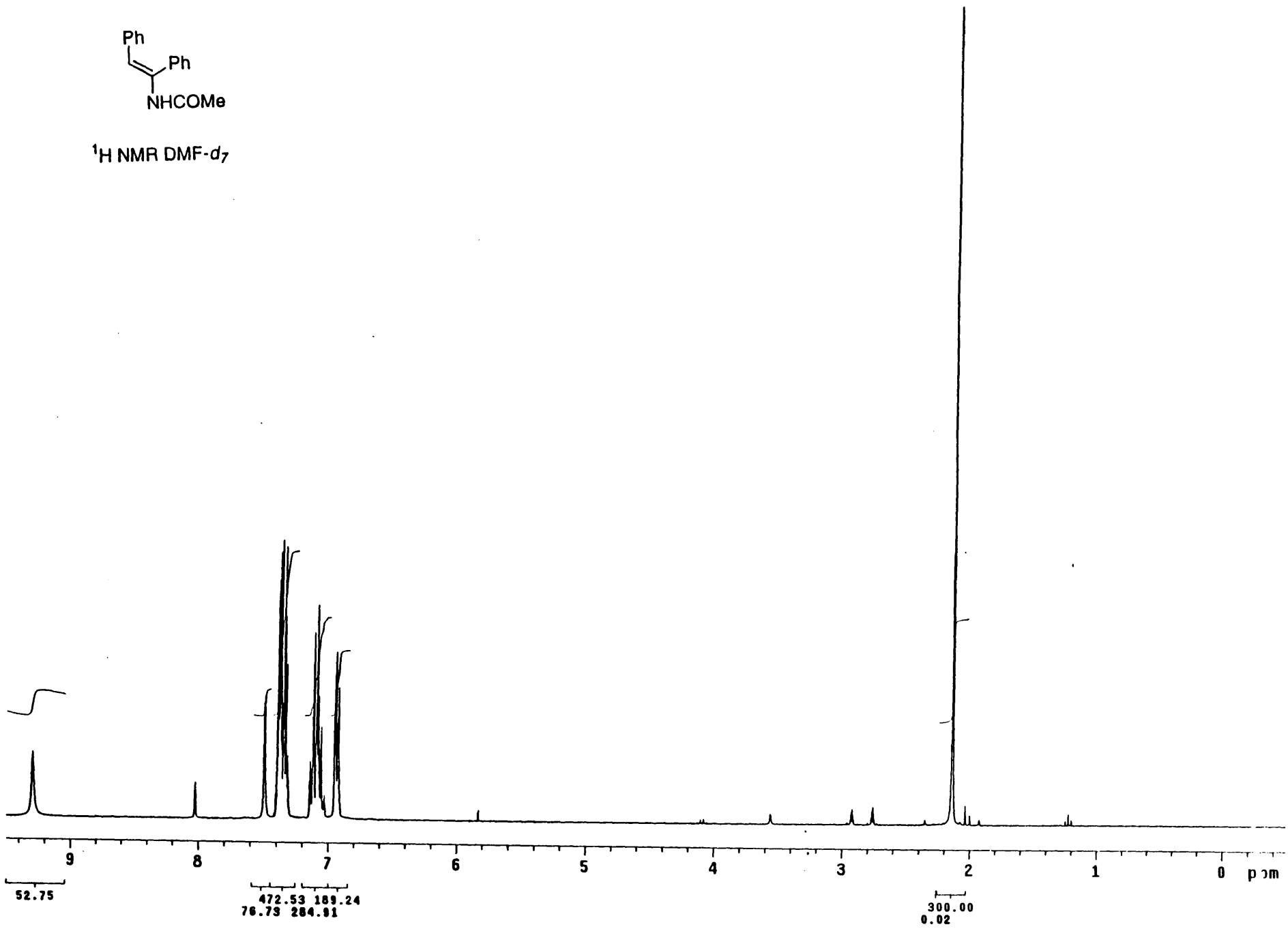
Ph
Ph
NHCOMe
1H NMR DMF-d7
9
8
7
6
5
4
3
2
1
0
ppm
52.75
472.53
76.73
189.24
284.91
300.00
0.02

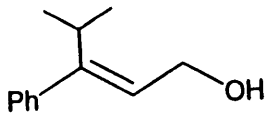

^{1}H NMR $CDCl_3$

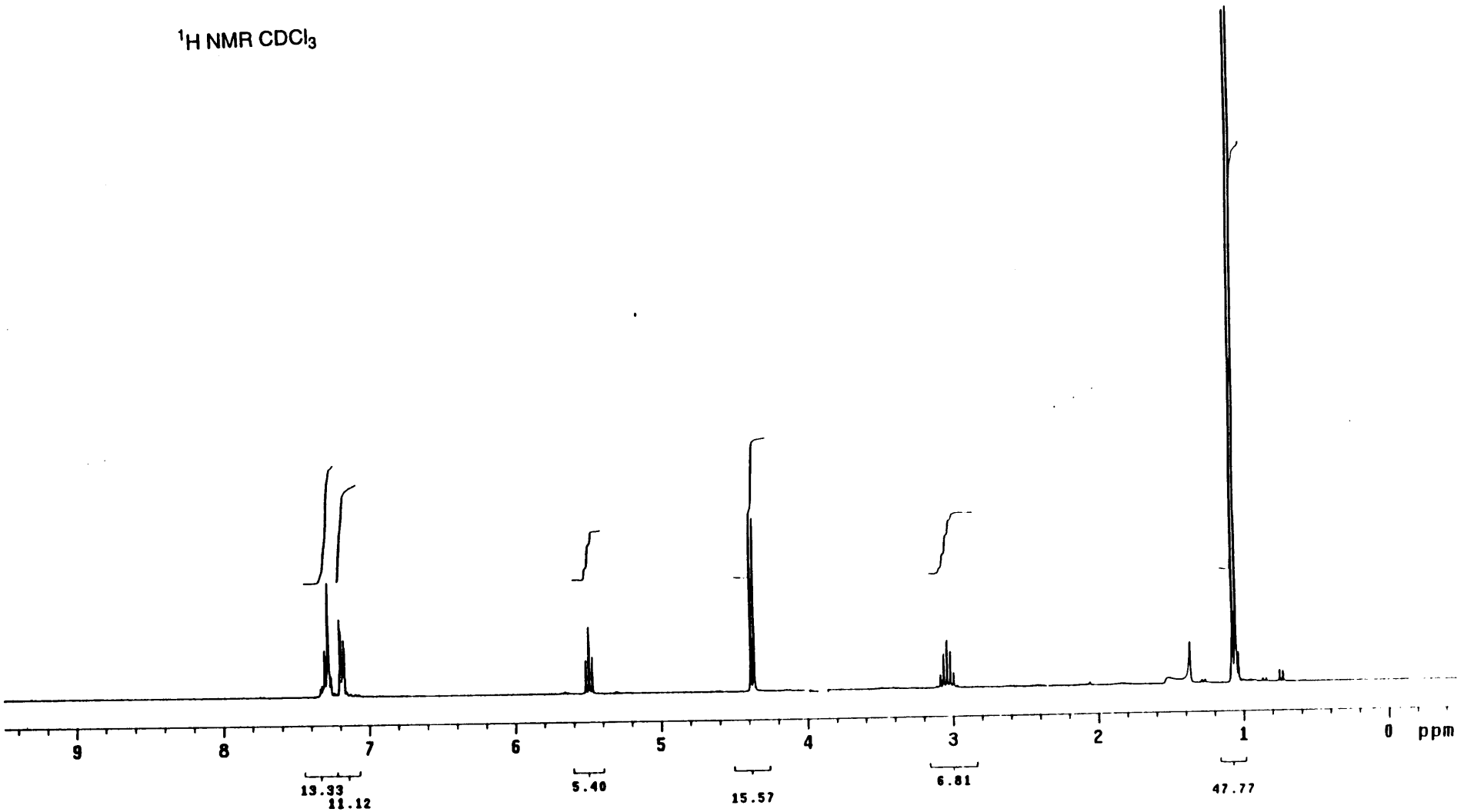

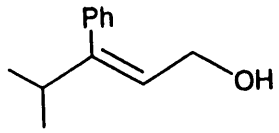

^{1}H NMR $CDCl_3$

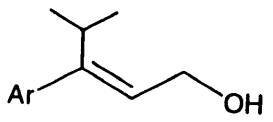

Ar = 4-Cl-Ph

^{1}H NMR $CDCl_3$

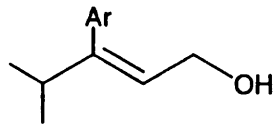

Ar = 4-Cl-Ph

^{1}H NMR $CDCl_3$

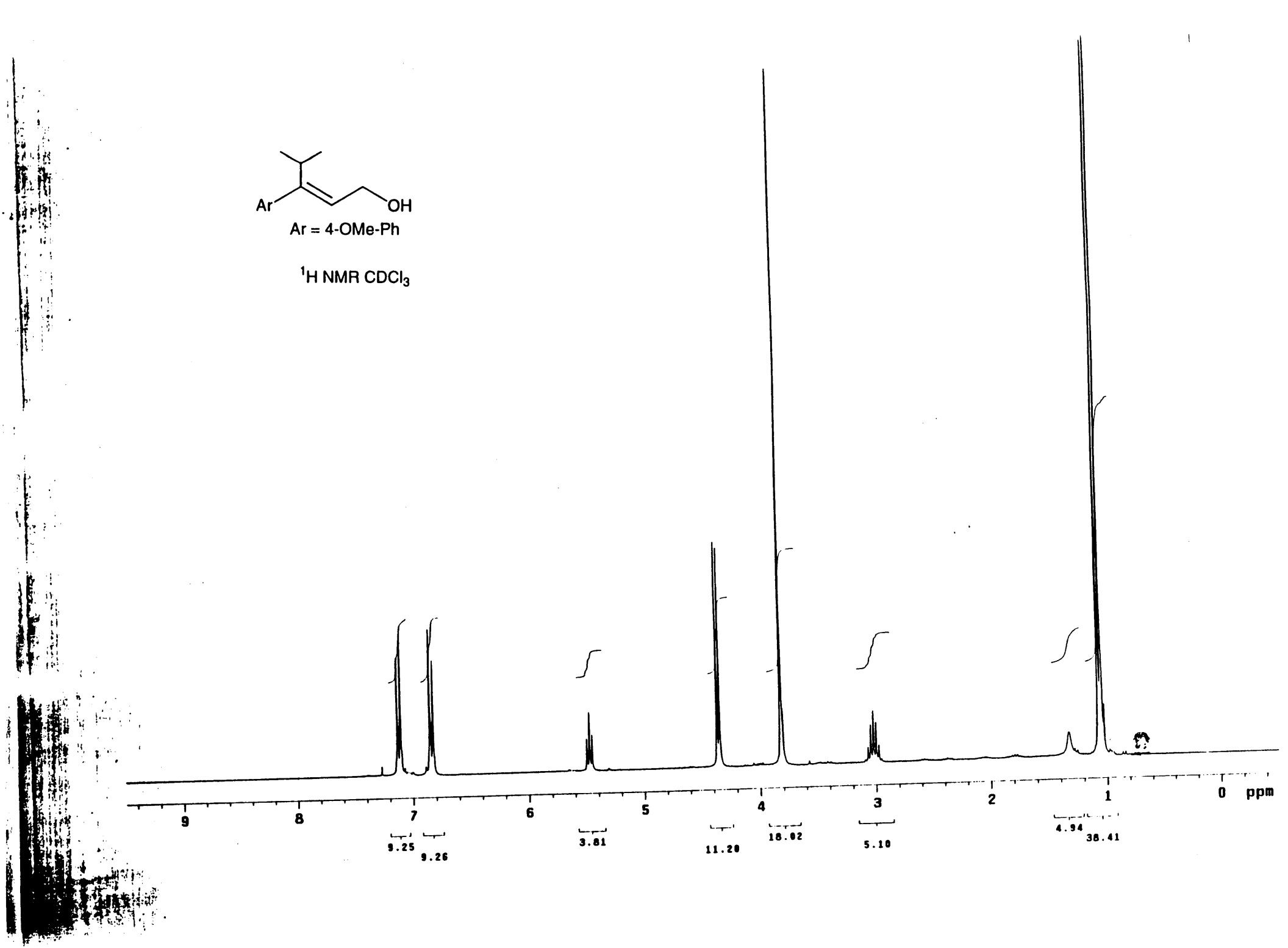
Ar
OH
Ar = 4-OMe-Ph
^{1}H NMR $CDCl_3$
9
8
7
6
5
4
3
2
1
0 ppm
9.25
9.26
3.81
11.20
18.02
5.10
4.94
38.41

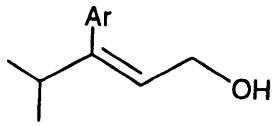

Ar = 4-OMe-Ph

^{1}H NMR $CDCl_3$